Close Out and Final Report For
NASA Glenn Cooperative Agreement NCC3-878

Multi-Scale Sizing of Lightweight Multifunctional Spacecraft Structural Components

Brett A. Bednarcyk
Ohio Aerospace Institute
Cleveland, Ohio

Table of Contents

Abstract

This document is the final report for the project entitled, "Multi-Scale Sizing of Lightweight Multifunctional Spacecraft Structural Components," funded under the NRA entitled "Cross-Enterprise Technology Development Program" issued by the NASA Office of Space Science in 2000. The project was funded in 2001, and spanned a four year period from March, 2001 to February, 2005. Through enhancements to and synthesis of unique, state of the art structural mechanics and micromechanics analysis software, a new multi-scale tool has been developed that enables design, analysis, and sizing of advance lightweight composite and smart materials and structures from the full vehicle, to the stiffened structure, to the micro (fiber and matrix) scales. The new software tool has broad, cross-cutting value to current and future NASA missions that will rely on advanced composite and smart materials and structures.

Introduction

The research project entitled "Multi-Scale Sizing of Lightweight Multifunctional Spacecraft Structural Components" was successfully completed on February 28, 2005. The overall goal of this endeavor was to develop and implement a unique software package for the design, analysis, and optimization of lightweight heterogeneous and smart materials and structures. Through enhancement and synthesis of three existing analysis technologies known as HyperSizer, MAC/GMC, and HOTFGM, the resulting software product now enables design, analysis, and sizing from the micro, through the meso, to the global (structural) scale in order to maximize component performance while minimizing weight. The need for and methodology of this type of multi-scale analysis technology is shown in Fig. 1. Most traditional aerospace structural component designs require computationally intensive explicit 3-D finite element analyses (on the global scale) using effective material properties. Then, in regions identified to be critical, a local finite element analysis is performed via submodeling to obtain a better approximation of the local behavior. This submodeling process is extremely operator intensive, and not well suited for design optimization, thus, while the component is rendered functional and safe via finite element analysis, it is rarely truly optimized to yield the best and most cost effective design. The new software developed in this project enables continuous and automatic homogenization and localization between the relevant material and structural scales. This, in turn enables engineers to produce significantly improved designs of smart and traditional spacecraft structures while consuming at least an order of magnitude fewer man-hours than currently required in the design process (for sufficiently complex components).

The project was undertaken by a collaborative team of engineers at four separate institutions: Ohio Aerospace Institute (Cleveland, Ohio), Collier Research Corporation (Hampton, Virginia), University of Virginia (Charlottesville, Virginia), and NASA Glenn Research Center (Cleveland, Ohio). While the tasks associated with the project were each the primary responsibility of one institution, there was a great deal of cooperation throughout the project.

The Micromechanics Analysis Code with Generalized Method of Cells (MAC/GMC) provides the core micro scale (see Fig. 1) design and analysis capability to the developed multi-scale software. Based on state of the art micromechanics analysis theories, this software determines the effective properties and response of nonlinear traditional and smart composite materials based on the constituent properties and their arrangement. Because MAC/GMC provides the local stress and strain fields throughout the fiber and matrix constituents, local models for viscoplasticity, damage, and failure can (and have been) implemented. Then, the effects of these local phenomena on the composite properties and nonlinear response are determined (via homogenization) and, as shown in Fig. 1, this information can be passed to higher-scale structural models. MAC/GMC is also extremely efficient, and within this project, new capabilities that enable analysis of so-called "smart" piezo-electro-magnetic materials and that provide the code with a new standard of micro scale accuracy have been implemented.

The Higher-Order Theory for Functionally Graded Materials (HOTFGM) is a higher-order micromechanics theory that analyzes the thermo-mechanical behavior of composites. Unlike MAC/GMC, in its standard form, HOTFGM considers simple composite structures that have boundaries (e.g., plates). MAC/GMC, on the other hand, considers a periodic composite material without boundaries. As the name implies, HOTFGM has found significant application in the area of functionally graded composite materials, but it is also applicable to a wide array of simple arbitrary structures. As part of this project, a new homogenized version of HOTFGM (now called HFGMC) has been developed and implemented within MAC/GMC. This enables the improved accuracy associated with the HOTFGM higher-order fields to impact the analysis of composite materials rather than structures. As a new analysis module within MAC/GMC, this homogenized version of HOTFGM has been incorporated within the developed multi-scale software tool. In addition, a loose coupling between HyperSizer and the standard HOTFGM capabilities has been accomplished through a product called HyperSizer NCell.

HyperSizer is a unique state of the art automated structural sizing software package that performs strength and stability analyses of a wide array stiffened panel and beam concepts, see Fig. 1. It is a commercial code sold and marketed by Collier Research Corporation. HyperSizer automatically

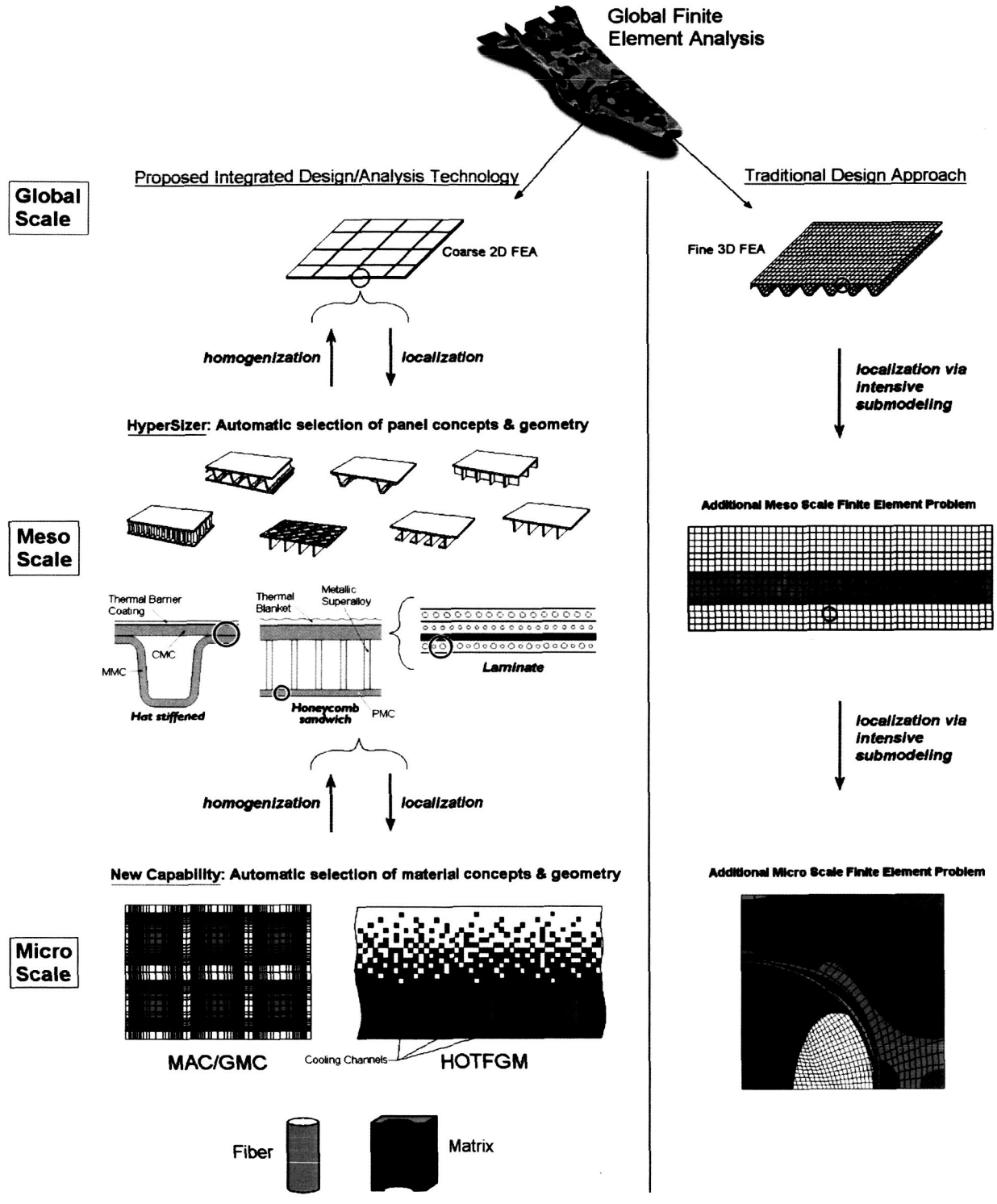

Fig. 1. The unique integrated structural design software synthesizes advanced analysis techniques to enable automatic sizing of multifunctional structural components on all scales. Thus micro scale changes can be made to improve the design, and the effects of these changes on the global scale can be determined. The traditional approach to structural design allows localization through an extremely intense process of submodeling, but a process for making improvements through micro scale changes and determining the effects of those changes on the global scale is intractable.

optimizes stiffened structures and selects from among stiffener concepts and geometric dimensions, materials, and composite ply layups to arrive at the lightest weight design. In order to enable full vehicle design and analysis, the software couples with finite element analysis as shown in Fig. 1. Because HyperSizer homogenizes stiffened panels to arrive at their effective plate-like response, a coarse two-dimensional shell element mesh can be employed for the stiffened panels within the vehicle level finite element analysis, as opposed to the fine three-dimensional mesh required to account for the stiffener geometry relying solely on the finite element method (see right hand side of Fig. 1). As a result, HyperSizer is orders of magnitude faster in terms if operator and execution time compared to the standard finite element approach. As part of this project, HyperSizer has been enhanced to include smart (piezo-electro-magnetic) material effects and time-dependence. This has significantly broadened the applicability of the code in the realm of advanced adaptive structures and time-dependent progressive failure analysis. Finally, as shown in Fig. 1, a tight coupling between MAC/GMC and HyperSizer has produced a new, integrated, multi-scale software tool. For each ply within a HyperSizer composite or smart structural analysis, MAC/GMC can be called to provide the micro scale response. Local damage can thus be predicted in the fiber and matrix constituents within each ply, and the effects will be felt on the meso and global scales. The result is more accurate, higher-fidelity analyses that enable improved aerospace structural designs in terms of cost, efficiency, reliability, and safety.

The most significant accomplishments of this project are outlined here, and discussed in more detail (along with general accomplishments) in the body of this report.

- **The High-Fidelity Generalized Method of Cells (HFGMC) has been developed and implemented within MAC/GMC.** Based on a homogenized version of HOTFGM, HFGMC is significantly more accurate at the micro fiber and matrix constituent scale compared to the standard generalized method of cell (GMC), the previous micromechanics technology in MAC/GMC. Implemented in a separate analysis module within the software (see Fig. 2), HFGMC enables improved composite and laminate analyses, and when combined with the standard GMC capabilities, it provides MAC/GMC with variable fidelity analysis capabilities that maximize either efficiency or accuracy. HFGMC represents the state of the art for micromechanics theories.

- **Smart (piezo-electro-magnetic) material analysis has been implemented within MAC/GMC.** Piezo-electro-magnetic materials, which exhibit coupling among their electric, magnetic, mechanical, and thermal responses, have vast potential for application in aerospace structures. Such materials enable structures to perform as lifelike, multifunctional systems that can sense and potentially react to various stimuli. The structural system can then be designed to adapt to a changing mission profile, enabling optimum performance, reliability, and safety under all conditions rather than at a single design-to load point. Smart composites and laminates provide additional flexibility as they introduce coupling of certain effects that can be exploited in a design, and their material properties can be tailored. A smart GMC composite analysis module has now been implemented within MAC/GMC (see Fig. 2), along with the ability to model smart composite laminates. This provides, for the first time, a tool for the systematic design and analysis of these new smart materials, thus filling a void needed to realize their vast potential.

- **A new streamlined and updated Version 4.0 of MAC/GMC has been released.** In order to facilitate incorporation of MAC/GMC within HyperSizer, a new and significantly improved version of MAC/GMC was released. This new version includes the HFGMC and smart material capabilities described above and has also been upgraded in terms of micro scale damage analysis and usability. The new version was rewritten in the FORTRAN 90 standard (from the previous FORTRAN 77 versions), and now takes advantage of dynamic memory allocation, data structures, and modules. These FORTRAN 90 features were critical to enabling the integration of MAC/GMC within HyperSizer in terms of data exchange between the codes and providing access to the needed MAC/GMC subprograms.

- **Graphical User Interfaces (GUIs) have been developed for MAC/GMC and HOTFGM.** In the case of HOTFGM, the GUI represents a separate module (now called HyperSizer NCell) enabling users to set up, execute, and post-process HOTFGM problems. The MAC/GMC GUI forms are fully integrated within HyperSizer. The new Micromechanics Architecture Form enables users to define a MAC/GMC composite material, in terms of the constituent materials and their arrangements, and to quickly calculate effective composite properties. The new Micromechanics Workspace Form enables users to perform stand alone MAC/GMC simulations (i.e., apply time-dependent loading) on MAC/GMC composite materials. Problems can be executed within the GUIs, and results can be displayed and stored within the HyperSizer database. These GUIs provide a clean and user-friendly environment for MAC/GMC and HOTFGM and take both codes to the commercial level.

- **A smart (piezo-electro-magnetic) version of HyperSizer has been developed and implemented.** New equations representing the coupling among the thermal, electric, magnetic, and mechanical behavior of stiffened panels were developed and added to the HyperSizer core analysis code. This enables HyperSizer to now impact designs of smart, adaptive, stiffened structures and to accept ply-level smart material information from MAC/GMC. These smart capabilities far exceed those of other commercial structural analysis software packages, including large finite element codes such as ABAQUS, ANSYS, and MSC/NASTRAN.

- **Time-Dependence has been implemented within HyperSizer.** By enabling HyperSizer to apply loads incrementally, several new and important classes of design problems can now be solved. HyperSizer can now call MAC/GMC for each composite material ply at each time step, and accept time-dependent information from the micro scale analysis. This enables progressive damage simulations in which local damage is simulated at the fiber-matrix scale. This local damage alters the composite ply-level properties, which the affects the panel level response (making it nonlinear), and can eventually lead to structural failure. This new capability fills a gap for HyperSizer in that, previously, only ply-level damage initiation could be accounted for. In addition, HyperSizer now admits a design-to load profile, rather than a single design-to load. The software now progressively applies each load level within the profile, stepping between the load points, and properly accounting for accumulated damage in evaluating the structure's margin of safety at each specified design-to load in the profile.

- **Fully coupled smart, time-dependent HyperSizer – MAC/GMC software for multiscale analysis of multifunctional structures has been developed.** This new integrated software package is the crown jewel of the project. Analysis can now progress from the full vehicle, to the stiffened panel, to the laminate ply, to the micro fiber and matrix scales (see Fig. 1). Effects and phenomena modeled on the micro scale can then affect the ply, panel, and full vehicle designs. This provides a new and unique level of fidelity and accuracy to the HyperSizer predictions by granting access to the wide range of powerful MAC/GMC micromechanics capabilities. This coupling has been accomplished not only for the standard composite material analyses, but also for the new smart material analyses made available within MAC/GMC and HyperSizer as part of this project. The integrated, multi-scale, multifunctional HyperSizer – MAC/GMC software package's innovative combination of features far exceeds those of any other structural analysis product and will have a major impact on aerospace structural systems in terms of cost, reliability, efficiency, and safety.

The remainder of this report provides details on the work performed and results of the specific project tasks.

Project Team

The project team consisted of engineers from three institutions: the Ohio Aerospace Institute (OAI) in Cleveland, Ohio, Collier Research Corporation (CRC) in Hampton, Virginia, NASA Glenn Research Center (GRC) in Cleveland, Ohio, and the University of Virginia (U.Va.) in Charlottesville, Virginia. The project team members and their affiliations are given below.

Team Member	Title	Affiliation
Dr. Brett A. Bednarcyk (Principal Investigator)	Senior Scientist	OAI
Mr. Craig S. Collier	President	CRC
Mr. Phillip W. Yarrington	Lead Software Engineer	CRC
Dr. Steven M. Arnold	Senior Research Engineer	NASA GRC
Dr. Marek-Jerzy Pindera	Professor	U.Va.
Dr. Jacob Aboudi	Visiting Professor	U.Va.
Ms. Melissa J.B. Rogers	Educational Specialist	OAI

Dr. Dale A. Hopkins, Senior Research Engineer at NASA GRC, served as NASA COTR for the project.

Task 1. Enhancements to MAC/GMC

NASA GRC's Micromechanics Analysis Code with Generalized Method of Cells (MAC/GMC) (Bednarcyk and Arnold, 2002a,b) functions at the lowest scale in the new integrated software toolset (i.e., the micro scale, see Fig. 1). MAC/GMC models both continuous and discontinuous composite materials using a repeating unit cell, which represents the geometric arrangement of the composite constituents. It relies on a family of micromechanics theories, known collectively as the Generalized Method of Cells (GMC), which are implemented in MAC/GMC as analysis modules as shown in Fig. 2. Then, on the level of the individual constituents, the MAC/GMC libraries of features and local deformation and failure models operate in concert, enabling realistic modeling of composite response and life. Two of the analysis modules depicted in Fig. 2 resulted from Task 1 of this project: 1) the GMC Smart Piezo-Electro-Magnetic Composite Analysis Module and 2) the HFGMC continuous composite analysis module. The development of these modules is described as the subtasks below.

1.1 Inclusion of Electromagnetic Effects

A new fully coupled thermo-electro-magneto-inelastic version of the GMC theory has been incorporated within MAC/GMC as an analysis module (see Fig. 2). This enables analysis of composites and laminates containing piezoelectric materials, which exhibit coupling between their electric and mechanical responses, and piezomagnetic materials, which exhibit coupling between their magnetic and mechanical responses. Temperature changes also affect these materials' electric and magnetic behavior, respectively. These new "smart" composites, and structures composed of them, have the ability to sense and/or react to particular thermal, mechanical, electric, and magnetic conditions. They thus can be used to create multifunctional structures that can detect and possibly react so as to mitigate the deleterious effects of damage. However, design and analysis tools for these smart materials and structures have been lacking.

Like standard GMC, piezo-electro-magnetic GMC considers a periodic composite material through identification of a repeating unit cell, as shown in Fig. 3. As the figure indicates, piezo-electro-magnetic GMC considers a triply-periodic, three-dimensional repeating unit cell composed of an arbitrary number of three-dimensional subcells identified by the indices $\alpha\beta\gamma$. N_α, N_β, and N_γ are the number of subcells in each of the three coordinate directions. By placing different monolithic materials within each subcell, the repeating unit cell can represent an arbitrary periodic composite material.

The basic approach to incorporating piezo-electro-magnetic effects within GMC involves expanding the subcell and repeating unit cell constitutive equations. The subcell constitutive equation is given by,

$$\begin{bmatrix} \sigma_{11} \\ \sigma_{22} \\ \sigma_{33} \\ \sigma_{23} \\ \sigma_{13} \\ \sigma_{12} \\ D_1 \\ D_2 \\ D_3 \\ B_1 \\ B_2 \\ B_3 \end{bmatrix}^{(\alpha\beta\gamma)} = \begin{bmatrix} C_{11} & C_{12} & C_{13} & C_{14} & C_{15} & C_{16} & e_{11} & e_{21} & e_{31} & q_{11} & q_{21} & q_{31} \\ C_{12} & C_{22} & C_{23} & C_{24} & C_{25} & C_{26} & e_{12} & e_{22} & e_{32} & q_{12} & q_{22} & q_{32} \\ C_{13} & C_{23} & C_{33} & C_{34} & C_{35} & C_{36} & e_{13} & e_{23} & e_{33} & q_{13} & q_{23} & q_{33} \\ C_{14} & C_{24} & C_{34} & C_{44} & C_{45} & C_{46} & e_{14} & e_{24} & e_{34} & q_{14} & q_{24} & q_{34} \\ C_{15} & C_{25} & C_{35} & C_{45} & C_{55} & C_{56} & e_{15} & e_{25} & e_{35} & q_{15} & q_{25} & q_{35} \\ C_{16} & C_{26} & C_{36} & C_{46} & C_{56} & C_{66} & e_{16} & e_{26} & e_{36} & q_{16} & q_{26} & q_{36} \\ e_{11} & e_{12} & e_{13} & e_{14} & e_{15} & e_{16} & -\kappa_{11} & -\kappa_{12} & -\kappa_{13} & -a_{11} & -a_{12} & -a_{13} \\ e_{21} & e_{22} & e_{23} & e_{24} & e_{25} & e_{26} & -\kappa_{12} & -\kappa_{22} & -\kappa_{23} & -a_{21} & -a_{22} & -a_{23} \\ e_{31} & e_{32} & e_{33} & e_{34} & e_{35} & e_{36} & -\kappa_{13} & -\kappa_{23} & -\kappa_{33} & -a_{31} & -a_{32} & -a_{33} \\ q_{11} & q_{12} & q_{13} & q_{14} & q_{15} & q_{16} & -a_{11} & -a_{21} & -a_{31} & -\mu_{11} & -\mu_{12} & -\mu_{13} \\ q_{21} & q_{22} & q_{23} & q_{24} & q_{25} & q_{26} & -a_{12} & -a_{22} & -a_{32} & -\mu_{12} & -\mu_{22} & -\mu_{23} \\ q_{31} & q_{32} & q_{33} & q_{34} & q_{35} & q_{36} & -a_{13} & -a_{23} & -a_{33} & -\mu_{13} & -\mu_{23} & -\mu_{33} \end{bmatrix}^{(\alpha\beta\gamma)} \begin{bmatrix} \varepsilon_{11} - \varepsilon_{11}^I - \varepsilon_{11}^T \\ \varepsilon_{22} - \varepsilon_{22}^I - \varepsilon_{22}^T \\ \varepsilon_{33} - \varepsilon_{33}^I - \varepsilon_{33}^T \\ 2\varepsilon_{23} - 2\varepsilon_{23}^I - 2\varepsilon_{23}^T \\ 2\varepsilon_{13} - 2\varepsilon_{13}^I - 2\varepsilon_{13}^T \\ 2\varepsilon_{12} - 2\varepsilon_{12}^I - 2\varepsilon_{12}^T \\ -E_1 - E_1^T \\ -E_2 - E_2^T \\ -E_3 - E_3^T \\ -H_1 - H_1^T \\ -H_2 - H_2^T \\ -H_3 - H_3^T \end{bmatrix}^{(\alpha\beta\gamma)} \quad (1.1)$$

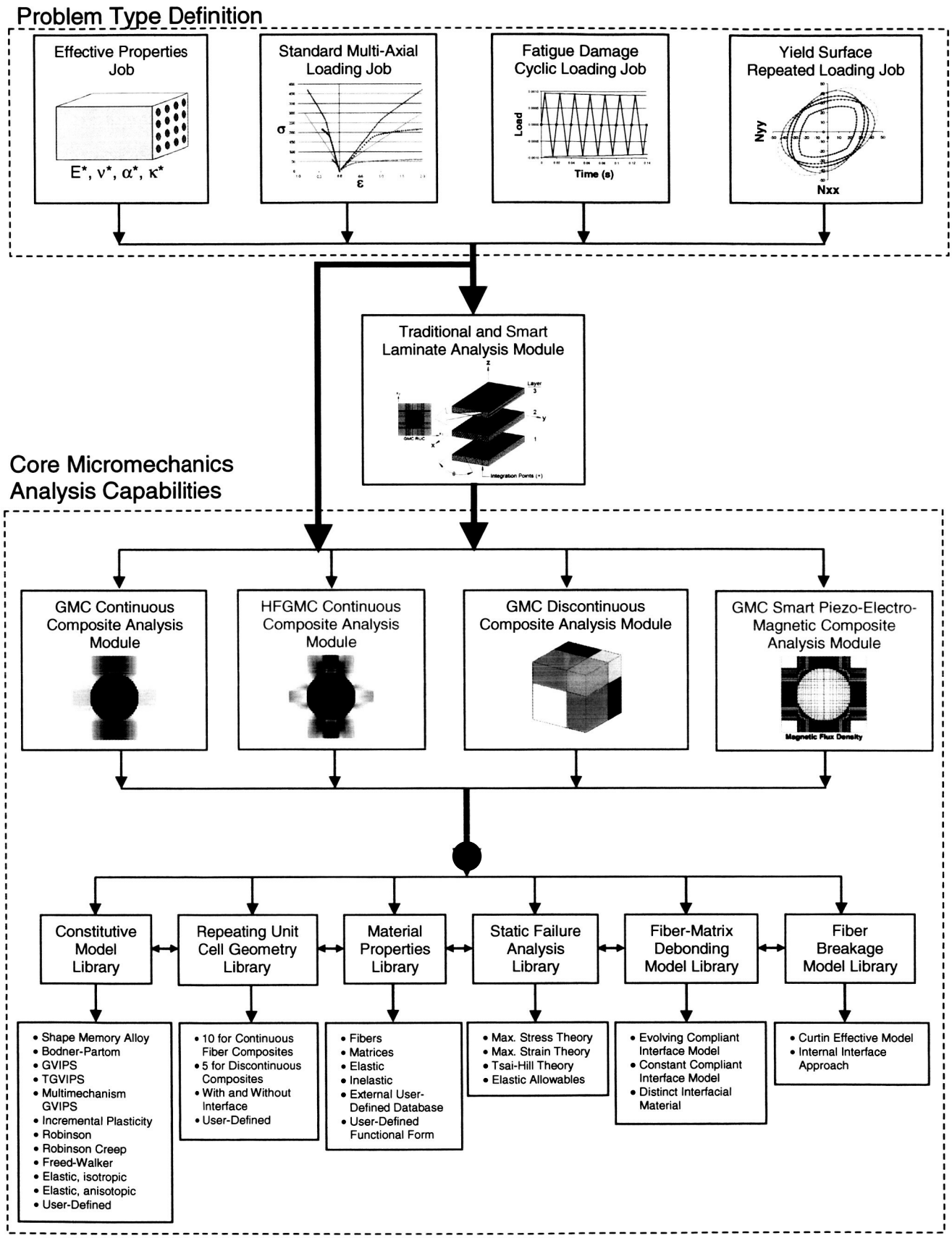

Fig. 2. Functionality diagram for the Micromechanics Analysis Code with Generalized Method of Cells (MAC/GMC). The software enables execution of four types of analysis jobs on either a composite laminate or a non-laminated composite material. The four core micromechanics analysis modules may thus be accessed directly or through the laminate analysis module, which then uses the core micromechanics modules to simulate the response of each ply. Alternatively, as integrated with HyperSizer, HyperSizer accesses the core modules directly. The libraries of local models, properties, and features function in concert within the micromechanics modules to provide MAC/GMC with its full array of analysis and simulation capabilities. The HFGMC and Smart Composite Analysis Modules were developed as part of this project.

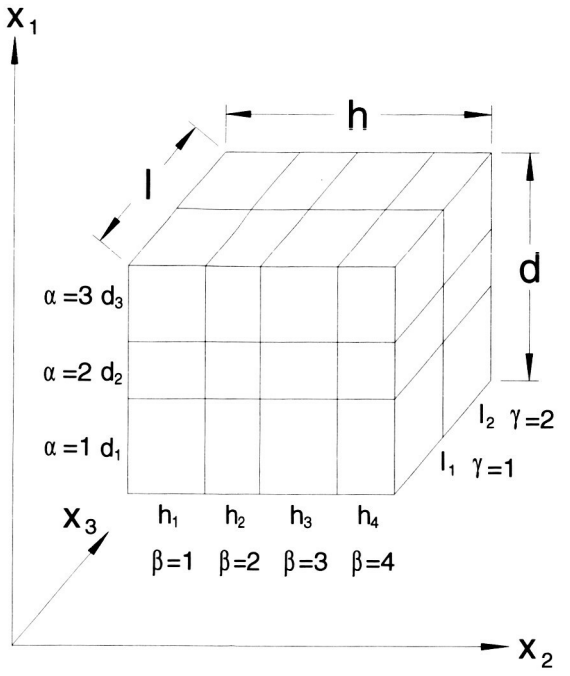

Fig. 3. Triply-periodic generalized method of cells geometry with $N_\alpha = 3$, $N_\beta = 4$, and $N_\gamma = 2$.

where $\sigma_{ij}^{(\alpha\beta\gamma)}$ are the stress components, $D_k^{(\alpha\beta\gamma)}$ are the electric displacement components, $B_k^{(\alpha\beta\gamma)}$ are the magnetic flux density components, $\varepsilon_{ij}^{(\alpha\beta\gamma)}$ are the total strain components, $\varepsilon_{ij}^{I(\alpha\beta\gamma)}$ are the inelastic strain components, $\varepsilon_{ij}^{T(\alpha\beta\gamma)}$ are the thermal strain components, $E_k^{(\alpha\beta\gamma)}$ are the electric field components, $E_k^{T(\alpha\beta\gamma)}$ are the thermo-electric field components, $H_k^{(\alpha\beta\gamma)}$ are the magnetic field components, $H_k^{T(\alpha\beta\gamma)}$ are the thermo-magnetic field components, $C_{ij}^{(\alpha\beta\gamma)}$ are the material stiffness components, $e_{kj}^{(\alpha\beta\gamma)}$ are the material piezoelectric components, $q_{kj}^{(\alpha\beta\gamma)}$ are the material piezomagnetic components, $\kappa_{ij}^{(\alpha\beta\gamma)}$ are the material dielectric components, $a_{ij}^{(\alpha\beta\gamma)}$ are the material magnetoelectric components, and $\mu_{ij}^{(\alpha\beta\gamma)}$ are the material magnetic permeability components of a given subcell (denoted by the indices $\alpha\beta\gamma$). The inelastic strain components of each subcell, $\varepsilon_{ij}^{I(\alpha\beta\gamma)}$, can be obtained from an arbitrary local inelastic constitutive theory, as the local field quantities for the subcell will be known. The thermal strain and thermal field components are related to a change in temperature from a given reference temperature (i.e., ΔT) by,

$$\left[\varepsilon_{11}^T \;\; \varepsilon_{22}^T \;\; \varepsilon_{33}^T \;\; 2\varepsilon_{23}^T \;\; 2\varepsilon_{13}^T \;\; 2\varepsilon_{12}^T \;\; E_1^T \;\; E_2^T \;\; E_3^T \;\; H_1^T \;\; H_2^T \;\; H_3^T\right]^{(\alpha\beta\gamma)} = \left[\alpha_{11} \;\; \alpha_{22} \;\; \alpha_{33} \;\; \alpha_{23} \;\; \alpha_{13} \;\; \alpha_{12} \;\; \zeta_1 \;\; \zeta_2 \;\; \zeta_3 \;\; \psi_1 \;\; \psi_2 \;\; \psi_3\right]^{(\alpha\beta\gamma)} \Delta T \tag{1.2}$$

where $\alpha_{ij}^{(\alpha\beta\gamma)}$ are the subcell material coefficients of thermal expansion (CTEs), $\zeta_k^{(\alpha\beta\gamma)}$ are the subcell material pyroelectric constants, and $\psi_k^{(\alpha\beta\gamma)}$ are the subcell material pyromagnetic constants. Clearly, Eq. (1.1) is an extension of the standard anisotropic thermo-inelastic constitutive equation that now treats

electric displacement, electric field, magnetic flux density, and magnetic field components as additional field variables.

The piezo-electro-magnetic GMC formulation treats the electric displacement and magnetic flux density components similar to stress components and treats the electric and magnetic field components similar to strain components. For details, see Bednarcyk (2003). By assuming linear local displacement and electric and magnetic potential fields, along with application of continuity and periodicity conditions, we arrive at a system of linear equations of the form,

$$\tilde{\mathbf{G}}\mathbf{T} = \mathbf{f}^M - \mathbf{f}^I - \mathbf{f}^T \tag{1.3}$$

whose solution provides the unique subcell stress, electric displacement, and magnetic flux density components in the subcells of the repeating unit cell given the global strain components, global electric field components, global magnetic field components, subcell inelastic strain components, subcell thermal strain components, subcell thermo-electric field components, and subcell thermo-magnetic field components. The vector $\mathbf{T}$ contains the unknown subcell stress, electric displacement, and magnetic flux density components, the square $\tilde{\mathbf{G}}$ matrix contains material constants and geometric terms, the vector $\mathbf{f}^M$ contains the applied global components, the vector $\mathbf{f}^I$ contains local inelastic strains and geometric terms, and the vector $\mathbf{f}^T$ contains thermal strains, thermo-electric field components, thermo-magnetic field components, and geometric terms.

Equation (1.3) is solved for the vector $\mathbf{T}$ to yield mixed thermo-electro-magneto-elasto-plastic concentration equations for the repeating unit cell,

$$\mathbf{T} = \mathbf{G}\left[\mathbf{f}^M - \mathbf{f}^I - \mathbf{f}^T\right] \tag{1.4}$$

Then, considering the repeating unit cell stress, electric displacement, and magnetic flux density components to be volume-weighted sums of their corresponding local subcell components (see Bednarcyk, 2003, for details), one arrives at the global constitutive equation that represents the piezo-electro-magnetic composite material,

$$\begin{bmatrix} \bar{\sigma}_{11} \\ \bar{\sigma}_{22} \\ \bar{\sigma}_{33} \\ \bar{\sigma}_{23} \\ \bar{\sigma}_{13} \\ \bar{\sigma}_{12} \\ \bar{D}_1 \\ \bar{D}_2 \\ \bar{D}_3 \\ \bar{B}_1 \\ \bar{B}_2 \\ \bar{B}_3 \end{bmatrix} = \begin{bmatrix} C^*_{11} & C^*_{12} & C^*_{13} & C^*_{14} & C^*_{15} & C^*_{16} & e^*_{11} & e^*_{21} & e^*_{31} & q^*_{11} & q^*_{21} & q^*_{31} \\ C^*_{12} & C^*_{22} & C^*_{23} & C^*_{24} & C^*_{25} & C^*_{26} & e^*_{12} & e^*_{22} & e^*_{32} & q^*_{12} & q^*_{22} & q^*_{32} \\ C^*_{13} & C^*_{23} & C^*_{33} & C^*_{34} & C^*_{35} & C^*_{36} & e^*_{13} & e^*_{23} & e^*_{33} & q^*_{13} & q^*_{23} & q^*_{33} \\ C^*_{14} & C^*_{24} & C^*_{34} & C^*_{44} & C^*_{45} & C^*_{46} & e^*_{14} & e^*_{24} & e^*_{34} & q^*_{14} & q^*_{24} & q^*_{34} \\ C^*_{15} & C^*_{25} & C^*_{35} & C^*_{45} & C^*_{55} & C^*_{56} & e^*_{15} & e^*_{25} & e^*_{35} & q^*_{15} & q^*_{25} & q^*_{35} \\ C^*_{16} & C^*_{26} & C^*_{36} & C^*_{46} & C^*_{56} & C^*_{66} & e^*_{16} & e^*_{26} & e^*_{36} & q^*_{16} & q^*_{26} & q^*_{36} \\ e^*_{11} & e^*_{12} & e^*_{13} & e^*_{14} & e^*_{15} & e^*_{16} & -\kappa^*_{11} & -\kappa^*_{12} & -\kappa^*_{13} & -a^*_{11} & -a^*_{12} & -a^*_{13} \\ e^*_{21} & e^*_{22} & e^*_{23} & e^*_{24} & e^*_{25} & e^*_{26} & -\kappa^*_{12} & -\kappa^*_{22} & -\kappa^*_{23} & -a^*_{21} & -a^*_{22} & -a^*_{23} \\ e^*_{31} & e^*_{32} & e^*_{33} & e^*_{34} & e^*_{35} & e^*_{36} & -\kappa^*_{13} & -\kappa^*_{23} & -\kappa^*_{33} & -a^*_{31} & -a^*_{32} & -a^*_{33} \\ q^*_{11} & q^*_{12} & q^*_{13} & q^*_{14} & q^*_{15} & q^*_{16} & -a^*_{11} & -a^*_{21} & -a^*_{31} & -\mu^*_{11} & -\mu^*_{12} & -\mu^*_{13} \\ q^*_{21} & q^*_{22} & q^*_{23} & q^*_{24} & q^*_{25} & q^*_{26} & -a^*_{12} & -a^*_{22} & -a^*_{32} & -\mu^*_{12} & -\mu^*_{22} & -\mu^*_{23} \\ q^*_{31} & q^*_{32} & q^*_{33} & q^*_{34} & q^*_{35} & q^*_{36} & -a^*_{13} & -a^*_{23} & -a^*_{33} & -\mu^*_{13} & -\mu^*_{23} & -\mu^*_{33} \end{bmatrix} \begin{bmatrix} \bar{\varepsilon}_{11} - \bar{\varepsilon}^I_{11} - \bar{\varepsilon}^T_{11} \\ \bar{\varepsilon}_{22} - \bar{\varepsilon}^I_{22} - \bar{\varepsilon}^T_{22} \\ \bar{\varepsilon}_{33} - \bar{\varepsilon}^I_{33} - \bar{\varepsilon}^T_{33} \\ 2\bar{\varepsilon}_{23} - 2\bar{\varepsilon}^I_{23} - 2\bar{\varepsilon}^T_{23} \\ 2\bar{\varepsilon}_{13} - 2\bar{\varepsilon}^I_{13} - 2\bar{\varepsilon}^T_{13} \\ 2\bar{\varepsilon}_{12} - 2\bar{\varepsilon}^I_{12} - 2\bar{\varepsilon}^T_{12} \\ -\bar{E}_1 - \bar{E}^T_1 \\ -\bar{E}_2 - \bar{E}^T_2 \\ -\bar{E}_3 - \bar{E}^T_3 \\ -\bar{H}_1 - \bar{H}^T_1 \\ -\bar{H}_2 - \bar{H}^T_2 \\ -\bar{H}_3 - \bar{H}^T_3 \end{bmatrix} \tag{1.5}$$

where overbars and asterisks refer to effective composite level quantities. Equation (1.5) provides the effective thermo-piezo-electro-magnetic properties of the composite, and also enables the application of loading in the form of stresses/strains, electric displacements/fields, magnetic flux densities/fields, and a temperature change. Note in particular that the piezo-electro-magnetic GMC theory includes inelasticity

as well. As documented by Bednarcyk (2003), this work represented the first time that smart materials and inelastic materials were combined within a single theory.

Because Eq. (1.5) is applicable to a material, rather than a structure, it can be used to represent the effective behavior and properties of smart materials located at points within a structure. This is why it was possible to incorporate the piezo-electro-magnetic GMC theory within HyperSizer to enable analysis of smart stiffened structures. Also, the work performed under Task 1.1 of the present project involved incorporation the piezo-electro-magnetic GMC theory within lamination theory to represent the ply-level response, as shown in Fig. 4. The expanded form of the composite material constitutive equation (1.5) is employed, and the laminate-level equations are developed (see Bednarcyk, 2003, for details). The laminate constitutive equation is given by,

$$\begin{bmatrix} N_x \\ N_y \\ N_{xy} \\ M_x \\ M_y \\ M_{xy} \end{bmatrix} = \begin{bmatrix} \mathbf{A} & \mathbf{B} \\ \mathbf{B} & \mathbf{D} \end{bmatrix} \begin{bmatrix} \varepsilon^0_{xx} \\ \varepsilon^0_{yy} \\ 2\varepsilon^0_{xy} \\ \kappa^0_{xx} \\ \kappa^0_{yy} \\ \kappa^0_{xy} \end{bmatrix} - \begin{bmatrix} N^I_x \\ N^I_y \\ N^I_{xy} \\ M^I_x \\ M^I_y \\ M^I_{xy} \end{bmatrix} - \begin{bmatrix} N^T_x \\ N^T_y \\ N^T_{xy} \\ M^T_x \\ M^T_y \\ M^T_{xy} \end{bmatrix} - \begin{bmatrix} N^E_x \\ N^E_y \\ N^E_{xy} \\ M^E_x \\ M^E_y \\ M^E_{xy} \end{bmatrix} - \begin{bmatrix} N^{ET}_x \\ N^{ET}_y \\ N^{ET}_{xy} \\ M^{ET}_x \\ M^{ET}_y \\ M^{ET}_{xy} \end{bmatrix} - \begin{bmatrix} N^M_x \\ N^M_y \\ N^M_{xy} \\ M^M_x \\ M^M_y \\ M^M_{xy} \end{bmatrix} - \begin{bmatrix} N^{MT}_x \\ N^{MT}_y \\ N^{MT}_{xy} \\ M^{MT}_x \\ M^{MT}_y \\ M^{MT}_{xy} \end{bmatrix} \tag{1.6}$$

where the standard thermo-inelastic lamination theory terms are the force and moment resultants ($N_\bullet$ and $M_\bullet$), the ABD matrix, the midplane strains and curvatures ($\varepsilon^0_\bullet$ and $\kappa^0_\bullet$), the inelastic force and moment resultants ($N^I_\bullet$ and $M^I_\bullet$), and the thermal force and moment resultants ($N^T_\bullet$ and $M^T_\bullet$). The new terms, which account for the thermo-piezo-electro-magnetic effects are the electric force and moment resultants ($N^E_\bullet$ and $M^E_\bullet$), the thermo-electric force and moment resultants ($N^{ET}_\bullet$ and $M^{ET}_\bullet$), the magnetic force and moment resultants ($N^M_\bullet$ and $M^M_\bullet$), and the thermo-magnetic force and moment resultants ($N^{MT}_\bullet$ and $M^{MT}_\bullet$).

As indicated in Fig. 2, the piezo-electro-magnetic GMC theory has been implemented within MAC/GMC as a module. Further, this module is callable from the MAC/GMC lamination theory module, enabling analysis of smart laminates.

A journal article, a NASA Contractor Report, and a conference paper/presentation resulted directly from the work performed under Task 1.1. These publications are:

1) Bednarcyk, B.A. (2003) "An Inelastic Micro/Macro Theory for Hybrid Smart/Metal Composites" Composites: Part B 34, 175-197.

2) Bednarcyk, B.A. (2002) "A Fully Coupled Micro/Macro Theory for Thermo-Electro-Magneto-Elasto-Plastic Composite Laminates" NASA/CR-2002-211468.

3) Bednarcyk, B.A. (2003) "An Inelastic Micro/Macro Theory for Hybrid Smart/Metal Composites" in Proc. Tenth International Symposium on Plasticity, July, Quebec City, Canada.

Results of piezo-electro-magnetic MAC/GMC are given in the above publications. Here we show results that appeared only in the conference presentation. Consider the piezoelectric/aluminum laminate shown in Fig. 5. By using opposite poling directions for the top and bottom PZT-7A (a piezoelectric material) plies, the laminate will bend in response to an applied through-thickness electric field (E_z). These type of piezoelectric elements are sold as sensors and actuators, and usually come with a metallic

middle layer (aluminum in this case). If the applied electric field is cyclic, then the laminate will experience fatigue. MAC/GMC was used to simulated fatigue loading on the laminate for the cases both with and without the aluminum middle layer. The results shown in Fig. 6 indicate that the predicted fatigue life for the laminate that includes the aluminum layer is approximately an order of magnitude greater than the laminate without the aluminum layer. Clearly, inclusion of the aluminum middle layer has a significant beneficial effect on the laminate.

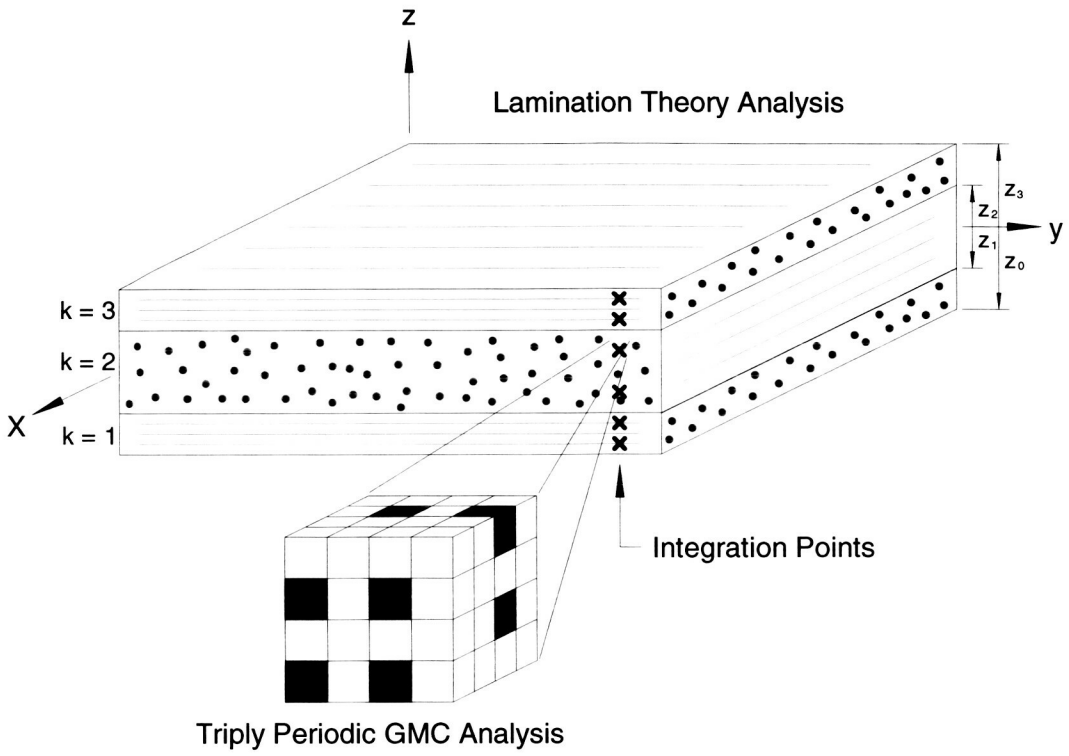

Fig. 4. Laminate plate geometry and schematic of the use of GMC to represent the ply-level composite material.

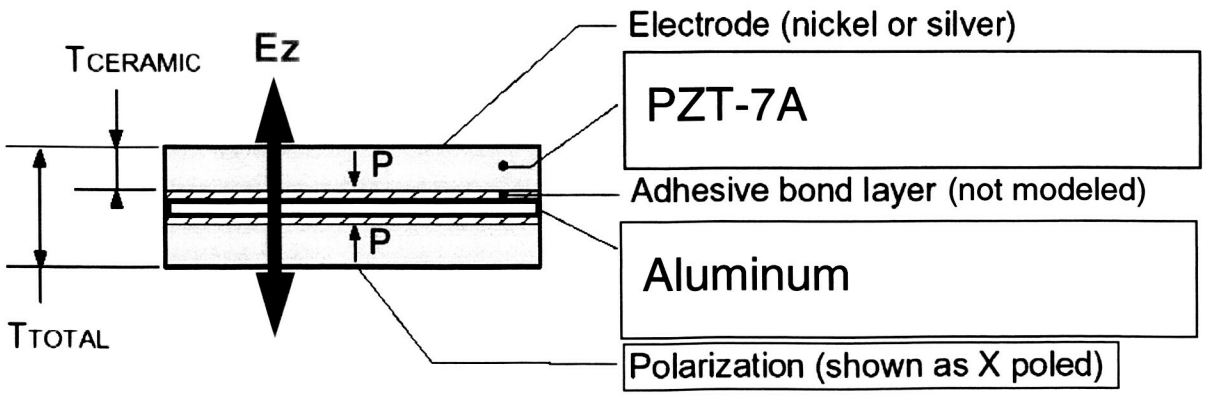

Fig. 5. Geometry of a piezo-aluminum laminate modeled using MAC/GMC.

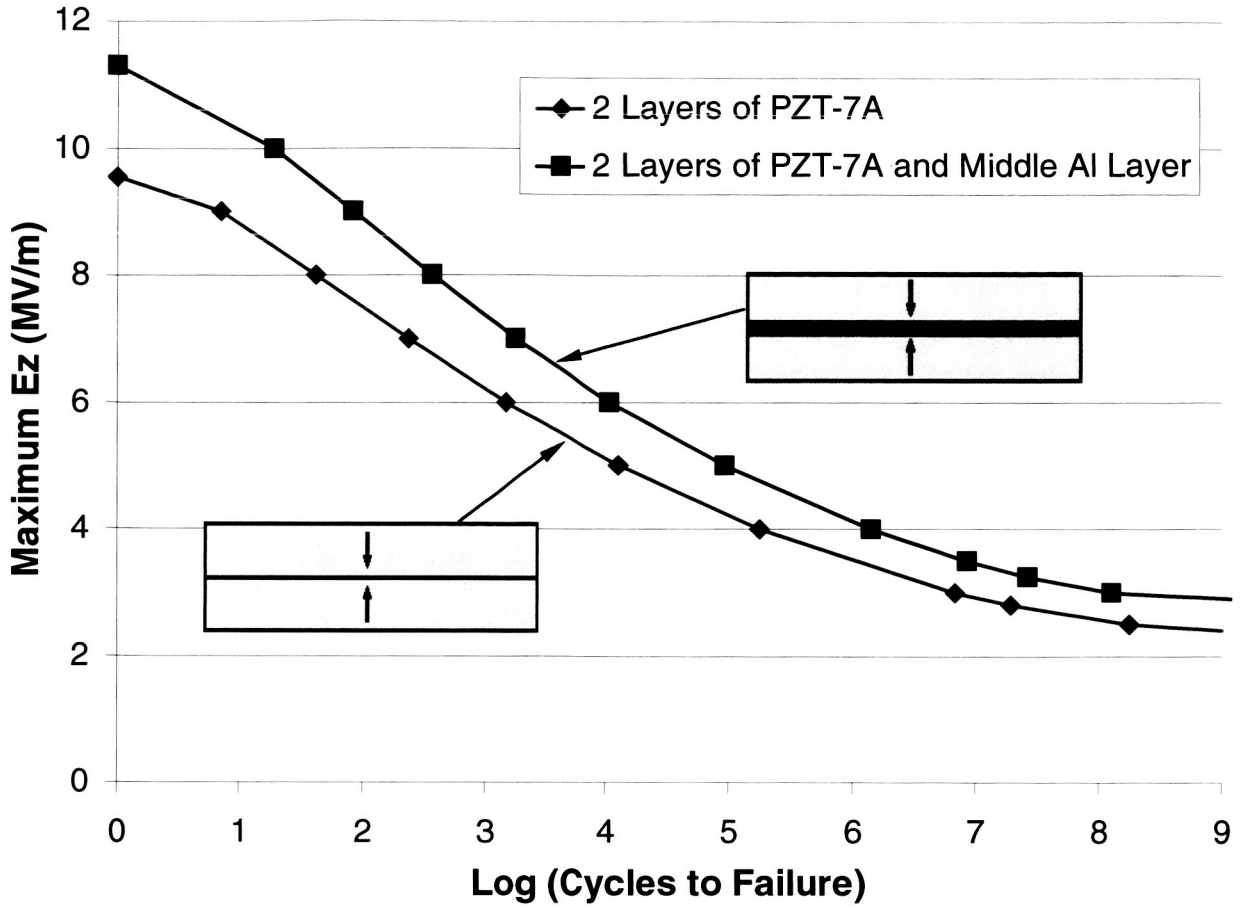

Fig. 6. Fatigue life predictions for piezo-aluminum and piezo laminates. The hybrid laminate with the aluminum layer is approximately an order magnitude more fatigue resistant.

1.2 Inclusion of Normal-Shear Stress Coupling

Due to the first-order displacement field assumed within the subcells in GMC, the theory lacks coupling between normal and shear stresses and strains. That is, GMC predicts that if only normal stresses and strains are applied to a composite material, only shear stresses and strains will result internally, with no shear stresses or strains. It is well-known that this is not the case as, especially in the vicinity of the fiber-matrix interface, significant local shear stresses and strains arise. The lack of shear coupling thus limits the local accuracy of the stress and strain fields within the composite fiber and matrix constituents predicted by GMC. Note that it is also this lack of shear coupling that provides GMC with its extreme level of computational efficiency.

A new version of the GMC theory, called High-Fidelity GMC (HFGMC), has been developed under Task 2.2 of this project (Aboudi et al., 2001, 2002, 2003). HFGMC (which is based largely on HOTFGM, see Task 2), like GMC, considers a repeating unit cell to represent a periodic composite material. However, HFGMC employs a quadratic local displacement field, which leads to the shear coupling that GMC is lacking. The result is far more accurate local stress and strain fields throughout the composite material repeating unit cell, while the overall composite level deformation predictions using GMC and HFGMC are usually very similar. The improved local accuracy, however, comes at a significant computational price, with HFGMC requiring more memory and execution time for comparable analyses.

As shown in Fig. 2, Task 1.2 of this project has involved the construction of a new analysis module for MAC/GMC based on the double-periodic version of HFGMC. Discussion of the HFGMC theory is given under Task 2.2 below. The improved local accuracy of HFGMC is most important in situations where local phenomena within the composite dominate the overall composite response such as local damage simulations. In the case of local damage, failure events occur on the level of the subcells within the composite repeating unit cell that have a major impact on the composite's global response. Because these local failure events are initiated based on the local stress or strain fields in the composite, the accuracy of these local fields becomes critical. MAC/GMC's new HFGMC capabilities have been applied to solve the problem of modeling fiber-matrix debonding in titanium matrix composites (TMCs), in which the accuracy of the local fields is critical. Two publications, a journal article and a conference presentation/paper, as well as an invited lecture resulted from Task 1.2 and the application of the HFGMC capability to debonding in TMCs:

1) Bednarcyk, B.A., Arnold, S.M., Aboudi, J., and Pindera, M.-J. (2004) "Local Field Effects in Titanium Matrix Composites Subject to Fiber-Matrix Debonding" International Journal of Plasticity 20, 1707-1737.

2) Bednarcyk, B.A., Arnold, S.M., Aboudi, J., and Pindera, M.-J. (2002) "Accurate Micro/Macro Field Simulation for Composites Subject to Fiber-Matrix Debonding Using HFGMC" in Proc. 15th ASCE Engineering Mechanics Conference, June, New York.

3) Bednarcyk, B.A. (2002) "Micromechanics of Fiber-Matrix Debonding in Titanium Matrix Composites" Invited Lecture, University of Virginia Dept. Civil Engineering Seminar Series, February, Charlottesville, Virginia.

Three key components were needed to solve the TMC debonding modeling problem: 1) an accurate micromechanics model, provided by the new MAC/GMC HFGMC analysis module, 2) an accurate debonding model, provided by MAC/GMC's existing evolving compliant interface (ECI) model, and 3) an accurate viscoplastic constitutive model for the titanium matrix, provided by MAC/GMC's existing generalized viscoplasticity with potential structure (GVIPS) model. Thanks to the incorporation of HFGMC within the MAC/GMC framework, these three needed components were able to work in concert to simulate the behavior of the TMC.

Previous work aimed at solving the TMC debonding modeling problem using GMC proved cumbersome (Bednarcyk and Arnold, 2000, 2002c). In order to match the experimental transverse response of TMCs, a great deal of effort was required. A refined circular fiber representation repeating unit cell was required, and, as shown in Fig. 7, each interface between fiber and matrix subcells required a different bond strength. Even then, GMC did not perform well in making pure predictions. This is because GMC's lack of shear coupling caused the local stresses at the fiber-matrix interface, which are used to predict the onset of debonding, to be inaccurate. HFGMC, on the other hand, with its accurate local fields, was able to use a less refined circular fiber representation along with a single set of bond strengths used for every fiber-matrix subcell interface.

Results for the TMC debonding problem at elevated temperature are shown in Fig. 8. Although these results represent correlation (i.e., these experimental results were used to select the debonding model parameters), it is clear the HFGMC is far superior to GMC. In fact, for the 8×8 subcell repeating unit cell shown in Fig. 8, GMC cannot match experiment unless some fiber-matrix subcell interfaces are required to be strongly bonded (see Fig. 7). The reason for this becomes clear when examining the local stress fields, shown in Fig. 9, at an applied global strain level of 0.005, which is after debonding has initiated. First, we see that GMC predicts zero shear stress (σ_{23}) throughout the repeating unit cell, while significant shear stresses arise in the HFGMC predictions. Second, comparing the σ_{22} fields (stress in the loading direction), we see that, in the case of GMC, all subcell in line with the fiber subcells have unloaded their stress due to the debonding at the fiber-matrix interface. In the case of HFGMC, the σ_{22}

field is completely different. The stress has unloaded at the fiber-matrix interface, but due to the interaction between shear and normal stresses, the matrix material in line with the fiber is able to still carry significant stress levels. As shown in Fig. 8, the result is that HFGMC is able to match the experimental results, while the GMC simulations are too compliant.

Figure 10 shows predictions for the TMC transverse response, now at room temperature. We see that the HFGMC predictions are very good (the discrepancy is likely due to inaccuracies in the GVIPS viscoplastic constitutive model for the titanium matrix), while the GMC predictions are once again too compliant. HFGMC has thus enabled, for the first time, accurate modeling of the debonding phenomenon within TMCs.

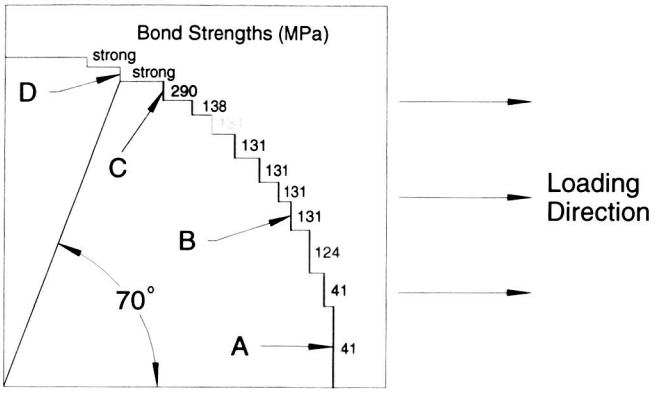

Fig. 7. With GMC, in order to match experimental results for the transverse TMC response, each fiber-matrix interface required a distinct bond strength.

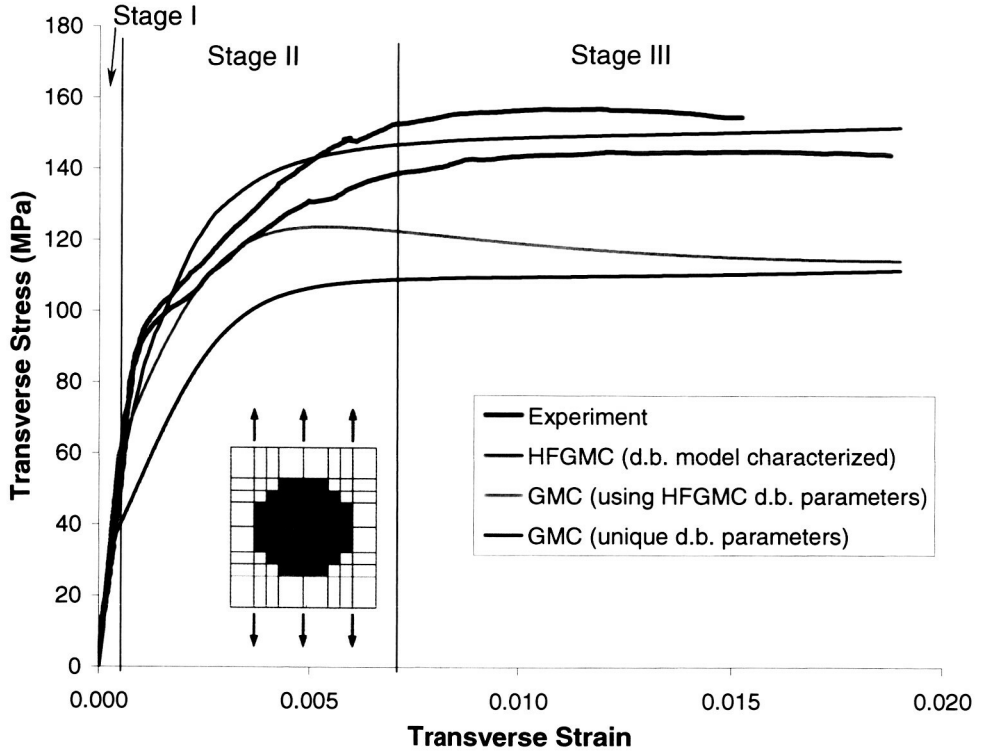

Fig. 8. Experimental and simulated response of 33% SCS-6/TIMETAL21S at 650 °C, strain rate = 1.67×10^{-4} / sec.

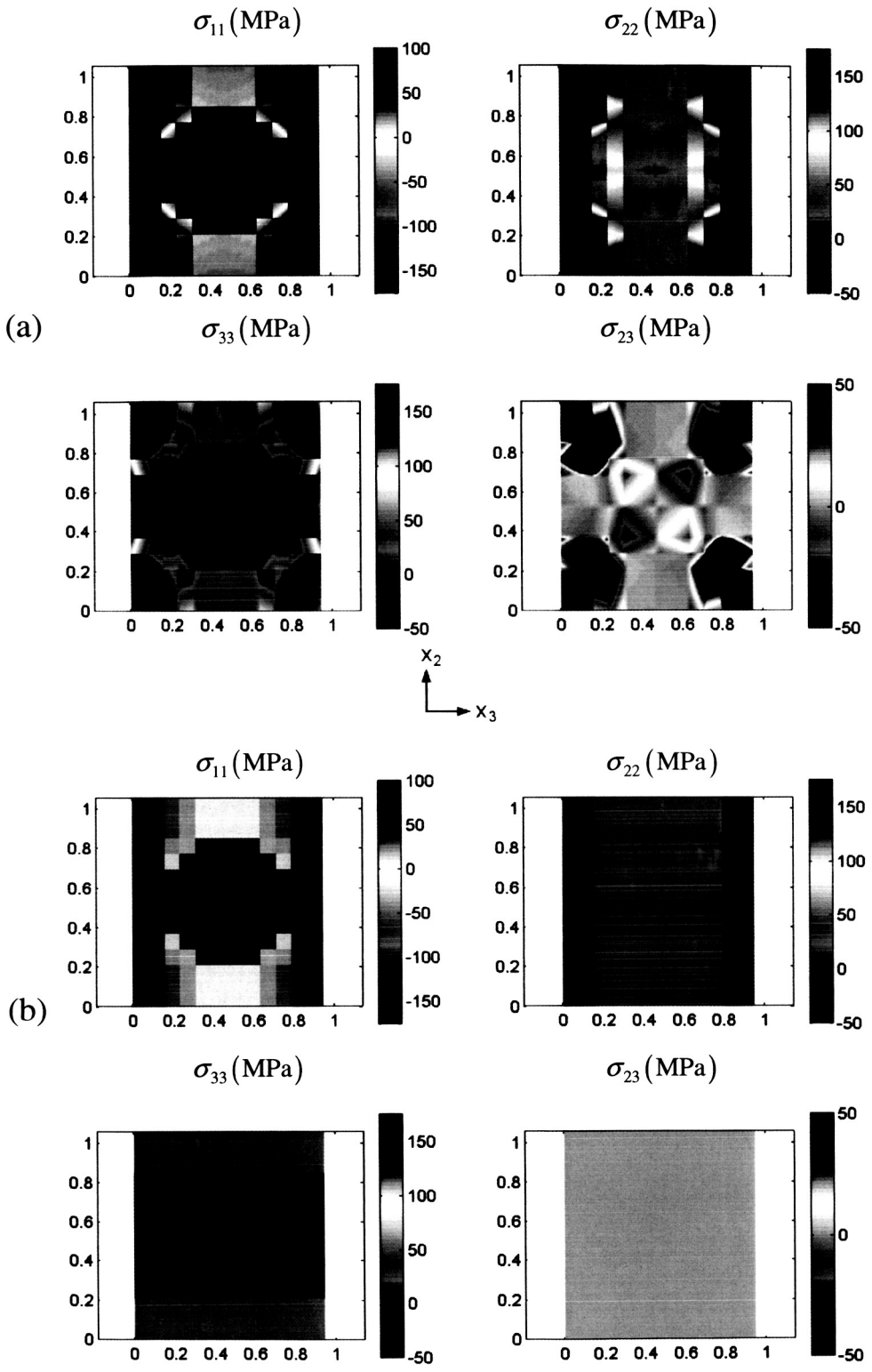

Fig. 9. Local stress fields: (a) HFGMC, (b) GMC; 650 °C, 33% SCS-6/TIMETAL21S, applied global transverse strain of 0.005.

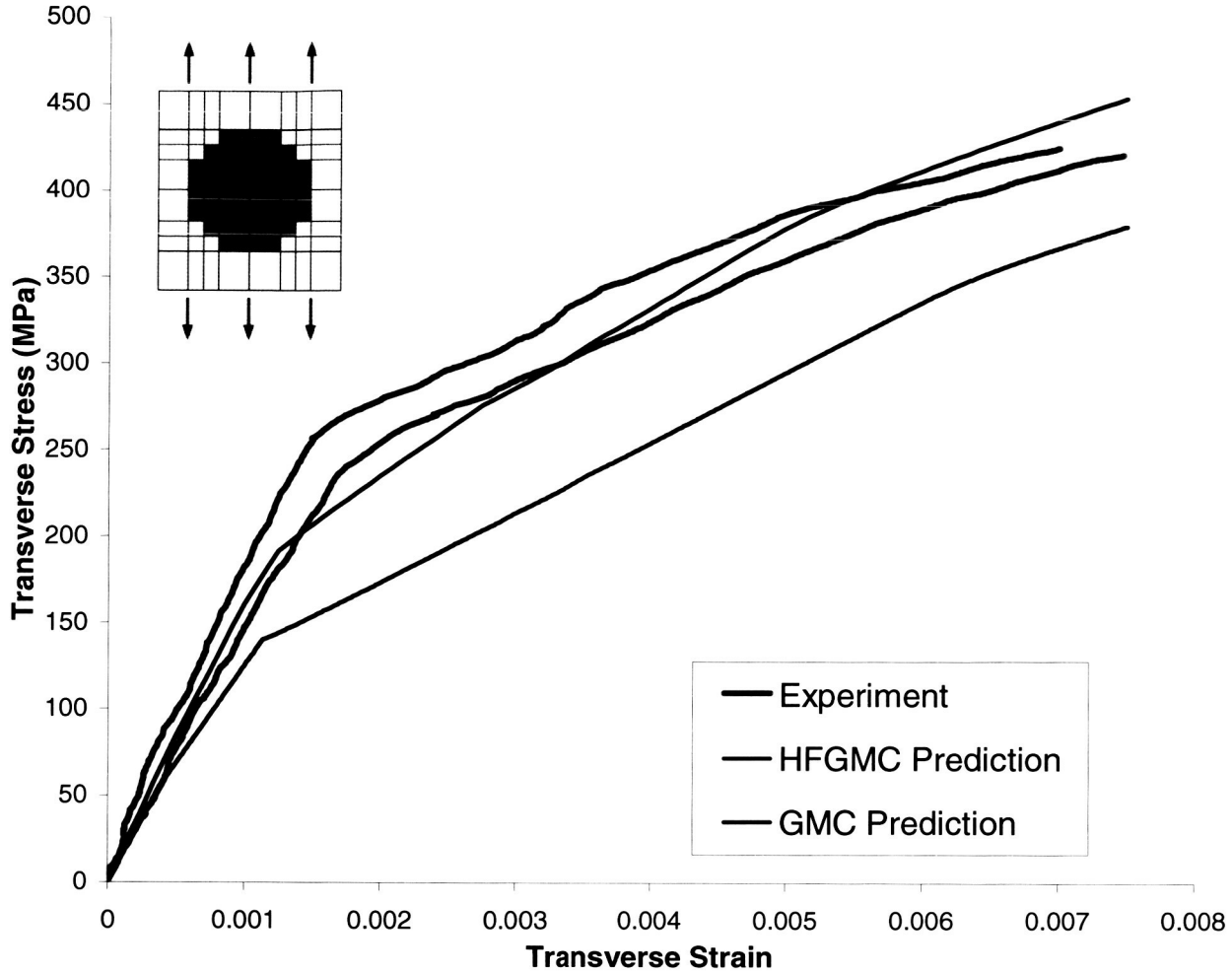

Fig. 10. Experimental and predicted response of 33% SCS-6/TIMETAL21S at 23 °C, strain rate = 1.67×10^{-4} / sec.

Task 2. Enhancements to HOTFGM

The Higher-Order Theory for Functionally Graded Materials (HOTFGM) is a micromechanics theory that analyzes heterogeneous composite material, but does not employ homogenization. That is, rather than considering a composite material and generating effective properties (like GMC and HFGMC), HOTFGM considers composite structures that have boundaries. Due to the presence of these boundaries, the geometry and arrangement of the constituent materials are explicitly coupled with the overall structural dimensions. This dimensional coupling is not present when homogenization is employed, as in GMC and HFGMC. In certain situations, such as large fiber composites and functionally graded composite materials, this coupling becomes important.

The geometry considered by the two-dimensional version of HOTFGM is shown in Fig. 11. Like GMC and HFGMC, the geometry is discretized into a number of subvolumes, each of which may contain a distinct monolithic material. The HOTFGM versions employed in this project employs a two-level geometric discretization, as shown in Fig. 11, in which the overall geometry is discretized into cells that contain four subcells. It has been recently shown, however, that this two-level discretization is unnecessary (Bansal and Pindera, 2002; Arnold et. al, 2004). The most important difference between HOTFGM and the homogenized micromechanics theories is that the geometry shown in Fig. 11 has boundaries. The GMC and HFGMC analysis geometries, on the other hand, are repeating unit cells, and are thus adjacent on all sides to identical repeating unit cells. Obvious, in the context of HOTFGM, boundary conditions must therefore be applied. Also, HOTFGM, unlike GMC and HFGMC, solves the thermal problem (i.e., the temperature distribution) for the composite structure based on applied temperature, heat flux, and convection boundary conditions.

Task 2 of this project involved enhancing, extending, and synthesizing HOTFGM into an analysis module for use within the HyperSizer framework. Originally, tight coupling of all HOTFGM capabilities with HyperSizer was envisioned. However, during the course of the project it was deemed that the homogenized version of HOTFGM, now called HFGMC, which was developed under Task 2.2 was a priority in terms of usefulness. The standard HOTFGM theory, due to the presence of boundaries, is not well suited for full integration so as to be automatically called from HyperSizer. HFGMC on the other hand, which represents a material without boundaries, is perfect for such full integration. For these reasons, only HFGMC has been fully integrated, while the standard HOTFGM capabilities reside in a stand alone HyperSizer module. Note that this module was original called HOT-SMAC, and then called HyperSizer FGM, and is now called NCell (Nodeless Cell). This alteration to Task 2 was approved by the project NASA COTR in year 2 of the project.

2.1 Synthesis of HOTFGM Codes

The synthesis of several versions of HOTFGM into one succinct, all encompassing code was completed during year 1 of the project. This involved transforming the research codes, provided by U.Va., from FORTRAN 77 to FORTRAN 90, subdividing the codes into subroutines, and combining them such that all the functionality of each research code was preserved. In addition, due to the large size of the system that must be solved within HOTFGM, a state of the art sparse linear equation solver was incorporated. This synthesized HOTFGM code was renamed Higher Order Theory – Structural/Micro Analysis Code (HOT-SMAC), then renamed again to Nodeless Cell (NCell). Two publications: a journal article and a NASA Technical Memorandum, resulted in part from the work on this task.

1) Pindera, M-J., Aboudi, J., and Arnold, S. M. (2002a) "Analysis of Spallation Mechanism in Thermal Barrier Coatings with Graded Bond Coats Using the Higher-Order Theory for FGMs," International Journal of Engineering Fracture Mechanics, 69, 1587-1606.

2) Pindera, M-J., Aboudi, J., and Arnold, S. M. (2002b) "Analysis of Plasma-Sprayed TBCs with Homogeneous and Heterogeneous Bond Coats Under Spatially Uniform Cyclic Thermal Loading," NASA/TM-2001-210803.

Details on the final HyperSizer module resulting from this task are described under Task 4.3, which involved the development of the graphical user interface (GUI) for the module.

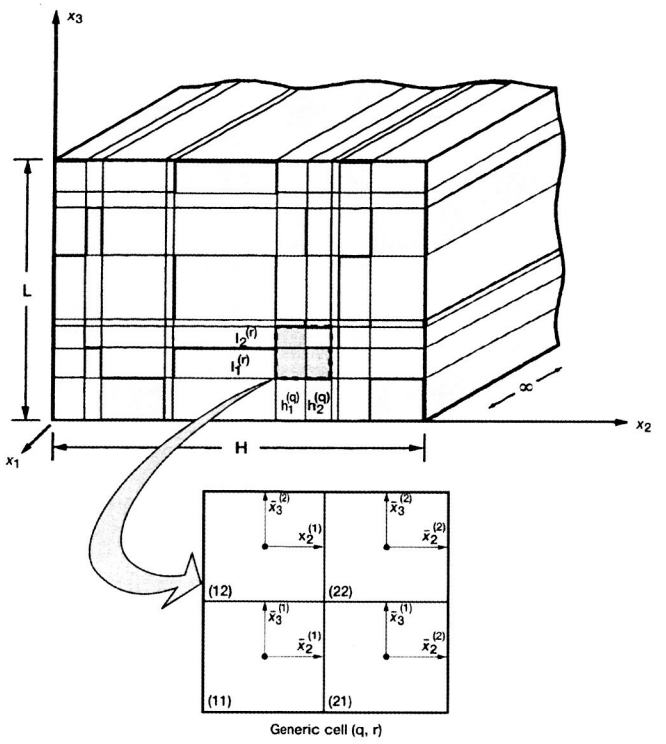

Fig. 11. A geometric model of a heterogeneous graded material in the $x_2 - x_3$ plane illustrating the volume discretization employed in HOTFGM.

2.2 Development of Homogenized HOTFGM

As discussed under Task 1.2 above, the High-Fidelity Generalized Method of Cells (HFGMC) micromechanics theory, which models the response of composite materials, as opposed to the composite structures with boundaries modeled by HOTFGM, was developed from the HOTFGM equations. The quadratic displacement field from HOTFGM, now active in HFGMC, provides the new micromechanics theory with shear coupling, enabling far more accurate local fields compared to GMC. Under Task 2.2 of the project, the doubly-periodic HFGMC theory has been successfully developed and implemented in a research computer code. Elements of this code then served as the starting point for the HFGMC analysis module that was incorporated within MAC/GMC in Task 1.2.

The geometry of the doubly-periodic repeating unit cell employed by both GMC and HFGMC is shown in Fig. 12. The rectangular repeating unit cell is infinite in the out of plane direction (generalized plane strain) and is composed of an arbitrary number of rectangular subcells, each of which may contain an arbitrary monolithic material. The local (subcell) constitutive equation for both the GMC and HFGMC micromechanics theories is given by,

$$\boldsymbol{\sigma}^{(\beta\gamma)} = \mathbf{C}^{(\beta\gamma)}\left(\boldsymbol{\varepsilon}^{(\beta\gamma)} - \boldsymbol{\varepsilon}^{I(\beta\gamma)} - \boldsymbol{\varepsilon}^{T(\beta\gamma)}\right) \tag{2.1}$$

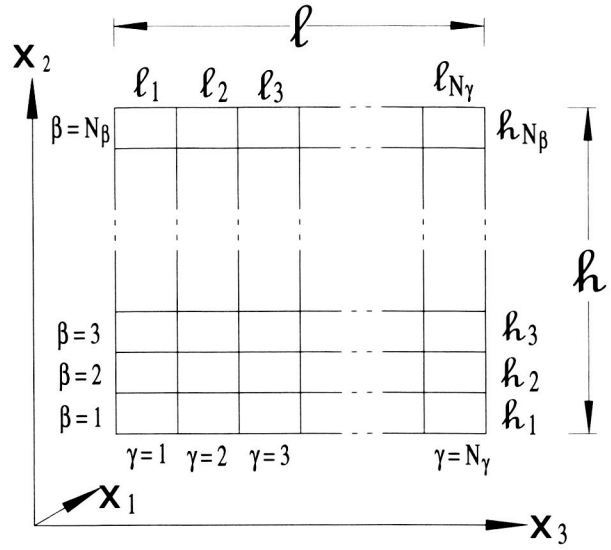

Fig. 12. Geometry of the doubly-periodic GMC and HFGMC repeating unit cell.

where $\boldsymbol{\sigma}^{(\beta\gamma)}$ is the vector of average subcell stresses, $\mathbf{C}^{(\beta\gamma)}$ is the subcell elastic stiffness matrix, and $\boldsymbol{\varepsilon}^{(\beta\gamma)}$, $\boldsymbol{\varepsilon}^{I(\beta\gamma)}$, and $\boldsymbol{\varepsilon}^{T(\beta\gamma)}$ are the vectors of average subcell total strain, inelastic strain, and thermal strain, respectively.

The basic assumption in GMC is that the displacement vector in each subcell varies linearly with the local subcell coordinates ($\bar{y}_2^{(\beta)}$, $\bar{y}_3^{(\gamma)}$) located at the center of each subcell,

$$u_i^{(\beta\gamma)} = W_{i(00)}^{(\beta\gamma)} + \bar{y}_2^{(\beta)} W_{i(10)}^{(\beta\gamma)} + \bar{y}_3^{(\gamma)} W_{i(01)}^{(\beta\gamma)} \tag{2.2}$$

whereas, in HFGMC, a quadratic displacement field is employed,

$$u_i^{(\beta\gamma)} = \bar{\varepsilon}_{ij}\, x_j + W_{i(00)}^{(\beta\gamma)} + \bar{y}_2^{(\beta)} W_{i(10)}^{(\beta\gamma)} + \bar{y}_3^{(\gamma)} W_{i(01)}^{(\beta\gamma)} + \frac{1}{2}\left(3\bar{y}_2^{(\beta)2} - \frac{h_\beta^2}{4} \right) W_{i(20)}^{(\beta\gamma)} + \frac{1}{2}\left(3\bar{y}_3^{(\gamma)2} - \frac{l_\gamma^2}{4} \right) W_{i(02)}^{(\beta\gamma)} \tag{2.3}$$

The GMC formulation involves imposition of continuity of displacements and tractions between adjacent subcells and repeating unit cells in an integral, or average, sense. In the original work of Paley and Aboudi (1992), this procedure resulted in a system of $6N_\beta N_\gamma$ linear algebraic equations in which the strains in the subcells (which are constant within each subcell) serve as the basic unknown quantities. Note that N_β and N_γ are the number of subcells within the repeating unit cell in the two in-plane directions (see Fig. 12). The GMC equations have been computationally optimized by Pindera and Bednarcyk (1999) such that subcell stress components serve as the unknown variables, which leads to an alternative system of linear algebraic equations with only $N_\beta + N_\gamma$ equations plus additional decoupled equations (assuming at most orthotropic local subcell behavior). This reduced number of unknown quantities (e.g., degrees of freedom) provides GMC with a high level of computational efficiency. This system of equations (involving the normal stress components) can be written as,

$$\tilde{\mathbf{G}}\mathbf{T} = \mathbf{f}^m - \mathbf{f}^I - \mathbf{f}^T \tag{2.4}$$

while the additional decoupled equations (involving the shear stress components) can be written as,

$$\tilde{G}_{12}^{(\gamma)} T_{12}^{(\gamma)} = f_{12}^{m} - f_{12}^{I(\gamma)}, \quad \tilde{G}_{13}^{(\beta)} T_{13}^{(\beta)} = f_{13}^{m} - f_{13}^{I(\beta)}, \quad \tilde{G}_{23} T_{23} = f_{23}^{m} - f_{23}^{I} \tag{2.5}$$

where the $\tilde{\mathbf{G}}$ matrix and the $\tilde{G}_{ij}^{(\square)}$ terms contain information on the subcell material elastic properties and the subcell dimensions, the $\mathbf{T}$ vector and the $T_{ij}^{(\square)}$ terms are the unique subcell stress components, the $\mathbf{f}^m$ vector and the f_{ij}^{m} terms contain information on the repeating unit cell dimensions and the global (unit cell) strains, the $\mathbf{f}^I$ vector and the $f_{ij}^{I(\square)}$ terms contain the inelastic effects, and the $\mathbf{f}^T$ vector contains the thermal effects.

HFGMC, on the other hand, with its higher-order displacement field (Eq. 2.3), requires supplementary equations in its formulation. In addition to the imposition of continuity of displacements and tractions between subcells in an integral sense, the zeroth, first, and second moments of the local (subcell) equilibrium equations are satisfied in a volumetric sense. Finally, periodic boundary conditions are imposed at the repeating unit cell boundaries, resulting in a linear system of $15N_\beta N_\gamma$ algebraic equations,

$$\mathbf{KU} = \mathbf{f} + \mathbf{g} \tag{2.6}$$

where the $\mathbf{K}$ matrix contains information on the subcell material elastic properties and the subcell dimensions, $\mathbf{U}$ contains the unknown terms $W_{i(\square)}^{(\beta\gamma)}$ in the displacement field (Eq. 2.3), the $\mathbf{f}$ vector contains information on the global (unit cell) strains and the thermal effects, and $\mathbf{g}$ contains integrals of inelastic strains. Clearly, solving Eq. (2.6) for the $15N_\beta N_\gamma$ unknowns in HFGMC is considerably more computationally demanding than solving Eq. (2.4) for the $N_\beta + N_\gamma$ unknowns (in addition to the $N_\beta + N_\gamma + 1$ decoupled equations (2.5)) in GMC.

Once Eqs. (2.4 – 2.6) are solved, the local stress and strain fields throughout the repeating unit cell can be determined from the standard kinematics equations and the local constitutive equations (2.1) in both GMC and HFGMC. Then the terms in the global constitutive equation,

$$\overline{\boldsymbol{\sigma}} = \mathbf{C}^* \left(\overline{\boldsymbol{\varepsilon}} - \overline{\boldsymbol{\varepsilon}}^I - \overline{\boldsymbol{\varepsilon}}^T \right) \tag{2.7}$$

can be determined using the definition of average (global) stress,

$$\overline{\boldsymbol{\sigma}} = \frac{1}{hl} \sum_{\beta=1}^{N_\beta} \sum_{\gamma=1}^{N_\gamma} h_\beta l_\gamma \boldsymbol{\sigma}^{(\beta\gamma)} \tag{2.8}$$

where $\mathbf{C}^*$ is the average or effective stiffness matrix, and $\overline{\boldsymbol{\varepsilon}}$, $\overline{\boldsymbol{\varepsilon}}^I$, and $\overline{\boldsymbol{\varepsilon}}^T$ are the average or effective total, inelastic, and thermal strain vectors, respectively.

Eq. (2.7) is the effective (macro) constitutive equation for the homogenized composite material represented by the GMC or HFGMC repeating unit cell. It allows one to impose an admissible combination of global stress and strain components, in addition to spatially constant thermal loading, and to determine the remaining global stresses and strains acting on the composite material. Then, via Eqs.

(2.4 – 2.6) the local stress and strain fields can be determined as well. These local-global fields constitute the complete micromechanics solution.

Table 1 provides a comparison of the features of the GMC and HFGMC micromechanics models. GMC, with its first-order displacement field (Eq. 2.2) lacks shear coupling. That is, if the global stress-strain state imposed on the composite material involves only normal components, GMC will predict only normal local stresses and strains. While this is a limitation in terms of local field accuracy, it is this lack of shear coupling that enabled GMC to be reformulated in order to provide its superior computational efficiency. This limitation has been overcome by HFGMC, which now includes shear coupling, but the associated improved local field accuracy comes at an additional computational cost. Further, GMC's lack of shear coupling is manifested in piece-wise uniform stress and strain fields throughout the repeating unit cell. In contrast, the fields in HFGMC vary within the subcells, and in the presence of inelasticity, this spatial field variation is arbitrary. As a result, HFGMC must employ a number of integration points within each subcell to represent the higher-order local fields, while GMC requires the local field variables to be stored only once for each subcell.

The work involved in developing the HFGMC theory and research code in Task 2.2 of the project resulted in three publication: two journal articles and a NASA report.

1) Aboudi, J., Pindera, M.J. and Arnold, S.M. (2001) "Linear Thermoelastic Higher-Order Theory for Periodic Multiphase Materials" Journal of Applied Mechanics 68, 697-707, 2001.

2) Aboudi, J., Pindera, M.-J., and Arnold, S.M. (2002) "High-Fidelity Generalized Method of Cells for Inelastic Periodic Multiphase Materials" NASA/TM-2002-211469.

3) Aboudi, J., Pindera, M.-J., and Arnold, S.M. (2003) "Higher-Order Theory for Periodic Multiphase Materials with Inelastic Phases" International Journal Plasticity 19, 805-847.

Sample HFGMC results are shown in Figs. 13 and 14. Fig. 13 compares the overall composite level deformation predictions of HFGMC with finite element analysis for 5% graphite/aluminum and 25% graphite/aluminum unidirectional composites. The finite element and HFGMC predictions are virtually identical. The local effective stress ($\sigma_e = \sqrt{3S_{ij}S_{ij}/2}$, S_{ij} = deviatoric stress components) fields are plotted for the same composite in Fig. 14. In this case, GMC predictions are shown as well. The results indicate that the HFGMC theory predicts point-wise stress and strain fields that are on par with finite element results. The HFGMC theory represents a significant step forward in the state of the art micromechanics models and it is a major accomplishment of this project.

Table 1. Comparison of the GMC and HFGMC micromechanics models.

	GMC	**HFGMC**
General global accuracy	Very good	Excellent
Computational efficiency	Excellent	Fair
Local field accuracy	Fair	Excellent
Shear coupling	No	Yes
Subcell mesh dependence	No	Yes
Admits local inelasticity	Yes	Yes
Suitable for inclusion in structural models	Yes	Yes
Multi-axial	Yes	Yes

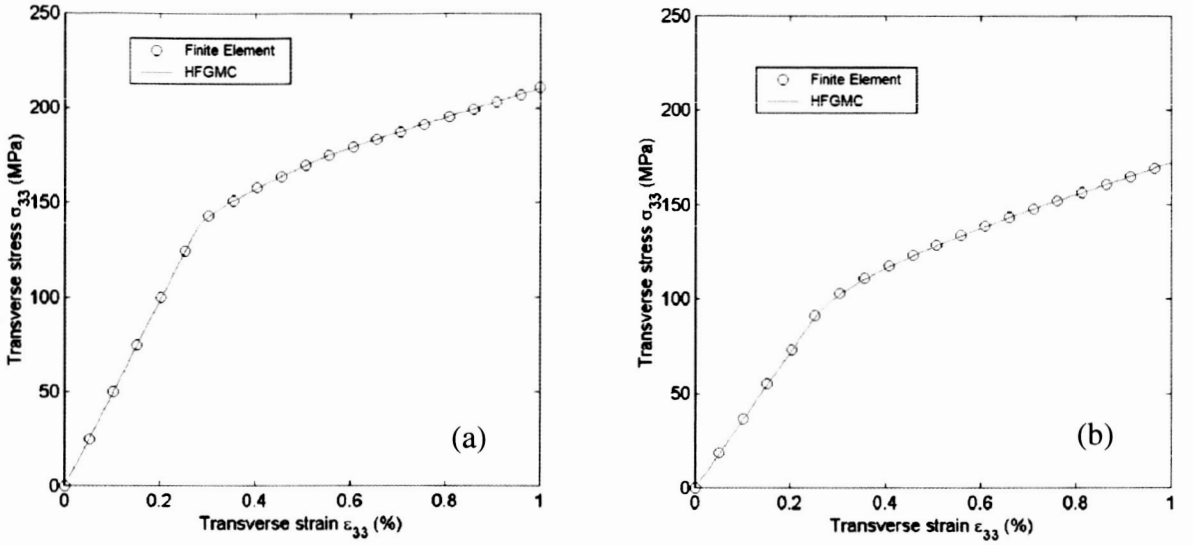

Fig. 13. Graphite/aluminum transverse stress strain response due to loading: $\overline{\varepsilon}_{22} = -\overline{\varepsilon}_{33}$, $\overline{\varepsilon}_{11} = 0$, (a) fiber volume fraction = 5%, (b) fiber volume fraction = 25%. HFGMC predictions compared to finite element analysis.

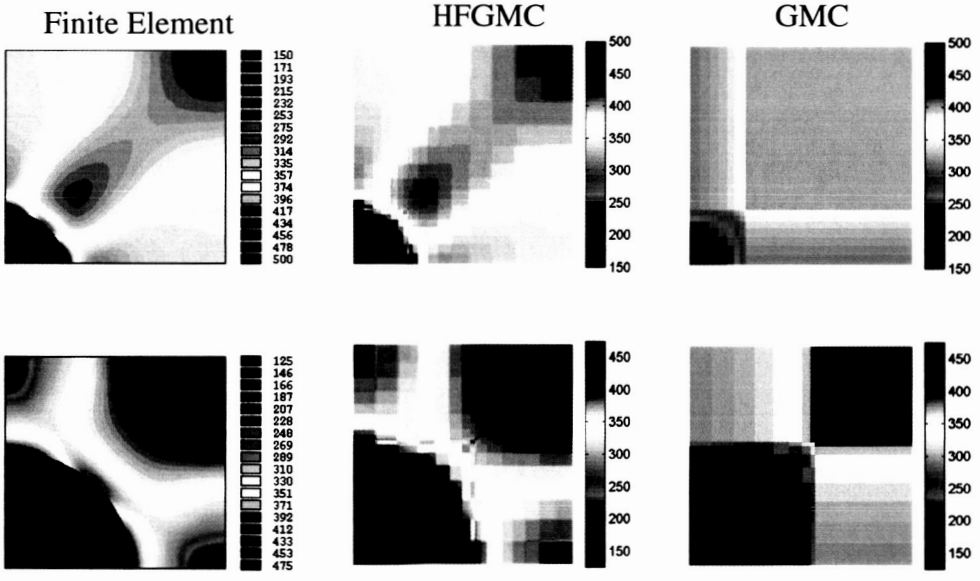

Fig. 14. Comparison of local effective stress fields predicted by finite element analysis, HFGMC, and GMC. 5% (top) and 25% (bottom) graphite/aluminum subjected to loading: $\overline{\varepsilon}_{22} = -\overline{\varepsilon}_{33}$, $\overline{\varepsilon}_{11} = 0$.

2.3 Inclusion of Electromagnetic Effects

This task was originally envisioned to involve inclusion of electromagnetic effects within both Cartesian and cylindrical versions of HOTFGM. However, it was determined that a 3-D Cartesian version of HOTFGM, while more complex, would be most useful in the context of HyperSizer problems

as it has the potential to solve the laminate interlaminar and free-edge stress distribution problem. As such, it was decided that this task would focus on the 3-D Cartesian HOTFGM and that work on the cylindrical version of HOTFGM would be indefinitely postponed. This alteration to the project was approved by the NASA COTR during year 2 of the project.

The 3-D Cartesian version of HOTFGM code was completed by U.Va. on schedule, however, in the course of validating the code results, a significant technical issue arose. While solving a classical punch problem with the code, it was found that, while the results were correct when advantage was taken of geometric symmetry, a problem was encountered when the entire geometry was modeled and symmetry boundary conditions were replaced by traction free conditions. In this case, while the in-plane quantities compared well with analytical elasticity results, the stress and displacement fields in the direction orthogonal to the plane of loading were not accurately captured by HOTFGM. A good deal of effort was expended examining this technical issue, and it was overcome by the end of the project. The correctly functioning research code was delivered, but, due to the long delay associated with the code, it was not incorporated within NCell.

Task 3. Enhancements to HyperSizer

HyperSizer is a unique, state-of-the-art, automated, structural sizing software package that currently performs strength and stability analyses of stiffened panels and beams when subjected to thermomechanical environments and provides analytical weight predictions (http://www.hypersizer .com/). Optimization capabilities include automatic selection from forty different stiffened panel, sandwich panel, and beam concepts constructed of advanced composite, metallic, honeycomb, and foam materials. Currently, the meso scale analysis technologies represented by HyperSizer are directly linked to FEA (see Fig. 1). Thus, global scale FEA can be performed extremely efficiently, without sacrificing accuracy, using a coarse 2D mesh for the structure rather than a fine 3D mesh. Furthermore, HyperSizer automatically adjusts all meso scale design parameters to yield an optimum design and then re-analyzes the global structure. Task 3 of the project has involved enhancements to HyperSizer that enable analysis of smart structures and time-dependent analysis. As commercial software, the new HyperSizer capabilities are now available to the HyperSizer customer base, including the major aerospace corporations (Boeing, Lockheed Martin, Northrup Grumman).

Work on Task 3 focused on the major effort required within HyperSizer to enable time-dependent analyses (Task 3.3) and piezo-electro-magnetic effects (Task 3.2). These efforts were successful and represent two major accomplishments of the project. Details are given below.

3.1 Cylindrical Formulation

The original plan for this task involved extending HyperSizer's capabilities based on an analytical formulation for the thermomechanical response of stiffened cylindrical shell geometries. Due to the lack of pressing need for these capabilities and increased emphasis and effort level allocated to Tasks 3.2 and 3.3, during year 2 of the project, Task 3.1 was postponed to the final six months of the project. Rather than implementation of a cylindrical formulation, the effort on this task was limited to the preliminary level, focusing on evaluating HyperSizer's limitations with respect to modeling cylindrical geometries using its flat panel capabilities. This alteration of the project scope was approved by the NASA COTR during year 2 of the project.

The HyperSizer approach, when coupled with finite element analysis (see Fig. 1), involves representing a finite thickness structure with a single plane of finite elements. That is, a finite thickness panel is homogenized by HyperSizer to arrive at a plate-like mathematical representation, which is passed to a single plane of elements in the global analysis. A limitation exists within HyperSizer when this approach is used to represent cylindrical structures. The single plane of elements approach used by HyperSizer assumes that for a uniform membrane load, the top and bottom facesheets of the panel will strain equally. As an example, Fig. 15 shows the displacement due to internal pressure of a cylindrical sandwich structure. As the pressure is applied, the actual structure is displaced as shown in Fig. 15a. The outer facesheet strains more than the inner facesheet due to the difference in radial location of these facesheets. In HyperSizer's single plane approach however, the simulated displacement is shown in Fig. 15b, because the single plane of elements does not account for radial location difference between the inner and outer facesheets. By modeling a cylindrical sandwich structure subjected to internal pressure with: a) a single plane of elements; and b) two planes of elements separated by a solid model core, the differences between the two approaches can be quantified. As shown in Table 2, only when the radius over thickness (r/t) ratio is fairly small, does the inaccuracy become significant.

3.2 Inclusion of Electromagnetic Effects

A great deal of effort was expended to include piezo-electro-magnetic effects within HyperSizer involving not only coding, but also development of new methods. These new methods are outlined below. HyperSizer analyzes stiffened panels composed of arbitrary composite laminates through stiffener homogenization, or "smearing", techniques. The result is an effective constitutive equation for the stiffened panel that is suitable for use in a full vehicle-scale finite element analysis via MSC/NASTRAN. This task has extended the existing thermo-elastic capabilities of HyperSizer to include coupled thermo-

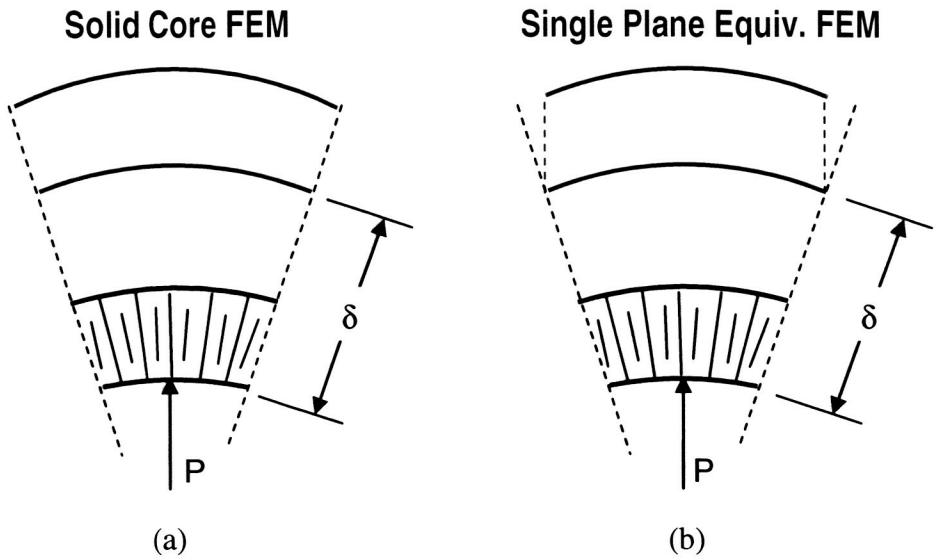

Fig. 15. The single plane equivalent FEM approach of HyperSizer introduces inaccuracies when modeling cylindrical structures with small r/t ratios. (a) Realistic displacements obtained when accounting for finite thickness using a solid core model. (b) Displacements predicted using the HyperSizer single plane approach requires the inner and outer face sheets to strain equally.

Table 2. Difference between hoop force resultants (lb/in.) in the inner and outer facesheets of a cylindrical sandwich panel subjected to internal pressure predicted using the HyperSizer homogenized single plane approach and the full finite element solid core approach as a function of radius/thickness (r/t) ratio.

	Inner Facesheet			Outer Facesheet		
r/t	Single Plane	Solid Core	% dif.	Single Plane	Solid Core	% dif.
12	926	980	5.6	590	535	10.3
24	1851	1893	2.3	1179	1136	3.8
48	3702	3737	1.1	2357	2321	1.5
96	7404	7436	0.4	4713	4682	0.6

electro-magneto-elastic analysis capabilities. This represents a significant step toward realization of design tools capable of guiding the development of the next generation of smart aerospace structures. Verification results are presented that compare the developed smart HyperSizer capability with an ABAQUS piezoelectric finite element solution for a facesheet – flange combination. These results show good agreement between HyperSizer and ABAQUS, but highlight a limitation of the HyperSizer formulation in that constant electric field components are assumed.

Piezo-electro-magnetic materials are those that exhibit coupling among their electric, magnetic, mechanical, and thermal responses. That is, for example, in response to an applied voltage or current, a piezoelectric material (such as lead zirconium titanate, or PZT) will respond mechanically with a change in strain or stress. Conversely, if piezoelectric materials are loaded mechanically or thermally, a change in their electric field or flux results. Thus, piezoelectric materials can serve as both actuators and sensors and have the potential to perform tasks passively through utilization of an induced field/flux to cause a desired mechanical response. Piezomagnetic materials (such as $CoFe_2O_4$) exhibit similar coupling between their magnetic and mechanical behaviors, and by forming a composite of piezoelectric and

piezomagnetic materials, a fully coupled piezo-electro-magnetic material can be produced. Piezo-electro-magnetic materials are characterized by their fast response times to applied (or sensed) stimuli (on the order of 10^{-2} to 10^{1} milliseconds) and thus have found significant application as vibration dampers. Reviews of piezo-electro-magnetic concepts and materials are available from Gandhi and Thompson (1992), Uchino (1997), Parton and Krudryavtsev (1988), and Krudryavtsev et al. (1990).

In order to realize the potential embodied by smart materials and structures, advances in modeling and simulation technologies are needed. The standard tools for structural design are finite element analysis (FEA) models (e.g., ANSYS, NASTRAN, ABAQUS). However, FEA models are ill-suited (i.e., inefficient, subject to operator error) for rapid design and sizing (i.e., trade studies) for structural components. Further, the lack of well-developed and robust capabilities related to intelligent materials underscores the shortcomings of the FEA approach when it comes to adaptive structures. There is thus a need for physics-based design, analysis, and sizing tools that capture the essential characteristics of piezo-electro-magnetic materials and enable the analysis of structures composed of these materials.

The methods and procedures that have been developed to enable the analysis of piezo-electro-magnetic materials within HyperSizer are described below. Starting with the analysis of a piezo-electro-magnetic laminate, new laminate level matrices that account for the electric, magnetic, thermo-electric and thermo-magnetic effects are developed. These then can be treated in a way analogous to the HyperSizer treatment of the laminate thermal matrix, enabling use of homogenization, or "smearing" techniques to develop stiffened panel level electric, magnetic, thermo-electric, and thermo-magnetic terms. The developed methods are based on a classical lamination theory treatment of the laminates comprising a given stiffened panel, and the homogenization of the stiffened panel so it can be represented with classical lamination theory terms. It is this simplicity that provides the methods with the level of efficiency needed to consider many design cases rapidly while still capturing the dominant first-order effects. A good body of work exists for the analysis of piezoelectric laminates, using both analytical (Lee, 1990; Crawley and Lazurus, 1991; Tauchert, 1992; Tzou, 1993; Jonnalagadda et al., (1994); Carrera, 1997; Saravanos and Heyliger (1999); Gopinathan et al. (2000); Schultz and Hyer, 2003; Fernandes and Pouget, 2004) and finite element (Robbins and Reddy, 1993; Saravanos et al., 1997; Lee and Saravanos, 1997, 2000; Bansal and Ramaswamy, 2002) approaches. The piezomagnetic laminates have also received some attention (Pan, 2001; Pan and Heyliger, 2003; Heyliger et al., 2004). The work most closely related to the methods developed herein involve the extension of classical lamination theory to include piezoelectric plies by Lee (1990), Crawley and Lazarus (1991), and Tauchert (1992), and to include piezomagnetic and inelastic behavior by Bednarcyk (2003).

Reference Plane Shifting Procedure for a Thermo-Electro-Magneto-Elastic Laminate

Because a stiffened panel is, in general, composed of a number of laminates, each of which has properties that are typically calculated with respect to its own midplane, a first step in calculating properties of the panel as a whole involves shifting the reference plane of a given laminate. As will be shown, if the reference plane of each laminate comprising a stiffened panel can be shifted to a common reference plane, the homogenization of the laminate properties to form the properties of the stiffened panel properties becomes straightforward.

Consider and arbitrary number of composite laminates, each of which has its constitutive behavior defined with respect to its midplane via the standard thermo-elastic lamination theory equation (Jones, 1975; Herakovich, 1998),

$$\begin{bmatrix} \mathbf{N} \\ \mathbf{M} \end{bmatrix} = \begin{bmatrix} \mathbf{A}^0 & \mathbf{B}^0 \\ \mathbf{B}^0 & \mathbf{D}^0 \end{bmatrix} \begin{bmatrix} \boldsymbol{\varepsilon}^0 \\ \boldsymbol{\kappa}^0 \end{bmatrix} - \begin{bmatrix} \mathbf{N}_0^T \\ \mathbf{M}_0^T \end{bmatrix} \tag{3.1}$$

In this equation, $\mathbf{N}$ and $\mathbf{M}$ are the force and moment resultant vectors, which are related to the midplane strain and curvature vectors, $\boldsymbol{\varepsilon}^0$ and $\boldsymbol{\kappa}^0$, by the laminate extensional, coupling, and bending stiffness matrices (measured with respect to the midplane), $\mathbf{A}^0$, $\mathbf{B}^0$, and $\mathbf{D}^0$, and the thermal force and moment

resultant vectors (measured with respect to the midplane), $\mathbf{N}_0^T$ and $\mathbf{M}_0^T$. The laminate midplane stiffness matrices and thermal resultants are given by,

$$\mathbf{A}^0 = \sum_k \bar{\mathbf{Q}}_k \left[z_{k-1}^0 - z_k^0 \right] \quad \mathbf{B}^0 = -\frac{1}{2} \sum_k \bar{\mathbf{Q}}_k \left[\left(z_{k-1}^0 \right)^2 - \left(z_k^0 \right)^2 \right] \quad \mathbf{D}^0 = \frac{1}{3} \sum_k \bar{\mathbf{Q}}_k \left[\left(z_{k-1}^0 \right)^3 - \left(z_k^0 \right)^3 \right] \tag{3.2}$$

$$\begin{aligned} \mathbf{N}_0^T &= \sum_k \bar{\mathbf{Q}}_k \boldsymbol{\alpha}_k \left[z_{k-1}^0 - z_k^0 \right] \Delta T_0 + \frac{1}{2} \sum_k \bar{\mathbf{Q}}_k \boldsymbol{\alpha}_k \left[\left(z_{k-1}^0 \right)^2 - \left(z_k^0 \right)^2 \right] \Delta G \\ \mathbf{M}_0^T &= -\frac{1}{2} \sum_k \bar{\mathbf{Q}}_k \boldsymbol{\alpha}_k \left[\left(z_{k-1}^0 \right)^2 - \left(z_k^0 \right)^2 \right] \Delta T_0 - \frac{1}{3} \sum_k \bar{\mathbf{Q}}_k \boldsymbol{\alpha}_k \left[\left(z_{k-1}^0 \right)^3 - \left(z_k^0 \right)^3 \right] \Delta G \end{aligned} \tag{3.3}$$

where $\bar{\mathbf{Q}}_k$ is the reduced stiffness matrix of ply k, $\boldsymbol{\alpha}_k$ is the coefficient of thermal expansion vector of ply k, z_k^0 is the z-coordinate position of the top of ply k measured with respect to the laminate midplane, ΔT_0 is the temperature change from reference temperature at the laminate midplane, and ΔG is the linear laminate through-thickness temperature gradient, i.e., $T(z) - T_{ref} = \Delta T_0 + z\, \Delta G$, with $T(z)$ being the temperature at any z-coordinate location and T_{ref} being the reference temperature.

We now consider a shift of the reference plane from the laminate midplane to an arbitrary z-coordinate position and seek to determine the effect on the quantities given in Eqs. (3.2 – 3.3). This arbitrary reference plane shift is depicted in Fig. 16. Considering point A, in the original, laminate midplane coordinate system, this point is located at $z_A^0 = -h/2$, whereas, in the new shifted coordinate system, this point is located at $z_A^{new} = -h/2 - \Delta z$. Thus, for an arbitrary shift of reference plane we have

$$z^{\text{new}} = z^0 - \Delta z \tag{3.4}$$

where Δz measures the distance in the positive z-direction from original laminate reference plane to the new laminate reference plane. The temperature change from reference temperature at the new reference plane is given based on the linear through-thickness temperature gradient as,

$$\Delta T_{\text{new}} = \Delta T_0 + \Delta G\ \Delta z \tag{3.5}$$

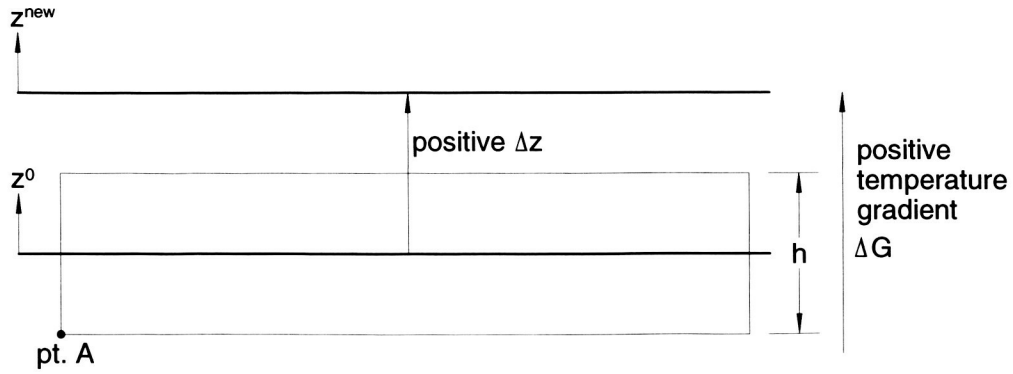

Fig. 16. Arbitrary reference plane shift from the laminate midplane.

The laminate stiffness matrices, measured with respect to the new shifted reference plane are given by,

$$\mathbf{A}^{\text{new}} = \sum_k \bar{\mathbf{Q}}_k \left[z_{k-1}^{\text{new}} - z_k^{\text{new}} \right] \tag{3.6}$$

$$\mathbf{B}^{\text{new}} = -\frac{1}{2} \sum_k \bar{\mathbf{Q}}_k \left[\left(z_{k-1}^{\text{new}} \right)^2 - \left(z_k^{\text{new}} \right)^2 \right] \tag{3.7}$$

$$\mathbf{D}^{\text{new}} = \frac{1}{3} \sum_k \bar{\mathbf{Q}}_k \left[\left(z_{k-1}^{\text{new}} \right)^3 - \left(z_k^{\text{new}} \right)^3 \right] \tag{3.8}$$

Substituting for z^{new} in Eqs. (3.6 – 3.8) using Eq. (3.4) we arrive at,

$$\mathbf{A}^{\text{new}} = \sum_k \bar{\mathbf{Q}}_k \left[z_{k-1}^{\text{new}} - z_k^{\text{new}} \right] = \sum_k \bar{\mathbf{Q}}_k \left[\left(z_{k-1}^0 - \Delta z \right) - \left(z_k^0 - \Delta z \right) \right] = \sum_k \bar{\mathbf{Q}}_k \left[z_{k-1}^0 - z_k^0 \right] = \mathbf{A}^0$$

$$\boxed{\mathbf{A}^{\text{new}} = \mathbf{A}^0} \tag{3.9}$$

$$\begin{aligned}
\mathbf{B}^{\text{new}} &= -\frac{1}{2} \sum_k \bar{\mathbf{Q}}_k \left[\left(z_{k-1}^{\text{new}} \right)^2 - \left(z_k^{\text{new}} \right)^2 \right] = -\frac{1}{2} \sum_k \bar{\mathbf{Q}}_k \left[\left(z_{k-1}^0 - \Delta z \right)^2 - \left(z_k^0 - \Delta z \right)^2 \right] \\
&= -\frac{1}{2} \sum_k \bar{\mathbf{Q}}_k \left[\left(z_{k-1}^0 \right)^2 - 2\, z_{k-1}^0 \Delta z + \Delta z^2 - \left(z_k^0 \right)^2 + 2\, z_k^0 \Delta z - \Delta z^2 \right] \\
&= -\frac{1}{2} \sum_k \bar{\mathbf{Q}}_k \left[\left(z_{k-1}^0 \right)^2 - \left(z_k^0 \right)^2 - 2\Delta z \left(z_{k-1}^0 - z_k^0 \right) \right] \\
&= -\frac{1}{2} \sum_k \bar{\mathbf{Q}}_k \left[\left(z_{k-1}^0 \right)^2 - \left(z_k^0 \right)^2 \right] - \frac{1}{2} \sum_k \bar{\mathbf{Q}}_k \left[-2\Delta z \left(z_{k-1}^0 - z_k^0 \right) \right] \\
&= -\frac{1}{2} \sum_k \bar{\mathbf{Q}}_k \left[\left(z_{k-1}^0 \right)^2 - \left(z_k^0 \right)^2 \right] + \Delta z \sum_k \bar{\mathbf{Q}}_k \left[z_{k-1}^0 - z_k^0 \right] \\
&= \mathbf{B}^0 + \Delta z\, \mathbf{A}^0
\end{aligned}$$

$$\boxed{\mathbf{B}^{\text{new}} = \mathbf{B}^0 + \Delta z\, \mathbf{A}^0} \tag{3.10}$$

$$\begin{aligned}
\mathbf{D}^{\text{new}} &= \frac{1}{3} \sum_k \bar{\mathbf{Q}}_k \left[\left(z_{k-1}^{\text{new}} \right)^3 - \left(z_k^{\text{new}} \right)^3 \right] = \frac{1}{3} \sum_k \bar{\mathbf{Q}}_k \left[\left(z_{k-1}^0 - \Delta z \right)^3 - \left(z_k^0 - \Delta z \right)^3 \right] \\
&= \frac{1}{3} \sum_k \bar{\mathbf{Q}}_k \left\{ \left[\left(z_{k-1}^0 \right)^3 - 3\Delta z \left(z_{k-1}^0 \right)^2 + 3\Delta z^2 z_{k-1}^0 - \Delta z^3 \right] - \left[\left(z_k^0 \right)^3 - 3\Delta z \left(z_k^0 \right)^2 + 3\Delta z^2 z_k^0 - \Delta z^3 \right] \right\} \\
&= \frac{1}{3} \sum_k \bar{\mathbf{Q}}_k \left[\left(z_{k-1}^0 \right)^3 - \left(z_k^0 \right)^3 \right] + \frac{1}{3} \sum_k \bar{\mathbf{Q}}_k \left(-3\Delta z \right) \left[\left(z_{k-1}^0 \right)^2 - \left(z_k^0 \right)^2 \right] + \frac{1}{3} \sum_k \bar{\mathbf{Q}}_k \left(3\Delta z^2 \right) \left[z_{k-1}^0 - z_k^0 \right] \\
&= \frac{1}{3} \sum_k \bar{\mathbf{Q}}_k \left[\left(z_{k-1}^0 \right)^3 - \left(z_k^0 \right)^3 \right] - \Delta z \sum_k \bar{\mathbf{Q}}_k \left[\left(z_{k-1}^0 \right)^2 - \left(z_k^0 \right)^2 \right] + \Delta z^2 \sum_k \bar{\mathbf{Q}}_k \left[z_{k-1}^0 - z_k^0 \right] \\
&= \mathbf{D}^0 + 2\, \Delta z \mathbf{B}^0 + \Delta z^2\, \mathbf{A}^0
\end{aligned}$$

$$\boxed{\mathbf{D}^{\text{new}} = \mathbf{D}^0 + 2\, \Delta z \mathbf{B}^0 + \Delta z^2\, \mathbf{A}^0} \tag{3.11}$$

Likewise, for the thermal force and moment resultants measured with respect to the new shifted reference plane, we have,

$$\begin{aligned}\mathbf{N}^T_{\text{new}} &= \sum_k \bar{\mathbf{Q}}_k \boldsymbol{\alpha}_k \left[z^{\text{new}}_{k-1} - z^{\text{new}}_k \right] \Delta T_{\text{new}} + \frac{1}{2} \sum_k \bar{\mathbf{Q}}_k \boldsymbol{\alpha}_k \left[\left(z^{\text{new}}_{k-1} \right)^2 - \left(z^{\text{new}}_k \right)^2 \right] \Delta G \\ \mathbf{M}^T_{\text{new}} &= -\frac{1}{2} \sum_k \bar{\mathbf{Q}}_k \boldsymbol{\alpha}_k \left[\left(z^{\text{new}}_{k-1} \right)^2 - \left(z^{\text{new}}_k \right)^2 \right] \Delta T_{\text{new}} - \frac{1}{3} \sum_k \bar{\mathbf{Q}}_k \boldsymbol{\alpha}_k \left[\left(z^{\text{new}}_{k-1} \right)^3 - \left(z^{\text{new}}_k \right)^3 \right] \Delta G \end{aligned} \tag{3.12}$$

Substituting for z^{new} in Eq. (3.12) using Eq. (3.4) and for ΔT_{new} using Eq. (3.5), we arrive at,

$$\begin{aligned}
\mathbf{N}^T_{\text{new}} &= \sum_k \bar{\mathbf{Q}}_k \boldsymbol{\alpha}_k \left[z^0_{k-1} - \Delta z - z^0_k + \Delta z \right] \left(\Delta T_0 + \Delta G \; \Delta z \right) + \frac{1}{2} \sum_k \bar{\mathbf{Q}}_k \boldsymbol{\alpha}_k \left[\left(z^0_{k-1} - \Delta z \right)^2 - \left(z^0_k - \Delta z \right)^2 \right] \Delta G \\
&= \sum_k \bar{\mathbf{Q}}_k \boldsymbol{\alpha}_k \left[z^0_{k-1} - z^0_k \right] \left(\Delta T_0 + \Delta G \; \Delta z \right) + \frac{1}{2} \sum_k \bar{\mathbf{Q}}_k \boldsymbol{\alpha}_k \left[\left(z^0_{k-1} \right)^2 - 2 \; z^0_{k-1} \Delta z + \Delta z^2 - \left(z^0_k \right)^2 + 2 \; z^0_k \Delta z - \Delta z^2 \right] \Delta G \\
&= \sum_k \bar{\mathbf{Q}}_k \boldsymbol{\alpha}_k \left[z^0_{k-1} - z^0_k \right] \Delta T_0 + \sum_k \bar{\mathbf{Q}}_k \boldsymbol{\alpha}_k \left[z^0_{k-1} - z^0_k \right] \Delta G \; \Delta z + \frac{1}{2} \sum_k \bar{\mathbf{Q}}_k \boldsymbol{\alpha}_k \left[\left(z^0_{k-1} \right)^2 - \left(z^0_k \right)^2 - 2 \Delta z \left(z^0_{k-1} - z^0_k \right) \right] \Delta G \\
&= \sum_k \bar{\mathbf{Q}}_k \boldsymbol{\alpha}_k \left[z^0_{k-1} - z^0_k \right] \Delta T_0 + \frac{1}{2} \sum_k \bar{\mathbf{Q}}_k \boldsymbol{\alpha}_k \left[\left(z^0_{k-1} \right)^2 - \left(z^0_k \right)^2 \right] \Delta G + \sum_k \bar{\mathbf{Q}}_k \boldsymbol{\alpha}_k \left[z^0_{k-1} - z^0_k \right] \Delta G \; \Delta z - \sum_k \bar{\mathbf{Q}}_k \boldsymbol{\alpha}_k \left[z^0_{k-1} - z^0_k \right] \Delta G \Delta z \\
&= \sum_k \bar{\mathbf{Q}}_k \boldsymbol{\alpha}_k \left[z^0_{k-1} - z^0_k \right] \Delta T_0 + \frac{1}{2} \sum_k \bar{\mathbf{Q}}_k \boldsymbol{\alpha}_k \left[\left(z^0_{k-1} \right)^2 - \left(z^0_k \right)^2 \right] \Delta G \\
&= \mathbf{N}^T_0
\end{aligned}$$

$$\boxed{\mathbf{N}^T_{\text{new}} = \mathbf{N}^T_0} \tag{3.13}$$

$$\begin{aligned}
\mathbf{M}^T_{\text{new}} &= -\frac{1}{2} \sum_k \bar{\mathbf{Q}}_k \boldsymbol{\alpha}_k \left[\left(z^0_{k-1} - \Delta z \right)^2 - \left(z^0_k - \Delta z \right)^2 \right] \left(\Delta T_0 + \Delta G \; \Delta z \right) - \frac{1}{3} \sum_k \bar{\mathbf{Q}}_k \boldsymbol{\alpha}_k \left[\left(z^0_{k-1} - \Delta z \right)^3 - \left(z^0_k - \Delta z \right)^3 \right] \Delta G \\
&= -\frac{1}{2} \sum_k \bar{\mathbf{Q}}_k \boldsymbol{\alpha}_k \left[\left(z^0_{k-1} \right)^2 - 2 \; z^0_{k-1} \Delta z + \Delta z^2 - \left(z^0_k \right)^2 + 2 \; z^0_k \Delta z - \Delta z^2 \right] \left(\Delta T_0 + \Delta G \; \Delta z \right) \\
&\quad - \frac{1}{3} \sum_k \bar{\mathbf{Q}}_k \boldsymbol{\alpha}_k \left[\left[\left(z^0_{k-1} \right)^3 - 3 \Delta z \left(z^0_{k-1} \right)^2 + 3 \Delta z^2 \; z^0_{k-1} - \Delta z^3 \right] - \left[\left(z^0_k \right)^3 - 3 \Delta z \left(z^0_k \right)^2 + 3 \Delta z^2 \; z^0_k - \Delta z^3 \right] \right] \Delta G
\end{aligned}$$

$$\begin{aligned}
&= -\frac{1}{2} \sum_k \bar{\mathbf{Q}}_k \boldsymbol{\alpha}_k \left[\left(z^0_{k-1} \right)^2 - \left(z^0_k \right)^2 \right] \left(\Delta T_0 + \Delta G \; \Delta z \right) - \frac{1}{2} \sum_k \bar{\mathbf{Q}}_k \boldsymbol{\alpha}_k \left[-2 \Delta z \left(z^0_{k-1} - z^0_k \right) \right] \left(\Delta T_0 + \Delta G \; \Delta z \right) \\
&\quad - \frac{1}{3} \sum_k \bar{\mathbf{Q}}_k \boldsymbol{\alpha}_k \left[\left(z^0_{k-1} \right)^3 - \left(z^0_k \right)^3 \right] \Delta G - \frac{1}{3} \sum_k \bar{\mathbf{Q}}_k \boldsymbol{\alpha}_k \left[-3 \Delta z \left[\left(z^0_{k-1} \right)^2 - \left(z^0_k \right)^2 \right] \right] \Delta G \\
&\quad - \frac{1}{3} \sum_k \bar{\mathbf{Q}}_k \boldsymbol{\alpha}_k \left[3 \Delta z^2 \left(z^0_{k-1} - z^0_k \right) \right] \Delta G
\end{aligned}$$

$$= -\frac{1}{2}\sum_k \bar{\mathbf{Q}}_k \boldsymbol{\alpha}_k \left[\left(z_{k-1}^0\right)^2 - \left(z_k^0\right)^2 \right] \Delta T_0 - \frac{1}{2}\sum_k \bar{\mathbf{Q}}_k \boldsymbol{\alpha}_k \left[\left(z_{k-1}^0\right)^2 - \left(z_k^0\right)^2 \right] \Delta G\, \Delta z$$
$$+ \sum_k \bar{\mathbf{Q}}_k \boldsymbol{\alpha}_k \left[z_{k-1}^0 - z_k^0 \right] \Delta T_0 \Delta z + \sum_k \bar{\mathbf{Q}}_k \boldsymbol{\alpha}_k \left[z_{k-1}^0 - z_k^0 \right] \Delta G\, \Delta z^2$$
$$- \frac{1}{3}\sum_k \bar{\mathbf{Q}}_k \boldsymbol{\alpha}_k \left[\left(z_{k-1}^0\right)^3 - \left(z_k^0\right)^3 \right] \Delta G + \sum_k \bar{\mathbf{Q}}_k \boldsymbol{\alpha}_k \left[\left(z_{k-1}^0\right)^2 - \left(z_k^0\right)^2 \right] \Delta G \Delta z$$
$$- \sum_k \bar{\mathbf{Q}}_k \boldsymbol{\alpha}_k \left[z_{k-1}^0 - z_k^0 \right] \Delta G \Delta z^2$$

$$= -\frac{1}{2}\sum_k \bar{\mathbf{Q}}_k \boldsymbol{\alpha}_k \left[\left(z_{k-1}^0\right)^2 - \left(z_k^0\right)^2 \right] \Delta T_0 - \frac{1}{3}\sum_k \bar{\mathbf{Q}}_k \boldsymbol{\alpha}_k \left[\left(z_{k-1}^0\right)^3 - \left(z_k^0\right)^3 \right] \Delta G$$
$$+ \frac{1}{2}\sum_k \bar{\mathbf{Q}}_k \boldsymbol{\alpha}_k \left[\left(z_{k-1}^0\right)^2 - \left(z_k^0\right)^2 \right] \Delta G\, \Delta z + \sum_k \bar{\mathbf{Q}}_k \boldsymbol{\alpha}_k \left[z_{k-1}^0 - z_k^0 \right] \Delta T_0 \Delta z$$

$$= \mathbf{M}_0^T + \Delta z\, \mathbf{N}_0^T$$

$$\boxed{\mathbf{M}_{\text{new}}^T = \mathbf{M}_0^T + \Delta z\, \mathbf{N}_0^T} \tag{3.14}$$

HyperSizer employs an alternate non-classical form of the laminate constitutive Eq. (3.1) in which the thermal effects are accounted for using "thermal ABD" terms (Collier, 1993). In this case, the laminate constitutive equation is written as,

$$\begin{bmatrix} \mathbf{N} \\ \mathbf{M} \end{bmatrix} = \begin{bmatrix} \mathbf{A}^0 & \mathbf{B}^0 \\ \mathbf{B}^0 & \mathbf{D}^0 \end{bmatrix} \begin{bmatrix} \boldsymbol{\varepsilon}^0 \\ \boldsymbol{\kappa}^0 \end{bmatrix} - \begin{bmatrix} \mathbf{A}_0^\alpha & \mathbf{B}_0^\alpha \\ \mathbf{B}_0^\alpha & \mathbf{D}_0^\alpha \end{bmatrix} \begin{bmatrix} \Delta T_0 \\ -\Delta G \end{bmatrix} \tag{3.15}$$

where,

$$\mathbf{A}_0^\alpha = \sum_k \bar{\mathbf{Q}}_k \boldsymbol{\alpha}_k \left[z_{k-1}^0 - z_k^0 \right] \tag{3.15a}$$

$$\mathbf{B}_0^\alpha = -\frac{1}{2}\sum_k \bar{\mathbf{Q}}_k \boldsymbol{\alpha}_k \left[\left(z_{k-1}^0\right)^2 - \left(z_k^0\right)^2 \right] \tag{3.15b}$$

$$\mathbf{D}_0^\alpha = \frac{1}{3}\sum_k \bar{\mathbf{Q}}_k \boldsymbol{\alpha}_k \left[\left(z_{k-1}^0\right)^3 - \left(z_k^0\right)^3 \right] \tag{3.15c}$$

the thermal force and moment resultants are related to the thermal ABD terms by,

$$\mathbf{N}_0^T = \mathbf{A}_0^\alpha \Delta T_0 - \mathbf{B}_0^\alpha \Delta G \tag{3.16}$$

$$\mathbf{M}_0^T = \mathbf{B}_0^\alpha \Delta T_0 - \mathbf{D}_0^\alpha \Delta G \tag{3.17}$$

With respect to the new shifted reference plane, we have,

$$\mathbf{N}_{\text{new}}^T = \mathbf{A}_{\text{new}}^\alpha \Delta T_{\text{new}} - \mathbf{B}_{\text{new}}^\alpha \Delta G \tag{3.18}$$

$$\mathbf{M}_{\text{new}}^T = \mathbf{B}_{\text{new}}^\alpha \Delta T_{\text{new}} - \mathbf{D}_{\text{new}}^\alpha \Delta G \tag{3.19}$$

Substituting Eq. (3.5) into Eq. (3.18) yields,

$$\begin{aligned}\mathbf{N}^{T}_{\text{new}} &= \mathbf{A}^{\alpha}_{\text{new}}\left(\Delta T_0 + \Delta G\ \Delta z\right) - \mathbf{B}^{\alpha}_{\text{new}}\,\Delta G = \mathbf{A}^{\alpha}_{\text{new}}\Delta T_0 + \mathbf{A}^{\alpha}_{\text{new}}\Delta G\ \Delta z - \mathbf{B}^{\alpha}_{\text{new}}\,\Delta G \\ &= \mathbf{A}^{\alpha}_{\text{new}}\Delta T_0 - \left(\mathbf{B}^{\alpha}_{\text{new}} - \mathbf{A}^{\alpha}_{\text{new}}\Delta z\right)\Delta G\end{aligned} \tag{3.20}$$

Using Eq. (3.13) and comparing the terms present in Eq. (3.20) with those in Eq. (3.16) gives,

$$\boxed{\mathbf{A}^{\alpha}_{\text{new}} = \mathbf{A}^{\alpha}_{0}} \tag{3.21}$$

and,

$$\mathbf{B}^{\alpha}_{0} = \mathbf{B}^{\alpha}_{\text{new}} - \mathbf{A}^{\alpha}_{\text{new}}\Delta z \tag{3.22}$$

Substituting using Eq. (3.21) and rearranging yields,

$$\boxed{\mathbf{B}^{\alpha}_{\text{new}} = \mathbf{B}^{\alpha}_{0} + \Delta z\,\mathbf{A}^{\alpha}_{0}} \tag{3.23}$$

Substituting Eq. (3.5) into (3.18) gives,

$$\begin{aligned}\mathbf{M}^{T}_{\text{new}} &= \mathbf{B}^{\alpha}_{\text{new}}\left(\Delta T_0 + \Delta G\ \Delta z\right) - \mathbf{D}^{\alpha}_{\text{new}}\,\Delta G = \mathbf{B}^{\alpha}_{\text{new}}\Delta T_0 + \mathbf{B}^{\alpha}_{\text{new}}\Delta G\ \Delta z - \mathbf{D}^{\alpha}_{\text{new}}\,\Delta G \\ &= \mathbf{B}^{\alpha}_{\text{new}}\Delta T_0 - \left(\mathbf{D}^{\alpha}_{\text{new}} - \mathbf{B}^{\alpha}_{\text{new}}\Delta z\right)\Delta G\end{aligned} \tag{3.24}$$

Using Eq. (3.14) and substituting using Eqs. (3.16 – 3.17) yields,

$$\begin{aligned}\mathbf{M}^{T}_{\text{new}} &= \mathbf{B}^{\alpha}_{0}\,\Delta T_0 - \mathbf{D}^{\alpha}_{0}\,\Delta G + \Delta z\left(\mathbf{A}^{\alpha}_{0}\,\Delta T_0 - \mathbf{B}^{\alpha}_{0}\,\Delta G\right) \\ &= \left(\mathbf{B}^{\alpha}_{0} + \Delta z\,\mathbf{A}^{\alpha}_{0}\right)\Delta T_0 - \left(\mathbf{D}^{\alpha}_{0} + \mathbf{B}^{\alpha}_{0}\Delta z\right)\Delta G\end{aligned} \tag{3.25}$$

Comparing the terms in Eq. (3.25) with those in Eq. (3.24), we confirm Eq. (3.23) and also have,

$$\mathbf{D}^{\alpha}_{\text{new}} - \mathbf{B}^{\alpha}_{\text{new}}\Delta z = \mathbf{D}^{\alpha}_{0} + \mathbf{B}^{\alpha}_{0}\Delta z \tag{3.26}$$

Rearranging Eq. (3.26) and substituting using Eq. (3.23) then yields,

$$\boxed{\mathbf{D}^{\alpha}_{\text{new}} = \mathbf{D}^{\alpha}_{0} + 2\Delta z\mathbf{B}^{\alpha}_{0} + \Delta z^{2}\,\mathbf{A}^{\alpha}_{0}} \tag{3.27}$$

Equations (3.9 – 3.11), (3.13), (3.14), (3.21), (3.23), and (3.27) thus enable the determination of the thermo-elastic laminate constitutive equation terms with respect to an arbitrary reference plane from the reference plane thermo-elastic laminate constitutive equation terms and the reference plane shift, Δz.

Thermo-piezo-electro-magnetic effects can be included within the midplane laminate constitutive equation (3.1) (see Bednarcyk, 2003, for details) as,

$$\begin{bmatrix}\mathbf{N}\\ \mathbf{M}\end{bmatrix}=\begin{bmatrix}\mathbf{A}^0 & \mathbf{B}^0\\ \mathbf{B}^0 & \mathbf{D}^0\end{bmatrix}\begin{bmatrix}\boldsymbol{\varepsilon}^0\\ \boldsymbol{\kappa}^0\end{bmatrix}-\begin{bmatrix}\mathbf{N}_0^T\\ \mathbf{M}_0^T\end{bmatrix}-\begin{bmatrix}\mathbf{N}_0^E\\ \mathbf{M}_0^E\end{bmatrix}-\begin{bmatrix}\mathbf{N}_0^{ET}\\ \mathbf{M}_0^{ET}\end{bmatrix}-\begin{bmatrix}\mathbf{N}_0^M\\ \mathbf{M}_0^M\end{bmatrix}-\begin{bmatrix}\mathbf{N}_0^{MT}\\ \mathbf{M}_0^{MT}\end{bmatrix} \tag{3.28}$$

where $\mathbf{N}_0^E$ and $\mathbf{M}_0^E$ are the electric force an moment resultant vectors, $\mathbf{N}_0^{ET}$ and $\mathbf{M}_0^{ET}$ are the thermo-electric force and moment resultant vectors, $\mathbf{N}_0^M$ and $\mathbf{M}_0^M$ are the magnetic force and moment resultant vectors, and $\mathbf{N}_0^{MT}$ and $\mathbf{M}_0^{MT}$ are the thermo-magnetic force and moment resultant vectors, all determined with respect to the laminate midplane. These thermo-piezo-electro-magnetic force and moment resultant vectors are given by,

$$\mathbf{N}_0^E=\begin{bmatrix}N_x^E\\ N_y^E\\ N_{xy}^E\end{bmatrix}_0=\sum_{k=1}^{N}[\hat{\mathbf{e}}_k]\begin{bmatrix}E_x\\ E_y\\ E_z\end{bmatrix}_k(z_k-z_{k-1}) \qquad \mathbf{M}_0^E=\begin{bmatrix}M_x^E\\ M_y^E\\ M_{xy}^E\end{bmatrix}_0=-\frac{1}{2}\sum_{k=1}^{N}[\hat{\mathbf{e}}_k]\begin{bmatrix}E_x\\ E_y\\ E_z\end{bmatrix}_k\left(z_k^2-z_{k-1}^2\right) \tag{3.29}$$

$$\mathbf{N}_0^{ET}=\begin{bmatrix}N_x^{ET}\\ N_y^{ET}\\ N_{xy}^{ET}\end{bmatrix}_0=\sum_{k=1}^{N}[\hat{\mathbf{e}}_k]\int_{z_{k-1}}^{z_k}\begin{bmatrix}E_x^T\\ E_y^T\\ E_z^T\end{bmatrix}_k dz \qquad \mathbf{M}_0^{ET}=\begin{bmatrix}M_x^{ET}\\ M_y^{ET}\\ M_{xy}^{ET}\end{bmatrix}_0=-\sum_{k=1}^{N}[\hat{\mathbf{e}}_k]\int_{z_{k-1}}^{z_k}\begin{bmatrix}E_x^T\\ E_y^T\\ E_z^T\end{bmatrix}_k z\,dz \tag{3.30}$$

$$\mathbf{N}_0^M=\begin{bmatrix}N_x^M\\ N_y^M\\ N_{xy}^M\end{bmatrix}_0=\sum_{k=1}^{N}[\hat{\mathbf{q}}_k]\int_{z_{k-1}}^{z_k}\begin{bmatrix}H_x\\ H_y\\ H_z\end{bmatrix}_k dz \qquad \mathbf{M}_0^E=\begin{bmatrix}M_x^M\\ M_y^M\\ M_{xy}^M\end{bmatrix}_0=-\frac{1}{2}\sum_{k=1}^{N}[\hat{\mathbf{q}}_k]\begin{bmatrix}H_x\\ H_y\\ H_z\end{bmatrix}_k\left(z_k^2-z_{k-1}^2\right) \tag{3.31}$$

$$\mathbf{N}_0^{MT}=\begin{bmatrix}N_x^{MT}\\ N_y^{MT}\\ N_{xy}^{MT}\end{bmatrix}_0=\sum_{k=1}^{N}[\hat{\mathbf{q}}_k]\int_{z_{k-1}}^{z_k}\begin{bmatrix}H_x^T\\ H_y^T\\ H_z^T\end{bmatrix}_k dz \qquad \mathbf{M}_0^{MT}=\begin{bmatrix}M_x^{MT}\\ M_y^{MT}\\ M_{xy}^{MT}\end{bmatrix}_0=-\sum_{k=1}^{N}[\hat{\mathbf{q}}_k]\int_{z_{k-1}}^{z_k}\begin{bmatrix}H_x^T\\ H_y^T\\ H_z^T\end{bmatrix}_k z\,dz \tag{3.32}$$

where E_i are the electric field components, E_i^T are the thermo-electric field components, H_i are the magnetic field components, H_i^T are the thermo-magnetic field components, $\hat{\mathbf{e}}_k$ is the 3×3 reduced piezoelectric coefficient matrix (for layer k),

$$[\hat{\mathbf{e}}_k] = \begin{bmatrix} \hat{e}_{11} & \hat{e}_{21} & \hat{e}_{31} \\ \hat{e}_{12} & \hat{e}_{22} & \hat{e}_{32} \\ \hat{e}_{16} & \hat{e}_{26} & \hat{e}_{36} \end{bmatrix}_k \tag{3.33}$$

and $\hat{\mathbf{q}}_k$ is the 3×3 reduced piezomagnetic matrix (for layer k),

$$[\hat{\mathbf{q}}_k] = \begin{bmatrix} \hat{\mathbf{q}}_{11} & \hat{\mathbf{q}}_{21} & \hat{\mathbf{q}}_{31} \\ \hat{\mathbf{q}}_{12} & \hat{\mathbf{q}}_{22} & \hat{\mathbf{q}}_{32} \\ \hat{\mathbf{q}}_{16} & \hat{\mathbf{q}}_{26} & \hat{\mathbf{q}}_{36} \end{bmatrix}_k \tag{3.34}$$

(see Bednarcyk, 2003, for details). It should be noted that the minus signs present in the above moment resultant equations (3.29 – 3.32) are due to the coordinate system employed shown in Fig. 16. This coordinate system differs from that used by Bednarcyk (2003), in which the aforementioned minus signs do not appear.

For consistency, we now develop an alternative representation of these force and moment resultants that by introducing terms analogous to the thermal ABD terms present in Eq. (3.15). Restricting the applied electric field components to the case in which they are constant throughout the laminate, Eq. (3.29) can be written as,

$$\mathbf{N}_0^E = \left[\sum_{k=1}^{N} [\hat{\mathbf{e}}_k](z_{k-1} - z_k)\right] \begin{bmatrix} E_x \\ E_y \\ E_z \end{bmatrix} \qquad \mathbf{M}_0^E = \left[-\frac{1}{2}\sum_{k=1}^{N} [\hat{\mathbf{e}}_k]\left(z_{k-1}^2 - z_k^2\right)\right] \begin{bmatrix} E_x \\ E_y \\ E_z \end{bmatrix} \tag{3.35}$$

Combining Eq. (3.35),

$$\begin{bmatrix} \mathbf{N}_0^E \\ \mathbf{M}_0^E \end{bmatrix} = \begin{bmatrix} \sum_{k=1}^{N} [\hat{\mathbf{e}}_k](z_{k-1} - z_k) \\ -\frac{1}{2}\sum_{k=1}^{N} [\hat{\mathbf{e}}_k]\left(z_{k-1}^2 - z_k^2\right) \end{bmatrix} \begin{bmatrix} E_x \\ E_y \\ E_z \end{bmatrix} \tag{3.36}$$

or,

$$\underbrace{\begin{bmatrix} \mathbf{N}_0^E \\ \mathbf{M}_0^E \end{bmatrix}}_{6\times1} = \underbrace{\begin{bmatrix} \mathbf{A}_0^E \\ \mathbf{B}_0^E \end{bmatrix}}_{6\times3} \underbrace{\begin{bmatrix} E_x \\ E_y \\ E_z \end{bmatrix}}_{3\times1} \tag{3.37}$$

where,

$$\boxed{\mathbf{A}_0^E = \sum_{k=1}^{N} [\hat{e}_k](z_{k-1} - z_k)} \qquad \boxed{\mathbf{B}_0^E = -\frac{1}{2}\sum_{k=1}^{N} [\hat{e}_k]\left(z_{k-1}^2 - z_k^2\right)} \tag{3.38}$$

Here $\mathbf{A}_0^E$ and $\mathbf{B}_0^E$ are each 3×3 matrices and combine to form the laminate electric AB matrix, as shown in Eq. (3.37).

Similarly, restricting the applied magnetic field components to the case in which they are constant throughout the laminate, we can write Eq. (3.31) as,

$$\underbrace{\begin{bmatrix} \mathbf{N}_0^M \\ \mathbf{M}_0^M \end{bmatrix}}_{6\times 1} = \underbrace{\begin{bmatrix} \mathbf{A}_0^M \\ \mathbf{B}_0^M \end{bmatrix}}_{6\times 3} \underbrace{\begin{bmatrix} H_x \\ H_y \\ H_z \end{bmatrix}}_{3\times 1} \tag{3.39}$$

where,

$$\boxed{\mathbf{A}_0^M = \sum_{k=1}^{N} [\hat{q}_k](z_{k-1} - z_k)} \qquad \boxed{\mathbf{B}_0^M = -\frac{1}{2}\sum_{k=1}^{N} [\hat{q}_k]\left(z_{k-1}^2 - z_k^2\right)} \tag{3.40}$$

Here $\mathbf{A}_0^M$ and $\mathbf{B}_0^M$ are each 3×3 matrices and combine to form the laminate magnetic AB matrix, as shown in Eq. (3.39).

The temperature change from reference at any point within a ply is given by $T(z) - T_{ref} = \Delta T_0 + z\,\Delta G$, and the thermo-electric and thermo-magnetic field components, appearing in Eqs. (3.30) and (3.32), are related to this temperature change by,

$$\begin{bmatrix} E_x^T \\ E_y^T \\ E_z^T \end{bmatrix}_k = \boldsymbol{\zeta}_k^* \left(\Delta T_0 + z\,\Delta G\right) \qquad \begin{bmatrix} H_x^T \\ H_y^T \\ H_z^T \end{bmatrix}_k = \boldsymbol{\psi}_k^* \left(\Delta T_0 + z\,\Delta G\right) \tag{3.41}$$

where $\boldsymbol{\zeta}_k^*$ is the effective pyroelectric constant vector of ply k and $\boldsymbol{\psi}_k^*$ is the effective pyromagnetic constant vector for ply k, both in the global laminate coordinate system. Note that the relations between the thermal field quantities and the pyroelectric and pyromagnetic constants in Eq. (3.40) is analogous to that of the thermal strain and the coefficient of thermal expansion. Substituting Eq. (3.40) into Eqs. (3.30) and (3.32) yields,

$$\mathbf{N}_0^{ET} = \sum_{k=1}^{N} [\hat{\mathbf{e}}_k] \int_{z_{k-1}}^{z_k} \boldsymbol{\zeta}_k^* \left(\Delta T_0 + z\,\Delta G\right) dz \qquad \mathbf{M}_0^{ET} = -\sum_{k=1}^{N} [\hat{\mathbf{e}}_k] \int_{z_{k-1}}^{z_k} \boldsymbol{\zeta}_k^* \left(\Delta T_0 + z\,\Delta G\right) z\,dz \tag{3.42}$$

$$\mathbf{N}_0^{MT} = \sum_{k=1}^{N} [\hat{\mathbf{q}}_k] \int_{z_{k-1}}^{z_k} \boldsymbol{\psi}_k^* \left(\Delta T_0 + z\,\Delta G\right) dz \qquad \mathbf{M}_0^{MT} = -\sum_{k=1}^{N} [\hat{\mathbf{q}}_k] \int_{z_{k-1}}^{z_k} \boldsymbol{\psi}_k^* \left(\Delta T_0 + z\,\Delta G\right) z\,dz \tag{3.43}$$

or,

$$\begin{bmatrix}\mathbf{N}_0^{ET}\\ \mathbf{M}_0^{ET}\end{bmatrix}=\begin{bmatrix}\sum_{k=1}^{N}[\hat{\mathbf{e}}_k]\zeta_k^*\left(z_{k-1}-z_k\right)\Delta T_0+\frac{1}{2}\sum_{k=1}^{N}[\hat{\mathbf{e}}_k]\zeta_k^*\left(z_{k-1}^2-z_k^2\right)\Delta G\\ -\frac{1}{2}\sum_{k=1}^{N}[\hat{\mathbf{e}}_k]\zeta_k^*\left(z_{k-1}^2-z_k^2\right)\Delta T_0-\frac{1}{3}\sum_{k=1}^{N}[\hat{\mathbf{e}}_k]\zeta_k^*\left(z_{k-1}^3-z_k^3\right)\Delta G\end{bmatrix} \tag{3.44}$$

$$\begin{bmatrix}\mathbf{N}_0^{MT}\\ \mathbf{M}_0^{MT}\end{bmatrix}=\begin{bmatrix}\sum_{k=1}^{N}[\hat{\mathbf{q}}_k]\psi_k^*\left(z_{k-1}-z_k\right)\Delta T_0+\frac{1}{2}\sum_{k=1}^{N}[\hat{\mathbf{q}}_k]\psi_k^*\left(z_{k-1}^2-z_k^2\right)\Delta G\\ -\frac{1}{2}\sum_{k=1}^{N}[\hat{\mathbf{q}}_k]\psi_k^*\left(z_{k-1}^2-z_k^2\right)\Delta T_0-\frac{1}{3}\sum_{k=1}^{N}[\hat{\mathbf{q}}_k]\psi_k^*\left(z_{k-1}^3-z_k^3\right)\Delta G\end{bmatrix} \tag{3.45}$$

or,

$$\underbrace{\begin{bmatrix}\mathbf{N}_0^{ET}\\ \mathbf{M}_0^{ET}\end{bmatrix}}_{6\times1}=\underbrace{\begin{bmatrix}\mathbf{A}_0^{ET} & \mathbf{B}_0^{ET}\\ \mathbf{B}_0^{ET} & \mathbf{D}_0^{ET}\end{bmatrix}}_{6\times2}\underbrace{\begin{bmatrix}\Delta T_0\\ -\Delta G\end{bmatrix}}_{2\times1} \qquad \underbrace{\begin{bmatrix}\mathbf{N}_0^{MT}\\ \mathbf{M}_0^{MT}\end{bmatrix}}_{6\times1}=\underbrace{\begin{bmatrix}\mathbf{A}_0^{MT} & \mathbf{B}_0^{MT}\\ \mathbf{B}_0^{MT} & \mathbf{D}_0^{MT}\end{bmatrix}}_{6\times2}\underbrace{\begin{bmatrix}\Delta T_0\\ -\Delta G\end{bmatrix}}_{2\times1} \tag{3.46}$$

where,

$$\mathbf{A}_0^{ET}=\sum_{k=1}^{N}[\hat{\mathbf{e}}_k]\zeta_k^*\left(z_{k-1}-z_k\right) \qquad \mathbf{B}_0^{ET}=-\frac{1}{2}\sum_{k=1}^{N}[\hat{\mathbf{e}}_k]\zeta_k^*\left(z_{k-1}^2-z_k^2\right) \qquad \mathbf{D}_0^{ET}=\frac{1}{3}\sum_{k=1}^{N}[\hat{\mathbf{e}}_k]\zeta_k^*\left(z_{k-1}^3-z_k^3\right) \tag{3.47}$$

$$\mathbf{A}_0^{MT}=\sum_{k=1}^{N}[\hat{\mathbf{q}}_k]\psi_k^*\left(z_{k-1}-z_k\right) \qquad \mathbf{B}_0^{MT}=-\frac{1}{2}\sum_{k=1}^{N}[\hat{\mathbf{q}}_k]\psi_k^*\left(z_{k-1}^2-z_k^2\right) \qquad \mathbf{D}_0^{MT}=\frac{1}{3}\sum_{k=1}^{N}[\hat{\mathbf{q}}_k]\psi_k^*\left(z_{k-1}^3-z_k^3\right) \tag{3.48}$$

Note that each of the above thermo-electric and thermo-magnetic ABD terms is a 3×1 matrix. We can now write the laminate constitutive equation (3.15) and (3.28) as,

$$\begin{aligned}\begin{bmatrix}\mathbf{N}\\ \mathbf{M}\end{bmatrix}=&\begin{bmatrix}\mathbf{A}^0 & \mathbf{B}^0\\ \mathbf{B}^0 & \mathbf{D}^0\end{bmatrix}\begin{bmatrix}\boldsymbol{\varepsilon}^0\\ \boldsymbol{\kappa}^0\end{bmatrix}-\begin{bmatrix}\mathbf{A}_0^{\alpha} & \mathbf{B}_0^{\alpha}\\ \mathbf{B}_0^{\alpha} & \mathbf{D}_0^{\alpha}\end{bmatrix}\begin{bmatrix}\Delta T_0\\ -\Delta G\end{bmatrix}-\begin{bmatrix}\mathbf{A}_0^{E}\\ \mathbf{B}_0^{E}\end{bmatrix}\begin{bmatrix}E_x\\ E_y\\ E_z\end{bmatrix}-\begin{bmatrix}\mathbf{A}_0^{M}\\ \mathbf{B}_0^{M}\end{bmatrix}\begin{bmatrix}H_x\\ H_y\\ H_z\end{bmatrix}\\ &-\begin{bmatrix}\mathbf{A}_0^{ET} & \mathbf{B}_0^{ET}\\ \mathbf{B}_0^{ET} & \mathbf{D}_0^{ET}\end{bmatrix}\begin{bmatrix}\Delta T_0\\ -\Delta G\end{bmatrix}-\begin{bmatrix}\mathbf{A}_0^{MT} & \mathbf{B}_0^{MT}\\ \mathbf{B}_0^{MT} & \mathbf{D}_0^{MT}\end{bmatrix}\begin{bmatrix}\Delta T_0\\ -\Delta G\end{bmatrix}\end{aligned} \tag{3.49}$$

Comparing the electric, magnetic, thermo-electric, and thermo-magnetic terms in Eq. (3.49) with the thermal terms in Eq. (3.49) (see Eqs. (3.15a – 3.15c), (3.38), (3.40), and (3.47 – 3.48), it is clear that there is a direct analogy among all $\mathbf{A}_0^j$ matrices, among all $\mathbf{B}_0^j$ matrices, and among all $\mathbf{D}_0^j$ matrices. Since the z_k functionality in all of these thermo-electro-magnetic ABD terms is the same as that of the thermal ABD terms, it can be shown that these thermo-electro-magnetic ABD terms will shift reference plane (see Fig. 16) in a way analogous to the shift in the thermal ABD terms given in Eqs. (3.21), (3.23), and (3.27). Thus, for a reference plane shift of Δz, we have,

$$\boxed{\mathbf{A}^j_{\text{new}} = \mathbf{A}^j_0} \qquad \boxed{\mathbf{B}^j_{\text{new}} = \mathbf{B}^j_0 + \Delta z\,\mathbf{A}^j_0}, \qquad j = E,\ M,\ ET,\ MT \tag{3.50}$$

$$\boxed{\mathbf{D}^j_{\text{new}} = \mathbf{D}^j_0 + 2\Delta z\mathbf{B}^j_0 + \Delta z^2\,\mathbf{A}^j_0}, \qquad j = ET,\ MT \tag{3.51}$$

In terms of the thermo-electro-magnetic force and moment resultants (Eqs. 3.35, 3.40, 3.44, and 3.45), we have,

$$\boxed{\mathbf{N}^j_{\text{new}} = \mathbf{N}^j_0}, \qquad j = E,\ M,\ ET,\ MT \tag{3.52}$$

$$\boxed{\mathbf{M}^j_{\text{new}} = \mathbf{M}^j_0 + \Delta z\,\mathbf{N}^j_0}, \qquad j = E,\ M,\ ET,\ MT \tag{3.53}$$

A simple procedure has thus been established for shifting all elements of the thermo-electro-magneto-elastic laminate constitutive equations (3.49) from the laminate midplane to an arbitrary reference plane. This new laminate constitutive equation is given by,

$$\begin{aligned}\begin{bmatrix}\mathbf{N}\\ \mathbf{M}\end{bmatrix} = &\begin{bmatrix}\mathbf{A}^{\text{new}} & \mathbf{B}^{\text{new}}\\ \mathbf{B}^{\text{new}} & \mathbf{D}^{\text{new}}\end{bmatrix}\begin{bmatrix}\boldsymbol{\varepsilon}^{\text{new}}\\ \boldsymbol{\kappa}^{\text{new}}\end{bmatrix} - \begin{bmatrix}\mathbf{A}^{\alpha}_{\text{new}} & \mathbf{B}^{\alpha}_{\text{new}}\\ \mathbf{B}^{\alpha}_{\text{new}} & \mathbf{D}^{\alpha}_{\text{new}}\end{bmatrix}\begin{bmatrix}\Delta T_{\text{new}}\\ -\Delta G\end{bmatrix} - \begin{bmatrix}\mathbf{A}^{E}_{\text{new}}\\ \mathbf{B}^{E}_{\text{new}}\end{bmatrix}\begin{bmatrix}E_x\\ E_y\\ E_z\end{bmatrix} - \begin{bmatrix}\mathbf{A}^{M}_{\text{new}}\\ \mathbf{B}^{M}_{\text{new}}\end{bmatrix}\begin{bmatrix}H_x\\ H_y\\ H_z\end{bmatrix}\\ &- \begin{bmatrix}\mathbf{A}^{ET}_{\text{new}} & \mathbf{B}^{ET}_{\text{new}}\\ \mathbf{B}^{ET}_{\text{new}} & \mathbf{D}^{ET}_{\text{new}}\end{bmatrix}\begin{bmatrix}\Delta T_{\text{new}}\\ -\Delta G\end{bmatrix} - \begin{bmatrix}\mathbf{A}^{MT}_{\text{new}} & \mathbf{B}^{MT}_{\text{new}}\\ \mathbf{B}^{MT}_{\text{new}} & \mathbf{D}^{MT}_{\text{new}}\end{bmatrix}\begin{bmatrix}\Delta T_{\text{new}}\\ -\Delta G\end{bmatrix}\end{aligned} \tag{3.54}$$

Homogenization Procedure for a Group of Laminates

Now that a reference plane shifting procedure has been established, it is possible to develop a simple methodology for homogenizing the constitutive equations of a group of laminates to arrive at an effective laminate constitutive equation of the laminate constituted by the group. Because each term in the laminate constitutive equation (3.49) is determined via summation of ply-level quantities, provided that the constitutive equations of all laminates in the group are determined with respect to the same reference plane (Eq. 3.54), the constitutive equation of the group can be determined via a simple summation. Thus, given a number of laminates and the z_{new} coordinate of the original reference plane of each laminate (given by l_k, see Fig. 17), we can shift the reference plane of each laminate to the common z_{new} reference plane and then sum the resulting ABD_p matrices to determine the new homogenized ABD of the entire group of laminates.

For each laminate (denoted by the subscript p) in Fig. 17 the reference plane shift is given by, $\Delta z^0_p = -l_p$ because Δz^0_p is measured from a laminate's original reference plane to the new reference plane, while l_p is measured in the opposite direction, from the new reference plane to the laminate's original reference plane. Considering first the standard laminate ABD matrix terms,

$$\mathbf{A}_{\text{Group}} = \sum_p \mathbf{A}^{\text{new}}_p = \sum_p \mathbf{A}^0_p \qquad \rightarrow \qquad \boxed{\mathbf{A}_{\text{Group}} = \sum_p \mathbf{A}^0_p} \tag{3.55}$$

$$\mathbf{B}_{\text{Group}} = \sum_k \mathbf{B}^{\text{new}}_p = \sum_p \left(\mathbf{B}^0_p + \Delta z_p\,\mathbf{A}^0_p\right) = \sum_p \left(\mathbf{B}^0_p - l_p\,\mathbf{A}^0_p\right) \qquad \rightarrow \qquad \boxed{\mathbf{B}_{\text{Group}} = \sum_p \left(\mathbf{B}^0_p - l_p\,\mathbf{A}^0_p\right)} \tag{3.56}$$

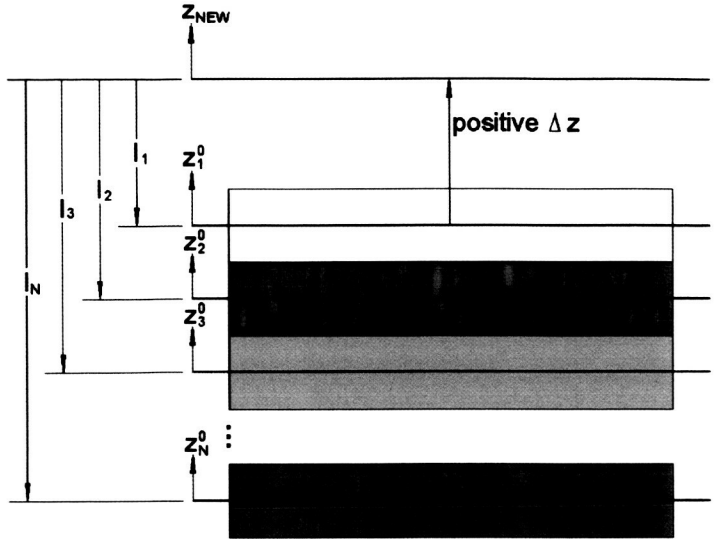

Fig. 17. A group of laminates whose constitutive equation terms have been determined with respect to a common reference plane, defined by the origin of the coordinate z_{new}. This allows determination of effective constitutive equation terms (with respect to the common reference plane) for the laminate constituted by the group.

$$\mathbf{D}_{\text{Group}} = \sum_p \mathbf{D}_p^{\text{new}} = \sum_p \left(\mathbf{D}_p^0 + 2\,\Delta z_p\,\mathbf{B}_p^0 + \Delta z_p{}^2\,\mathbf{A}_p^0 \right)$$
$$= \sum_k \left(\mathbf{D}_p^0 - 2\,l_p\,\mathbf{B}_p^0 + l_p{}^2\,\mathbf{A}_p^0 \right) \quad \rightarrow \quad \boxed{\mathbf{D}_{\text{Group}} = \sum_p \left(\mathbf{D}_p^0 - 2\,l_p\,\mathbf{B}_p^0 + l_p{}^2\,\mathbf{A}_p^0 \right)} \tag{3.57}$$

Similarly, the homogenized thermal terms are given by,

$$\mathbf{A}_{\text{Group}}^{\alpha} = \sum_p \left(\mathbf{A}_{\text{new}}^{\alpha} \right)_p = \sum_p \left(\mathbf{A}_0^{\alpha} \right)_p \quad \rightarrow \quad \boxed{\mathbf{A}_{\text{Group}}^{\alpha} = \sum_p \left(\mathbf{A}_0^{\alpha} \right)_p} \tag{3.58}$$

$$\mathbf{B}_{\text{Group}}^{\alpha} = \sum_p \left(\mathbf{B}_{\text{new}}^{\alpha} \right)_p = \sum_p \left[\left(\mathbf{B}_0^{\alpha} \right)_p + \Delta z_p \left(\mathbf{A}_0^{\alpha} \right)_p \right]$$
$$= \sum_p \left[\left(\mathbf{B}_0^{\alpha} \right)_p - l_p \left(\mathbf{A}_0^{\alpha} \right)_p \right] \quad \rightarrow \quad \boxed{\mathbf{B}_{\text{Group}}^{\alpha} = \sum_p \left[\left(\mathbf{B}_0^{\alpha} \right)_p - l_p \left(\mathbf{A}_0^{\alpha} \right)_p \right]} \tag{3.59}$$

$$\mathbf{D}_{\text{Group}}^{\alpha} = \sum_p \left(\mathbf{D}_{\text{new}}^{\alpha} \right)_p = \sum_k \left[\left(\mathbf{D}_0^{\alpha} \right)_p + 2\,\Delta z_p \left(\mathbf{B}_0^{\alpha} \right)_p + \Delta z_p{}^2 \left(\mathbf{A}_0^{\alpha} \right)_p \right]$$
$$= \sum_p \left[\left(\mathbf{D}_0^{\alpha} \right)_p - 2\,l_p \left(\mathbf{B}_0^{\alpha} \right)_p + l_p{}^2 \left(\mathbf{A}_0^{\alpha} \right)_p \right] \quad \rightarrow$$

$$\boxed{\mathbf{D}_{\text{Group}}^{\alpha} = \sum_p \left[\left(\mathbf{D}_0^{\alpha} \right)_p - 2\,l_p \left(\mathbf{B}_0^{\alpha} \right)_p + l_p{}^2 \left(\mathbf{A}_0^{\alpha} \right)_p \right]} \tag{3.60}$$

$$\mathbf{N}^T_{\text{Group}} = \sum_p \left(\mathbf{N}^T_{\text{new}}\right)_p = \sum_p \left(\mathbf{N}^T_0\right)_p \quad \rightarrow \quad \boxed{\mathbf{N}^T_{\text{Group}} = \sum_p \left(\mathbf{N}^T_0\right)_p} \tag{3.61}$$

$$\mathbf{M}^T_{\text{Group}} = \sum_p \left(\mathbf{M}^T_{\text{new}}\right)_p = \sum_p \left(\mathbf{N}^T_0 + \Delta z\ \mathbf{M}^T_0\right)_p = \sum_p \left(\mathbf{N}^T_0 - l_k\ \mathbf{M}^T_0\right)_p \quad \rightarrow \quad \boxed{\mathbf{M}^T_{\text{Group}} = \sum_p \left(\mathbf{M}^T_0 - l_k\ \mathbf{N}^T_0\right)_p} \tag{3.62}$$

Finally, the homogenized thermo-electro-magnetic terms are given by,

$$\boxed{\mathbf{A}^j_{\text{Group}} = \sum_p \left(\mathbf{A}^j_0\right)_p}, \qquad j = E,\ M,\ ET,\ MT \tag{3.63}$$

$$\boxed{\mathbf{B}^j_{\text{Group}} = \sum_p \left[\left(\mathbf{B}^j_0\right)_p - l_p \left(\mathbf{A}^j_0\right)_p\right]}, \qquad j = E,\ M,\ ET,\ MT \tag{3.64}$$

$$\boxed{\mathbf{D}^j_{\text{Group}} = \sum_p \left[\left(\mathbf{D}^j_0\right)_p - 2\, l_p \left(\mathbf{B}^j_0\right)_p + l_p{}^2 \left(\mathbf{A}^j_0\right)_p\right]}, \qquad j = ET,\ MT \tag{3.65}$$

$$\boxed{\mathbf{N}^j_{\text{Group}} = \sum_p \left(\mathbf{N}^j_0\right)_p}, \qquad j = E,\ M,\ ET,\ MT \tag{3.66}$$

$$\boxed{\mathbf{M}^j_{\text{Group}} = \sum_p \left(\mathbf{M}^j_0 - l_p\ \mathbf{N}^j_0\right)_p}, \qquad j = E,\ M,\ ET,\ MT \tag{3.67}$$

The homogenized constitutive equation for the group of laminates with respect to the reference plane defined by the origin of the z_{new} coordinate in Fig. 17 is given by,

$$\begin{bmatrix}\mathbf{N}\\ \mathbf{M}\end{bmatrix} = \begin{bmatrix}\mathbf{A}_{\text{Group}} & \mathbf{B}_{\text{Group}}\\ \mathbf{B}_{\text{Group}} & \mathbf{D}_{\text{Group}}\end{bmatrix}\begin{bmatrix}\boldsymbol{\varepsilon}^{\text{new}}\\ \boldsymbol{\kappa}^{\text{new}}\end{bmatrix} - \begin{bmatrix}\mathbf{A}^{\alpha}_{\text{Group}} & \mathbf{B}^{\alpha}_{\text{Group}}\\ \mathbf{B}^{\alpha}_{\text{Group}} & \mathbf{D}^{\alpha}_{\text{Group}}\end{bmatrix}\begin{bmatrix}\Delta T_{\text{new}}\\ -\Delta G\end{bmatrix} - \begin{bmatrix}\mathbf{A}^{E}_{\text{Group}}\\ \mathbf{B}^{E}_{\text{Group}}\end{bmatrix}\begin{bmatrix}E_x\\ E_y\\ E_z\end{bmatrix} - \begin{bmatrix}\mathbf{A}^{M}_{\text{Group}}\\ \mathbf{B}^{M}_{\text{Group}}\end{bmatrix}\begin{bmatrix}H_x\\ H_y\\ H_z\end{bmatrix} - \begin{bmatrix}\mathbf{A}^{ET}_{\text{Group}} & \mathbf{B}^{ET}_{\text{Group}}\\ \mathbf{B}^{ET}_{\text{Group}} & \mathbf{D}^{ET}_{\text{Group}}\end{bmatrix}\begin{bmatrix}\Delta T_{\text{new}}\\ -\Delta G\end{bmatrix} - \begin{bmatrix}\mathbf{A}^{MT}_{\text{Group}} & \mathbf{B}^{MT}_{\text{Group}}\\ \mathbf{B}^{MT}_{\text{Group}} & \mathbf{D}^{MT}_{\text{Group}}\end{bmatrix}\begin{bmatrix}\Delta T_{\text{new}}\\ -\Delta G\end{bmatrix} \tag{3.68}$$

Analysis of Blade Stiffened Panels

The geometry of a blade stiffened panel is shown in Fig. 18. The face sheet can be an arbitrary composite laminate that is oriented as shown in the x, y, z coordinate system such that the z-direction is the laminate through-thickness direction. This coordinate system is also used for the stiffened panel as a whole. The blade stiffener can also be an arbitrary laminate, but, as shown, it is oriented in the x_B, y_B, z_B coordinate system with the blade through-thickness direction, z_B, corresponding to the panel y-direction. Note that the x_B-direction for the blade corresponds to the x-direction of the face sheet and panel as a whole.

The key assumption made in incorporating the blade contribution to the overall behavior of the stiffened panel is that the contribution is largely decoupled from the face sheet contribution. That is, the response of the blade in its own y_B-direction is assumed not to affect the panel and face sheet response due to the small contact region between the components. Considering first the panel mechanical

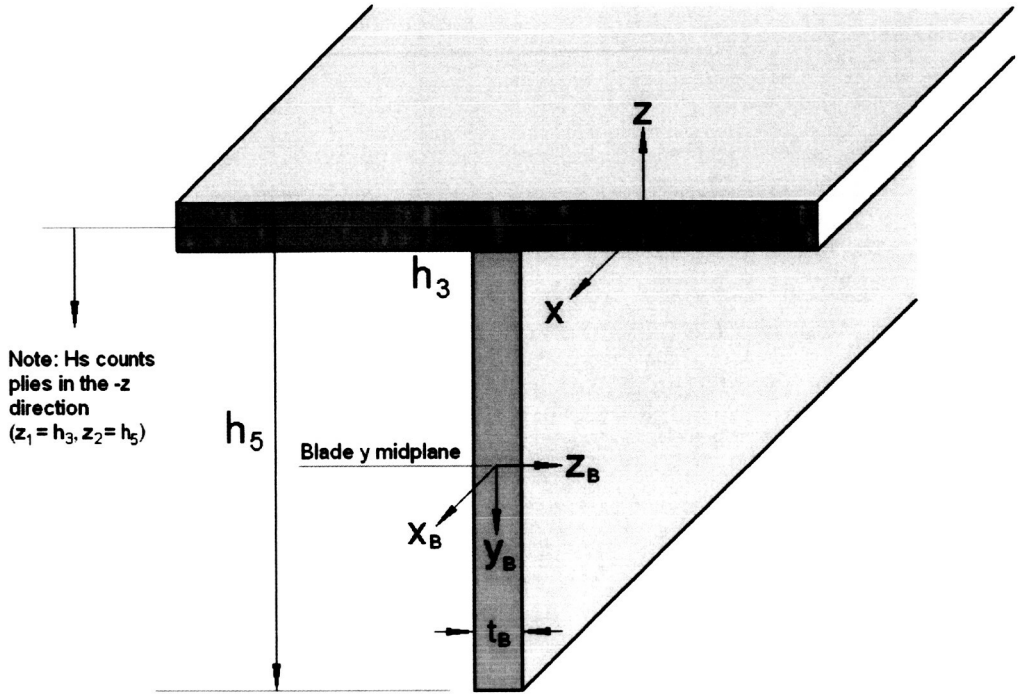

Fig. 18. Geometry of a blade stiffened panel. The face sheet is shown in blue, while the blade stiffener is shown in pink.

behavior, the decoupling assumption is embodied by assigning the blade the following effective in-plane properties (in the local blade coordinate system),

$$\bar{E}_x^B \neq 0, \quad \bar{E}_y^B = 0, \quad \bar{\nu}_{xy}^B = 0, \quad \bar{G}_{xy}^B = 0 \tag{3.69}$$

Thus, in terms of its effect on the panel response, the blade will have a contribution to the axial stiffness (x-direction), but no direct stiffness contribution and no Poisson contribution in the y_B-direction (panel z-direction), and no shear contribution. $\bar{E}_x^B$ is the effective (homogenized) axial stiffness of the blade. It can be calculated from the inverse of the blade laminate extensional stiffness matrix, $\mathbf{A}^{-1}$, as,

$$\bar{E}_x^B = \frac{1}{t_B \; AI_{11}^B} \tag{3.70}$$

where t_B is the thickness of the blade (see Fig. 18) and AI_{11}^B is the 11 component of the inverse of the blade laminate extensional stiffness matrix. Based on the effective properties given in Eq, (3.69), the uncoupled reduced stiffness matrix of the blade is,

$$\bar{\mathbf{Q}}_B^u = \begin{bmatrix} \bar{E}_x^B & 0 & 0 \\ 0 & 0 & 0 \\ 0 & 0 & 0 \end{bmatrix} \tag{3.71}$$

In the panel coordinate system (see Fig. 18), the blade stiffness contribution is taken to be the volume-weighted sum of the blade uncoupled reduced stiffness matrix and the empty space between the blades along the panel y-direction. If the blade spacing (i.e., distance between adjacent blades) is denoted as S, this blade contribution is given by,

$$\bar{\mathbf{Q}}_B^{\text{cont}} = \frac{t_B \bar{\mathbf{Q}}_B^u}{S} = \frac{t_B}{S}\begin{bmatrix} \bar{E}_x^B & 0 & 0 \\ 0 & 0 & 0 \\ 0 & 0 & 0 \end{bmatrix} = \frac{1}{S\ AI_B^{11}}\begin{bmatrix} 1 & 0 & 0 \\ 0 & 0 & 0 \\ 0 & 0 & 0 \end{bmatrix} \tag{3.72}$$

Employing Eq. (3.2), the blade contributions to the ABD terms with respect to the blade's midplane (see Fig. 18) are given by,

$$\mathbf{A}_B^0 = \bar{\mathbf{Q}}_B^{\text{cont}}\left[-\frac{h_5 - h_3}{2} - \frac{h_5 - h_3}{2}\right] = \bar{\mathbf{Q}}_B^{\text{cont}}\left(h_3 - h_5\right) \tag{3.73}$$

$$\mathbf{B}_B^0 = -\frac{1}{2}\bar{\mathbf{Q}}_B^{\text{cont}}\left[\left(-\frac{h_5 - h_3}{2}\right)^2 - \left(\frac{h_5 - h_3}{2}\right)^2\right] = 0 \tag{3.74}$$

$$\mathbf{D}_B^0 = \frac{1}{3}\bar{\mathbf{Q}}_B^{\text{cont}}\left[\left(-\frac{h_5 - h_3}{2}\right)^3 - \left(\frac{h_5 - h_3}{2}\right)^3\right] = \frac{1}{12}\bar{\mathbf{Q}}_B^{\text{cont}}\left(h_3 - h_5\right)^3 \tag{3.75}$$

Shifting these terms to the midplane of the face sheet, which serves as the reference plane for the panel, using Eqs. (3.9 – 3.11) with $\Delta z = \dfrac{h_5 + h_3}{2}$ yields,

$$\mathbf{A}_B^{\text{cont}} = \bar{\mathbf{Q}}_B^{\text{cont}}\left(h_3 - h_5\right) \tag{3.76}$$

$$\mathbf{B}_B^{\text{cont}} = \frac{h_3 + h_5}{2}\bar{\mathbf{Q}}_B^{\text{cont}}\left(h_3 - h_5\right) = \frac{1}{2}\bar{\mathbf{Q}}_B^{\text{cont}}\left(h_3^2 - h_5^2\right) \tag{3.77}$$

$$\mathbf{D}_B^{\text{cont}} = \frac{1}{12}\bar{\mathbf{Q}}_B^{\text{cont}}\left(h_3 - h_5\right)^3 + \left(\frac{h_3 + h_5}{2}\right)^2 \bar{\mathbf{Q}}_B^{\text{cont}}\left(h_3 - h_5\right) = \frac{1}{3}\bar{\mathbf{Q}}_B^{\text{cont}}\left(h_3^3 - h_5^3\right) \tag{3.78}$$

Then, as discussed in Section 3, the contributions of the blade and the face sheet to the panel ABD terms can be added to yield the effective panel ABD terms (since the blade and face sheet terms are now known with respect to the same reference plane). Thus,

$$\mathbf{A}_{\text{panel}} = \mathbf{A}_{\text{FS}} + \bar{\mathbf{Q}}_B^{\text{cont}}\left(h_3 - h_5\right) \tag{3.79}$$

$$\mathbf{B}_{\text{panel}} = \mathbf{B}_{\text{FS}} + \frac{1}{2}\bar{\mathbf{Q}}_B^{\text{cont}}\left(h_3^2 - h_5^2\right) \tag{3.80}$$

$$\mathbf{D}_{\text{panel}} = \mathbf{D}_{\text{FS}} + \frac{1}{3}\bar{\mathbf{Q}}_B^{\text{cont}}\left(h_3^3 - h_5^3\right) \tag{3.81}$$

where $\mathbf{A}_{\text{FS}}$, $\mathbf{B}_{\text{FS}}$, and $\mathbf{D}_{\text{FS}}$ are the face sheet laminate extensional, coupling, and bending stiffnesses, respectively.

Considering the thermal response of the blade stiffened panel, the decoupling of the blade from the panel thermal response indicates that only the x-direction thermal expansion of the blade will have an

effect. Thus, the effective coefficients of thermal expansion (in the blade coordinate system, Fig. 18) assigned to the blade for its thermal contribution are,

$$\bar{\alpha}_x^B \neq 0, \quad \bar{\alpha}_y^B = 0, \quad \bar{\alpha}_{xy}^B = 0 \tag{3.82}$$

$\bar{\alpha}_x^B$ is the effective thermal expansion coefficient in the x-direction. This term can be calculated by considering the inverted form of the general laminate constitutive equation (3.49),

$$\begin{aligned}\begin{bmatrix}\boldsymbol{\varepsilon}^0\\ \boldsymbol{\kappa}\end{bmatrix} &= \begin{bmatrix}\mathbf{A}^0 & \mathbf{B}^0\\ \mathbf{B}^0 & \mathbf{D}^0\end{bmatrix}^{-1}\begin{bmatrix}\mathbf{N}\\ \mathbf{M}\end{bmatrix} - \begin{bmatrix}\mathbf{A}^0 & \mathbf{B}^0\\ \mathbf{B}^0 & \mathbf{D}^0\end{bmatrix}^{-1}\begin{bmatrix}\mathbf{A}_0^{\alpha} & \mathbf{B}_0^{\alpha}\\ \mathbf{B}_0^{\alpha} & \mathbf{D}_0^{\alpha}\end{bmatrix}\begin{bmatrix}\Delta T_0\\ -\Delta G\end{bmatrix} - \begin{bmatrix}\mathbf{A}^0 & \mathbf{B}^0\\ \mathbf{B}^0 & \mathbf{D}^0\end{bmatrix}^{-1}\begin{bmatrix}\mathbf{A}_0^{E} \\ \mathbf{B}_0^{E}\end{bmatrix}\begin{bmatrix}E_x\\ E_y\\ E_z\end{bmatrix}\\ &- \begin{bmatrix}\mathbf{A}^0 & \mathbf{B}^0\\ \mathbf{B}^0 & \mathbf{D}^0\end{bmatrix}^{-1}\begin{bmatrix}\mathbf{A}_0^{M} \\ \mathbf{B}_0^{M}\end{bmatrix}\begin{bmatrix}H_x\\ H_y\\ H_z\end{bmatrix} - \begin{bmatrix}\mathbf{A}^0 & \mathbf{B}^0\\ \mathbf{B}^0 & \mathbf{D}^0\end{bmatrix}^{-1}\begin{bmatrix}\mathbf{A}_0^{ET} & \mathbf{B}_0^{ET}\\ \mathbf{B}_0^{ET} & \mathbf{D}_0^{ET}\end{bmatrix}\begin{bmatrix}\Delta T_0\\ -\Delta G\end{bmatrix} - \begin{bmatrix}\mathbf{A}^0 & \mathbf{B}^0\\ \mathbf{B}^0 & \mathbf{D}^0\end{bmatrix}^{-1}\begin{bmatrix}\mathbf{A}_0^{MT} & \mathbf{B}_0^{MT}\\ \mathbf{B}_0^{MT} & \mathbf{D}_0^{MT}\end{bmatrix}\begin{bmatrix}\Delta T_0\\ -\Delta G\end{bmatrix}\end{aligned} \tag{3.83}$$

Clearly, a thermal matrix can be identified as "CTE-like", and, as identified by Collier (1993),

$$\begin{bmatrix}\mathbf{A}^0 & \mathbf{B}^0\\ \mathbf{B}^0 & \mathbf{D}^0\end{bmatrix}^{-1}\begin{bmatrix}\mathbf{A}_0^{\alpha} & \mathbf{B}_0^{\alpha}\\ \mathbf{B}_0^{\alpha} & \mathbf{D}_0^{\alpha}\end{bmatrix} = \begin{bmatrix}\boldsymbol{\alpha}_{\text{lam}} & \boldsymbol{\delta}_{\text{lam}}^{\text{coupling}}\\ \boldsymbol{\alpha}_{\text{lam}}^{\text{coupling}} & \boldsymbol{\delta}_{\text{lam}}\end{bmatrix} \tag{3.84}$$

where $\boldsymbol{\alpha}_{\text{lam}}$ is a 3×1 vector relating strain to temperature change, $\boldsymbol{\alpha}_{\text{lam}}^{\text{coupling}}$ is a 3×1 vector relating curvature to temperature change, $\boldsymbol{\delta}_{\text{lam}}^{\text{coupling}}$ is a 3×1 vector relating strain to through-thickness temperature gradient, and $\boldsymbol{\delta}_{\text{lam}}$ is a 3×1 vector relating curvature to through-thickness temperature gradient. The x-direction effective thermal expansion coefficient for the laminate is then simply the first component of $\boldsymbol{\alpha}_{\text{lam}}$, that is,

$$\bar{\alpha}_x^B = \left(\alpha_{\text{lam}}\right)_1 \tag{3.85}$$

where $\left(\alpha_{\text{lam}}\right)_1$ is the 1,1 component of the 6×2 matrix formed by Eq. (3.84), and the blade CTE vector is given by,

$$\bar{\boldsymbol{\alpha}}_B = \begin{bmatrix}\bar{\alpha}_x^B\\ 0\\ 0\end{bmatrix} \tag{3.86}$$

Employing Eq. (3.15), the blade contributions to the panel thermal ABD terms with respect to the blade's midplane (see Fig. 18) are given by,

$$\left(\mathbf{A}_B^{\alpha}\right)^0 = \bar{\mathbf{Q}}_B^{\text{cont}}\,\bar{\boldsymbol{\alpha}}_B\left[-\frac{h_5-h_3}{2} - \frac{h_5-h_3}{2}\right] = \bar{\mathbf{Q}}_B^{\text{cont}}\,\bar{\boldsymbol{\alpha}}_B\left(h_3-h_5\right) \tag{3.87}$$

$$\left(\mathbf{B}_B^{\alpha}\right)^0 = -\frac{1}{2}\bar{\mathbf{Q}}_B^{\text{cont}}\bar{\boldsymbol{\alpha}}_B\left[\left(-\frac{h_5-h_3}{2}\right)^2-\left(\frac{h_5-h_3}{2}\right)^2\right]=0 \tag{3.88}$$

$$\left(\mathbf{D}_B^{\alpha}\right)^0 = \frac{1}{3}\bar{\mathbf{Q}}_B^{\text{cont}}\bar{\boldsymbol{\alpha}}_B\left[\left(-\frac{h_5-h_3}{2}\right)^3-\left(\frac{h_5-h_3}{2}\right)^3\right]=\frac{1}{12}\bar{\mathbf{Q}}_B^{\text{cont}}\bar{\boldsymbol{\alpha}}_B\left(h_3-h_5\right)^3 \tag{3.89}$$

Shifting these terms to the midplane of the face sheet, which serves as the reference plane for the panel, using Eqs. (3.21, 3.23, 3.27) with $\Delta z = \frac{h_5+h_3}{2}$ yields,

$$\left(\mathbf{A}_B^{\alpha}\right)^{\text{cont}} = \bar{\mathbf{Q}}_B^{\text{cont}}\bar{\boldsymbol{\alpha}}_B\left(h_3-h_5\right) \tag{3.90}$$

$$\left(\mathbf{B}_B^{\alpha}\right)^{\text{cont}} = \frac{h_3+h_5}{2}\bar{\mathbf{Q}}_B^{\text{cont}}\bar{\boldsymbol{\alpha}}_B\left(h_3-h_5\right)=\frac{1}{2}\bar{\mathbf{Q}}_B^{\text{cont}}\bar{\boldsymbol{\alpha}}_B\left(h_3^2-h_5^2\right) \tag{3.91}$$

$$\left(\mathbf{D}_B^{\alpha}\right)^{\text{cont}} = \frac{1}{12}\bar{\mathbf{Q}}_B^{\text{cont}}\bar{\boldsymbol{\alpha}}_B\left(h_3-h_5\right)^3+\left(\frac{h_3+h_5}{2}\right)^2\bar{\mathbf{Q}}_B^{\text{cont}}\bar{\boldsymbol{\alpha}}_B\left(h_3-h_5\right)=\frac{1}{3}\bar{\mathbf{Q}}_B^{\text{cont}}\bar{\boldsymbol{\alpha}}_B\left(h_3^3-h_5^3\right) \tag{3.92}$$

Then, as discussed in Section 3, the contributions of the blade and the face sheet to the panel thermal ABD terms can be added to yield the effective panel thermal ABD terms (since the blade and face sheet terms are now known with respect to the same reference plane). Thus,

$$\mathbf{A}_{\text{panel}}^{\alpha} = \mathbf{A}_{\text{FS}}^{\alpha}+\bar{\mathbf{Q}}_B^{\text{cont}}\bar{\boldsymbol{\alpha}}_B\left(h_3-h_5\right) \tag{3.93}$$

$$\mathbf{B}_{\text{panel}}^{\alpha} = \mathbf{B}_{\text{FS}}^{\alpha}+\frac{1}{2}\bar{\mathbf{Q}}_B^{\text{cont}}\bar{\boldsymbol{\alpha}}_B\left(h_3^2-h_5^2\right) \tag{3.94}$$

$$\mathbf{D}_{\text{panel}}^{\alpha} = \mathbf{D}_{\text{FS}}^{\alpha}+\frac{1}{3}\bar{\mathbf{Q}}_B^{\text{cont}}\bar{\boldsymbol{\alpha}}_B\left(h_3^3-h_5^3\right) \tag{3.95}$$

where $\mathbf{A}_{\text{FS}}^{\alpha}$, $\mathbf{B}_{\text{FS}}^{\alpha}$, and $\mathbf{D}_{\text{FS}}^{\alpha}$ are the face sheet laminate thermal ABD matrices.

A similar treatment applies to the thermo-electro-magnetic terms. The decoupling of the blade from the panel thermo-electro-magnetic response indicates that only the *x*-direction electric, magnetic, thermo-electric, and thermo-magnetic expansion of the blade will have an effect. Thus, the effective piezoelectric, piezomagnetic, pyroelectric and pyromagnetic coefficients (in the blade coordinate system, Fig. 18) assigned to the blade for its thermo-electro-magnetic contributions are,

$$\bar{\mathbf{e}}_B = \begin{bmatrix} \bar{e}_{11}^B & \bar{e}_{21}^B & \bar{e}_{31}^B \\ 0 & 0 & 0 \\ 0 & 0 & 0 \\ 0 & 0 & 0 \\ 0 & 0 & 0 \\ 0 & 0 & 0 \end{bmatrix} \tag{3.96}$$

$$\overline{\mathbf{q}}_B = \begin{bmatrix} \overline{q}_{11}^B & \overline{q}_{21}^B & \overline{q}_{31}^B \\ 0 & 0 & 0 \\ 0 & 0 & 0 \\ 0 & 0 & 0 \\ 0 & 0 & 0 \\ 0 & 0 & 0 \end{bmatrix} \tag{3.97}$$

$$\overline{\zeta}_B = \begin{bmatrix} \overline{\zeta}_1^B \\ 0 \\ 0 \end{bmatrix} \tag{3.98}$$

$$\overline{\psi}_B = \begin{bmatrix} \overline{\psi}_1^B \\ 0 \\ 0 \end{bmatrix} \tag{3.99}$$

where $\overline{e}_{ij}^B$, $\overline{q}_{ij}^B$, $\overline{\zeta}_1^B$, and $\overline{\psi}_1^B$ are the effective piezoelectric, piezomagnetic, pyroelectric, and pyromagnetic coefficients, respectively, that influence the x-direction. In Eq. (3.83) the following identifications can be made,

$$\begin{bmatrix} \mathbf{A}^0 & \mathbf{B}^0 \\ \mathbf{B}^0 & \mathbf{D}^0 \end{bmatrix}^{-1} \begin{bmatrix} \mathbf{A}_0^E \\ \mathbf{B}_0^E \end{bmatrix} = \begin{bmatrix} \mathbf{e}_{\text{lam}} \\ \mathbf{e}_{\text{lam}}^{\text{coupling}} \end{bmatrix} \tag{3.100}$$

$$\begin{bmatrix} \mathbf{A}^0 & \mathbf{B}^0 \\ \mathbf{B}^0 & \mathbf{D}^0 \end{bmatrix}^{-1} \begin{bmatrix} \mathbf{A}_0^M \\ \mathbf{B}_0^M \end{bmatrix} = \begin{bmatrix} \mathbf{q}_{\text{lam}} \\ \mathbf{q}_{\text{lam}}^{\text{coupling}} \end{bmatrix} \tag{3.101}$$

$$\begin{bmatrix} \mathbf{A}^0 & \mathbf{B}^0 \\ \mathbf{B}^0 & \mathbf{D}^0 \end{bmatrix}^{-1} \begin{bmatrix} \mathbf{A}_0^{ET} & \mathbf{B}_0^{ET} \\ \mathbf{B}_0^{ET} & \mathbf{D}_0^{ET} \end{bmatrix} = \begin{bmatrix} \boldsymbol{\alpha}\mathbf{e}_{\text{lam}} & \boldsymbol{\delta}\mathbf{e}_{\text{lam}}^{\text{coupling}} \\ \boldsymbol{\alpha}\mathbf{e}_{\text{lam}}^{\text{coupling}} & \boldsymbol{\delta}\mathbf{e}_{\text{lam}} \end{bmatrix} \tag{3.102}$$

$$\begin{bmatrix} \mathbf{A}^0 & \mathbf{B}^0 \\ \mathbf{B}^0 & \mathbf{D}^0 \end{bmatrix}^{-1} \begin{bmatrix} \mathbf{A}_0^{MT} & \mathbf{B}_0^{MT} \\ \mathbf{B}_0^{MT} & \mathbf{D}_0^{MT} \end{bmatrix} = \begin{bmatrix} \boldsymbol{\alpha}\mathbf{q}_{\text{lam}} & \boldsymbol{\delta}\mathbf{q}_{\text{lam}}^{\text{coupling}} \\ \boldsymbol{\alpha}\mathbf{q}_{\text{lam}}^{\text{coupling}} & \boldsymbol{\delta}\mathbf{q}_{\text{lam}} \end{bmatrix} \tag{3.103}$$

where $\mathbf{e}_{\text{lam}}$ and $\mathbf{q}_{\text{lam}}$ are 3×3 matrices relating strain to electric and magnetic field, respectively, $\mathbf{e}_{\text{lam}}^{\text{coupling}}$ and $\mathbf{q}_{\text{lam}}^{\text{coupling}}$ are 3×3 matrices relating curvature to electric and magnetic field, respectively, $\boldsymbol{\alpha}\mathbf{e}_{\text{lam}}$ and $\boldsymbol{\alpha}\mathbf{q}_{\text{lam}}$ are 3×1 vectors relating strain to temperature changes (due to thermo-electric and thermo-magnetic coupling, respectively), $\boldsymbol{\alpha}\mathbf{e}_{\text{lam}}^{\text{coupling}}$ and $\boldsymbol{\alpha}\mathbf{q}_{\text{lam}}^{\text{coupling}}$ are 3×1 matrices relating curvature to temperature change (due to thermo-electric and thermo-magnetic coupling, respectively), $\boldsymbol{\delta}\mathbf{e}_{\text{lam}}^{\text{coupling}}$ and $\boldsymbol{\delta}\mathbf{q}_{\text{lam}}^{\text{coupling}}$ are 3×1

matrices relating strain to through-thickness temperature gradient (due to thermo-electric and thermo-magnetic coupling, respectively), and $\boldsymbol{\delta}\mathbf{e}_{\text{lam}}$ and $\boldsymbol{\delta}\mathbf{q}_{\text{lam}}$ are 3×1 matrices relating curvature to through-thickness temperature gradient (due to thermo-electric and thermo-magnetic coupling, respectively).

As was the case for the blade thermal expansion coeffients, the thermo-electro-magnetic coefficients present in Eqs. (3.96 – 3.99) can be extracted from Eqs. (3.100 – 3.103). The $\bar{e}_{ij}^{B}$ and $\bar{q}_{ij}^{B}$ terms are simply the first rows of the $\mathbf{e}_{\text{lam}}$ matrix and the $\mathbf{q}_{\text{lam}}$ matrix, respectively, while $\bar{\zeta}_{1}^{B}$, and $\bar{\psi}_{1}^{B}$ are simply the first term in the $\boldsymbol{\alpha}\mathbf{e}_{\text{lam}}$ and $\boldsymbol{\alpha}\mathbf{q}_{\text{lam}}$ vectors.

Employing Eqs. (3.38, 3.40, 3.47, 3.48), the blade contributions to the panel electric, magnetic, thermo-electric, and thermo-magnetic ABD terms with respect to the blade's midplane (see Fig. 18) are given by,

$$\left(\mathbf{A}_{B}^{E}\right)^{0}=\bar{\mathbf{Q}}_{B}^{\text{cont}}\,\bar{\mathbf{e}}_{B}\left[-\frac{h_5-h_3}{2}-\frac{h_5-h_3}{2}\right]=\bar{\mathbf{Q}}_{B}^{\text{cont}}\,\bar{\mathbf{e}}_{B}\left(h_3-h_5\right) \tag{3.104}$$

$$\left(\mathbf{B}_{B}^{E}\right)^{0}=-\frac{1}{2}\bar{\mathbf{Q}}_{B}^{\text{cont}}\,\bar{\mathbf{e}}_{B}\left[\left(-\frac{h_5-h_3}{2}\right)^{2}-\left(\frac{h_5-h_3}{2}\right)^{2}\right]=0 \tag{3.105}$$

$$\left(\mathbf{A}_{B}^{M}\right)^{0}=\bar{\mathbf{Q}}_{B}^{\text{cont}}\,\bar{\mathbf{q}}_{B}\left[-\frac{h_5-h_3}{2}-\frac{h_5-h_3}{2}\right]=\bar{\mathbf{Q}}_{B}^{\text{cont}}\,\bar{\mathbf{q}}_{B}\left(h_3-h_5\right) \tag{3.106}$$

$$\left(\mathbf{B}_{B}^{M}\right)^{0}=-\frac{1}{2}\bar{\mathbf{Q}}_{B}^{\text{cont}}\,\bar{\mathbf{q}}_{B}\left[\left(-\frac{h_5-h_3}{2}\right)^{2}-\left(\frac{h_5-h_3}{2}\right)^{2}\right]=0 \tag{3.107}$$

$$\left(\mathbf{A}_{B}^{ET}\right)^{0}=\bar{\mathbf{Q}}_{B}^{\text{cont}}\,\bar{\zeta}_{B}\left[-\frac{h_5-h_3}{2}-\frac{h_5-h_3}{2}\right]=\bar{\mathbf{Q}}_{B}^{\text{cont}}\,\bar{\zeta}_{B}\left(h_3-h_5\right) \tag{3.108}$$

$$\left(\mathbf{B}_{B}^{ET}\right)^{0}=-\frac{1}{2}\bar{\mathbf{Q}}_{B}^{\text{cont}}\,\bar{\zeta}_{B}\left[\left(-\frac{h_5-h_3}{2}\right)^{2}-\left(\frac{h_5-h_3}{2}\right)^{2}\right]=0 \tag{3.109}$$

$$\left(\mathbf{D}_{B}^{ET}\right)^{0}=\frac{1}{3}\bar{\mathbf{Q}}_{B}^{\text{cont}}\,\bar{\zeta}_{B}\left[\left(-\frac{h_5-h_3}{2}\right)^{3}-\left(\frac{h_5-h_3}{2}\right)^{3}\right]=\frac{1}{12}\bar{\mathbf{Q}}_{B}^{\text{cont}}\,\bar{\zeta}_{B}\left(h_3-h_5\right)^{3} \tag{3.110}$$

$$\left(\mathbf{A}_{B}^{MT}\right)^{0}=\bar{\mathbf{Q}}_{B}^{\text{cont}}\,\bar{\psi}_{B}\left[-\frac{h_5-h_3}{2}-\frac{h_5-h_3}{2}\right]=\bar{\mathbf{Q}}_{B}^{\text{cont}}\,\bar{\psi}_{B}\left(h_3-h_5\right) \tag{3.111}$$

$$\left(\mathbf{B}_{B}^{MT}\right)^{0}=-\frac{1}{2}\bar{\mathbf{Q}}_{B}^{\text{cont}}\,\bar{\psi}_{B}\left[\left(-\frac{h_5-h_3}{2}\right)^{2}-\left(\frac{h_5-h_3}{2}\right)^{2}\right]=0 \tag{3.112}$$

$$\left(\mathbf{D}_{B}^{MT}\right)^{0}=\frac{1}{3}\bar{\mathbf{Q}}_{B}^{\text{cont}}\,\bar{\psi}_{B}\left[\left(-\frac{h_5-h_3}{2}\right)^{3}-\left(\frac{h_5-h_3}{2}\right)^{3}\right]=\frac{1}{12}\bar{\mathbf{Q}}_{B}^{\text{cont}}\,\bar{\psi}_{B}\left(h_3-h_5\right)^{3} \tag{3.113}$$

Shifting these terms to the midplane of the face sheet, which serves as the reference plane for the panel, using Eqs. (3.50, 3.51) with $\Delta z=\frac{h_5+h_3}{2}$ yields,

$$\left(\mathbf{A}_B^E\right)^{\text{cont}} = \bar{\mathbf{Q}}_B^{\text{cont}}\,\bar{\mathbf{e}}_B\left(h_3 - h_5\right) \tag{3.114}$$

$$\left(\mathbf{B}_B^E\right)^{\text{cont}} = \frac{h_3 + h_5}{2}\bar{\mathbf{Q}}_B^{\text{cont}}\,\bar{\mathbf{e}}_B\left(h_3 - h_5\right) = \frac{1}{2}\bar{\mathbf{Q}}_B^{\text{cont}}\,\bar{\mathbf{e}}_B\left(h_3^2 - h_5^2\right) \tag{3.115}$$

$$\left(\mathbf{A}_B^M\right)^{\text{cont}} = \bar{\mathbf{Q}}_B^{\text{cont}}\,\bar{\mathbf{q}}_B\left(h_3 - h_5\right) \tag{3.116}$$

$$\left(\mathbf{B}_B^M\right)^{\text{cont}} = \frac{h_3 + h_5}{2}\bar{\mathbf{Q}}_B^{\text{cont}}\,\bar{\mathbf{q}}_B\left(h_3 - h_5\right) = \frac{1}{2}\bar{\mathbf{Q}}_B^{\text{cont}}\,\bar{\mathbf{q}}_B\left(h_3^2 - h_5^2\right) \tag{3.117}$$

$$\left(\mathbf{A}_B^{ET}\right)^{\text{cont}} = \bar{\mathbf{Q}}_B^{\text{cont}}\,\bar{\boldsymbol{\zeta}}_B\left(h_3 - h_5\right) \tag{3.118}$$

$$\left(\mathbf{B}_B^{ET}\right)^{\text{cont}} = \frac{h_3 + h_5}{2}\bar{\mathbf{Q}}_B^{\text{cont}}\,\bar{\boldsymbol{\zeta}}_B\left(h_3 - h_5\right) = \frac{1}{2}\bar{\mathbf{Q}}_B^{\text{cont}}\,\bar{\boldsymbol{\zeta}}_B\left(h_3^2 - h_5^2\right) \tag{3.119}$$

$$\left(\mathbf{D}_B^{ET}\right)^{\text{cont}} = \frac{1}{12}\bar{\mathbf{Q}}_B^{\text{cont}}\,\bar{\boldsymbol{\zeta}}_B\left(h_3 - h_5\right)^3 + \left(\frac{h_3 + h_5}{2}\right)^2\bar{\mathbf{Q}}_B^{\text{cont}}\,\bar{\boldsymbol{\zeta}}_B\left(h_3 - h_5\right) = \frac{1}{3}\bar{\mathbf{Q}}_B^{\text{cont}}\,\bar{\boldsymbol{\alpha}}_B\left(h_3^3 - h_5^3\right) \tag{3.120}$$

$$\left(\mathbf{A}_B^{MT}\right)^{\text{cont}} = \bar{\mathbf{Q}}_B^{\text{cont}}\,\bar{\boldsymbol{\psi}}_B\left(h_3 - h_5\right) \tag{3.121}$$

$$\left(\mathbf{B}_B^{MT}\right)^{\text{cont}} = \frac{h_3 + h_5}{2}\bar{\mathbf{Q}}_B^{\text{cont}}\,\bar{\boldsymbol{\psi}}_B\left(h_3 - h_5\right) = \frac{1}{2}\bar{\mathbf{Q}}_B^{\text{cont}}\,\bar{\boldsymbol{\psi}}_B\left(h_3^2 - h_5^2\right) \tag{3.122}$$

$$\left(\mathbf{D}_B^{MT}\right)^{\text{cont}} = \frac{1}{12}\bar{\mathbf{Q}}_B^{\text{cont}}\,\bar{\boldsymbol{\psi}}_B\left(h_3 - h_5\right)^3 + \left(\frac{h_3 + h_5}{2}\right)^2\bar{\mathbf{Q}}_B^{\text{cont}}\,\bar{\boldsymbol{\psi}}_B\left(h_3 - h_5\right) = \frac{1}{3}\bar{\mathbf{Q}}_B^{\text{cont}}\,\bar{\boldsymbol{\alpha}}_B\left(h_3^3 - h_5^3\right) \tag{3.123}$$

Then, as discussed in Section 3, the contributions of the blade and the face sheet to the panel electric, magnetic, thermo-electric, and thermo-magnetic ABD terms can be added to yield the corresponding effective panel ABD terms (since the blade and face sheet terms are now known with respect to the same reference plane). Thus,

$$\mathbf{A}_{\text{panel}}^E = \mathbf{A}_{\text{FS}}^E + \bar{\mathbf{Q}}_B^{\text{cont}}\,\bar{\mathbf{e}}_B\left(h_3 - h_5\right) \tag{3.124}$$

$$\mathbf{B}_{\text{panel}}^E = \mathbf{B}_{\text{FS}}^E + \frac{1}{2}\bar{\mathbf{Q}}_B^{\text{cont}}\,\bar{\mathbf{e}}_B\left(h_3^2 - h_5^2\right) \tag{3.125}$$

$$\mathbf{A}_{\text{panel}}^M = \mathbf{A}_{\text{FS}}^M + \bar{\mathbf{Q}}_B^{\text{cont}}\,\bar{\mathbf{q}}_B\left(h_3 - h_5\right) \tag{3.126}$$

$$\mathbf{B}_{\text{panel}}^M = \mathbf{B}_{\text{FS}}^M + \frac{1}{2}\bar{\mathbf{Q}}_B^{\text{cont}}\,\bar{\mathbf{q}}_B\left(h_3^2 - h_5^2\right) \tag{3.127}$$

$$\mathbf{A}_{\text{panel}}^{ET} = \mathbf{A}_{\text{FS}}^{ET} + \bar{\mathbf{Q}}_B^{\text{cont}}\,\bar{\boldsymbol{\zeta}}_B\left(h_3 - h_5\right) \tag{3.128}$$

$$\mathbf{B}_{\text{panel}}^{ET} = \mathbf{B}_{\text{FS}}^{ET} + \frac{1}{2}\bar{\mathbf{Q}}_B^{\text{cont}}\,\bar{\boldsymbol{\zeta}}_B\left(h_3^2 - h_5^2\right) \tag{3.129}$$

$$\mathbf{D}_{\text{panel}}^{ET} = \mathbf{D}_{\text{FS}}^{ET} + \frac{1}{3}\bar{\mathbf{Q}}_B^{\text{cont}}\,\bar{\boldsymbol{\zeta}}_B\left(h_3^3 - h_5^3\right) \tag{3.130}$$

$$\mathbf{A}_{\text{panel}}^{MT} = \mathbf{A}_{\text{FS}}^{MT} + \bar{\mathbf{Q}}_B^{\text{cont}}\,\bar{\boldsymbol{\psi}}_B\left(h_3 - h_5\right) \tag{3.131}$$

$$\mathbf{B}_{\text{panel}}^{MT} = \mathbf{B}_{\text{FS}}^{MT} + \frac{1}{2}\bar{\mathbf{Q}}_B^{\text{cont}}\,\bar{\boldsymbol{\psi}}_B\left(h_3^2 - h_5^2\right) \tag{3.132}$$

$$\mathbf{D}^{MI}_{\text{panel}} = \mathbf{D}^{MI}_{\text{FS}} + \frac{1}{3}\bar{\mathbf{Q}}^{\text{cont}}_{B}\,\bar{\Psi}_{B}\left(h_3^3 - h_5^3\right) \tag{3.133}$$

where $\mathbf{A}^{\bullet}_{\text{FS}}$, $\mathbf{B}^{\bullet}_{\text{FS}}$, and $\mathbf{D}^{\bullet}_{\text{FS}}$ are the face sheet laminate electric, magnetic, thermo-electric, and thermo-magnetic ABD matrices.

It should be noted that if the blade stiffened panel includes a bottom face sheet, its contribution can be included by simply shifting its mechanical, thermal, electric, magnetic, thermo-electric, and thermo-magnetic ABD terms to the face sheet midplane according to Eqs. (3.9 – 3.11, 3.21, 3.23, 3.27, 3.50, 3.51) and adding these shifted terms to the corresponding panel ABD terms.

Analysis of Panels with Flanged Stiffeners

Considering a flanged stiffened panel, as shown in Fig. 19, the outlined region is referred to as "Segment 8". Comparing Fig. 19 to Fig. 18, it is clear that the only difference between the flanged stiffened panel and the blade stiffened panel is the presence of the flange. Thus, the development of effective ABD terms for the flanged stiffened panel necessitates only the additional analysis of Segment 8. As shown in Fig. 20, Segment 8 is composed of two other segments, Segments 1 and 6.

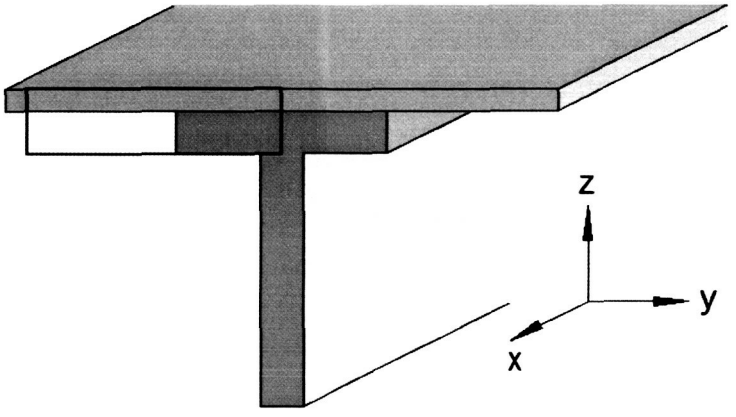

Fig. 19. A flanged stiffened panel with the segment 8 region outlined.

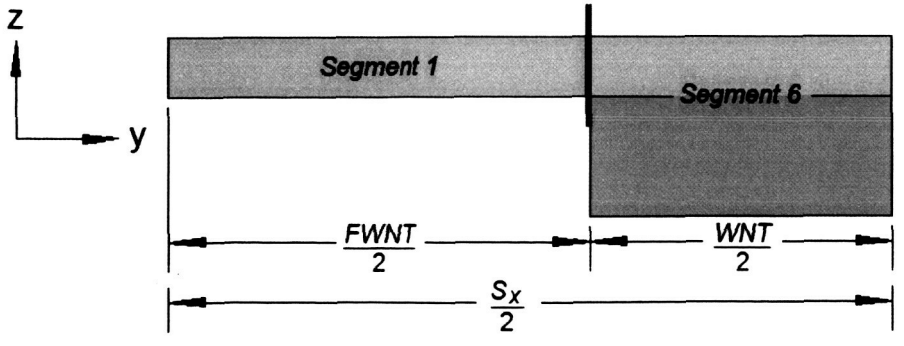

Fig. 20. The Segment 8 region divided into Segments 1 and 6.

In the x-direction, which is the direction of the stiffener (and thus the strong direction), iso-strain and iso-curvature conditions are employed. It is further assumed that the homogenized Segment 8 x-direction force and moment resultants are the sum of the volume-weighted x-direction force and moment resultants of the constituent segments (Segment 1 and 6). This is analogous to the "mechanics of materials" micromechanics approach presented by Herakovich (1998) that homogenizes continuous fiber composites to obtain effective properties. The conditions employed for the stiffener direction are,

$$\left(\varepsilon_{xx}^{0}\right)^{1} = \left(\varepsilon_{xx}^{0}\right)^{6} = \left(\varepsilon_{xx}^{0}\right)^{8} \tag{3.134}$$

$$\left(\kappa_{xx}\right)^{1} = \left(\kappa_{xx}\right)^{6} = \left(\kappa_{xx}\right)^{8} \tag{3.135}$$

$$\left(N_{xx}\right)^{8} = \frac{1}{S_x}\left[\left(FWNT\right)\left(N_{xx}\right)^{1} + \left(WNT\right)\left(N_{xx}\right)^{6}\right] \tag{3.136}$$

$$\left(M_{xx}\right)^{8} = \frac{1}{S_x}\left[\left(FWNT\right)\left(M_{xx}\right)^{1} + \left(WNT\right)\left(M_{xx}\right)^{6}\right] \tag{3.137}$$

where Sx is the stiffener spacing, $FWNT$ is the distance between flanges, and WNT is the flange width.

In the y-direction and for the in plane shear effect (xy-components), the converse assumptions are employed. That is, iso-force and moment resultant conditions are imposed, along with volume-weighted summing for the strain and curvature components. These conditions are,

$$\left(N_{yy}\right)^{1} = \left(N_{yy}\right)^{6} = \left(N_{yy}\right)^{8} \tag{3.138}$$

$$\left(N_{xy}\right)^{1} = \left(N_{xy}\right)^{6} = \left(N_{xy}\right)^{8} \tag{3.139}$$

$$\left(M_{yy}\right)^{1} = \left(M_{yy}\right)^{6} = \left(M_{yy}\right)^{8} \tag{3.140}$$

$$\left(M_{xy}\right)^{1} = \left(M_{xy}\right)^{6} = \left(M_{xy}\right)^{8} \tag{3.141}$$

$$\left(\varepsilon_{yy}^{0}\right)^{8} = \frac{1}{S_x}\left[\left(FWNT\right)\left(\varepsilon_{yy}^{0}\right)^{1} + \left(WNT\right)\left(\varepsilon_{yy}^{0}\right)^{6}\right] \tag{3.142}$$

$$\left(\gamma_{xy}^{0}\right)^{8} = \frac{1}{S_x}\left[\left(FWNT\right)\left(\gamma_{xy}^{0}\right)^{1} + \left(WNT\right)\left(\gamma_{xy}^{0}\right)^{6}\right] \tag{3.143}$$

$$\left(\kappa_{xx}\right)^{8} = \frac{1}{S_x}\left[\left(FWNT\right)\left(\kappa_{xx}\right)^{1} + \left(WNT\right)\left(\kappa_{xx}\right)^{6}\right] \tag{3.144}$$

$$\left(\kappa_{xy}\right)^{8} = \frac{1}{S_x}\left[\left(FWNT\right)\left(\kappa_{xy}\right)^{1} + \left(WNT\right)\left(\kappa_{xy}\right)^{6}\right] \tag{3.145}$$

The constitutive equation for each segment is given by,

$$\begin{bmatrix} N_{xx} \\ N_{yy} \\ N_{xy} \\ M_{xx} \\ M_{yy} \\ M_{xy} \end{bmatrix} = \begin{bmatrix} \mathbf{A} & \mathbf{B} \\ \mathbf{B}^{\mathrm{T}} & \mathbf{D} \end{bmatrix} \begin{bmatrix} \varepsilon_{xx}^{0} \\ \varepsilon_{yy}^{0} \\ \gamma_{xy}^{0} \\ \kappa_{xx} \\ \kappa_{yy} \\ \kappa_{xy} \end{bmatrix} - \begin{bmatrix} \mathbf{A}^{\alpha} & \mathbf{B}^{\alpha} \\ \mathbf{B}^{\alpha} & \mathbf{D}^{\alpha} \end{bmatrix} \begin{bmatrix} \Delta T \\ -\Delta G \end{bmatrix} - \begin{bmatrix} \mathbf{A}^{E} \\ \mathbf{B}^{E} \end{bmatrix} \begin{bmatrix} E_1 \\ E_2 \\ E_3 \end{bmatrix} - \begin{bmatrix} \mathbf{A}^{M} \\ \mathbf{B}^{M} \end{bmatrix} \begin{bmatrix} H_1 \\ H_2 \\ H_3 \end{bmatrix} - \begin{bmatrix} \mathbf{A}^{ET} & \mathbf{B}^{ET} \\ \mathbf{B}^{ET} & \mathbf{D}^{ET} \end{bmatrix} \begin{bmatrix} \Delta T \\ -\Delta G \end{bmatrix} - \begin{bmatrix} \mathbf{A}^{MT} & \mathbf{B}^{MT} \\ \mathbf{B}^{MT} & \mathbf{D}^{MT} \end{bmatrix} \begin{bmatrix} \Delta T \\ -\Delta G \end{bmatrix} \tag{3.146}$$

where $\mathbf{B}^{\mathrm{T}}$ is the transpose of the **B** matrix, which is necessary because the **B** matrix itself is typically asymmetric for Segment 8 (although the ABD matrix remains symmetric). The equations are rearranged such that all components that fall under the iso- assumptions appear on the left hand side,

$$\begin{bmatrix} \varepsilon_{xx}^{0} \\ N_{yy} \\ N_{xy} \\ \kappa_{xx} \\ M_{yy} \\ M_{xy} \end{bmatrix} = \begin{bmatrix} \hat{\mathbf{C}} \end{bmatrix} \begin{bmatrix} N_{xx} \\ \varepsilon_{yy}^{0} \\ \gamma_{xy}^{0} \\ M_{xx} \\ \kappa_{yy} \\ \kappa_{xy} \end{bmatrix} - \begin{bmatrix} \hat{\mathbf{C}}^{\alpha} \end{bmatrix} \begin{bmatrix} \Delta T \\ -\Delta G \end{bmatrix} - \begin{bmatrix} \hat{\mathbf{C}}^{E} \end{bmatrix} \begin{bmatrix} E_1 \\ E_2 \\ E_3 \end{bmatrix} - \begin{bmatrix} \hat{\mathbf{C}}^{M} \end{bmatrix} \begin{bmatrix} H_1 \\ H_2 \\ H_3 \end{bmatrix} - \begin{bmatrix} \hat{\mathbf{C}}^{ET} \end{bmatrix} \begin{bmatrix} \Delta T \\ -\Delta G \end{bmatrix} - \begin{bmatrix} \hat{\mathbf{C}}^{MT} \end{bmatrix} \begin{bmatrix} \Delta T \\ -\Delta G \end{bmatrix} \tag{3.147}$$

or, in simplified notation,

$$(\mathbf{R}_{\mathbf{A}}) = \begin{bmatrix} \hat{\mathbf{C}} \end{bmatrix} (\mathbf{R}_{\mathbf{B}}) - \begin{bmatrix} \hat{\mathbf{C}}^{\alpha} \end{bmatrix} \begin{bmatrix} \Delta T \\ -\Delta G \end{bmatrix} - \begin{bmatrix} \hat{\mathbf{C}}^{E} \end{bmatrix} \begin{bmatrix} E_1 \\ E_2 \\ E_3 \end{bmatrix} - \begin{bmatrix} \hat{\mathbf{C}}^{M} \end{bmatrix} \begin{bmatrix} H_1 \\ H_2 \\ H_3 \end{bmatrix} - \begin{bmatrix} \hat{\mathbf{C}}^{ET} \end{bmatrix} \begin{bmatrix} \Delta T \\ -\Delta G \end{bmatrix} - \begin{bmatrix} \hat{\mathbf{C}}^{MT} \end{bmatrix} \begin{bmatrix} \Delta T \\ -\Delta G \end{bmatrix} \tag{3.148}$$

where the hatted matrices represent ABD matrices altered via the rearrangement required in forming Eq. (3.147) from Eq. (3.146). Solving Eq. (3.148) for $\mathbf{R}_{\mathbf{B}}$ yields,

$$(\mathbf{R}_{\mathbf{B}}) = \begin{bmatrix} \hat{\mathbf{C}} \end{bmatrix}^{-1} \left\{ (\mathbf{R}_{\mathbf{A}}) + \begin{bmatrix} \hat{\mathbf{C}}^{\alpha} \end{bmatrix} \begin{bmatrix} \Delta T \\ -\Delta G \end{bmatrix} + \begin{bmatrix} \hat{\mathbf{C}}^{E} \end{bmatrix} \begin{bmatrix} E_1 \\ E_2 \\ E_3 \end{bmatrix} + \begin{bmatrix} \hat{\mathbf{C}}^{M} \end{bmatrix} \begin{bmatrix} H_1 \\ H_2 \\ H_3 \end{bmatrix} + \begin{bmatrix} \hat{\mathbf{C}}^{ET} \end{bmatrix} \begin{bmatrix} \Delta T \\ -\Delta G \end{bmatrix} + \begin{bmatrix} \hat{\mathbf{C}}^{MT} \end{bmatrix} \begin{bmatrix} \Delta T \\ -\Delta G \end{bmatrix} \right\} \tag{3.149}$$

Now, employing the above simplified notation, all of the iso- assumptions can be expressed as,

$$(\mathbf{R}_{\mathbf{A}})^{1} = (\mathbf{R}_{\mathbf{A}})^{6} = (\mathbf{R}_{\mathbf{A}})^{8} \tag{3.150}$$

while all of the volume-weighted summation assumptions can be expressed as,

$$(\mathbf{R}_{\mathbf{B}})^{8} = \frac{1}{S_x} \left[(FWNT)(\mathbf{R}_{\mathbf{B}})^{1} + (WNT)(\mathbf{R}_{\mathbf{B}})^{6} \right] \tag{3.151}$$

The $\mathbf{R_B}$ vector for each segment in Eq. (3.151) can be replaced with the expression from Eq. (3.149),

$$S_x\left[\hat{\mathbf{C}}^8\right]^{-1}\left\{(\mathbf{R_A})+\left[\hat{\mathbf{C}}^{\alpha 8}\right]\begin{bmatrix}\Delta T\\ -\Delta G\end{bmatrix}+\left[\hat{\mathbf{C}}^{E8}\right]\begin{bmatrix}E_1\\ E_2\\ E_3\end{bmatrix}+\left[\hat{\mathbf{C}}^{M8}\right]\begin{bmatrix}H_1\\ H_2\\ H_3\end{bmatrix}+\left[\hat{\mathbf{C}}^{ET8}\right]\begin{bmatrix}\Delta T\\ -\Delta G\end{bmatrix}+\left[\hat{\mathbf{C}}^{MT8}\right]\begin{bmatrix}\Delta T\\ -\Delta G\end{bmatrix}\right\}=$$

$$(FWNT)\left[\hat{\mathbf{C}}^1\right]^{-1}\left\{(\mathbf{R_A})+\left[\hat{\mathbf{C}}^{\alpha 1}\right]\begin{bmatrix}\Delta T\\ -\Delta G\end{bmatrix}+\left[\hat{\mathbf{C}}^{E1}\right]\begin{bmatrix}E_1\\ E_2\\ E_3\end{bmatrix}+\left[\hat{\mathbf{C}}^{M1}\right]\begin{bmatrix}H_1\\ H_2\\ H_3\end{bmatrix}+\left[\hat{\mathbf{C}}^{ET1}\right]\begin{bmatrix}\Delta T\\ -\Delta G\end{bmatrix}+\left[\hat{\mathbf{C}}^{MT1}\right]\begin{bmatrix}\Delta T\\ -\Delta G\end{bmatrix}\right\}$$

$$+(WNT)\left[\hat{\mathbf{C}}^6\right]^{-1}\left\{(\mathbf{R_A})+\left[\hat{\mathbf{C}}^{\alpha 6}\right]\begin{bmatrix}\Delta T\\ -\Delta G\end{bmatrix}+\left[\hat{\mathbf{C}}^{E6}\right]\begin{bmatrix}E_1\\ E_2\\ E_3\end{bmatrix}+\left[\hat{\mathbf{C}}^{M6}\right]\begin{bmatrix}H_1\\ H_2\\ H_3\end{bmatrix}+\left[\hat{\mathbf{C}}^{ET6}\right]\begin{bmatrix}\Delta T\\ -\Delta G\end{bmatrix}+\left[\hat{\mathbf{C}}^{MT6}\right]\begin{bmatrix}\Delta T\\ -\Delta G\end{bmatrix}\right\} \tag{3.152}$$

Each effect present in Eq. (3.152) can be isolated by considering the case when only it is active. That is, if we assume that the panel has only mechanical loading and no thermal, electric, or magnetic loading, Eq. (3.152) simplifies to,

$$S_x\left[\hat{\mathbf{C}}^8\right]^{-1}(\mathbf{R_A})=(FWNT)\left[\hat{\mathbf{C}}^1\right]^{-1}(\mathbf{R_A})+(WNT)\left[\hat{\mathbf{C}}^6\right]^{-1}(\mathbf{R_A}) \tag{3.153}$$

or,

$$\left[\hat{\mathbf{C}}^8\right]^{-1}=\frac{1}{S_x}\left\{(FWNT)\left[\hat{\mathbf{C}}^1\right]^{-1}+(WNT)\left[\hat{\mathbf{C}}^6\right]^{-1}\right\} \tag{3.154}$$

Then, inverting Eq. (3.153) provides $\hat{\mathbf{C}}^8$, and rearranging the terms (see below) provides the homogenized ABD matrix for Segment 8.

For the thermal, electric, magnetic, thermo-electric, and thermo-magnetic terms appearing in Eq. (3.152), we have,

Thermal

$$S_x\left[\hat{\mathbf{C}}^8\right]^{-1}\left[\hat{\mathbf{C}}^{\alpha 8}\right]\begin{bmatrix}\Delta T\\ -\Delta G\end{bmatrix}=(FWNT)\left[\hat{\mathbf{C}}^1\right]^{-1}\left[\hat{\mathbf{C}}^{\alpha 1}\right]\begin{bmatrix}\Delta T\\ -\Delta G\end{bmatrix}+(WNT)\left[\hat{\mathbf{C}}^6\right]^{-1}\left[\hat{\mathbf{C}}^{\alpha 6}\right]\begin{bmatrix}\Delta T\\ -\Delta G\end{bmatrix} \tag{3.155}$$

or

$$\left[\hat{\mathbf{C}}^{\alpha 8}\right]=\frac{1}{S_x}\left[\hat{\mathbf{C}}^8\right]\left\{(FWNT)\left[\hat{\mathbf{C}}^1\right]^{-1}\left[\hat{\mathbf{C}}^{\alpha 1}\right]+(WNT)\left[\hat{\mathbf{C}}^6\right]^{-1}\left[\hat{\mathbf{C}}^{\alpha 6}\right]\right\} \tag{3.156}$$

Electric

$$S_x\left[\hat{\mathbf{C}}^8\right]^{-1}\left[\hat{\mathbf{C}}^{E8}\right]\begin{bmatrix}E_1\\ E_2\\ E_3\end{bmatrix}=(FWNT)\left[\hat{\mathbf{C}}^1\right]^{-1}\left[\hat{\mathbf{C}}^{E1}\right]\begin{bmatrix}E_1\\ E_2\\ E_3\end{bmatrix}+(WNT)\left[\hat{\mathbf{C}}^6\right]^{-1}\left[\hat{\mathbf{C}}^{E6}\right]\begin{bmatrix}E_1\\ E_2\\ E_3\end{bmatrix} \tag{3.157}$$

or

$$\left[\hat{\mathbf{C}}^{E^8}\right]=\frac{1}{S_x}\left[\hat{\mathbf{C}}^8\right]\left\{(FWNT)\left[\hat{\mathbf{C}}^1\right]^{-1}\left[\hat{\mathbf{C}}^{E^1}\right]+(WNT)\left[\hat{\mathbf{C}}^6\right]^{-1}\left[\hat{\mathbf{C}}^{E^6}\right]\right\} \tag{3.158}$$

Magnetic

$$S_x\left[\hat{\mathbf{C}}^8\right]^{-1}\left[\hat{\mathbf{C}}^{M^8}\right]\begin{bmatrix}H_1\\H_2\\H_3\end{bmatrix}=(FWNT)\left[\hat{\mathbf{C}}^1\right]^{-1}\left[\hat{\mathbf{C}}^{M^1}\right]\begin{bmatrix}H_1\\H_2\\H_3\end{bmatrix}+(WNT)\left[\hat{\mathbf{C}}^6\right]^{-1}\left[\hat{\mathbf{C}}^{M^6}\right]\begin{bmatrix}H_1\\H_2\\H_3\end{bmatrix} \tag{3.159}$$

or

$$\left[\hat{\mathbf{C}}^{M^8}\right]=\frac{1}{S_x}\left[\hat{\mathbf{C}}^8\right]\left\{(FWNT)\left[\hat{\mathbf{C}}^1\right]^{-1}\left[\hat{\mathbf{C}}^{M^1}\right]+(WNT)\left[\hat{\mathbf{C}}^6\right]^{-1}\left[\hat{\mathbf{C}}^{M^6}\right]\right\} \tag{3.160}$$

Thermo-Electric

$$S_x\left[\hat{\mathbf{C}}^8\right]^{-1}\left[\hat{\mathbf{C}}^{ET^8}\right]\begin{bmatrix}\Delta T\\-\Delta G\end{bmatrix}=(FWNT)\left[\hat{\mathbf{C}}^1\right]^{-1}\left[\hat{\mathbf{C}}^{ET^1}\right]\begin{bmatrix}\Delta T\\-\Delta G\end{bmatrix}+(WNT)\left[\hat{\mathbf{C}}^6\right]^{-1}\left[\hat{\mathbf{C}}^{ET^6}\right]\begin{bmatrix}\Delta T\\-\Delta G\end{bmatrix} \tag{3.161}$$

or

$$\left[\hat{\mathbf{C}}^{ET^8}\right]=\frac{1}{S_x}\left[\hat{\mathbf{C}}^8\right]\left\{(FWNT)\left[\hat{\mathbf{C}}^1\right]^{-1}\left[\hat{\mathbf{C}}^{ET^1}\right]+(WNT)\left[\hat{\mathbf{C}}^6\right]^{-1}\left[\hat{\mathbf{C}}^{ET^6}\right]\right\} \tag{3.162}$$

Thermo-Magnetic

$$S_x\left[\hat{\mathbf{C}}^8\right]^{-1}\left[\hat{\mathbf{C}}^{MT^8}\right]\begin{bmatrix}\Delta T\\-\Delta G\end{bmatrix}=(FWNT)\left[\hat{\mathbf{C}}^1\right]^{-1}\left[\hat{\mathbf{C}}^{MT^1}\right]\begin{bmatrix}\Delta T\\-\Delta G\end{bmatrix}+(WNT)\left[\hat{\mathbf{C}}^6\right]^{-1}\left[\hat{\mathbf{C}}^{MT^6}\right]\begin{bmatrix}\Delta T\\-\Delta G\end{bmatrix} \tag{3.163}$$

or

$$\left[\hat{\mathbf{C}}^{MT^8}\right]=\frac{1}{S_x}\left[\hat{\mathbf{C}}^8\right]\left\{(FWNT)\left[\hat{\mathbf{C}}^1\right]^{-1}\left[\hat{\mathbf{C}}^{MT^1}\right]+(WNT)\left[\hat{\mathbf{C}}^6\right]^{-1}\left[\hat{\mathbf{C}}^{MT^6}\right]\right\} \tag{3.164}$$

By rearranging each of Eqs. (3.154, 3.156, 3.158, 3.160, 3.162, 3.164), the Segment 8 thermal, electric, magnetic, thermoelectric, and thermomagnetic ABD matrices can be determined. However, for this to be accomplished, all of the hatted matrices for each segment must be determined. This is done by separating the segment constitutive equation as,

$$\begin{bmatrix} N_{yy} \\ N_{xy} \\ M_{yy} \\ M_{xy} \end{bmatrix} = \begin{bmatrix} A_{22} & A_{23} & B_{22} & B_{23} \\ A_{23} & A_{33} & B_{32} & B_{33} \\ B_{22} & B_{32} & D_{22} & D_{23} \\ B_{23} & B_{33} & D_{32} & D_{33} \end{bmatrix} \begin{bmatrix} \varepsilon_{yy}^0 \\ \gamma_{xy}^0 \\ \kappa_{yy} \\ \kappa_{xy} \end{bmatrix} + \begin{bmatrix} A_{12} & B_{21} \\ A_{13} & B_{31} \\ B_{12} & D_{12} \\ B_{13} & D_{13} \end{bmatrix} \begin{bmatrix} \varepsilon_{xx}^0 \\ \kappa_{xx} \end{bmatrix}$$
$$- \begin{bmatrix} A_2^\alpha & B_2^\alpha \\ A_3^\alpha & B_3^\alpha \\ B_2^\alpha & D_2^\alpha \\ B_3^\alpha & D_3^\alpha \end{bmatrix} \begin{bmatrix} \Delta T \\ -\Delta G \end{bmatrix} - \begin{bmatrix} A_{21}^E & A_{22}^E & A_{23}^E \\ A_{31}^E & A_{32}^E & A_{33}^E \\ B_{21}^E & B_{22}^E & B_{23}^E \\ B_{31}^E & B_{32}^E & B_{33}^E \end{bmatrix} \begin{bmatrix} E_1 \\ E_2 \\ E_3 \end{bmatrix} - \begin{bmatrix} A_{21}^M & A_{22}^M & A_{23}^M \\ A_{31}^M & A_{32}^M & A_{33}^M \\ B_{21}^M & B_{22}^M & B_{23}^M \\ B_{31}^M & B_{32}^M & B_{33}^M \end{bmatrix} \begin{bmatrix} H_1 \\ H_2 \\ H_3 \end{bmatrix} \tag{3.165}$$
$$- \begin{bmatrix} A_2^{ET} & B_2^{ET} \\ A_3^{ET} & B_3^{ET} \\ B_2^{ET} & D_2^{ET} \\ B_3^{ET} & D_3^{ET} \end{bmatrix} \begin{bmatrix} \Delta T \\ -\Delta G \end{bmatrix} - \begin{bmatrix} A_2^{MT} & B_2^{MT} \\ A_3^{MT} & B_3^{MT} \\ B_2^{MT} & D_2^{MT} \\ B_3^{MT} & D_3^{MT} \end{bmatrix} \begin{bmatrix} \Delta T \\ -\Delta G \end{bmatrix}$$

or, employing simplified notation,

$$\mathbf{v}_1 = \mathbf{S}_{11}\mathbf{u}_1 + \mathbf{S}_{12}\mathbf{u}_2 - \mathbf{S}_1^\alpha \Delta\mathbf{T} - \mathbf{S}_1^E \mathbf{E} - \mathbf{S}_1^M \mathbf{H} - \mathbf{S}_1^{ET} \Delta\mathbf{T} - \mathbf{S}_1^{MT} \Delta\mathbf{T} \tag{3.166}$$

and

$$\begin{bmatrix} N_{xx} \\ M_{xx} \end{bmatrix} = \begin{bmatrix} A_{12} & A_{13} & B_{12} & B_{13} \\ B_{21} & B_{31} & D_{12} & D_{13} \end{bmatrix} \begin{bmatrix} \varepsilon_{yy}^0 \\ \gamma_{xy}^0 \\ \kappa_{yy} \\ \kappa_{xy} \end{bmatrix} + \begin{bmatrix} A_{11} & B_{11} \\ B_{11} & D_{11} \end{bmatrix} \begin{bmatrix} \varepsilon_{xx}^0 \\ \kappa_{xx} \end{bmatrix}$$
$$- \begin{bmatrix} A_1^\alpha & B_1^\alpha \\ B_1^\alpha & D_1^\alpha \end{bmatrix} \begin{bmatrix} \Delta T \\ -\Delta G \end{bmatrix} - \begin{bmatrix} A_{11}^E & A_{12}^E & A_{13}^E \\ B_{11}^E & B_{12}^E & B_{13}^E \end{bmatrix} \begin{bmatrix} E_1 \\ E_2 \\ E_3 \end{bmatrix} - \begin{bmatrix} A_{11}^M & A_{12}^M & A_{13}^M \\ B_{11}^M & B_{12}^M & B_{13}^M \end{bmatrix} \begin{bmatrix} H_1 \\ H_2 \\ H_3 \end{bmatrix} \tag{3.167}$$
$$- \begin{bmatrix} A_1^{ET} & B_1^{ET} \\ B_1^{ET} & D_1^{ET} \end{bmatrix} \begin{bmatrix} \Delta T \\ -\Delta G \end{bmatrix} - \begin{bmatrix} A_1^{MT} & B_1^{MT} \\ B_1^{MT} & D_1^{MT} \end{bmatrix} \begin{bmatrix} \Delta T \\ -\Delta G \end{bmatrix}$$

or, employing simplified notation,

$$\mathbf{v}_2 = \mathbf{S}_{21}\mathbf{u}_1 + \mathbf{S}_{22}\mathbf{u}_2 - \mathbf{S}_2^\alpha \Delta\mathbf{T} - \mathbf{S}_2^E \mathbf{E} - \mathbf{S}_2^M \mathbf{H} - \mathbf{S}_2^{ET} \Delta\mathbf{T} - \mathbf{S}_2^{MT} \Delta\mathbf{T} \tag{3.168}$$

Equations (3.166) and (3.168) can be rearranged and combined as,

$$\begin{bmatrix} \mathbf{v}_1 \\ \mathbf{u}_2 \end{bmatrix} = \begin{bmatrix} \hat{\mathbf{S}}_{11} & \hat{\mathbf{S}}_{12} \\ \hat{\mathbf{S}}_{21} & \hat{\mathbf{S}}_{22} \end{bmatrix} \begin{bmatrix} \mathbf{u}_1 \\ \mathbf{v}_2 \end{bmatrix} - \begin{bmatrix} \hat{\mathbf{S}}_1^\alpha \\ \hat{\mathbf{S}}_2^\alpha \end{bmatrix} \Delta\mathbf{T} - \begin{bmatrix} \hat{\mathbf{S}}_1^E \\ \hat{\mathbf{S}}_2^E \end{bmatrix} \mathbf{E} - \begin{bmatrix} \hat{\mathbf{S}}_1^M \\ \hat{\mathbf{S}}_2^M \end{bmatrix} \mathbf{H} - \begin{bmatrix} \hat{\mathbf{S}}_1^{ET} \\ \hat{\mathbf{S}}_2^{ET} \end{bmatrix} \Delta\mathbf{T} - \begin{bmatrix} \hat{\mathbf{S}}_1^{MT} \\ \hat{\mathbf{S}}_2^{MT} \end{bmatrix} \Delta\mathbf{T} \tag{3.169}$$

where now all components subjected to the iso- conditions appear on the left hand side. Solving Eq. (3.168) for $\mathbf{u}_2$ yields,

$$\mathbf{u}_2 = [\mathbf{S}_{22}]^{-1}\left\{\mathbf{v}_2 - \mathbf{S}_{21}\mathbf{u}_1 + \mathbf{S}_2^{\alpha}\Delta\mathbf{T} + \mathbf{S}_2^{E}\mathbf{E} + \mathbf{S}_2^{M}\mathbf{H} + \mathbf{S}_2^{ET}\Delta\mathbf{T} + \mathbf{S}_2^{MT}\Delta\mathbf{T}\right\} \tag{3.170}$$

and substituting for $\mathbf{u}_2$ in Eq. (3.166) using Eq. (3.170) yields,

$$\begin{aligned}\mathbf{v}_1 = {} & \mathbf{S}_{11}\mathbf{u}_1 + \mathbf{S}_{12}[\mathbf{S}_{22}]^{-1}\left\{\mathbf{v}_2 - \mathbf{S}_{21}\mathbf{u}_1 + \mathbf{S}_2^{\alpha}\Delta\mathbf{T} + \mathbf{S}_2^{E}\mathbf{E} + \mathbf{S}_2^{M}\mathbf{H} + \mathbf{S}_2^{ET}\Delta\mathbf{T} + \mathbf{S}_2^{MT}\Delta\mathbf{T}\right\} \\ & - \mathbf{S}_1^{\alpha}\Delta\mathbf{T} - \mathbf{S}_1^{E}\mathbf{E} - \mathbf{S}_1^{M}\mathbf{H} - \mathbf{S}_1^{ET}\Delta\mathbf{T} - \mathbf{S}_1^{MT}\Delta\mathbf{T}\end{aligned} \tag{3.171}$$

or, with terms grouped,

$$\begin{aligned}\mathbf{v}_1 = {} & \left\{\mathbf{S}_{11} - \mathbf{S}_{12}[\mathbf{S}_{22}]^{-1}\mathbf{S}_{21}\right\}\mathbf{u}_1 + \mathbf{S}_{12}[\mathbf{S}_{22}]^{-1}\mathbf{v}_2 - \left\{\mathbf{S}_1^{\alpha} - \mathbf{S}_{12}[\mathbf{S}_{22}]^{-1}\mathbf{S}_2^{\alpha}\right\}\Delta\mathbf{T} - \left\{\mathbf{S}_1^{E} - \mathbf{S}_{12}[\mathbf{S}_{22}]^{-1}\mathbf{S}_2^{E}\right\}\mathbf{E} \\ & - \left\{\mathbf{S}_1^{M} - \mathbf{S}_{12}[\mathbf{S}_{22}]^{-1}\mathbf{S}_2^{M}\right\}\mathbf{H} - \left\{\mathbf{S}_1^{ET} - \mathbf{S}_{12}[\mathbf{S}_{22}]^{-1}\mathbf{S}_2^{ET}\right\}\Delta\mathbf{T} - \left\{\mathbf{S}_1^{MT} - \mathbf{S}_{12}[\mathbf{S}_{22}]^{-1}\mathbf{S}_2^{MT}\right\}\Delta\mathbf{T}\end{aligned} \tag{3.172}$$

Comparing Eqs. (3.172) and (3.170) with Eq. (3.169) allows the identification of the following hatted terms,

Mechanical

$$\hat{\mathbf{S}}_{11} = \mathbf{S}_{11} - \mathbf{S}_{12}[\mathbf{S}_{22}]^{-1}\mathbf{S}_{21} \tag{3.173}$$

$$\hat{\mathbf{S}}_{12} = \mathbf{S}_{12}[\mathbf{S}_{22}]^{-1} \tag{3.174}$$

$$\hat{\mathbf{S}}_{21} = -[\mathbf{S}_{22}]^{-1}\mathbf{S}_{21} \tag{3.175}$$

$$\hat{\mathbf{S}}_{22} = [\mathbf{S}_{22}]^{-1} \tag{3.176}$$

Thermal

$$\hat{\mathbf{S}}_1^{\alpha} = \mathbf{S}_1^{\alpha} - \mathbf{S}_{12}[\mathbf{S}_{22}]^{-1}\mathbf{S}_2^{\alpha} \tag{3.177}$$

$$\hat{\mathbf{S}}_2^{\alpha} = -[\mathbf{S}_{22}]^{-1}\mathbf{S}_2^{\alpha} \tag{3.178}$$

Electric

$$\hat{\mathbf{S}}_1^{E} = \mathbf{S}_1^{E} - \mathbf{S}_{12}[\mathbf{S}_{22}]^{-1}\mathbf{S}_2^{E} \tag{3.179}$$

$$\hat{\mathbf{S}}_2^{E} = -[\mathbf{S}_{22}]^{-1}\mathbf{S}_2^{E} \tag{3.180}$$

Magnetic

$$\hat{\mathbf{S}}_1^{M} = \mathbf{S}_1^{M} - \mathbf{S}_{12}[\mathbf{S}_{22}]^{-1}\mathbf{S}_2^{M} \tag{3.181}$$

$$\hat{\mathbf{S}}_2^{M} = -[\mathbf{S}_{22}]^{-1}\mathbf{S}_2^{M} \tag{3.182}$$

Thermo-electric

$$\hat{\mathbf{S}}_1^{ET} = \mathbf{S}_1^{ET} - \mathbf{S}_{12}\left[\mathbf{S}_{22}\right]^{-1}\mathbf{S}_2^{ET} \tag{3.183}$$

$$\hat{\mathbf{S}}_2^{ET} = -\left[\mathbf{S}_{22}\right]^{-1}\mathbf{S}_2^{ET} \tag{3.184}$$

Thermo-magnetic

$$\hat{\mathbf{S}}_1^{MT} = \mathbf{S}_1^{MT} - \mathbf{S}_{12}\left[\mathbf{S}_{22}\right]^{-1}\mathbf{S}_2^{MT} \tag{3.185}$$

$$\hat{\mathbf{S}}_2^{MT} = -\left[\mathbf{S}_{22}\right]^{-1}\mathbf{S}_2^{MT} \tag{3.186}$$

The equivalence between the $\hat{\mathbf{S}}^{\bullet}$ matrix terms in Eqs. (3.173 – 3.186) and the $\hat{\mathbf{C}}^{\bullet}$ matrix terms from Eqs. (3.152, 3.154, 3.156, 3.158, 3.160, 3.162) is,

$$\hat{\mathbf{C}} = \begin{bmatrix} \hat{S}_{22}(1,1) & \hat{S}_{21}(1,1) & \hat{S}_{21}(1,2) & \hat{S}_{22}(1,2) & \hat{S}_{21}(1,3) & \hat{S}_{21}(1,4) \\ \hat{S}_{12}(1,1) & \hat{S}_{11}(1,1) & \hat{S}_{11}(1,2) & \hat{S}_{12}(2,1) & \hat{S}_{11}(1,3) & \hat{S}_{11}(1,4) \\ \hat{S}_{12}(2,1) & \hat{S}_{11}(2,1) & \hat{S}_{11}(2,2) & \hat{S}_{12}(2,2) & \hat{S}_{11}(2,3) & \hat{S}_{11}(2,4) \\ \hat{S}_{22}(2,1) & \hat{S}_{21}(2,1) & \hat{S}_{21}(2,2) & \hat{S}_{22}(2,2) & \hat{S}_{21}(1,3) & \hat{S}_{21}(1,4) \\ \hat{S}_{12}(3,1) & \hat{S}_{11}(3,1) & \hat{S}_{11}(3,2) & \hat{S}_{12}(3,2) & \hat{S}_{11}(3,3) & \hat{S}_{11}(3,4) \\ \hat{S}_{12}(4,1) & \hat{S}_{11}(4,1) & \hat{S}_{11}(4,2) & \hat{S}_{12}(4,2) & \hat{S}_{11}(4,3) & \hat{S}_{11}(4,4) \end{bmatrix} \tag{3.187}$$

$$\hat{\mathbf{C}}^{\alpha} = \begin{bmatrix} \hat{S}_2^{\alpha}(1,1) & \hat{S}_2^{\alpha}(1,2) \\ \hat{S}_1^{\alpha}(1,1) & \hat{S}_1^{\alpha}(1,2) \\ \hat{S}_1^{\alpha}(2,1) & \hat{S}_1^{\alpha}(2,2) \\ \hat{S}_2^{\alpha}(2,1) & \hat{S}_2^{\alpha}(2,2) \\ \hat{S}_1^{\alpha}(3,1) & \hat{S}_1^{\alpha}(3,2) \\ \hat{S}_1^{\alpha}(4,1) & \hat{S}_1^{\alpha}(4,1) \end{bmatrix} \tag{3.188}$$

$$\hat{\mathbf{C}}^{E} = \begin{bmatrix} \hat{S}_2^{E}(1,1) & \hat{S}_2^{E}(1,2) & \hat{S}_2^{E}(1,3) \\ \hat{S}_1^{E}(1,1) & \hat{S}_1^{E}(1,2) & \hat{S}_1^{E}(1,3) \\ \hat{S}_1^{E}(2,1) & \hat{S}_1^{E}(2,2) & \hat{S}_1^{E}(2,3) \\ \hat{S}_2^{E}(2,1) & \hat{S}_2^{E}(2,2) & \hat{S}_2^{E}(2,3) \\ \hat{S}_1^{E}(3,1) & \hat{S}_1^{E}(3,2) & \hat{S}_1^{E}(3,3) \\ \hat{S}_1^{E}(4,1) & \hat{S}_1^{E}(4,2) & \hat{S}_1^{E}(4,3) \end{bmatrix} \tag{3.189}$$

$$\hat{\mathbf{C}}^{M} = \begin{bmatrix} \hat{S}_2^M(1,1) & \hat{S}_2^M(1,2) & \hat{S}_2^M(1,3) \\ \hat{S}_1^M(1,1) & \hat{S}_1^M(1,2) & \hat{S}_1^M(1,3) \\ \hat{S}_1^M(2,1) & \hat{S}_1^M(2,2) & \hat{S}_1^M(2,3) \\ \hat{S}_2^M(2,1) & \hat{S}_2^M(2,2) & \hat{S}_2^M(2,3) \\ \hat{S}_1^M(3,1) & \hat{S}_1^M(3,2) & \hat{S}_1^M(3,3) \\ \hat{S}_1^M(4,1) & \hat{S}_1^M(4,2) & \hat{S}_1^M(4,3) \end{bmatrix} \tag{3.190}$$

$$\hat{\mathbf{C}}^{ET} = \begin{bmatrix} \hat{S}_2^{ET}(1,1) & \hat{S}_2^{ET}(1,2) \\ \hat{S}_1^{ET}(1,1) & \hat{S}_1^{ET}(1,2) \\ \hat{S}_1^{ET}(2,1) & \hat{S}_1^{ET}(2,2) \\ \hat{S}_2^{ET}(2,1) & \hat{S}_2^{ET}(2,2) \\ \hat{S}_1^{ET}(3,1) & \hat{S}_1^{ET}(3,2) \\ \hat{S}_1^{ET}(4,1) & \hat{S}_1^{ET}(4,1) \end{bmatrix} \tag{3.191}$$

$$\hat{\mathbf{C}}^{MT} = \begin{bmatrix} \hat{S}_2^{MT}(1,1) & \hat{S}_2^{MT}(1,2) \\ \hat{S}_1^{MT}(1,1) & \hat{S}_1^{MT}(1,2) \\ \hat{S}_1^{MT}(2,1) & \hat{S}_1^{MT}(2,2) \\ \hat{S}_2^{MT}(2,1) & \hat{S}_2^{MT}(2,2) \\ \hat{S}_1^{MT}(3,1) & \hat{S}_1^{MT}(3,2) \\ \hat{S}_1^{MT}(4,1) & \hat{S}_1^{MT}(4,1) \end{bmatrix} \tag{3.192}$$

where the parenthetical indices refer to the indices of the components within each $\hat{S}_{ij}^{\bullet}$ and $\hat{S}_{k}^{\bullet}$ matrix.

Using Eqs. (3.154, 3.156, 3.158, 3.160, 3.162, 3.164) we can now determine the hatted quantities for Segment 8 from the hatted quantities of Segments 1 and 6 given by Eqs. (3.173 – 3.192). In order to then determine the non-hatted quantities for Segment 8, the reverse of the procedure embodied by Eqs. (3.166 – 3.192) is employed, resulting in equations of identical form of Eqs. (3.173 – 3.186), but with the rolls of hatted and unhatted quantities reversed. That is,

Mechanical

$$\mathbf{S}_{11} = \hat{\mathbf{S}}_{11} - \hat{\mathbf{S}}_{12}\left[\hat{\mathbf{S}}_{22}\right]^{-1}\hat{\mathbf{S}}_{21} \tag{3.193}$$

$$\mathbf{S}_{12} = \hat{\mathbf{S}}_{12}\left[\hat{\mathbf{S}}_{22}\right]^{-1} \tag{3.194}$$

$$\mathbf{S}_{21} = -\left[\hat{\mathbf{S}}_{22}\right]^{-1}\hat{\mathbf{S}}_{21} \tag{3.195}$$

$$\mathbf{S}_{22} = \left[\hat{\mathbf{S}}_{22}\right]^{-1} \tag{3.196}$$

Thermal

$$\mathbf{S}_1^{\alpha} = \hat{\mathbf{S}}_1^{\alpha} - \hat{\mathbf{S}}_{12}\left[\hat{\mathbf{S}}_{22}\right]^{-1}\hat{\mathbf{S}}_2^{\alpha} \tag{3.197}$$

$$\mathbf{S}_2^{\alpha} = -\left[\hat{\mathbf{S}}_{22}\right]^{-1}\hat{\mathbf{S}}_2^{\alpha} \tag{3.198}$$

Electric

$$\mathbf{S}_1^{E} = \hat{\mathbf{S}}_1^{E} - \hat{\mathbf{S}}_{12}\left[\hat{\mathbf{S}}_{22}\right]^{-1}\hat{\mathbf{S}}_2^{E} \tag{3.199}$$

$$\mathbf{S}_2^{E} = -\left[\hat{\mathbf{S}}_{22}\right]^{-1}\hat{\mathbf{S}}_2^{E} \tag{3.200}$$

Magnetic

$$\mathbf{S}_1^{M} = \hat{\mathbf{S}}_1^{M} - \hat{\mathbf{S}}_{12}\left[\hat{\mathbf{S}}_{22}\right]^{-1}\hat{\mathbf{S}}_2^{M} \tag{3.201}$$

$$\mathbf{S}_2^{M} = -\left[\hat{\mathbf{S}}_{22}\right]^{-1}\hat{\mathbf{S}}_2^{M} \tag{3.202}$$

Thermo-electric

$$\mathbf{S}_1^{ET} = \hat{\mathbf{S}}_1^{ET} - \hat{\mathbf{S}}_{12}\left[\hat{\mathbf{S}}_{22}\right]^{-1}\hat{\mathbf{S}}_2^{ET} \tag{3.203}$$

$$\mathbf{S}_2^{ET} = -\left[\hat{\mathbf{S}}_{22}\right]^{-1}\hat{\mathbf{S}}_2^{ET} \tag{3.204}$$

Thermo-magnetic

$$\mathbf{S}_1^{MT} = \hat{\mathbf{S}}_1^{MT} - \hat{\mathbf{S}}_{12}\left[\hat{\mathbf{S}}_{22}\right]^{-1}\hat{\mathbf{S}}_2^{MT} \tag{3.205}$$

$$\mathbf{S}_2^{MT} = -\left[\hat{\mathbf{S}}_{22}\right]^{-1}\hat{\mathbf{S}}_2^{MT} \tag{3.206}$$

Finally, the form of the equivalence between the $\mathbf{S}$ matrix terms and the $\mathbf{C}$ matrix terms is identical to the form of the equivalence between the $\hat{\mathbf{S}}$ matrix terms and the $\hat{\mathbf{C}}$ matrix terms given in Eqs. (3.187 – 3.192).

The Thermal Analogy

It is clear from the preceding development that an analogy exists between the thermal treatment of the material/laminate and each of the piezoelectric, piezomagnetic, thermoelectric, and thermomagnetic treatments of the material laminate. That is, the piezoelectric, piezomagnetic, thermoelectric, and thermomagnetic effects are each incorporated into the overall theory in a way that is analogous to the treatment of thermal effects. Therefore, it is possible to utilize the thermo-electro-magnetic terms within the theory to mimic thermal behavior, and conversely, it is possible to utilize the thermal terms within the theory to mimic the piezoelectric, piezomagnetic, thermoelectric, and thermomagnetic effects. This thermal analogy can be used to verify the thermo-electro-magnetic implementation vs. an established thermal implementation or to perform a piezoelectric, piezomagnetic, thermoelectric, and thermomagnetic analysis using an established thermal implementation. Côté et al. (2004) employed the latter approach to simulate the dynamic response of composite beam with an embedded piezoelectric actuator.

Material Level Thermo-Electro-Magnetic Terms Mimicking Thermal Response

The general thermo-piezo-electro-magnetic constitutive equation for a material is given by,

$$\begin{bmatrix}\sigma_{11}\\ \sigma_{22}\\ \sigma_{33}\\ \sigma_{23}\\ \sigma_{13}\\ \sigma_{12}\end{bmatrix}=\begin{bmatrix}C_{11} & C_{12} & C_{13} & C_{14} & C_{15} & C_{16}\\ C_{12} & C_{22} & C_{23} & C_{24} & C_{25} & C_{26}\\ C_{13} & C_{23} & C_{33} & C_{34} & C_{35} & C_{36}\\ C_{14} & C_{24} & C_{34} & C_{44} & C_{45} & C_{46}\\ C_{15} & C_{25} & C_{35} & C_{45} & C_{55} & C_{56}\\ C_{16} & C_{25} & C_{36} & C_{46} & C_{56} & C_{66}\end{bmatrix}\begin{bmatrix}\varepsilon_{11}-\alpha_{11}\Delta T\\ \varepsilon_{22}-\alpha_{22}\Delta T\\ \varepsilon_{33}-\alpha_{33}\Delta T\\ 2\varepsilon_{23}-2\alpha_{23}\Delta T\\ 2\varepsilon_{13}-2\alpha_{13}\Delta T\\ 2\varepsilon_{12}-2\alpha_{12}\Delta T\end{bmatrix}-\begin{bmatrix}e_{11} & e_{21} & e_{31}\\ e_{12} & e_{22} & e_{32}\\ e_{13} & e_{23} & e_{33}\\ e_{14} & e_{24} & e_{34}\\ e_{15} & e_{25} & e_{35}\\ e_{16} & e_{26} & e_{36}\end{bmatrix}\begin{bmatrix}E_1+\zeta_1\Delta T\\ E_2+\zeta_2\Delta T\\ E_3+\zeta_3\Delta T\end{bmatrix}-\begin{bmatrix}q_{11} & q_{21} & q_{31}\\ q_{12} & q_{22} & q_{32}\\ q_{13} & q_{23} & q_{33}\\ q_{14} & q_{24} & q_{34}\\ q_{15} & q_{25} & q_{35}\\ q_{16} & q_{26} & q_{36}\end{bmatrix}\begin{bmatrix}H_1+\psi_1\Delta T\\ H_2+\psi_2\Delta T\\ H_3+\psi_3\Delta T\end{bmatrix} \tag{3.207}$$

This equation can be written in contracted notation as,

$$\boldsymbol{\sigma}=\mathbf{C}[\boldsymbol{\varepsilon}-\boldsymbol{\alpha}\Delta T]-\mathbf{e}[\mathbf{E}+\boldsymbol{\zeta}\Delta T]-\mathbf{q}[\mathbf{H}+\boldsymbol{\psi}\Delta T] \tag{3.208}$$

or

$$\boldsymbol{\sigma}=\mathbf{C}\left[\boldsymbol{\varepsilon}-\boldsymbol{\alpha}\Delta T-\mathbf{C}^{-1}\mathbf{e}\mathbf{E}-\mathbf{C}^{-1}\mathbf{e}\boldsymbol{\zeta}\Delta T-\mathbf{C}^{-1}\mathbf{q}\mathbf{H}-\mathbf{C}^{-1}\mathbf{q}\boldsymbol{\psi}\Delta T\right] \tag{3.209}$$

Thus, in order to mimic the material level thermal effects using the piezoelectric terms, we seek a "Fake" piezoelectric coefficient matrix such that $\boldsymbol{\alpha}\Delta T=\mathbf{C}^{-1}\mathbf{e}^{Fake}\mathbf{E}$.

Assuming orthotropic behavior,

$$\begin{bmatrix}\alpha_1\\ \alpha_2\\ \alpha_3\\ 0\\ 0\\ 0\end{bmatrix}\Delta T=\begin{bmatrix}C_{11} & C_{12} & C_{13} & 0 & 0 & 0\\ C_{12} & C_{22} & C_{23} & 0 & 0 & 0\\ C_{13} & C_{23} & C_{33} & 0 & 0 & 0\\ 0 & 0 & 0 & C_{44} & 0 & 0\\ 0 & 0 & 0 & 0 & C_{55} & 0\\ 0 & 0 & 0 & 0 & 0 & C_{66}\end{bmatrix}^{-1}\begin{bmatrix}e_{11} & e_{21} & e_{31}\\ e_{12} & e_{22} & e_{32}\\ e_{13} & e_{23} & e_{33}\\ e_{14} & e_{24} & e_{34}\\ e_{15} & e_{25} & e_{35}\\ e_{16} & e_{26} & e_{36}\end{bmatrix}^{Fake}\begin{bmatrix}E_1\\ E_2\\ E_3\end{bmatrix} \tag{3.210}$$

Now, by setting $E_1=\Delta T,\ E_2=0,\ E_3=0$, we have,

$$\begin{bmatrix}\alpha_1\\ \alpha_2\\ \alpha_3\\ 0\\ 0\\ 0\end{bmatrix}\Delta T=\begin{bmatrix}C_{11} & C_{12} & C_{13} & 0 & 0 & 0\\ C_{12} & C_{22} & C_{23} & 0 & 0 & 0\\ C_{13} & C_{23} & C_{33} & 0 & 0 & 0\\ 0 & 0 & 0 & C_{44} & 0 & 0\\ 0 & 0 & 0 & 0 & C_{55} & 0\\ 0 & 0 & 0 & 0 & 0 & C_{66}\end{bmatrix}^{-1}\begin{bmatrix}e_{11} & e_{21} & e_{31}\\ e_{12} & e_{22} & e_{32}\\ e_{13} & e_{23} & e_{33}\\ e_{14} & e_{24} & e_{34}\\ e_{15} & e_{25} & e_{35}\\ e_{16} & e_{26} & e_{36}\end{bmatrix}^{Fake}\begin{bmatrix}\Delta T\\ 0\\ 0\end{bmatrix} \tag{3.211}$$

or

$$\begin{bmatrix}C_{11} & C_{12} & C_{13} & 0 & 0 & 0\\ C_{12} & C_{22} & C_{23} & 0 & 0 & 0\\ C_{13} & C_{23} & C_{33} & 0 & 0 & 0\\ 0 & 0 & 0 & C_{44} & 0 & 0\\ 0 & 0 & 0 & 0 & C_{55} & 0\\ 0 & 0 & 0 & 0 & 0 & C_{66}\end{bmatrix}\begin{bmatrix}\alpha_1\\ \alpha_2\\ \alpha_3\\ 0\\ 0\\ 0\end{bmatrix}\Delta T=\begin{bmatrix}e_{11}\\ e_{12}\\ e_{13}\\ e_{14}\\ e_{15}\\ e_{16}\end{bmatrix}^{Fake}\Delta T \tag{3.212}$$

which gives,

$$\begin{aligned} e_{11}^{Fake} &= C_{11}\alpha_1 + C_{12}\alpha_2 + C_{13}\alpha_3 \\ e_{12}^{Fake} &= C_{12}\alpha_1 + C_{22}\alpha_2 + C_{23}\alpha_3 \\ e_{13}^{Fake} &= C_{13}\alpha_1 + C_{23}\alpha_2 + C_{33}\alpha_3 \\ e_{14}^{Fake} &= 0 \\ e_{15}^{Fake} &= 0 \\ e_{16}^{Fake} &= 0 \end{aligned} \tag{3.213}$$

Thus, by utilizing the fake piezoelectric coefficients indicated by Eq. (3.213), along with $E_1 = \Delta T$, $E_2 = 0$, $E_3 = 0$ (and then also utilizing fake thermal expansion coefficients, $\boldsymbol{\alpha}^{Fake} = 0$), it is possible to determine the thermal behavior of a material through the piezoelectric terms. This can be used to verify the piezoelectric implementation.

Similarly, to verify the piezomagnetic effects, we set $H_1 = \Delta T$, $H_2 = 0$, $H_3 = 0$, and

$$\begin{aligned} q_{11}^{Fake} &= C_{11}\alpha_1 + C_{12}\alpha_2 + C_{13}\alpha_3 \\ q_{12}^{Fake} &= C_{12}\alpha_1 + C_{22}\alpha_2 + C_{23}\alpha_3 \\ q_{13}^{Fake} &= C_{13}\alpha_1 + C_{23}\alpha_2 + C_{33}\alpha_3 \\ q_{14}^{Fake} &= 0 \\ q_{15}^{Fake} &= 0 \\ q_{16}^{Fake} &= 0 \end{aligned} \tag{3.214}$$

For the thermo-electric effects, what we have $\boldsymbol{\alpha}\Delta T = \mathbf{C}^{-1}\mathbf{e}^{Fake}\boldsymbol{\zeta}^{Fake}\Delta T$. Again, assuming orthotropic material behavior,

$$\begin{bmatrix} C_{11} & C_{12} & C_{13} & 0 & 0 & 0 \\ C_{12} & C_{22} & C_{23} & 0 & 0 & 0 \\ C_{13} & C_{23} & C_{33} & 0 & 0 & 0 \\ 0 & 0 & 0 & C_{44} & 0 & 0 \\ 0 & 0 & 0 & 0 & C_{55} & 0 \\ 0 & 0 & 0 & 0 & 0 & C_{66} \end{bmatrix} \begin{bmatrix} \alpha_1 \\ \alpha_2 \\ \alpha_3 \\ 0 \\ 0 \\ 0 \end{bmatrix} = \begin{bmatrix} e_{11} & e_{21} & e_{31} \\ e_{12} & e_{22} & e_{32} \\ e_{13} & e_{23} & e_{33} \\ e_{14} & e_{24} & e_{34} \\ e_{15} & e_{25} & e_{35} \\ e_{16} & e_{26} & e_{36} \end{bmatrix}^{Fake} \begin{bmatrix} \zeta_1 \\ \zeta_2 \\ \zeta_3 \end{bmatrix}^{Fake} \tag{3.215}$$

Setting $\zeta_1^{Fake} = 1$, $\zeta_2^{Fake} = 0$, $\zeta_3^{Fake} = 0$, we have

$$\begin{bmatrix} C_{11} & C_{12} & C_{13} & 0 & 0 & 0 \\ C_{12} & C_{22} & C_{23} & 0 & 0 & 0 \\ C_{13} & C_{23} & C_{33} & 0 & 0 & 0 \\ 0 & 0 & 0 & C_{44} & 0 & 0 \\ 0 & 0 & 0 & 0 & C_{55} & 0 \\ 0 & 0 & 0 & 0 & 0 & C_{66} \end{bmatrix} \begin{bmatrix} \alpha_1 \\ \alpha_2 \\ \alpha_3 \\ 0 \\ 0 \\ 0 \end{bmatrix} = \begin{bmatrix} e_{11} & e_{21} & e_{31} \\ e_{12} & e_{22} & e_{32} \\ e_{13} & e_{23} & e_{33} \\ e_{14} & e_{24} & e_{34} \\ e_{15} & e_{25} & e_{35} \\ e_{16} & e_{26} & e_{36} \end{bmatrix}^{Fake} \begin{bmatrix} 1 \\ 0 \\ 0 \end{bmatrix} = \begin{bmatrix} e_{11} \\ e_{12} \\ e_{13} \\ e_{14} \\ e_{15} \\ e_{16} \end{bmatrix}^{Fake} \tag{3.216}$$

resulting in,

$$
\begin{aligned}
e_{11}^{Fake} &= C_{11}\alpha_1 + C_{12}\alpha_2 + C_{13}\alpha_3 \\
e_{12}^{Fake} &= C_{12}\alpha_1 + C_{22}\alpha_2 + C_{23}\alpha_3 \\
e_{13}^{Fake} &= C_{13}\alpha_1 + C_{23}\alpha_2 + C_{33}\alpha_3 \\
e_{14}^{Fake} &= 0 \\
e_{15}^{Fake} &= 0 \\
e_{16}^{Fake} &= 0
\end{aligned}
\tag{3.217}
$$

Similarly, for the thermo-magnetic terms, we set $\psi_1 = 1,\ \psi_2 = 0,\ \psi_3 = 0$ and obtain,

$$
\begin{aligned}
q_{11}^{Fake} &= C_{11}\alpha_1 + C_{12}\alpha_2 + C_{13}\alpha_3 \\
q_{12}^{Fake} &= C_{12}\alpha_1 + C_{22}\alpha_2 + C_{23}\alpha_3 \\
q_{13}^{Fake} &= C_{13}\alpha_1 + C_{23}\alpha_2 + C_{33}\alpha_3 \\
q_{14}^{Fake} &= 0 \\
q_{15}^{Fake} &= 0 \\
q_{16}^{Fake} &= 0
\end{aligned}
\tag{3.218}
$$

Material Level Thermal Terms Mimicking Thermo-Electro-Magnetic Response

In order to mimic the material piezoelectric behavior using the thermal terms, we again begin with Eqs. (3.207 – 3.209). Setting $\boldsymbol{\alpha}^{Fake}\,\Delta T^{Fake} = \mathbf{C}^{-1}\mathbf{e}\,\mathbf{E}$ and retaining anisotropic behavior,

$$
\begin{bmatrix} \alpha_1 \\ \alpha_2 \\ \alpha_3 \\ \alpha_4 \\ \alpha_5 \\ \alpha_6 \end{bmatrix}^{Fake} \Delta T^{Fake} = \begin{bmatrix} C_{11} & C_{12} & C_{13} & C_{14} & C_{15} & C_{16} \\ C_{21} & C_{22} & C_{23} & C_{24} & C_{25} & C_{26} \\ C_{31} & C_{32} & C_{33} & C_{34} & C_{35} & C_{36} \\ C_{41} & C_{42} & C_{43} & C_{44} & C_{45} & C_{46} \\ C_{51} & C_{52} & C_{53} & C_{54} & C_{55} & C_{56} \\ C_{61} & C_{62} & C_{63} & C_{64} & C_{65} & C_{66} \end{bmatrix}^{-1} \begin{bmatrix} e_{11} & e_{21} & e_{31} \\ e_{12} & e_{22} & e_{32} \\ e_{13} & e_{23} & e_{33} \\ e_{14} & e_{24} & e_{34} \\ e_{15} & e_{25} & e_{35} \\ e_{16} & e_{26} & e_{36} \end{bmatrix} \begin{bmatrix} E_1 \\ E_2 \\ E_3 \end{bmatrix}
\tag{3.219}
$$

Setting $\Delta T^{Fake} = E_1,\ E_2 = 0,\ E_3 = 0$, we have,

$$
\begin{bmatrix} \alpha_1 \\ \alpha_2 \\ \alpha_3 \\ \alpha_4 \\ \alpha_5 \\ \alpha_6 \end{bmatrix}^{Fake} E_1 = \begin{bmatrix} C_{11} & C_{12} & C_{13} & C_{14} & C_{15} & C_{16} \\ C_{21} & C_{22} & C_{23} & C_{24} & C_{25} & C_{26} \\ C_{31} & C_{32} & C_{33} & C_{34} & C_{35} & C_{36} \\ C_{41} & C_{42} & C_{43} & C_{44} & C_{45} & C_{46} \\ C_{51} & C_{52} & C_{53} & C_{54} & C_{55} & C_{56} \\ C_{61} & C_{62} & C_{63} & C_{64} & C_{65} & C_{66} \end{bmatrix}^{-1} \begin{bmatrix} e_{11} & e_{21} & e_{31} \\ e_{12} & e_{22} & e_{32} \\ e_{13} & e_{23} & e_{33} \\ e_{14} & e_{24} & e_{34} \\ e_{15} & e_{25} & e_{35} \\ e_{16} & e_{26} & e_{36} \end{bmatrix} \begin{bmatrix} E_1 \\ 0 \\ 0 \end{bmatrix}
\tag{3.220}
$$

or

$$
\begin{bmatrix} \alpha_1 \\ \alpha_2 \\ \alpha_3 \\ \alpha_4 \\ \alpha_5 \\ \alpha_6 \end{bmatrix}^{Fake} E_1 = \begin{bmatrix} C_{11} & C_{12} & C_{13} & C_{14} & C_{15} & C_{16} \\ C_{21} & C_{22} & C_{23} & C_{24} & C_{25} & C_{26} \\ C_{31} & C_{32} & C_{33} & C_{34} & C_{35} & C_{36} \\ C_{41} & C_{42} & C_{43} & C_{44} & C_{45} & C_{46} \\ C_{51} & C_{52} & C_{53} & C_{54} & C_{55} & C_{56} \\ C_{61} & C_{62} & C_{63} & C_{64} & C_{65} & C_{66} \end{bmatrix}^{-1} \begin{bmatrix} e_{11} \\ e_{12} \\ e_{13} \\ e_{14} \\ e_{15} \\ e_{16} \end{bmatrix} E_1
\tag{3.221}
$$

so

$$\begin{bmatrix}\alpha_1\\ \alpha_2\\ \alpha_3\\ \alpha_4\\ \alpha_5\\ \alpha_6\end{bmatrix}^{Fake} = \begin{bmatrix}C_{11} & C_{12} & C_{13} & C_{14} & C_{15} & C_{16}\\ C_{21} & C_{22} & C_{23} & C_{24} & C_{25} & C_{26}\\ C_{31} & C_{32} & C_{33} & C_{34} & C_{35} & C_{36}\\ C_{41} & C_{42} & C_{43} & C_{44} & C_{45} & C_{46}\\ C_{51} & C_{52} & C_{53} & C_{54} & C_{55} & C_{56}\\ C_{61} & C_{62} & C_{63} & C_{64} & C_{65} & C_{66}\end{bmatrix}^{-1}\begin{bmatrix}e_{11}\\ e_{12}\\ e_{13}\\ e_{14}\\ e_{15}\\ e_{16}\end{bmatrix} \tag{3.222}$$

Generally, for any single applied electric field component, E_i, set $\Delta T^{Fake} = E_i$ and $E_j = 0$ ($j \neq i$) along with,

$$\begin{bmatrix}\alpha_1\\ \alpha_2\\ \alpha_3\\ \alpha_4\\ \alpha_5\\ \alpha_6\end{bmatrix}^{Fake} = \begin{bmatrix}C_{11} & C_{12} & C_{13} & C_{14} & C_{15} & C_{16}\\ C_{21} & C_{22} & C_{23} & C_{24} & C_{25} & C_{26}\\ C_{31} & C_{32} & C_{33} & C_{34} & C_{35} & C_{36}\\ C_{41} & C_{42} & C_{43} & C_{44} & C_{45} & C_{46}\\ C_{51} & C_{52} & C_{53} & C_{54} & C_{55} & C_{56}\\ C_{61} & C_{62} & C_{63} & C_{64} & C_{65} & C_{66}\end{bmatrix}^{-1}\begin{bmatrix}e_{i1}\\ e_{i2}\\ e_{i3}\\ e_{i4}\\ e_{i5}\\ e_{i6}\end{bmatrix} \tag{3.223}$$

Similarly, to mimic the piezomagnetic effects using the thermal terms, set $\Delta T^{Fake} = H_i$ and $H_j = 0$ ($j \neq i$) along with,

$$\begin{bmatrix}\alpha_1\\ \alpha_2\\ \alpha_3\\ \alpha_4\\ \alpha_5\\ \alpha_6\end{bmatrix}^{Fake} = \begin{bmatrix}C_{11} & C_{12} & C_{13} & C_{14} & C_{15} & C_{16}\\ C_{21} & C_{22} & C_{23} & C_{24} & C_{25} & C_{26}\\ C_{31} & C_{32} & C_{33} & C_{34} & C_{35} & C_{36}\\ C_{41} & C_{42} & C_{43} & C_{44} & C_{45} & C_{46}\\ C_{51} & C_{52} & C_{53} & C_{54} & C_{55} & C_{56}\\ C_{61} & C_{62} & C_{63} & C_{64} & C_{65} & C_{66}\end{bmatrix}^{-1}\begin{bmatrix}q_{i1}\\ q_{i2}\\ q_{i3}\\ q_{i4}\\ q_{i5}\\ q_{i6}\end{bmatrix} \tag{3.224}$$

In order to mimic the thermo-electric effects, we set $\boldsymbol{\alpha}^{Fake}\Delta T^{Fake} = \mathbf{C}^{-1}\mathbf{e}\boldsymbol{\zeta}\Delta T$. Retaining anisotropic material behavior and setting $\Delta T^{Fake} = \Delta T$,

$$\begin{bmatrix}\alpha_1\\ \alpha_2\\ \alpha_3\\ \alpha_4\\ \alpha_5\\ \alpha_6\end{bmatrix}^{Fake} = \begin{bmatrix}C_{11} & C_{12} & C_{13} & C_{14} & C_{15} & C_{16}\\ C_{21} & C_{22} & C_{23} & C_{24} & C_{25} & C_{26}\\ C_{31} & C_{32} & C_{33} & C_{34} & C_{35} & C_{36}\\ C_{41} & C_{42} & C_{43} & C_{44} & C_{45} & C_{46}\\ C_{51} & C_{52} & C_{53} & C_{54} & C_{55} & C_{56}\\ C_{61} & C_{62} & C_{63} & C_{64} & C_{65} & C_{66}\end{bmatrix}^{-1}\begin{bmatrix}e_{11} & e_{21} & e_{31}\\ e_{12} & e_{22} & e_{32}\\ e_{13} & e_{23} & e_{33}\\ e_{14} & e_{24} & e_{34}\\ e_{15} & e_{25} & e_{35}\\ e_{16} & e_{26} & e_{36}\end{bmatrix}\begin{bmatrix}\zeta_1\\ \zeta_2\\ \zeta_3\end{bmatrix} \tag{3.225}$$

In order to mimic the thermo-magnetic effects, we set $\Delta T^{Fake} = \Delta T$, along with,

$$\begin{bmatrix} \alpha_1 \\ \alpha_2 \\ \alpha_3 \\ \alpha_4 \\ \alpha_5 \\ \alpha_6 \end{bmatrix}^{Fake} = \begin{bmatrix} C_{11} & C_{12} & C_{13} & C_{14} & C_{15} & C_{16} \\ C_{21} & C_{22} & C_{23} & C_{24} & C_{25} & C_{26} \\ C_{31} & C_{32} & C_{33} & C_{34} & C_{35} & C_{36} \\ C_{41} & C_{42} & C_{43} & C_{44} & C_{45} & C_{46} \\ C_{51} & C_{52} & C_{53} & C_{54} & C_{55} & C_{56} \\ C_{61} & C_{62} & C_{63} & C_{64} & C_{65} & C_{66} \end{bmatrix}^{-1} \begin{bmatrix} q_{11} & q_{21} & q_{31} \\ q_{12} & q_{22} & q_{32} \\ q_{13} & q_{23} & q_{33} \\ q_{14} & q_{24} & q_{34} \\ q_{15} & q_{25} & q_{35} \\ q_{16} & q_{26} & q_{36} \end{bmatrix} \begin{bmatrix} \zeta_1 \\ \zeta_2 \\ \zeta_3 \end{bmatrix} \tag{3.226}$$

It is thus possible to mimic the piezoelectric or piezomagnetic behavior of a material in response to a single electric or magnetic field component by using the fake coefficients of thermal expansion given by Eqs. (3.223) and (3.224). The thermo-electric and thermo-magnetic behavior can be mimicked by using the fake coefficients of thermal expansion given by Eqs. (3.225) and (3.226).

Panel Level Thermal Terms Mimicking Thermo-Electro-Magnetic Response

A simple thermal analogy is also in effect on the panel and laminate level. The laminate or stiffened panel constitutive equation is given by,

$$\begin{bmatrix} \mathbf{N} \\ \mathbf{M} \end{bmatrix} = \begin{bmatrix} \mathbf{A} & \mathbf{B} \\ \mathbf{B} & \mathbf{D} \end{bmatrix} \begin{bmatrix} \boldsymbol{\varepsilon}^0 \\ \boldsymbol{\kappa}^0 \end{bmatrix} - \begin{bmatrix} \mathbf{A}^\alpha & \mathbf{B}^\alpha \\ \mathbf{B}^\alpha & \mathbf{D}^\alpha \end{bmatrix} \begin{bmatrix} \Delta T \\ -\Delta G \end{bmatrix} - \begin{bmatrix} \mathbf{A}^E \\ \mathbf{B}^E \end{bmatrix} \begin{bmatrix} E_x \\ E_y \\ E_z \end{bmatrix} - \begin{bmatrix} \mathbf{A}^M \\ \mathbf{B}^M \end{bmatrix} \begin{bmatrix} H_x \\ H_y \\ H_z \end{bmatrix} - \begin{bmatrix} \mathbf{A}^{ET} & \mathbf{B}^{ET} \\ \mathbf{B}^{ET} & \mathbf{D}^{ET} \end{bmatrix} \begin{bmatrix} \Delta T \\ -\Delta G \end{bmatrix} - \begin{bmatrix} \mathbf{A}^{MT} & \mathbf{B}^{MT} \\ \mathbf{B}^{MT} & \mathbf{D}^{MT} \end{bmatrix} \begin{bmatrix} \Delta T \\ -\Delta G \end{bmatrix} \tag{3.227}$$

Equating fake thermal terms with the piezoelectric terms gives,

$$\begin{bmatrix} \mathbf{A}^\alpha & \mathbf{B}^\alpha \\ \mathbf{B}^\alpha & \mathbf{D}^\alpha \end{bmatrix}^{Fake} \begin{bmatrix} \Delta T \\ -\Delta G \end{bmatrix}^{Fake} = \begin{bmatrix} \mathbf{A}^E \\ \mathbf{B}^E \end{bmatrix} \begin{bmatrix} E_x \\ E_y \\ E_z \end{bmatrix} \tag{3.228}$$

or,

$$\begin{bmatrix} A_1^\alpha & B_1^\alpha \\ A_2^\alpha & B_2^\alpha \\ A_3^\alpha & B_3^\alpha \\ B_1^\alpha & D_1^\alpha \\ B_2^\alpha & D_2^\alpha \\ B_3^\alpha & D_3^\alpha \end{bmatrix}^{Fake} \begin{bmatrix} \Delta T \\ -\Delta G \end{bmatrix}^{Fake} = \begin{bmatrix} A_{11}^E & A_{12}^E & A_{13}^E \\ A_{21}^E & A_{22}^E & A_{23}^E \\ A_{31}^E & A_{32}^E & A_{33}^E \\ B_{11}^E & B_{12}^E & B_{13}^E \\ B_{21}^E & B_{22}^E & B_{23}^E \\ B_{31}^E & B_{32}^E & B_{33}^E \end{bmatrix} \begin{bmatrix} E_x \\ E_y \\ E_z \end{bmatrix} \tag{3.229}$$

Applying a single electric field component, E_i, we have,

$$\begin{bmatrix} A_1^{\alpha} & B_1^{\alpha} \\ A_2^{\alpha} & B_2^{\alpha} \\ A_3^{\alpha} & B_3^{\alpha} \\ B_1^{\alpha} & D_1^{\alpha} \\ B_2^{\alpha} & D_2^{\alpha} \\ B_3^{\alpha} & D_3^{\alpha} \end{bmatrix}^{Fake} \begin{bmatrix} \Delta T \\ -\Delta G \end{bmatrix}^{Fake} = \begin{bmatrix} A_{1i}^{E} \\ A_{2i}^{E} \\ A_{3i}^{E} \\ B_{1i}^{E} \\ B_{2i}^{E} \\ B_{3i}^{E} \end{bmatrix} E_i \tag{3.230}$$

Setting $\Delta T^{Fake} = E_i$ and $\Delta G^{Fake} = 0$ gives,

$$\begin{bmatrix} A_1^{\alpha} \\ A_2^{\alpha} \\ A_3^{\alpha} \\ B_1^{\alpha} \\ B_2^{\alpha} \\ B_3^{\alpha} \end{bmatrix}^{Fake} E_i = \begin{bmatrix} A_{1i}^{E} \\ A_{2i}^{E} \\ A_{3i}^{E} \\ B_{1i}^{E} \\ B_{2i}^{E} \\ B_{3i}^{E} \end{bmatrix} E_i \tag{3.231}$$

or,

$$\begin{bmatrix} A_1^{\alpha} \\ A_2^{\alpha} \\ A_3^{\alpha} \\ B_1^{\alpha} \\ B_2^{\alpha} \\ B_3^{\alpha} \end{bmatrix}^{Fake} = \begin{bmatrix} A_{1i}^{E} \\ A_{2i}^{E} \\ A_{3i}^{E} \\ B_{1i}^{E} \\ B_{2i}^{E} \\ B_{3i}^{E} \end{bmatrix} \tag{3.232}$$

Similarly, to determine fake thermal terms that mimic the panel/laminate piezomagnetic response, we set $\Delta T^{Fake} = H_i$ and $\Delta G^{Fake} = 0$ along with,

$$\begin{bmatrix} A_1^{\alpha} \\ A_2^{\alpha} \\ A_3^{\alpha} \\ B_1^{\alpha} \\ B_2^{\alpha} \\ B_3^{\alpha} \end{bmatrix}^{Fake} = \begin{bmatrix} A_{1i}^{M} \\ A_{2i}^{M} \\ A_{3i}^{M} \\ B_{1i}^{M} \\ B_{2i}^{M} \\ B_{3i}^{M} \end{bmatrix} \tag{3.233}$$

These results are useful because they enable the analysis of piezoelectric and piezomagnetic shells within NASTRAN using the software's thermal analysis capabilities. NASTRAN accepts thermal ABD matrices for the shell materials. Thus, by providing NASTRAN with the appropriate fake thermal

terms, the software will solve a thermal problem that is analogous to a desired piezoelectric or piezomagnetic problem. An even simpler analogy exists between the panel level thermal terms and the thermo-electric or thermo-magnetic terms. Simply setting,

$$\begin{bmatrix} \mathbf{A}^{\alpha} & \mathbf{B}^{\alpha} \\ \mathbf{B}^{\alpha} & \mathbf{D}^{\alpha} \end{bmatrix}^{Fake} = \begin{bmatrix} \mathbf{A}^{ET} & \mathbf{B}^{ET} \\ \mathbf{B}^{ET} & \mathbf{D}^{ET} \end{bmatrix} \tag{3.234}$$

or

$$\begin{bmatrix} \mathbf{A}^{\alpha} & \mathbf{B}^{\alpha} \\ \mathbf{B}^{\alpha} & \mathbf{D}^{\alpha} \end{bmatrix}^{Fake} = \begin{bmatrix} \mathbf{A}^{MT} & \mathbf{B}^{MT} \\ \mathbf{B}^{MT} & \mathbf{D}^{MT} \end{bmatrix} \tag{3.235}$$

will enable the thermal capabilities to mimic the thermo-electric or thermo-magnetic response. However, these analogies are less useful because their use assumes that the panel or laminate only reacts to the applied thermal loading through the thermo-electric or thermo-magnetic terms, and not through the standard thermal expansion terms. That is, these analogies would only be valid for the case in which the panel/laminate coefficients of thermal expansion are zero.

Results and Discussion

To verify the thermo-electro-magneto-elastic implementation within HyperSizer, we first consider a bonded facesheet – flange combination, which is identical to the HyperSizer Section 8 shown in Figs. 19 and 20. The geometry of this problem is shown in Fig. 21. Within HyperSizer, this case corresponds to a T-stiffened panel (see Fig. 19) with an infinitesimal web. The facesheet is composed of PZT-7A lead zirconium titanate piezoelectric material with a through-thickness poling direction, while the flange is composed of aluminum. The material properties employed for these materials are given in Tables 3 and 4. As indicated in Fig. 21, a voltage difference of 1×10^5 Volts is applied through the thickness of the face sheet. This corresponds to an electric field of (1×10^5 V) / (0.002286 m) = 43.74 MV/m. This problem has also been analyzed using the ABAQUS finite element analysis package, employing the finite element mesh shown in Fig. 22, consisting of a total of 21,200 elements. The facesheet is composed of CPE4E piezoelectric plane strain continuum elements, while the flange and adhesive are composed of CPE4R reduced integration plane strain continuum elements.

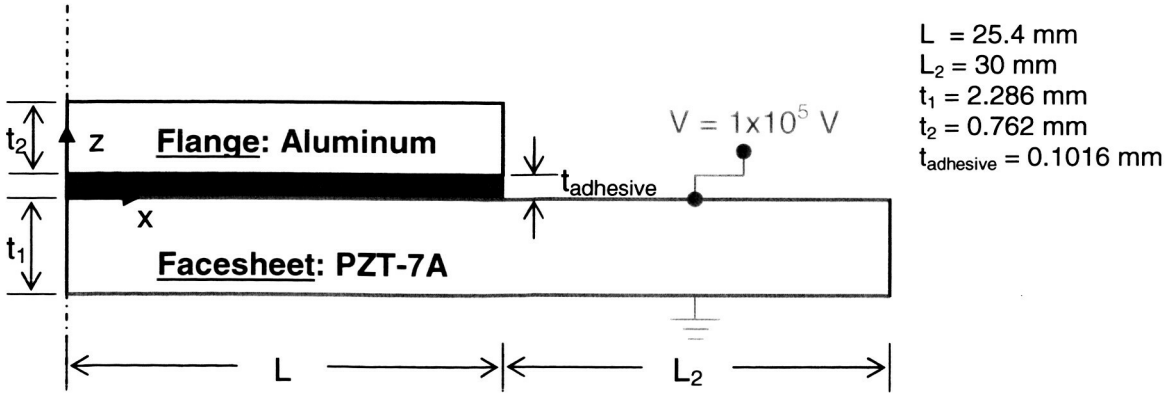

Fig. 21. ABAQUS solution domain for a facesheet – adhesive – flange combination.

Table 3. Elastic constants of the materials used in the analyses.

	E_{11} (GPa)	E_{22} (GPa)	E_{33} (GPa)	ν_{12}	ν_{13}	ν_{23}	G_{12} (GPa)	G_{13} (GPa)	G_{23} (GPa)
Aluminum	68.95	68.95	68.95	0.30	0.30	0.30	26.52	26.52	26.52
PZT-7A	94.97	81.90	94.97	0.384	0.323	0.331	25.40	25.40	35.90
Epoxy	3.068	3.068	3.068	0.3485	0.3485	0.3485	1.138	1.138	1.138

Table 4. Piezoelectric properties of the materials used in the analyses.

	e_{222} (C/m^2)	e_{233} (C/m^2)	e_{211} (C/m^2)	e_{323} (C/m^2)	e_{112} (C/m^2)	k_{22} (10^{-9} C/V m)	k_{33} (10^{-9} C/V m)	k_{11} (10^{-9} C/V m)
PZT-7A	12.25	-2.1	-2.1	9.2	9.2	2.07	4.07	4.07

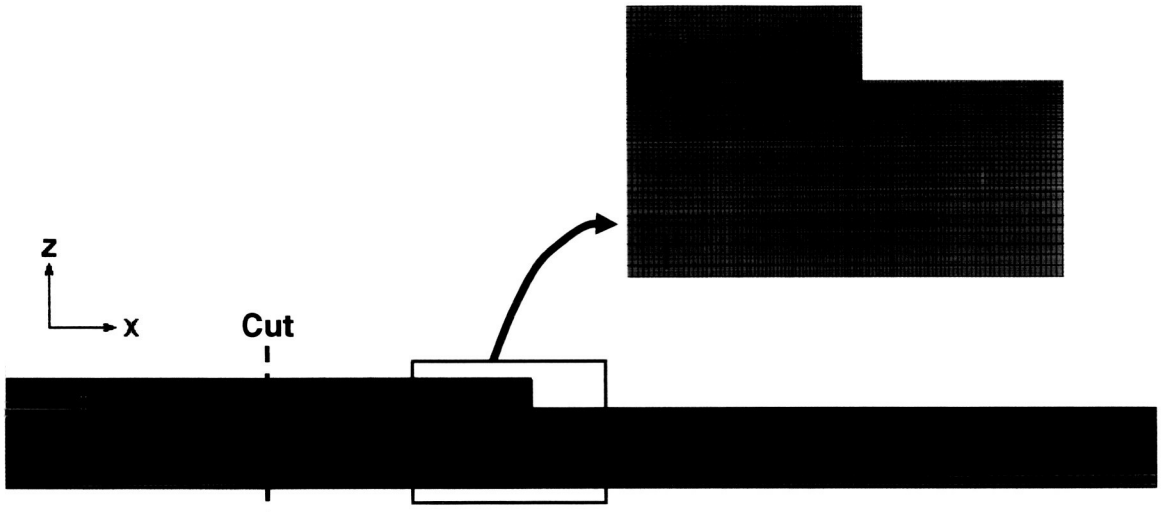

Fig. 22. ABAQUS mesh for the facesheet – adhesive – flange combination.

The normal stresses in the plane defined by the facesheet (x-y plane) arising due to the applied voltage along the cut shown in Fig. 22 are plotted in Figs. 23 and 24. The original ABAQUS solution (labeled "ABAQUS Fully Coupled") agrees reasonably well with the HyperSizer solution, but some deviation is evident. This deviation is caused by the fact that HyperSizer's formulation is based on the ability to apply constant panel (or laminate) level electric field components. In contrast, the ABAQUS continuum solution involves the application of electric potential at boundaries along with solution of a boundary value problem for the electric potential throughout the model. As will be shown, the ABAQUS solution does not result in constant electric field components.

In order to provide the ABAQUS solution with constant electric field components, which mimics the HyperSizer formulation, it is possible to employ artificially large dielectric constants (κ_{ij}) for the PZT-7A material. This, in effect, decouples the electric field components (E_i) in the piezoelectric material constitutive equation,

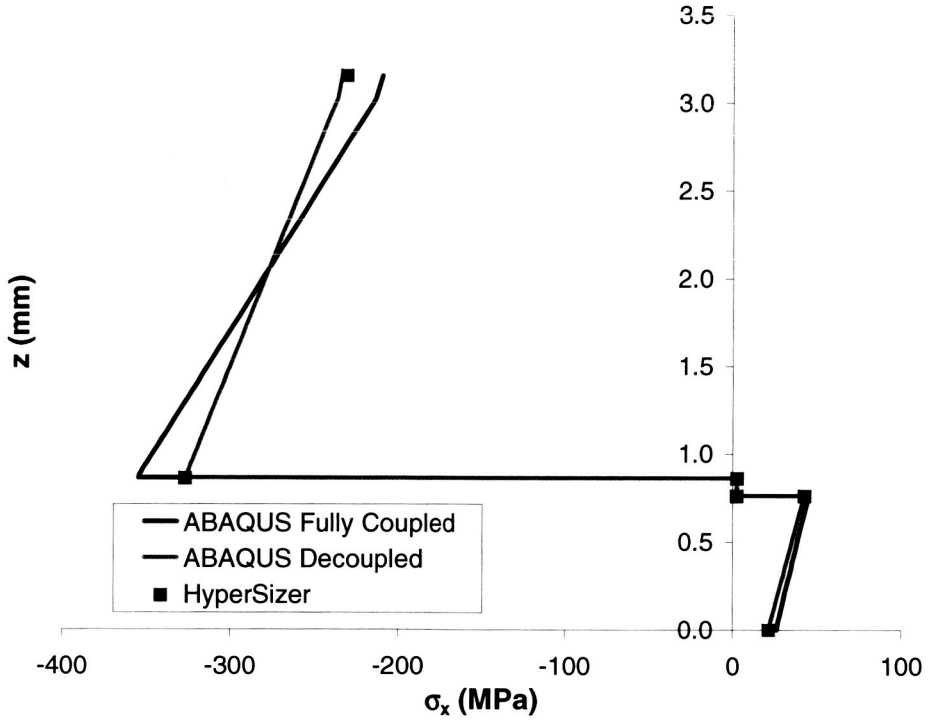

Fig. 23. Stress component (σ_x) along the cut through the flange adhesive and facesheet defined in Fig. 22 as predicted by HyperSizer and ABAQUS both with fully coupled and decoupled electric field components.

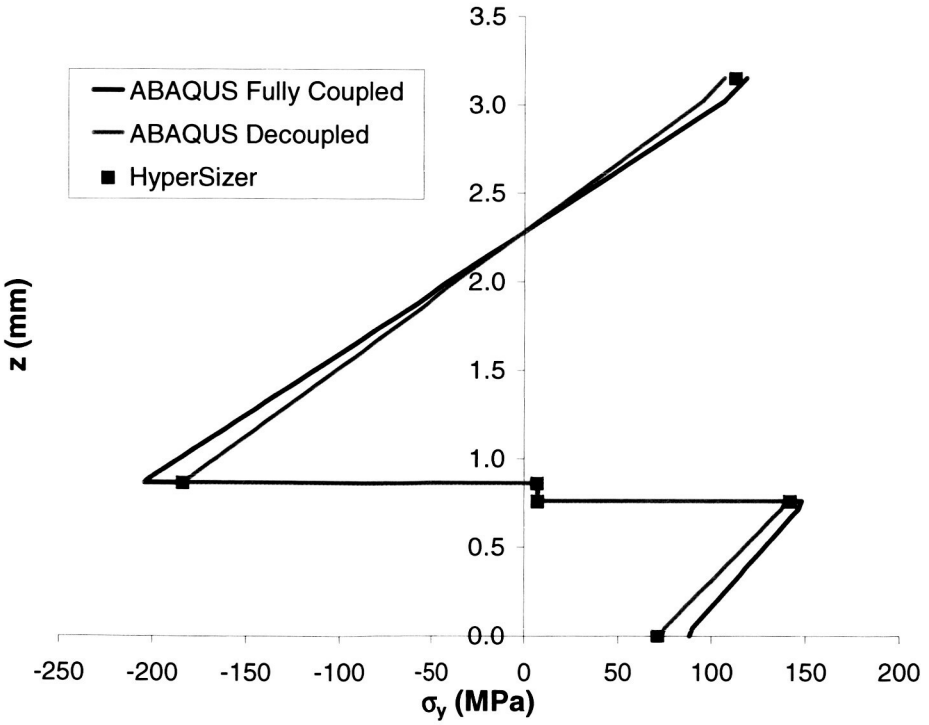

Fig. 24. Stress component (σ_y) along the cut through the flange adhesive and facesheet defined in Fig. 22 as predicted by HyperSizer and ABAQUS both with fully coupled and decoupled electric field components.

$$\begin{bmatrix} \sigma_{11} \\ \sigma_{22} \\ \sigma_{33} \\ \sigma_{23} \\ \sigma_{13} \\ \sigma_{12} \\ D_1 \\ D_2 \\ D_3 \end{bmatrix} = \begin{bmatrix} C_{11} & C_{12} & C_{13} & 0 & 0 & 0 & e_{11} & 0 & 0 \\ C_{12} & C_{22} & C_{23} & 0 & 0 & 0 & e_{12} & 0 & 0 \\ C_{13} & C_{23} & C_{33} & 0 & 0 & 0 & e_{13} & 0 & 0 \\ 0 & 0 & 0 & C_{44} & 0 & 0 & 0 & 0 & 0 \\ 0 & 0 & 0 & 0 & C_{55} & 0 & 0 & 0 & e_{35} \\ 0 & 0 & 0 & 0 & 0 & C_{66} & 0 & e_{26} & 0 \\ e_{11} & e_{12} & e_{13} & 0 & 0 & 0 & \kappa_{11} & 0 & 0 \\ 0 & 0 & 0 & 0 & 0 & e_{26} & 0 & \kappa_{22} & 0 \\ 0 & 0 & 0 & 0 & e_{35} & 0 & 0 & 0 & \kappa_{33} \end{bmatrix} \begin{bmatrix} \varepsilon_{11} \\ \varepsilon_{22} \\ \varepsilon_{33} \\ \gamma_{23} \\ \gamma_{13} \\ \gamma_{12} \\ E_1 \\ E_2 \\ E_3 \end{bmatrix} \tag{2.234}$$

where D_i are the electric displacement components and an x_1 poling direction has been assumed. By making the dielectric constants large, the stress, strain, and electric displacement components will depend on the electric field components, but the electric field components will not depend on the stress, strain, or electric displacement components. This condition is analogous to specifying constant electric field components, as is done in HyperSizer, such that they cannot vary due to the other field components.

To accomplish the decoupling of the electric field components described above, the dielectric constants given in Table 4 were increased by a factor of 10^5. Results for this case, labeled "ABAQUS Decoupled", in Figs. 23 and 24 now agree extremely well with the HyperSizer solution. Figures 25 – 28 provide further comparisons between the ABAQUS results with and without fully electric field coupling. Figure 25 indicates a slight difference in the von Mises stress field between the two cases. Likewise Fig. 26 shows only a small difference between the electric potential solution between the fully coupled and decoupled cases. However, the spatial derivatives of the electric potential, which are the electric field components in the two directions, do show significant differences. In Fig. 27(a), in the region of the facesheet directly beneath the flange, a through-thickness electric field gradient has arisen due to stress, strain, and electric displacement components that arise in the region due to the presence of the flange. In Fig. 27(b) on the other hand, the decoupling has eliminated this variation in the E_z electric field component, and a constant E_z value of 43.67 MV/m results in the facesheet, identical to the value applied in HyperSizer. The variation in E_z evident in Fig. 27(a) is approximately ±8% with respect to the constant decoupled value, which is not excessively large, but clearly is large enough to have an effect. In Fig. 28(a), a gradient in the E_x electric field component has arisen near the free edge of the adhesive bond within the facesheet. This is due to γ_{xz} shear strain that arises in this region which, thanks to a non-zero e_{26} (see Eq. (2.234)), gives rise to an electric displacement and field. In Fig. 28(b), the decoupling of the electric field components has eliminated this gradient, and a constant E_x field results with a value of zero. Again, this is identical to the condition imposed in the HyperSizer solution.

Next consider an I-stiffened panel composed of a PZT-7A facesheet, an aluminum I-stiffener, and an epoxy adhesive (between the stiffener and facesheet) as shown Figs. 29 and 30. The dimensions of the facesheet and top flange are identical to those used in the problem above identified in Fig. 21. The elastic and piezoelectric properties of the constituent materials are given in Tables 3 and 4. We once again consider a potential difference applied across the facesheet thickness, as shown in Fig. 21, that corresponds to an electric field of $(1\times10^5$ V) / (0.002286 m) = 43.74 MV/m. This problem is solved using the new HyperSizer smart material capabilities and the MSC/NASTRAN. Because MSC/ NASTRAN does not include piezoelectric capabilities, the thermal analogy discussed above, in which material level thermal terms are used to mimic the piezoelectric response (Eq. 3.223), has been employed. Applying Eq. (3.223) using the PZT-7A properties given in Tables 3 and 4, we arrive at the following "fake" coefficients of thermal expansion for the PZT-7A material,

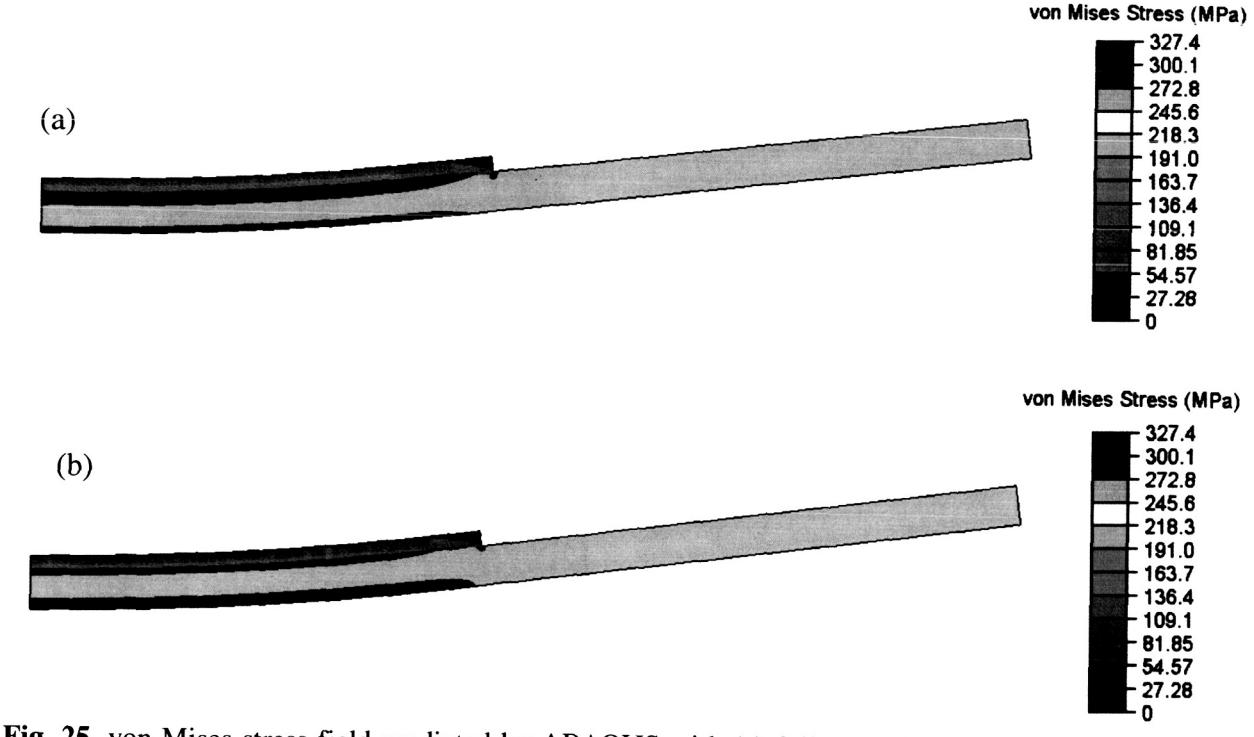

Fig. 25. von Mises stress field predicted by ABAQUS with (a) fully coupled and (b) decoupled electric field components.

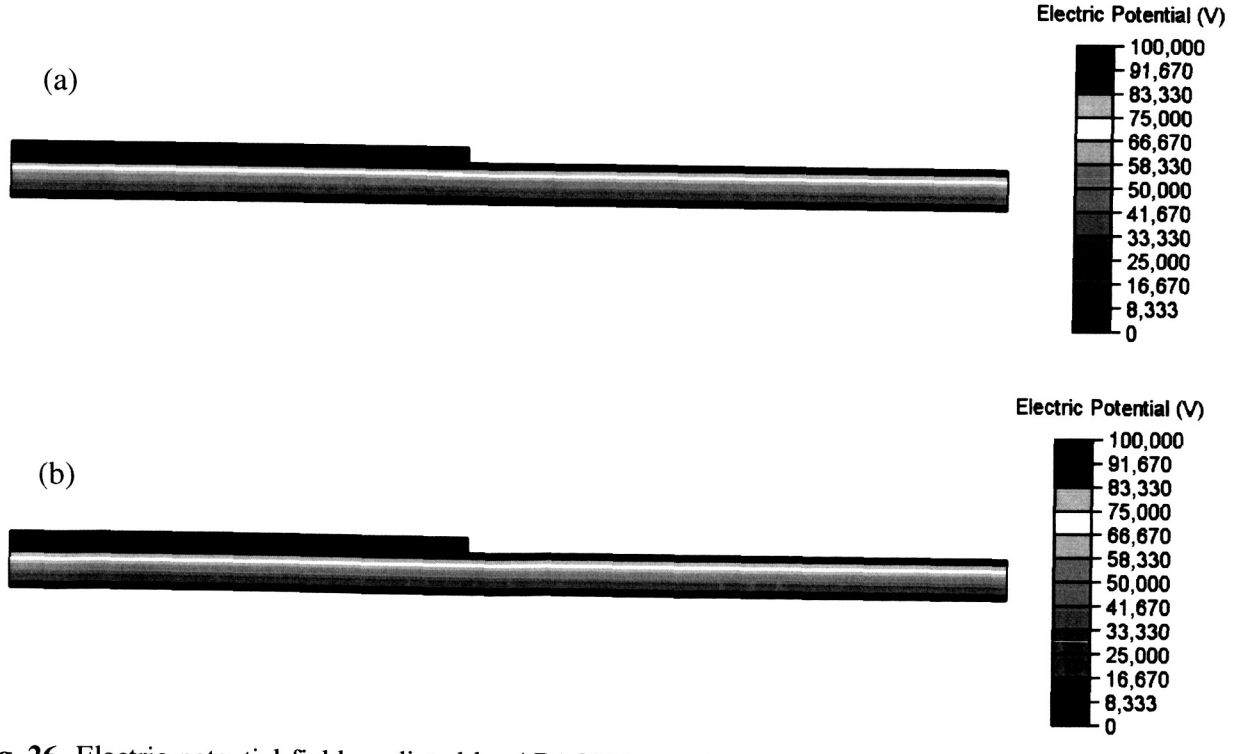

Fig. 26. Electric potential field predicted by ABAQUS with (a) fully coupled and (b) decoupled electric field components.

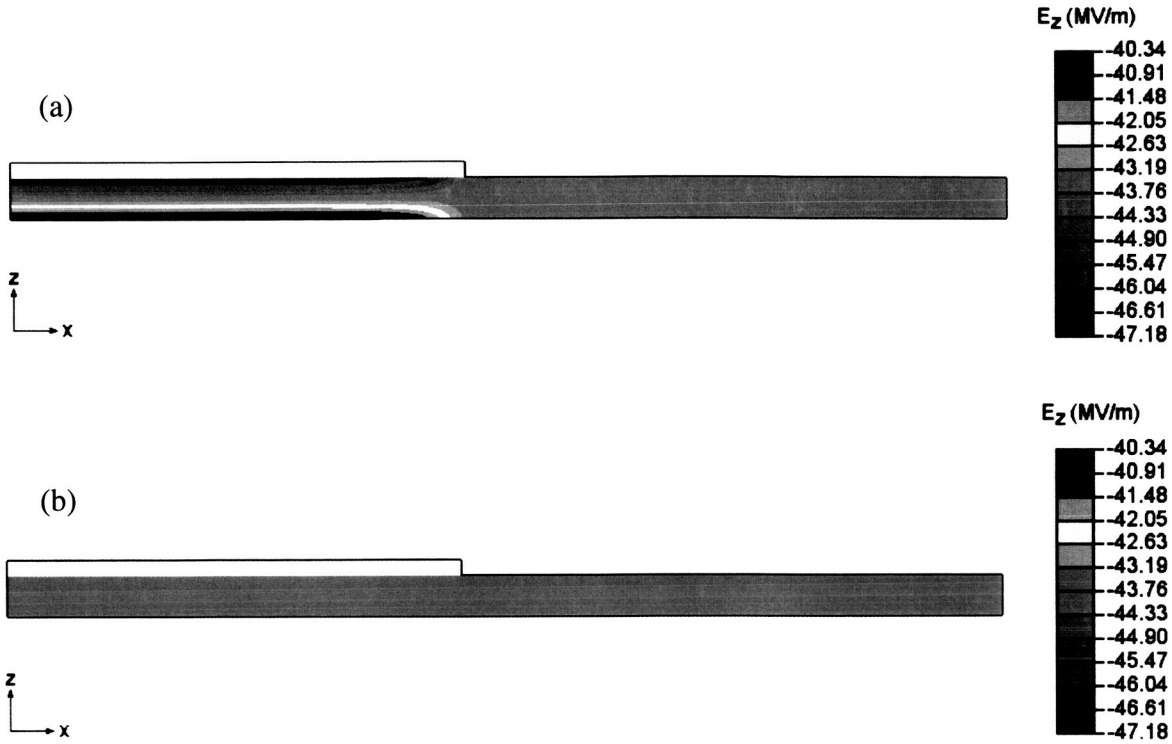

Fig. 27. Electric field component E_z predicted by ABAQUS with (a) fully coupled and (b) decoupled electric field components.

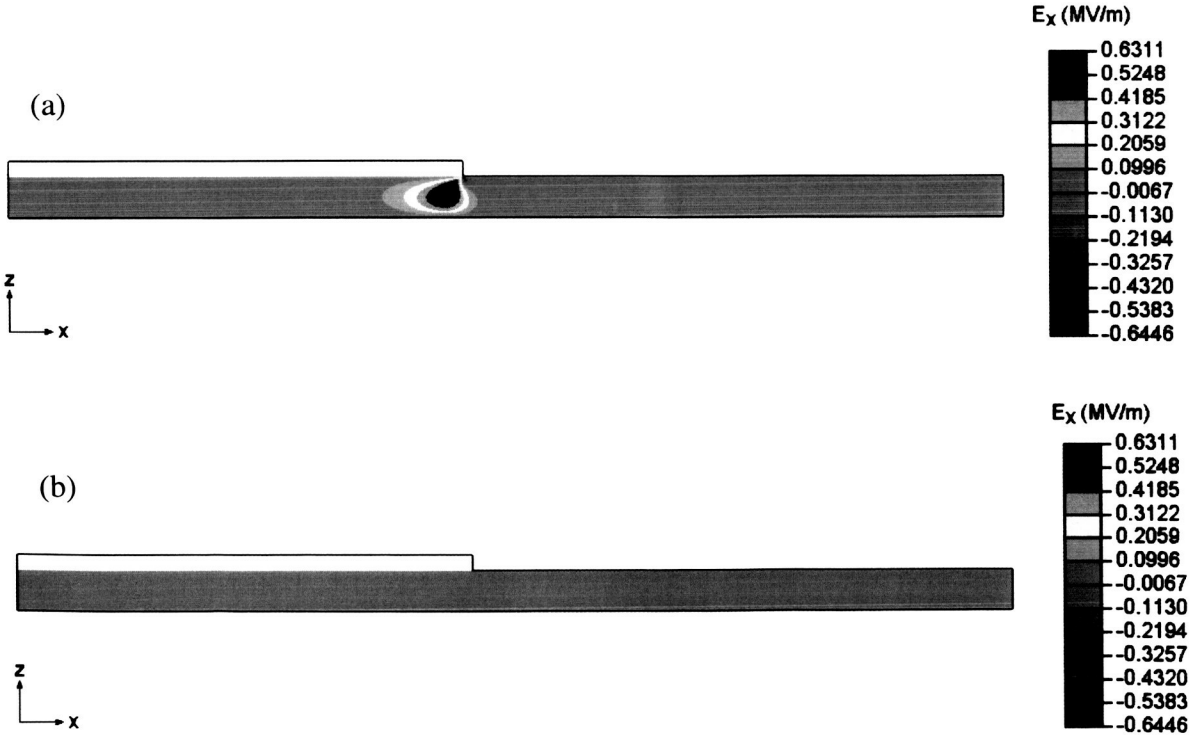

Fig. 28. Electric field component E_x predicted by ABAQUS with (a) fully coupled and (b) decoupled electric field components.

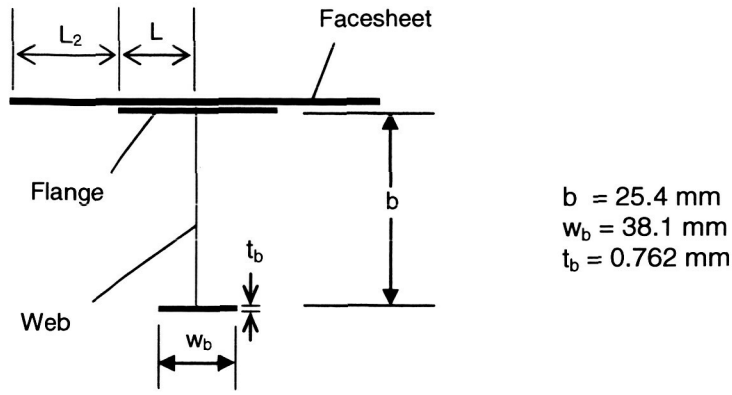

Fig. 29. Configuration of the bonded I-panel for piezoelectric analysis.

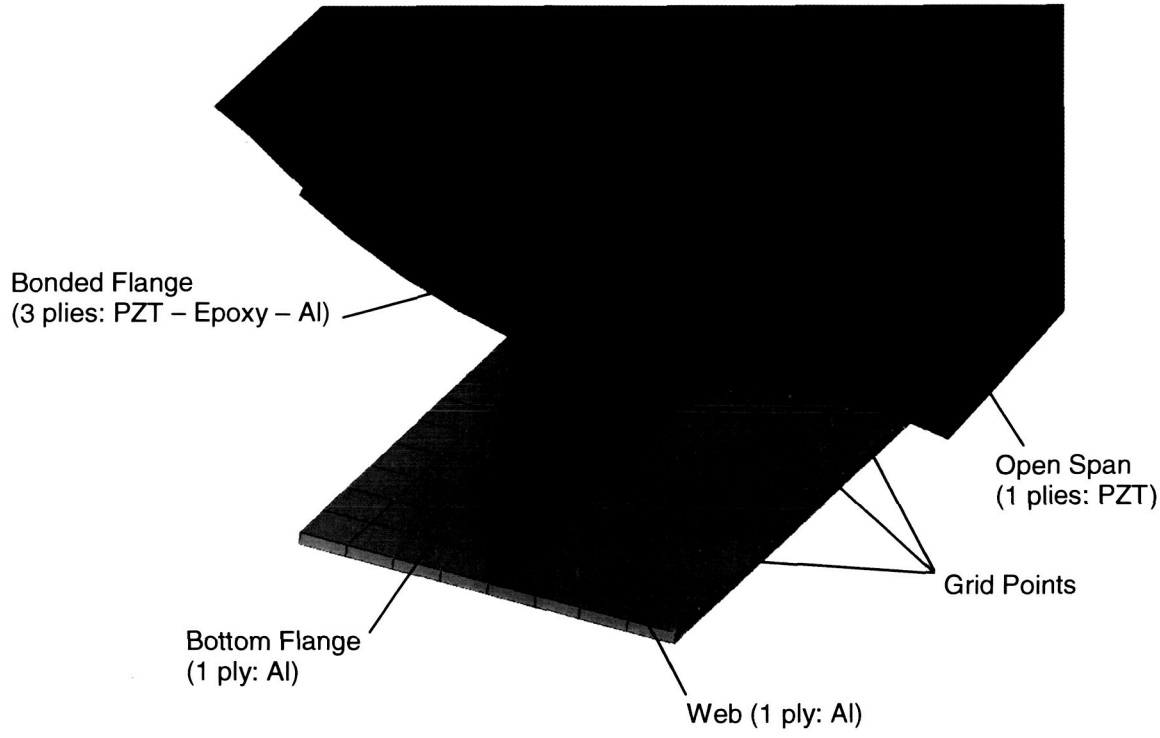

Fig. 30. Finite element representation of bonded I-panel using plate elements. To avoid overlap of material at nodal intersections, the plates were modeled using NASTRAN PCOMP property cards, with offset from the reference plane grids as shown.

$$\begin{bmatrix} \alpha_1 \\ \alpha_2 \\ \alpha_3 \\ \alpha_4 \\ \alpha_5 \\ \alpha_6 \end{bmatrix}^{Fake} = \begin{bmatrix} 1.666\times10^{-10}\,\text{C/N} \\ -0.645\times10^{-10}\,\text{C/N} \\ -0.645\times10^{-10}\,\text{C/N} \\ 0 \\ 0 \\ 0 \end{bmatrix}$$

which are used for the PZT-7A within MSC/NASTRAN, along with the "fake" temperature change $\Delta T^{Fake} = 4.374$ MV/m.

The MSC/NASTRAN finite element model employed is shown in Fig. 30. Each object (Open Span, Bonded Flange, etc.) is modeled in MSC/NASTRAN using PCOMP composite material cards in combination with MAT1 isotropic or MAT8 orthotropic material cards. The reference plane, or location of grid points, for the Bonded Flange and Open Span objects were both at the bottom surface of the Bonded Flange object. This allowed the FEA to represent the geometry of the stiffener and flange without any overlap of the web and flanges. This shift of reference plane was accomplished using the ZOFFS offset flag on the PCOMP card, which represents the distance from the reference plane and the bottom of the layup.

Figure 31 compares the HyperSizer results (which explicitly account for the smart piezoelectric material effect) with the MSC/NASTRAN results (which utilize the thermal analogy to account for the smart piezoelectric material effect) for the smart I-stiffened panel. The MSC/NASTRAN panel level strains are calculated from the model's object strains as shown. The HyperSizer and MSC/NASTRAN panel level strain results are in excellent agreement: 0.25326% vs. 0.25337% for ε_x, and 0.27555% vs. 0.27566% for ε_y.

Table 5 shows that, at the "detail" level, that is, analysis object and ply level stresses and strains, the MSC/NASTRAN and HyperSizer results match to within 3 significant figures, aside from the small moment resultant in the bottom flange.

Table 5. Force resultants (lb/in) and moments resultants (lb-in/in) at the analysis object level.

Object		Nx	Ny	Nxy	Mx	My	Mxy
Open Span	HyperSizer	-351.5	0	0	-2.226	0	0
	NASTRAN	-351.7	0	0	-2.227	0	0
Bonded Flange	HyperSizer	351.2	0	0	42.63	0	0
	NASTRAN	351.4	0	0	42.65	0	0
Web (Average)	HyperSizer	297.7	0	0	-	-	-
	NASTRAN	297.9	0	0	-	-	-
Bottom Flange	HyperSizer	-113.2	0	0	-0.066	0	0
	NASTRAN	-113.3	0	0	-0.060	0	0

At the analysis object level, the element force results from the finite element analysis match the element force results calculated by HyperSizer very closely. Figure 31 shows the raw output of object level forces from HyperSizer (center screen snapshot) and the MSC/NASTRAN results file. Because the reference plane for the FEA was shifted as described above, comparing the object moments between HyperSizer and FEA requires a reference plane shift on the moments using the parallel axis theorem. The moments extracted from the FEA at the grid points are combined with the forces multiplied by the shift (0.079") to the Hypersizer reference plane. The shifted moments can then be directly compared between HyperSizer and FEA. Once again, the HyperSizer and MSC/NASTRAN results exhibit excellent agreement. Excellent agreement has also been achieve in the ply level stress results shown in Table 6.

The axial stress in the web varies linearly from the top flange to the bottom as the panel is undergoing a constant curvature in the x-direction, as shown in Fig. 32. HyperSizer reports stress only at the top and bottom of the flange, while MSC/NASTRAN reports stresses at the midpoint of each element. Plotting these stresses (Fig. 32) shows that the HyperSizer and MSC/NASTRAN predicted web stresses match very closely.

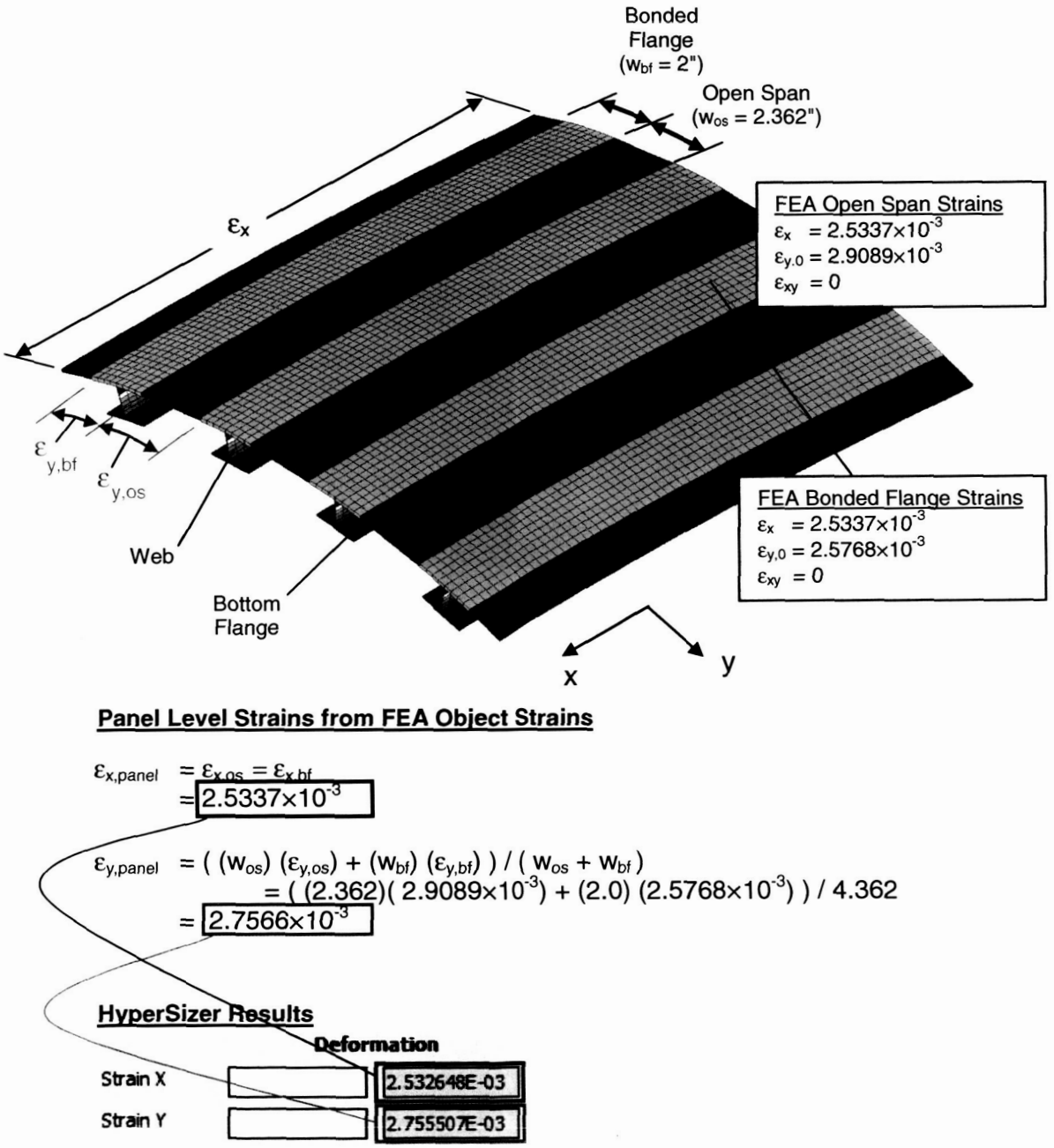

Fig. 31. The panel level results calculated by HyperSizer are the overall forces and strains of the panel as a whole rather than the individual objects. These quantities are obtained from the FEA results by extracting element strains from individual elements and combining them as shown above.

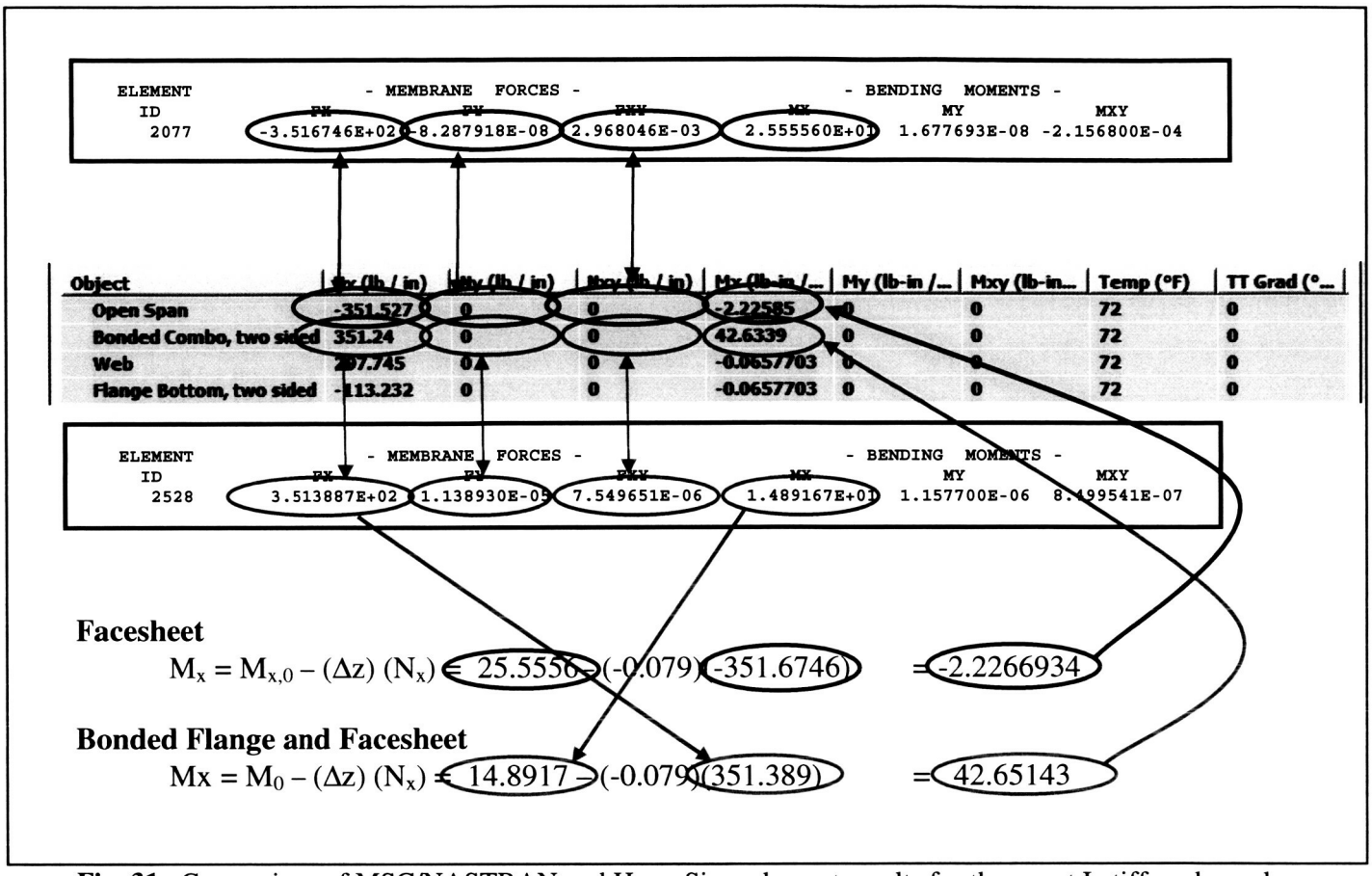

Fig. 31. Comparison of MSC/NASTRAN and HyperSizer element results for the smart I-stiffened panel.

Table 6. Comparison of the HyperSizer and MSC/NASTRAN ply stresses (psi) at the analysis object level.

Object			σ_1	σ_2	τ_{12}
Open Span	MidPlane	HyperSizer	-3906	0	0
		NASTRAN	-3907	0	0
Bonded Flange	Flange MidPlane	HyperSizer	28180	15180	0
		NASTRAN	28190	15180	0
	Adhesive Midplane	HyperSizer	1427	1022	0
		NASTRAN	1428	1022	0
	Facesheet Midplane	HyperSizer	-5553	-5105	0
		NASTRAN	-5555	-5107	0
Web	Top	HyperSizer	21990	0	0
		NASTRAN	21571	0	0
	Bottom	HyperSizer	-2034	0	0
		NASTRAN	-1714	0	0
Bottom Flange	MidPlane	HyperSizer	-3774	0	0
		NASTRAN	-3776	0	0

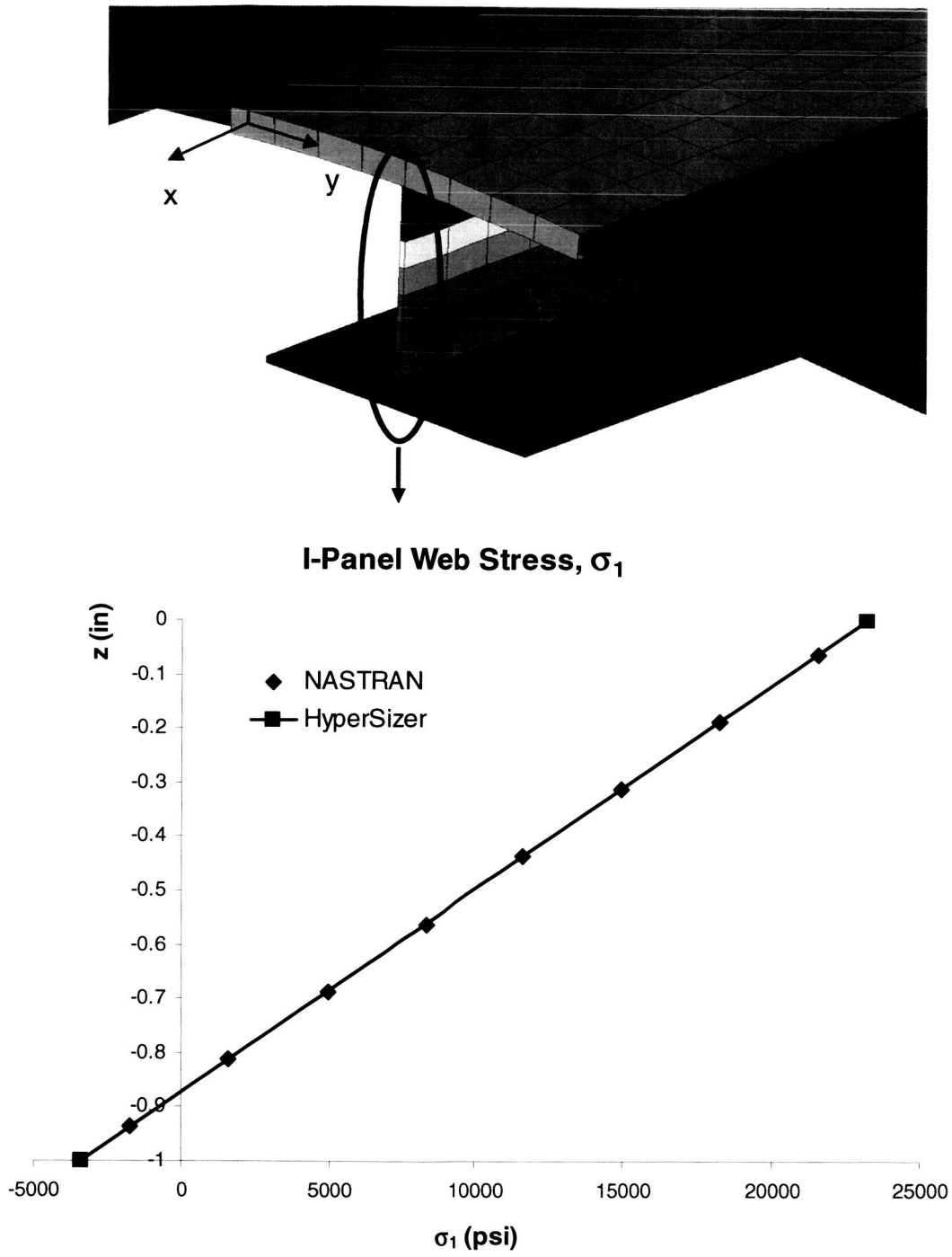

Fig. 32. Plot of the axial stress distribution through the web's height as predicted by MSC/NASTRAN and HyperSizer

The methods employed within HyperSizer to analyze composite stiffened panels with thermo-electro-magneto-elastic coupling have been presented. Starting on the level of the laminate, classical lamination theory is employed, and new electric, magnetic, thermo-electric, and thermo-magnetic ABD terms have been identified. Homogenization techniques have been presented for blade and flanged

stiffeners that result in stiffened panel level constitutive equations that are analogous to thermo-electro-magnetic laminate constitutive equations. These allow the stiffened panel to be included in a higher scale structural model via methods that accept laminate constitutive equation terms such as MSC/NASTRAN. While MSC/NASTRAN does not presently accept the newly developed thermo-electro-magnetic terms, the ability to calculate these terms allows the easy quantification and analysis of a new class of smart stiffened panels.

The analogy between standard lamination theory thermal expansion effects and the newly developed thermo-electro-magnetic effect was also discussed. This thermal analogy can be used to model the response of smart structure through a method's existing thermal capabilities as done with MSC/NASTRAN for the I-stiffened panel, or to model a thermal response of a structure through a method's electro-magnetic material capabilities. The former is useful for generating results for comparison with a known method, while the latter is useful for verifying a thermo-electro-magnetic method by generating known thermal results. In both cases, the coefficients needed to take advantage of the thermal analogy have been identified.

Verification results have been presented that compare HyperSizer piezoelectric results with ABAQUS piezoelectric finite results for a facesheet – adhesive – flange combination and with MSC/NASTRAN results for a full I-stiffened panel analysis. Because the ABAQUS capabilities are limited to piezoelectric materials, the new piezomagnetic, thermo-electric, and thermo-magnetic capabilities of HyperSizer were not compared. The results indicated generally good agreement between HyperSizer and ABAQUS. However, because ABAQUS solves a piezoelectric boundary value problem subject to prescribed electric potential, the electric field components can vary spatially within the model. The HyperSizer implementation, on the other hand, is based on classical lamination theory with prescribed spatially constant electric field components. This limitation leads to some discrepancy in the results. By decoupling the electric field components within the ABAQUS solution by significantly increasing the piezoelectric material dielectric constants, the electric field components are forced to remain constant. ABAQUS results in this decoupled condition match the HyperSizer results nearly exactly, serving to verify the HyperSizer piezoelectric implementation.

Because MSC/NASTRAN does not include piezoelectric analysis capabilities, the thermal analogy derived above was employed to enable the analysis of a smart I-stiffened panel with a PZT-7A facesheet. Comparison of the HyperSizer explicit smart panel analysis with the MSC/NASTRAN thermal analogy results showed that the results of the two methods are virtually identical in terms of the global and local strains, force resultants, and stresses throughout the stiffened panel. These results verify not only the correctness of the HyperSizer smart structural analysis capabilities, but also the correctness and utility of the thermal analogy that can be employed within finite element analysis to simulate smart structures.

3.3 Inclusion of Time-Dependence

A major accomplishment of the project is the incorporation of time-dependent load analysis capabilities within the HyperSizer structural sizing software package. This extension enables HyperSizer to step through a thermo-mechanical loading profile on a stiffened composite structure rather than considering loads as static points at which an analysis is performed. Now, when coupled with HyperSizer's new MAC/GMC micromechanics capabilities (see Tasks 4 and 5), the MAC/GMC code is called for each ply in each stiffened panel component at each step of the applied global loading. Local damage and failures can then occur at the level of the fiber and matrix constituents throughout the panel and affect the local ply stiffness. The reduced stiffness of the plies in turn affects the ABD matrices of their laminates, which affects the response of the panel as a whole. Thus, progressive damage and failure analysis of composite laminates and stiffened panels can now be performed within HyperSizer, which represents a major leap in the state of the art. In addition, a new panel-level global failure criterion has been developed and implemented in order to predict overall failure as a result of accumulated local

damage. Finally, a methodology for determining design margins of safety, quantities critical to the core HyperSizer capabilities, based on progressive failure analysis, has been developed and implemented.

HyperSizer's new time-dependent capabilities allow the code to apply loading in an incremental fashion, linearly stepping to a given load level rather than applying the load all at once. The time stepping procedure is outlined as,

1) Zero all stress and strain fields
2) Loop over the plies of the stiffened structure, calling MAC/GMC at each ply to obtain effective elastic properties. These properties take into account any damage that has occurred during any previous step.
3) Integrate the local ply properties to calculate the global ABD matrices for the stiffened structure.
4) Apply loads (global N_x, N_y, etc.) and determine global response (ε, κ, etc.).
5) Resolve ply-level strains from global strains and curvatures.
6) Pass ply-level strains to MAC/GMC library. MAC/GMC calculates subcell local fields, determines damage (if any), and returns margins of safety for given ply strains to HyperSizer.
7) Return to step 2 for the next time step, where any damage occurring during the present step will be reflected in the ABD matrix during the next step.

In the context of time-dependent analysis, HyperSizer's ability to consider multiple load cases now enables consideration of a history-dependent loading profile. A load case is a panel-level set of loading conditions consisting of N_x or ε_x, N_y or κ_y, N_{xy} or κ_{xy}, M_x or κ_x, M_y or κ_y, M_{xy} or κ_{xy}, Q_x, Q_y, temperature change from reference, and through-thickness temperature gradient. HyperSizer traditionally has considered each such load case separately, determining margins of safety for each. With the new time-dependent capabilities, each load case has an associated time and a time step size, and HyperSizer treats the load cases as a load profile, as shown in Fig. 33. The load cases thus form a number of points, and HyperSizer steps linearly from zero load to the first load point, then to the second, and so on. While stepping to a load point, local damage can potentially occur, thus making the panel response history dependent. As shown in Fig. 33, this potential path dependence could render the panel response to the two depicted load profiles different, despite the fact that all load points are identical. In contrast, HyperSizer's previous time-independent capabilities would predict the panel response to both load profiles as identical.

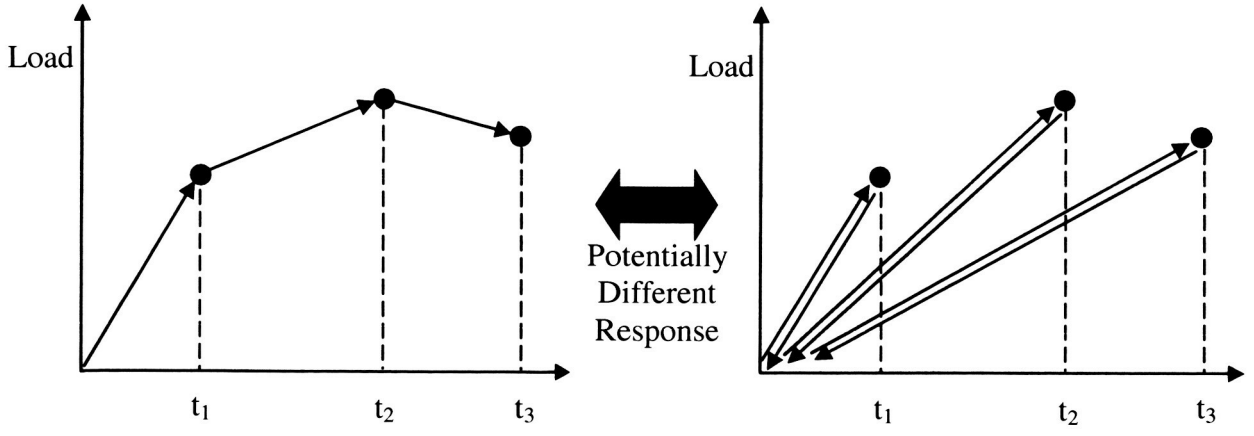

Fig. 33. HyperSizer's new time-dependent capabilities transform its existing load cases into a load profile through which the code steps. The two profiles shown, consisting of identical load points, now potentially yield different panel responses.

In order to predict overall panel failure during a time-dependent analysis, and thus determine a margin of safety for load levels below failure, a panel level failure criterion is needed. In the case of static HyperSizer panel analyses, ply-level failure theories are used to calculate the panel margin of safety. That is, the panel stresses and strains are localized to determine ply-level stresses and strains, which are then used in anisotropic failure theories such as the maximum stress criterion and the Tsai-Wu criterion. This type of static analysis thus considers panel failure to occur upon failure of the first ply. In the new time-dependent HyperSizer analyses, a ply may damage considerably before its contribution to the panel is no longer important, and several plies may damage completely (i.e., fail) before final failure of the panel. Clearly, a traditional failure theory, based on panel- or ply-level stresses or strains is not appropriate in this context. Rather, a criterion that evaluates the panel's global ability to support further loading is needed. Candidate criteria related to the rate of change of the panel strain energy density and to the trace of the panel ABD matrix were considered and evaluated. It was determined that the strain energy density rate experiences a disturbance (i.e., large drop) upon each local failure within the panel, and was thus not well-suited, while the trace of the ABD matrix did not experience a large change as a given laminate failed, even when the overall apparent stiffness of the laminate was reduced to near zero. The trace of the inverse of the panel ABD matrix, on the other hand, did exhibit large changes during failure, without the unwanted disturbances. After several trials of this procedure, an increase of an order of magnitude in the trace of the panel inverse ABD matrix has been chosen as the failure criterion in HyperSizer. Upon fulfillment of this criterion, the time stepping within HyperSizer stops, and the highest previously achieved load level is chosen as the panel or laminate ultimate load.

A sample laminate progressive failure response illustrating the implemented trace inverse ABD failure criterion is given in Fig. 34. Damage initiates at an applied midplane strain of 0.005, but it is not until a midplane strain of 0.01 that a large drop in the force resultant is observed. The trace of the laminate inverse ABD matrix increases by a factor of 4.8, and as Fig. 34 shows, the laminate force resultant continues to rise. It is not until the applied midplane strain reaches a value of 0.02 that the inverse ABD increases by an order of magnitude from its original value, signaling global failure in HyperSizer. Clearly, at this point the laminate cannot support any additional loading. HyperSizer then uses the highest achieved load level, $N_x = 4.85$ kips/in. in the example, as the failure load for the laminate or panel.

Predicting overall failure based on progressive micro scale failure is a new capability for HyperSizer, but for full implementation, the new capability must automatically calculate a margin of safety (MOS) based on a user specified load. With the new HyperSizer time-dependent capabilities, users can now specify an entire load profile (i.e., load vs. time points, see Fig. 33), but MOS values must be calculated for each specified load level. The MOS is defined as:

$$MOS = \frac{Allowable\ Load}{Actual\ Load} - 1 \tag{3.235}$$

It is a measure of how close the actual (i.e., specified) load is to the allowable (i.e., failure) load. If the actual load is small compared to the allowable load, the MOS will be large, indicating a safe load. If the actual load is at or below the allowable load, the MOS will be zero or negative, indicating an unsafe load. In the context of time-dependence, if the user specifies load levels that are below the allowable load, a question arises as to how to determine the MOS since the allowable load will not be known. That is, if a specified load is below the failure load, HyperSizer will reach that load without detecting final failure, so the allowable load will not be known. The procedure developed and implemented within HyperSizer for determining time-dependent MOS is depicted in Fig. 35. If a user-specified load point is reached without reaching overall failure, HyperSizer stores the information at that point, and then continues loading until overall failure is predicted. This then establishes the allowable load, and the MOS for that load point can be calculated from Eq. (3.235). HyperSizer then returns to the specified load point and continues loading along the path to the next load point. If failure is not detect before this next load point is reached,

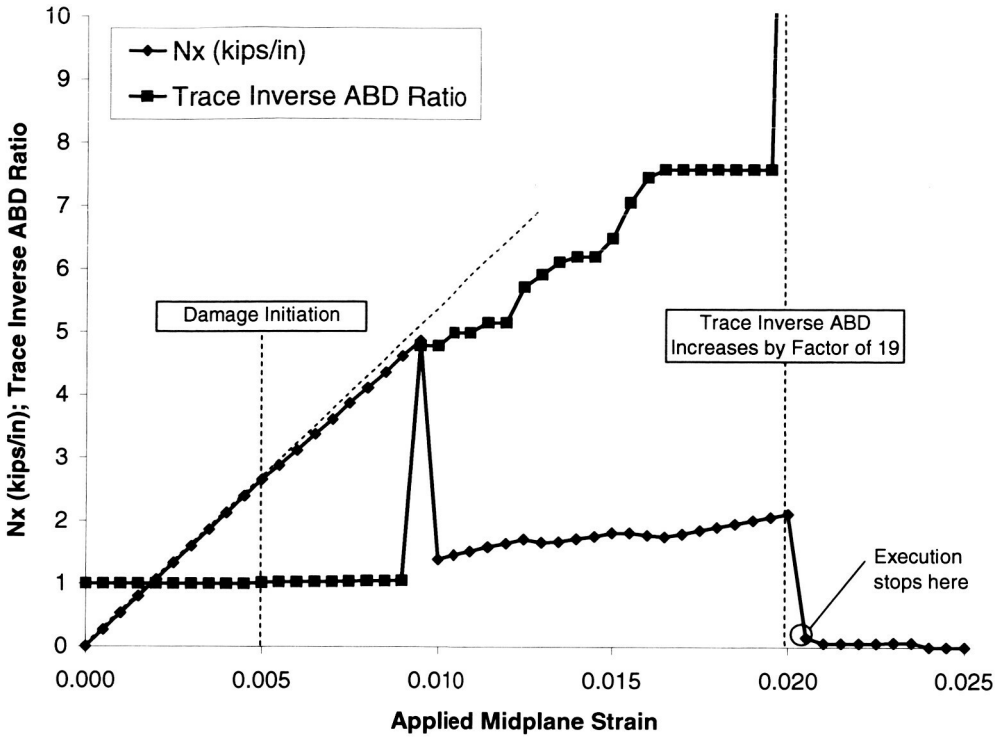

Fig. 34. HyperSizer progressive failure simulation of a quasi-isotropic graphite epoxy laminate; force resultant vs. applied midplane strain and trace inverse ABD ratio (trace inverse ABD / original trace inverse ABD) vs. applied midplane strain. An increase of 10 times of the trace of the inverse ABD from its initial (undamaged) value was chosen as the failure criterion for cessation of the time stepping in HyperSizer. HyperSizer then chooses the highest previous load level as the ultimate load.

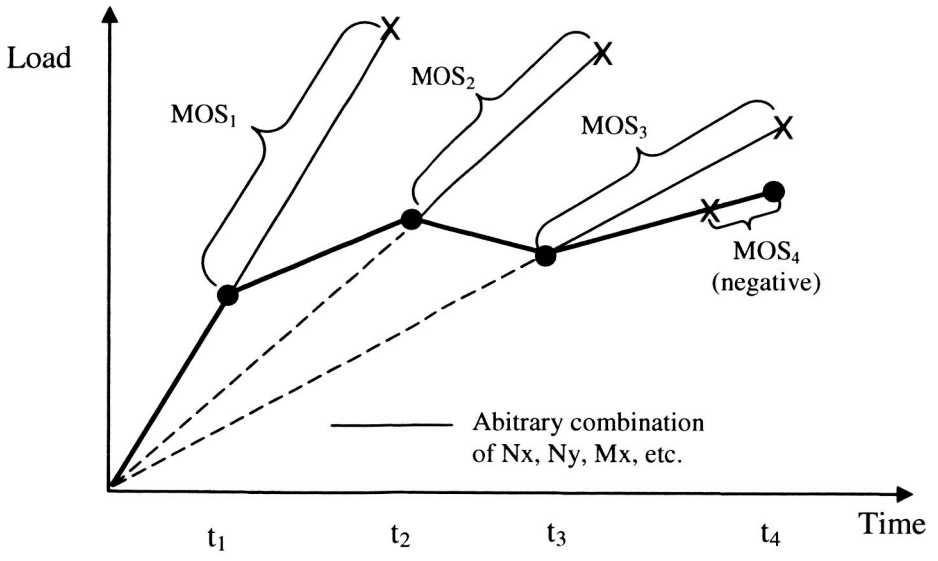

Fig. 35. The procedure developed and implemented within HyperSizer for determining time-dependent margins of safety (MOS) for each specified load point involves automatically stepping along a path connecting the origin with the load point until overall failure occurs.

HyperSizer again stores the information at the point and continues loading. However, as shown in Fig. 35, the loading continues not along the path between the load points, but along the path defined by the origin and load point. This then gives a true measure of how close the specified load point is to failure and accounts for any previous damage that has occurred in reaching the specified load point. If HyperSizer predicts overall failure along the path between two specified load points, then the negative MOS is calculated based on how far along the path the panel progressed before the overall failure. It should be noted that the load points are, in general, multi-axial, and thus Fig. 35 is just a schematic representation of the procedure. Fig. 36 provides actual HyperSizer intermediate ASCII data for a time-dependent HyperSizer progressive failure analysis.

HyperSizer time-dependent progressive failure analysis results were verified via comparison to MAC/GMC time-dependent results at the laminate level. Note that the HyperSizer panel-level time-dependent progressive failure analysis results are unique and thus not able to be verified. A verification example involving progressive failure of a fictional complex symmetric laminate consisting of doubly- and triply-periodic layers is shown in Fig. 37. Results for two different time step sizes are shown and in both cases, MAC/GMC and HyperSizer predictions are virtually identical. The example also indicates the location at which the overall failure criterion employed in HyperSizer (based on the trace of the inverse of the ABD matrix) is fulfilled, thus stopping the code's execution. Fig. 38 shows a verification case for similarly complex asymmetric laminate, which due to the asymmetry, experiences bending. Results for two different time step sizes are again shown, and the MAC/GMC and HyperSizer results are very similar. Slight differences occur in the vicinity of local failures due to the fact that MAC/GMC tracks damage at two points per ply, while HyperSizer tracks damage at only one.

The new HyperSizer time-dependent progressive failure analysis capabilities were applied to analyze a composite laminate studied as part of the World Wide Failure Exercise (WWFE) (Soden et al., 1998). The WWFE provided ply level properties for four polymer matrix composites and invited leading composite failure theory researchers to predict the deformation and strength of several laminate lay-ups without prior access to the laminate level results. In subsequent papers, the WWFE compared the theoretical predictions with experimental results (Soden et al.m 2002). The WWFE results have thus become a standard for polymer matrix composite laminate failure analysis. In Figs. 39 and 40, the HyperSizer time-dependent progressive failure predictions are compared with the biaxial WWFE experimental results for a quasi-isotropic $[0/\pm45/90]_s$ AS4 graphite/3501-6 epoxy composite. The applied stress ratios ($SR = \sigma_{xx} : \sigma_{yy}$) are 20:1 and 2:1, respectively. These results show that the new HyperSizer time-dependent progressive failure capabilities are able to capture the non-linear deformation response (due to local damage) of the laminates accurately, as well as provide a good, slightly conservative prediction of the laminate strength. Fig. 41 shows compares the full $[0/\pm45/90]_s$ AS4/3501-6 failure envelope predicted by the new HyperSizer time-dependent progressive failure capabilities with the WWFE experimental results. The HyperSizer predictions for final failure as well as initiation are plotted, along with the corresponding WWFE experimental results. Also plotted for comparison are first ply failure envelopes predicted by other leading ply-level failure theories. These results clearly indicate the dramatic improvement represented by HyperSizer's new time-dependent capabilities (when functioning in conjunction with a MAC/GMC micro scale analysis). Failure initiation can now be predicted by HyperSizer, and as shown in Fig. 41, the failure initiation surface is close to the failure predictions made using most ply-level theories. More importantly, the final failure envelope predicted by HyperSizer is excellent agreement with the WWFE experimental results and far superior to the ply-level theory envelopes.

The next step, as shown schematically in Fig. 42, is to perform analysis of a stiffened panel. A T-stiffened panel, like that shown in Fig. 43, composed of a $[0/\pm45/90]_s$ AS4/3501-6 facesheet and a $[0/\pm45/90]_s$ AS4/3501-6 T-stiffener, has been analyzed using HyperSizer. Deformation results for a stress ration of 1:0 are shown in Fig. 43. Note the presence of nonlinearity due to local damage of the epoxy matrix. Fig. 44 shows the full predicted failure envelope for the T-stiffened panel for both damage initiation and final failure. Envelopes predicted by other ply-level failure theories are once again plotted

```
==========================================
Current Load Segment:      1
Current timestep:     64
Current time:     3.2000

  "Applied" load (Nx, Ny, Nxy, Mx, My, Mxy, Qx, Qy):
 1500.0000      .0000      .0000      .0000      .0000      .0000      .0000      .0000

  "Ultimate" load (Nx, Ny, Nxy, Mx, My, Mxy, Qx, Qy):
 4725.0000      .0000      .0000      .0000      .0000      .0000      .0000      .0000

Ultimate Load MOS =      2.1500
==========================================

==========================================
Current Load Segment:      2
Current timestep:     64
Current time:     3.2000

  "Applied" load (Nx, Ny, Nxy, Mx, My, Mxy, Qx, Qy):
 1500.0000-1500.0000      .0000      .0000      .0000      .0000      .0000      .0000

  "Ultimate" load (Nx, Ny, Nxy, Mx, My, Mxy, Qx, Qy):
 3225.0000-3225.0000      .0000      .0000      .0000      .0000      .0000      .0000

Ultimate Load MOS =      1.1500
==========================================

==========================================
Current Load Segment:      3
Current timestep:    108
Current time:     5.4000

  "Applied" load (Nx, Ny, Nxy, Mx, My, Mxy, Qx, Qy):
 1500.0000 1500.0000      .0000      .0000      .0000      .0000      .0000      .0000

  "Ultimate" load (Nx, Ny, Nxy, Mx, My, Mxy, Qx, Qy):
 5025.0000 5025.0000      .0000      .0000      .0000      .0000      .0000      .0000

Ultimate Load MOS =      2.3500
==========================================

==========================================
Current Load Segment:      4
Current timestep:     93
Current time:     3.6600

Component failed within this time segment...

Ultimate Load MOS =      -.3400
==========================================
```

Fig. 36. Results of a HyperSizer progressive failure analysis involving multiple user-specified load points for which margins of safety (MOS) were determined. The specified load levels were: 1) Nx = 1500 Ny = 0, 2) Nx = 1500 Ny = -1500, 3) Nx = 1500 Ny = 1500, and 4) Nx = 7000 Ny = 0 (all lb/in.). For load level 1, HyperSizer stepped to Nx = 1500 lb/in, and then out to an ultimate load of Nx = 4725 lb/in, for a predicted MOS of 2.15. Then, the code returned to the stored micro/macro state at Nx = 1500 lb/in, stepped to Nx = 1500 Ny = -1500, and then out to failure for a predicted MOS of 1.15. Next, after returning to the state at Nx = 1500 Ny = -1500 and stepping to Nx = 1500 Ny = 1500, a MOS of 2.35 was predicted (correctly capturing the biaxial tensile load interaction effect). Finally, in attempting to reach a load level of Nx = 7000 Ny = 0, ultimate failure was predicted, resulting in a negative margin for this load level.

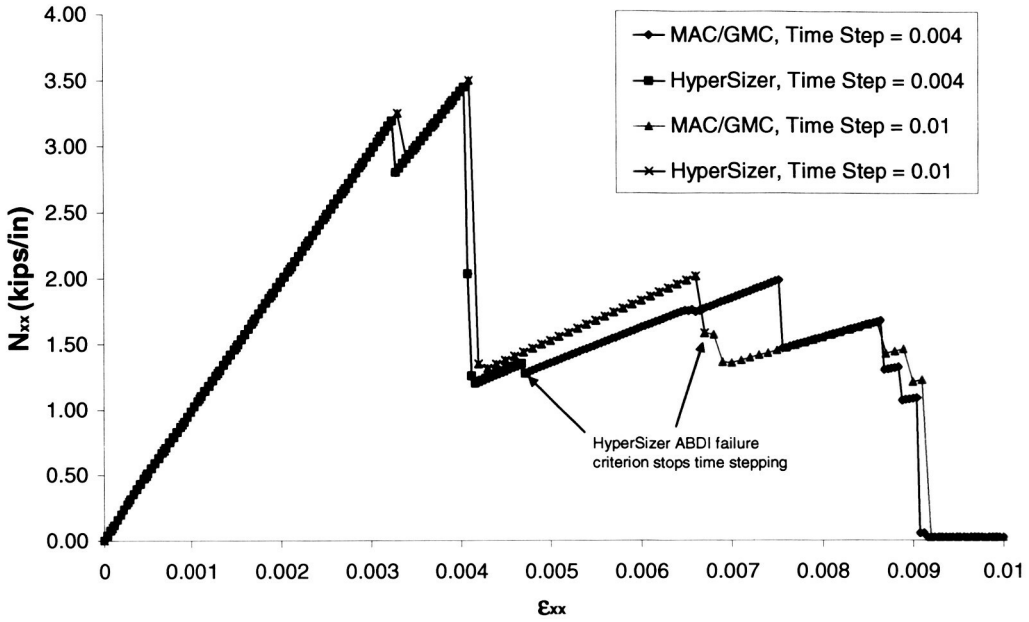

Fig. 37. Comparison of HyperSizer to MAC/GMC for the predicted progressive failure response of a fictional symmetric laminate containing both doubly-periodic and triply-periodic composite layers. Results are nearly identical.

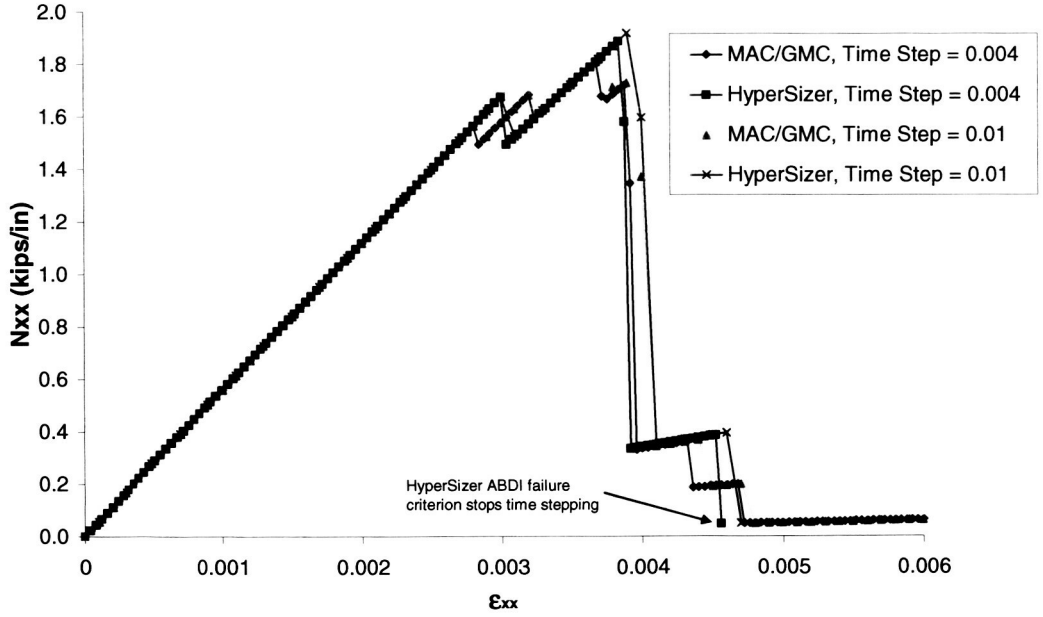

Fig. 38. Comparison of HyperSizer to MAC/GMC for the predicted progressive failure response of a fictional asymmetric laminate. The differences are due to the fact that MAC/GMC tracks the damage at two points per ply, while HyperSizer only employs one. This has an effect when, as in this asymmetric case, bending occurs.

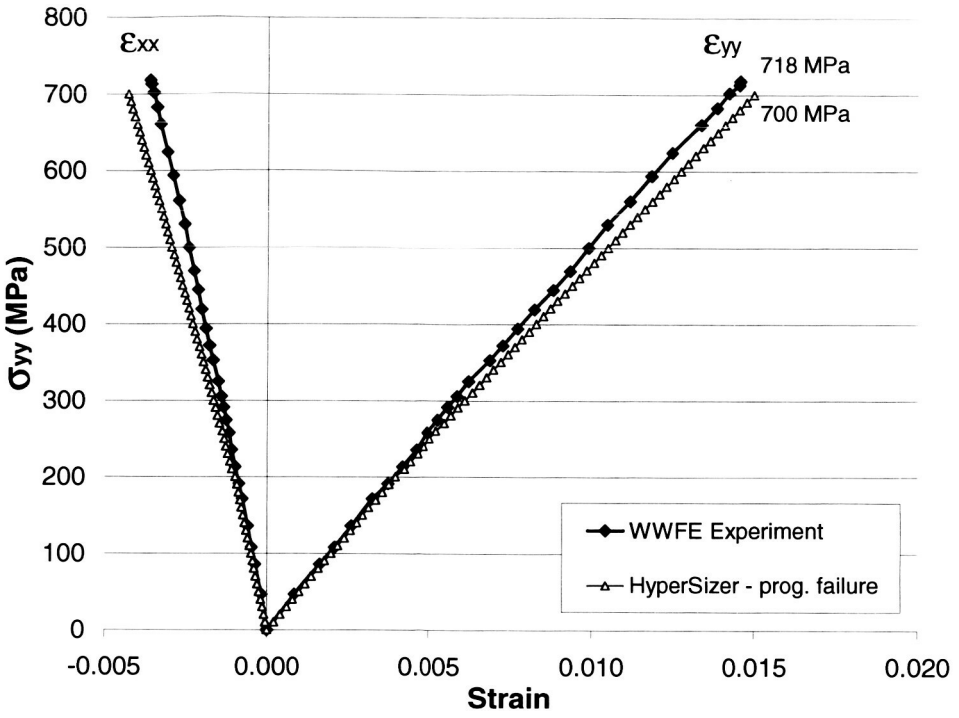

Fig. 39. Comparison of time-dependent HyperSizer progressive failure deformation predictions with WWFE biaxial experimental results for $[0/\pm45/90]_s$ AS4/3501-6 with SR=20:1.

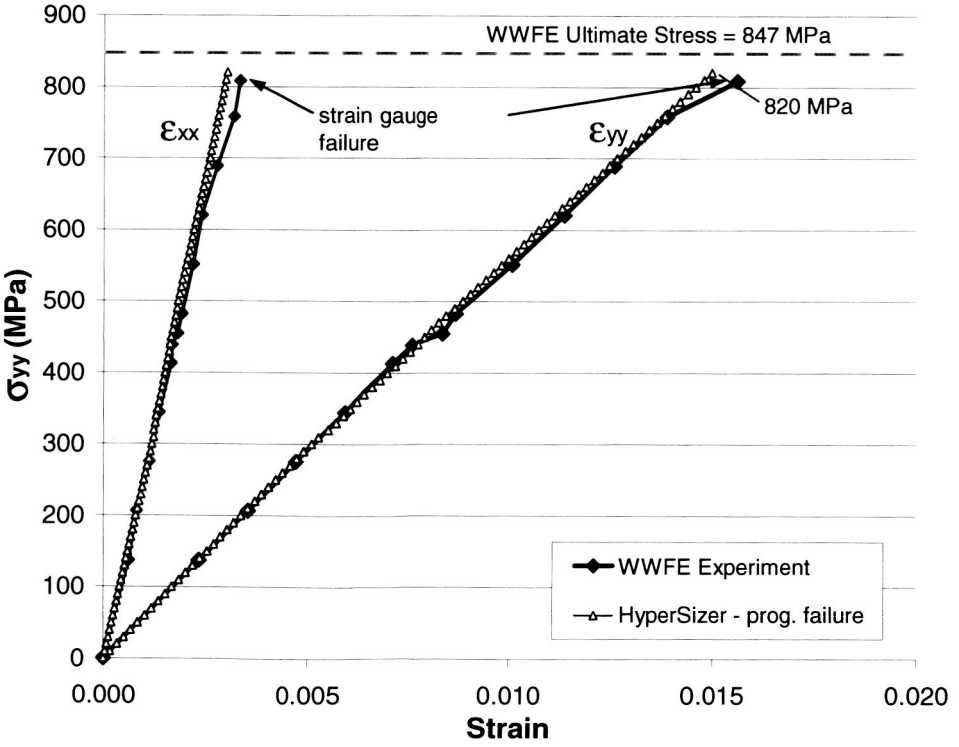

Fig. 40. Comparison of time-dependent HyperSizer progressive failure deformation predictions with WWFE biaxial experimental results for $[0/\pm45/90]_s$ AS4/3501-6 with SR=2:1.

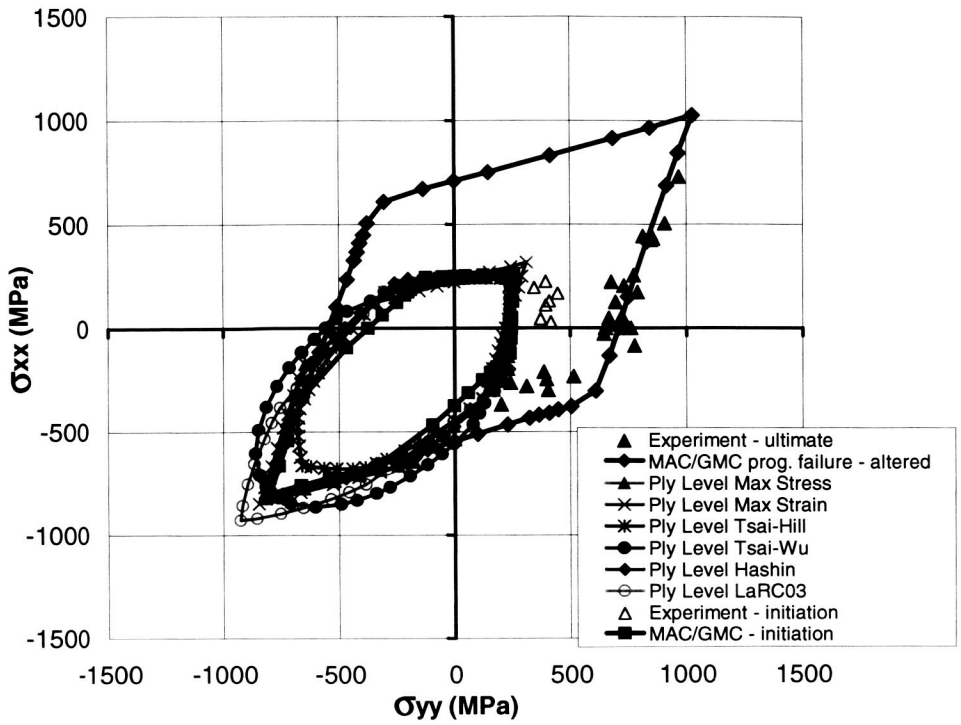

Fig. 41. Comparison of time-dependent HyperSizer progressive failure deformation predictions with WWFE experimental results for the $[0/\pm45/90]_s$ AS4/3501-6 failure envelope. Predictions made with other ply-level failure criteria are plotted as well.

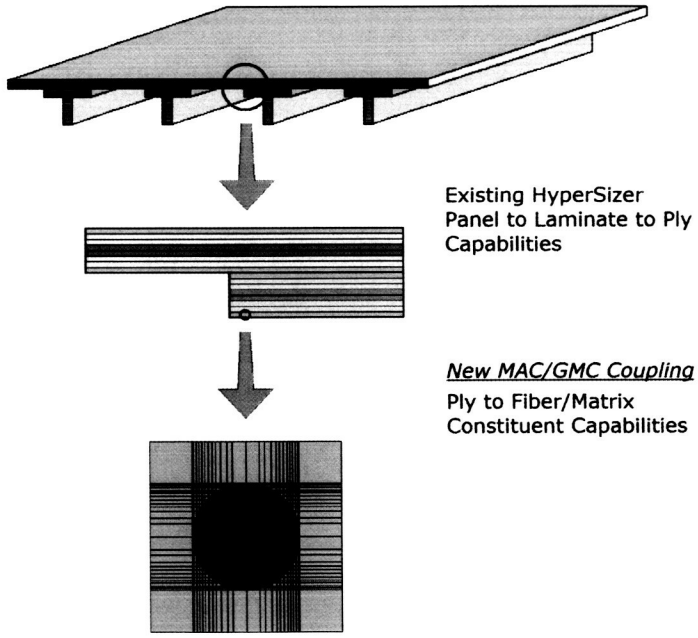

Fig. 42. Schematic of the T-panel to ply to micromechanics simulations now available within HyperSizer in the context of time-dependence and progressive failure. This new capability is a major accomplishment of this project.

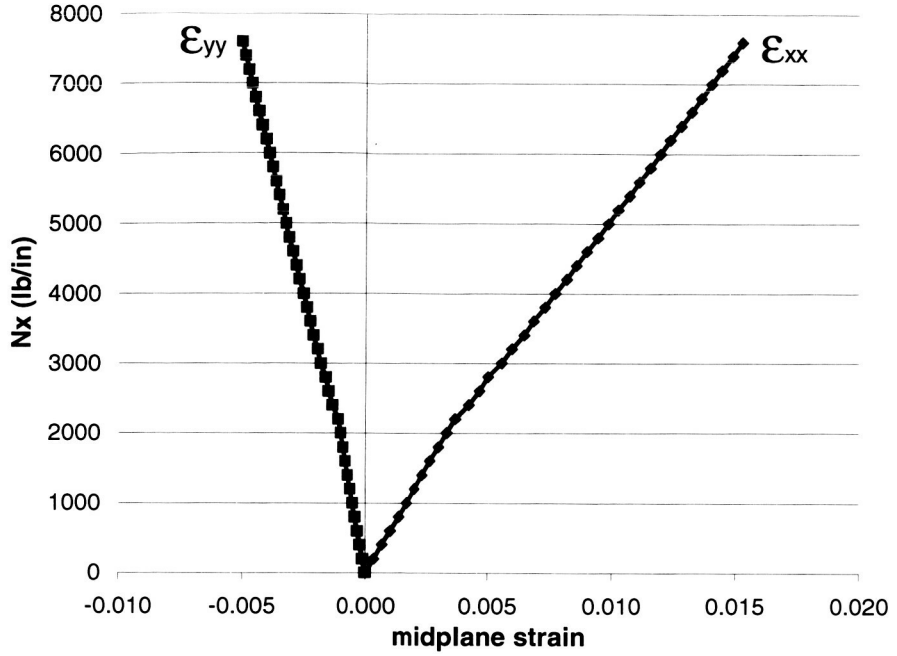

Fig. 43. Time-dependent HyperSizer progressive failure deformation predictions for a $[0/\pm45/90]_s$ AS4/3501-6 T-stiffened panel, SR=1:0.

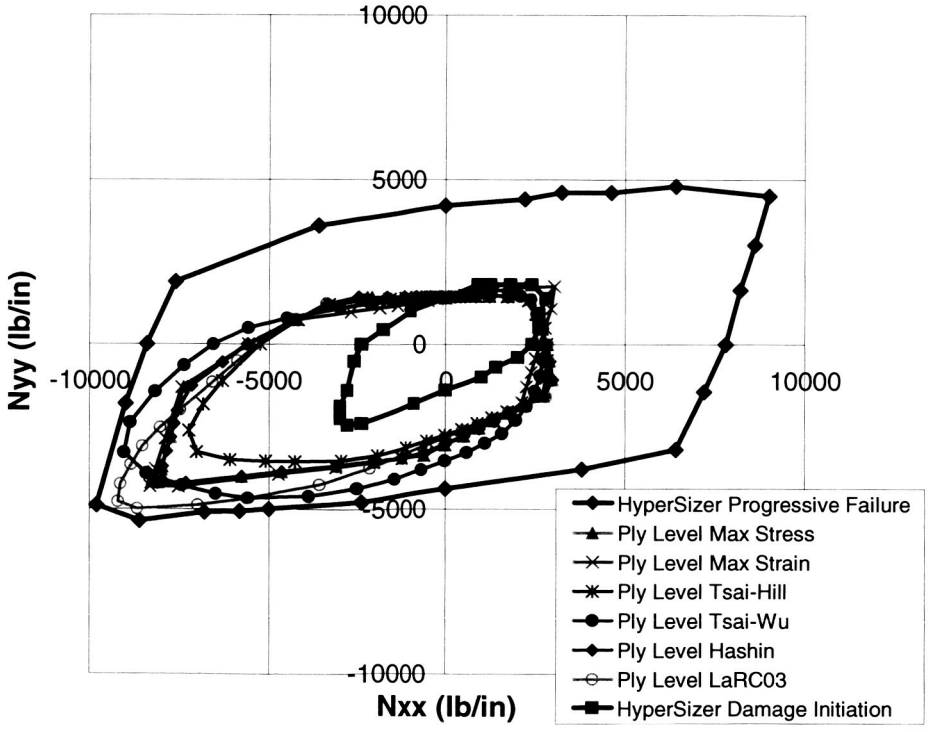

Fig. 44. Time-dependent HyperSizer progressive failure predictions for the failure envelope of a $[0/\pm45/90]_s$ AS4/3501-6 T-stiffened panel. Predictions made with other ply-level failure criteria are plotted as well.

for comparison. Although experimental data are not available for this panel, considering the superior predictions made by HyperSizer for the $[0/\pm45/90]_s$ AS4/3501-6 laminate (of which the T-panel facesheet and T-stiffener is made), it is likely that the HyperSizer time-dependent progressive failure results would once again match experiment much better than the ply-level theories.

Task 4. MAC/GMC and HOTFGM Linked to HyperSizer

Development of the linkages between HyperSizer and the micro scale models involved enabling access to MAC/GMC and HOTFGM as separate modules within HyperSizer that can function as stand-alone analysis tools. This intermediate step in the development of the fully integrated technology was needed to design the proper protocols to allow the models to function as one in an efficient manner.

4.1 Streamline MAC/GMC, Develop Protocol

In association with this task, an entirely new version of the MAC/GMC code was released (Version 4.0) along with extensive documentation (Bednarcyk and Arnold 2002a,b), see Fig. 2. One of the main focuses of this release involved streamlining the code and the input requirements so as to facilitate the coupling of the code with HyperSizer. Version 4.0 of MAC/GMC has been completely rewritten in the FORTRAN 90 code standard, as opposed to previous versions that utilized FORTRAN 77. This has enabled use of dynamic memory allocation, which is critical to the code's incorporation within HyperSizer. This dynamic memory allocation has eliminated static problem size limitations and enabled streamlined use of computer resources as only the memory needed for a particular MAC/GMC problem or problems is allocated. Advantage has also been taken of FORTRAN 90 modules, providing easy access to data throughout all MAC/GMC subprograms. This, in turn, has enabled streamlining of many different features of the software and provided much more interoperability of the various MAC/GMC libraries (see Fig. 2). The MAC/GMC Version 4.0 input file has been streamlined as well. Significantly more logical keywords and specifiers are now utilized, and the organization of the input data is now more logical and straightforward.

Two distinct protocols were developed for the linkage between HyperSizer and MAC/GMC. The first is for executing stand alone MAC/GMC problems with HyperSizer (using the new HyperSizer Micromechanics Workspace GUI, see Task 4.3). The second, discussed under Task 5.1, is for executing fully integrated HyperSizer – MAC/GMC problems. For stand alone MAC/GMC problems, the linkage protocol between HyperSizer and MAC/GMC is based on transferring data through ASCII files. That is, a stand alone MAC/GMC problem set up and executed within HyperSizer causes a MAC/GMC input file to be written and the code executed. MAC/GMC results are then written to ASCII files, which are then read, displayed, and stored by HyperSizer. This weak linkage was established early in the project as it was a logical starting point for enabling the linkage. Because stand alone analyses are typically far less computationally and memory intensive than coupled HyperSizer – MAC/GMC problems, the inefficiency associated with the read/write cycle is barely noticeable. Obviously, for fully coupled analyses, which typically call MAC/GMC thousands of times, such read/write cycles are not used (see Task 5.1). Finally, by writing input to a standard MAC/GMC input file for stand alone MAC/GMC problems, the input file is available for examination and future use by the user.

This task resulted directly in two NASA publications:

1) Bednarcyk, B.A. and Arnold, S.M. (2002a) "MAC/GMC 4.0 User's Manual Volume 2: Keywords Manual" NASA/TM-2002-212077/Vol 2.

2) Bednarcyk, B.A. and Arnold, S.M. (2002b) "MAC/GMC 4.0 User's Manual Volume 3: Example Manual" NASA/TM-2002-212077/Vol 3.

4.2 Streamline HOTFGM, Develop Protocol

Like MAC/GMC, HOTFGM was streamlined to maximize efficiency, and a protocol was developed so it can be called from the HyperSizer GUI (now called NCell). As with the stand alone MAC/GMC problem protocol, the protocol for HOTFGM involves the use of ASCII files to exchange information. As discussed in Task 2, the tight coupling original envisioned between standard HOTFGM and HyperSizer was not pursued. The homogenized version of HOTFGM, developed in Task 2.2 and now

called HFGMC, was incorporated within MAC/GMC in Task 1.2. Tight coupling between MAC/GMC (and thus HFGMC) and HyperSizer has been accomplished and is discussed in Task 5.1. For stand alone standard HOTFGM problems, the HyperSizer NCell GUI (see Task 4.3) writes a standard HOTFGM input file and executes the problem. HOTFGM then writes ASCII results files which are read and displayed by HyperSizer NCell.

4.3 Develop HyperSizer GUIs

Three new HyperSizer graphical user interfaces (GUIs) have been developed under this project. The first is the HOTFGM GUI, enabling stand alone standard HOTFGM problems to be set up and executed, and the results post-processed. Note that this GUI was original called HOT-SMAC, and then called HyperSizer FGM, and is now called NCell (Nodeless Cell).

NCell is a Microsoft Windows native product providing all software options on a single multi-tabbed GUI form, see Fig. 45. The user begins the analysis by selecting the local material constitutive models (Elastic, Plastic, Creep, etc.) to be employed and entering or loading material properties on the built-in material editor form. On the Geometry tab, shown in Fig. 46, the problem's overall dimensions, number of analysis subcells in each direction, and local dimensions are specified in a variety of ways. The graphical control allows the user to specify the height and width of selected subcells and linearly grade the subcell dimensions in either direction. The Materials tab, shown in Fig. 47, allows the arbitrary distribution of materials for each subcell. The user selects individual subcells or ranges of subcells on the graphical control for material assignment. In addition to material assignment, the user can designate portions of the domain as "windows", or voids, to include features such as active cooling channels. The user can automatically grade the material in a variety of ways over any range of subcells. In Fig. 47, the shown domain is graded linearly in the x_3-direction from "Material 1" at the left border to "Material 3", and then from "Material 3" to "Material 2" at the right border.

After specifying the dimensions and materials, boundary conditions are entered on the Thermal B.C. and Mechanical B.C. tabs, Fig. 48. The boundary conditions are specified at the appropriate edge(s) for each border subcell, including external boundaries and internal windows. Permissible thermal boundary conditions include specified temperature, heat flux, or specified convection. Mechanical boundary conditions include three "pre-defined" boundary types, free (zero traction), pinned (zero displacement) and rollered. In addition, general mechanical boundary conditions can be entered with options for specified traction, displacement, or gradients of these in either direction.

After the problem is defined and the thermo-mechanical analysis is performed by depressing the "Analyze" button in the upper right of the GUI (see Fig. 45), NCell automatically imports results and displays them on the Results tab. This tab presents the results in two ways. First, they can be plotted with color fringes, as shown in Fig. 49. Second, the user can specify rows and/or columns in the problem domain for line plots of results. The software will also export these line plots to a comma separated value (CSV) file for plotting in Microsoft Excel or any other post-processing software. A more detailed description of the HOT-SMAC software is provided by Yarrington (2001).

In addition to the HyperSizer NCell GUI for stand alone standard HOTFGM problems, two GUIs associated with MAC/GMC were developed and incorporated within HyperSizer. The first, the Micromechanics Architecture Form, is used to define a MAC/GMC composite material and generate effective composite properties. This form is accessed from the standard HyperSizer orthotropic material form shown in Fig. 50. As shown in the figure, if the Micromechanics Architecture box is checked, one can specify or edit the micromechanics parameters that define the orthotropic composite material. If the box is checked, the Micromechanics Architecture form can be accessed by pressing the "Edit..." button.

The Micromechanics Architecture Form is shown in Fig. 51. Note that this form is not used to perform full MAC/GMC analyses; this is done via the Micromechanics Workspace GUI. The micromechanics architecture form only defines the composite material and determines effective properties. Within the Micromechanics Architecture Form, the repeating unit cell geometry can be chosen from the MAC/GMC repeating unit cell library displayed on the Unit Cell tab, as shown in Fig. 51, or it can be graphically defined by the user on the Geometry Tab by checking the User-Defined Geometry box, shown in Fig. 52. The composite constituent materials are chosen on the Materials tab, as

shown in Fig. 53. If the User-Defined Materials box is checked, the used can graphically distribute the materials throughout the repeating unit cell. Materials can be added or deleted to the active material system (consisting of fiber and matrix materials) through the Manage Material System Form, shown in Fig. 54. This form is accessed from the Options drop-down list in the Micromechanics Architecture Form. The Summary tab, shown in Fig. 55, displays the effective properties after they are generated by MAC/GMC by depressing the "Effective Properties" button. The "Update Orthotropic Effective Properties" button then transfers these effective material properties to the HyperSizer database and into the Orthotropic Material Form (Fig. 50). When this is done, the orthotropic material basis is automatically set to "PRED" and a note is made in the material description in the Orthotropic Material Form in order to ensure that the user realizes that the materials have been predicted via micromechanics rather than representing test results. At this point, the MAC/GMC composite material is available for use with all HyperSizer features, whether they employ micro scale analysis or use only the generated effective properties.

In order to perform full stand alone MAC/GMC analyses, the new HyperSizer Micromechanics Workspace GUI Form is used. This form is shown in Fig. 56. The analysis starts by selecting a material from the HyperSizer database that has an associated MAC/GMC Micromechanics Architecture. That is, the Micromechanics Architecture form must exist for the selected material. Users can specify analysis options, loading, failure option, and yield surface options using the tabs on the Micromechanics Workspace Form, and then execute the MAC/GMC problem by depressing the "Analyze" button. Results are automatically displayed on the Results tab in the form of macro and micro x-y plots and contour fringe plots, as shown in Fig. 57.

The availability of the HyperSizer GUI forms for executing and storing MAC/GMC stand alone problems and results is a significant accomplishment of the project. It frees MAC/GMC users from having to use the standard MAC/GMC ASCII input and output files, but preserves these files for those users that are accustomed to using them.

Seven publications have resulted all or in part from the work on Task 4.3, including two journal papers, two NASA contractor reports, and four conference papers/presentations:

1) Arnold, S.M., Bednarcyk, B.A., and Aboudi, J. (2004) "Analysis of Internally Cooled Structures Using a Higher Order Theory" Computers and Structures 82, 659-688.

2) Bednarcyk, B.A., Zhang, J., Collier, C.S., Bansal, Y., and Pindera, M.-J. (2005) "Analysis Tools for Adhesively Bonded Composite Joints, Part I: Higher-Order Theory" AIAA Journal, In Press.

3) Bednarcyk, B.A. and Yarrington, P.W. (2004) "Elasto-Plastic Analysis of Tee Joints Using HOT-SMAC" NASA/CR-2004-213067.

4) Yarrington, P. (2001) "User's Manual and Final Report for HOT-SMAC GUI Development," NASA/CR-2001-211294.

5) Yarrington, P.W., Collier, C.S., Bednarcyk, B.A., Arnold, S.M., Pindera, M.-J., and Aboudi, J. (2003) "Higher Order Theory –Structural/Micro Analysis Code (HOT-SMAC) Software for Thermo-Mechanical Analysis of FGMs" in Proc. Fifth International Congress on Thermal Stresses and Related Topics, June, Blacksburg, Virginia.

6) Collier, C.S., Yarrington, P.W., Aboudi, J., Pindera, M.-J., Arnold, S.M., and Bednarcyk, B.A. (2002) "Higher Order Theory –Structural/Micro Analysis Code (HOT-SMAC) for Thermo-Mechanical Analysis of FGMs" in Proc. MPIF 2002 International Conference on Functionally Graded Materials, May 6-7, Denver, Colorado.

7) Zhang, J., Bansal, Y., Bednarcyk, B.A., Collier, C.S., and Pindera, M.-J. (2004) "Analysis of Adhesively Bonded Composite Joints Using a Higher-Order Theory" in Proc. 45nd AIAA/ASME/ASCE/AHS/ASC Structures, Structural Dynamics, and Materials Conference, Palm Springs, California.

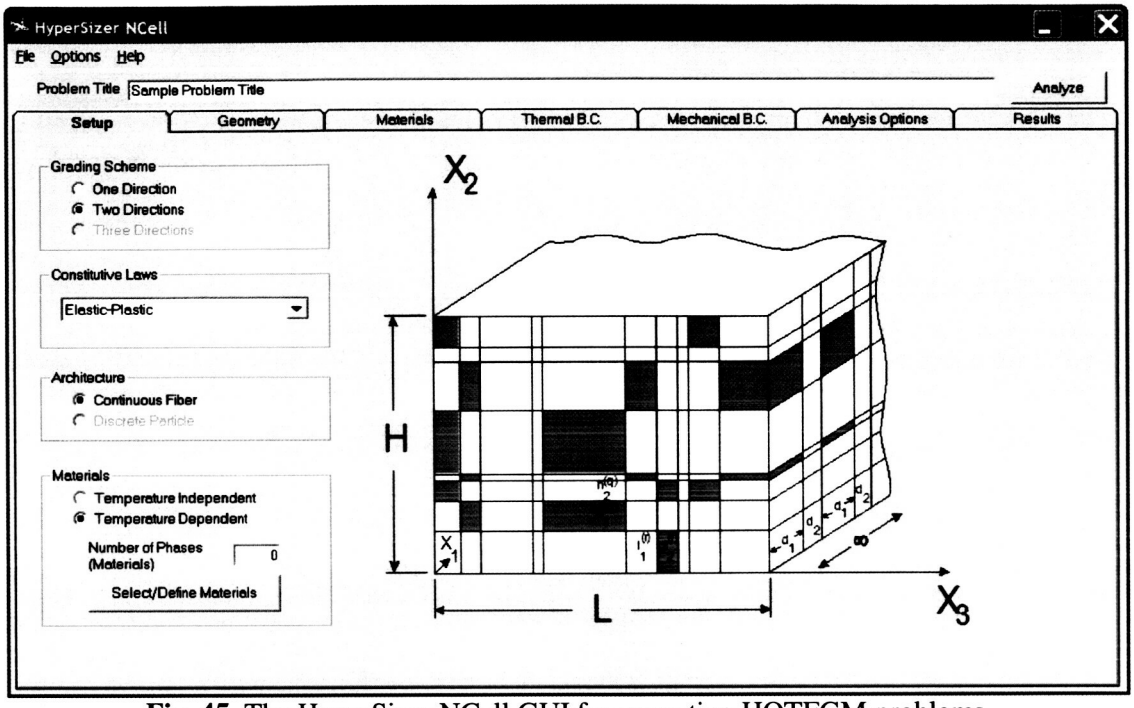

Fig. 45. The HyperSizer NCell GUI for executing HOTFGM problems.

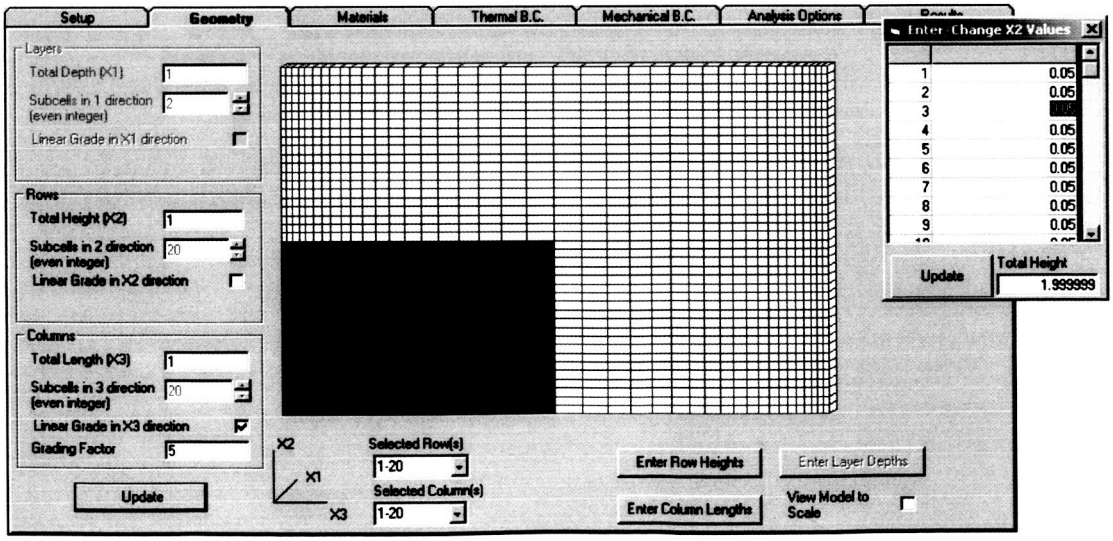

Fig. 46. The HyperSizer NCell Geometry tab

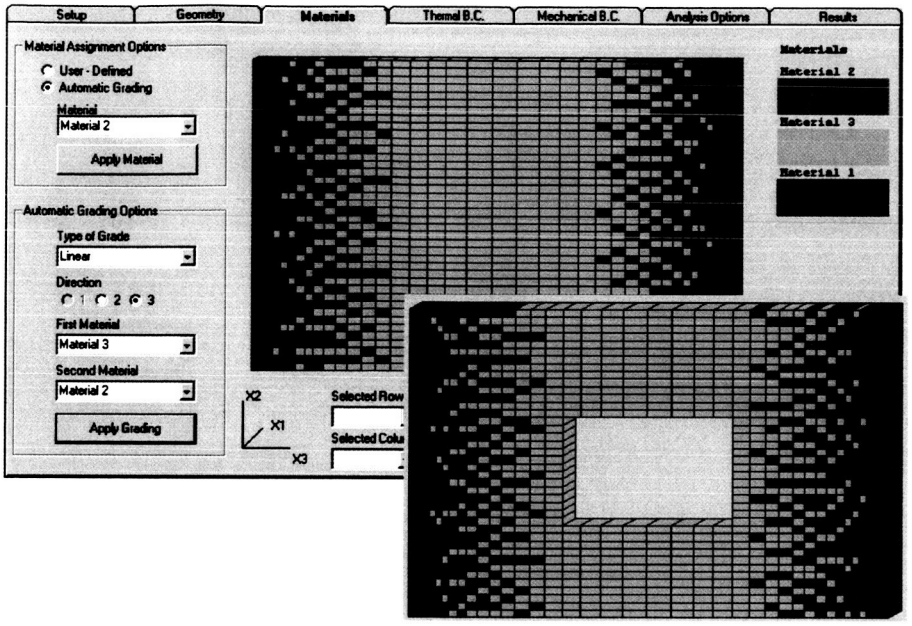

Fig. 47. The HyperSizer NCell materials tab.

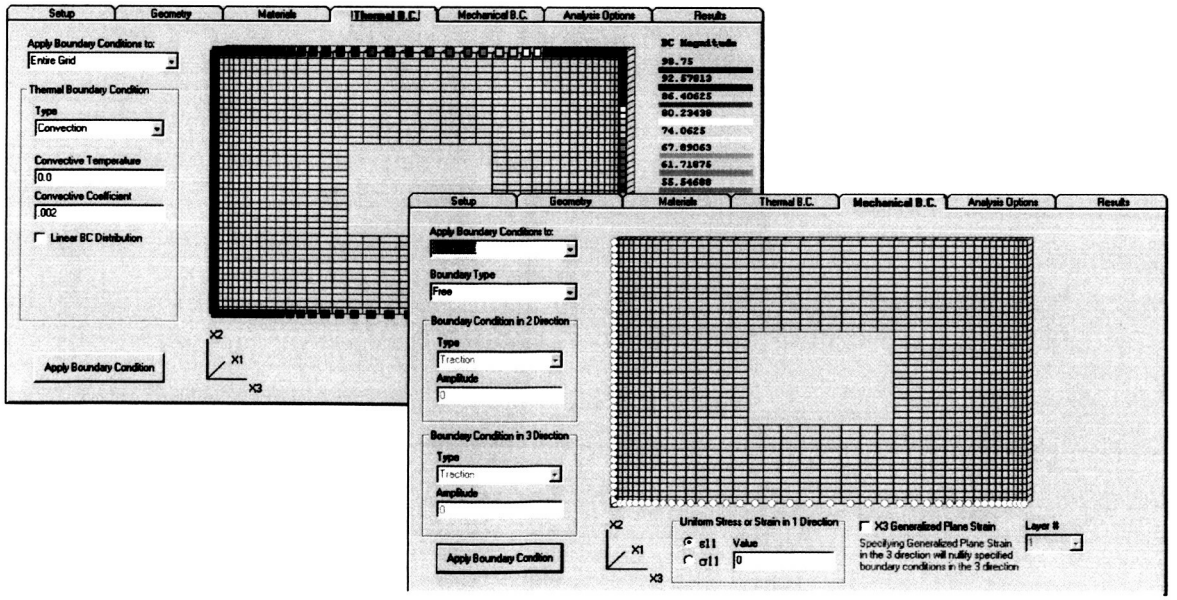

Fig. 48. The HyperSizer NCell B.C. tabs.

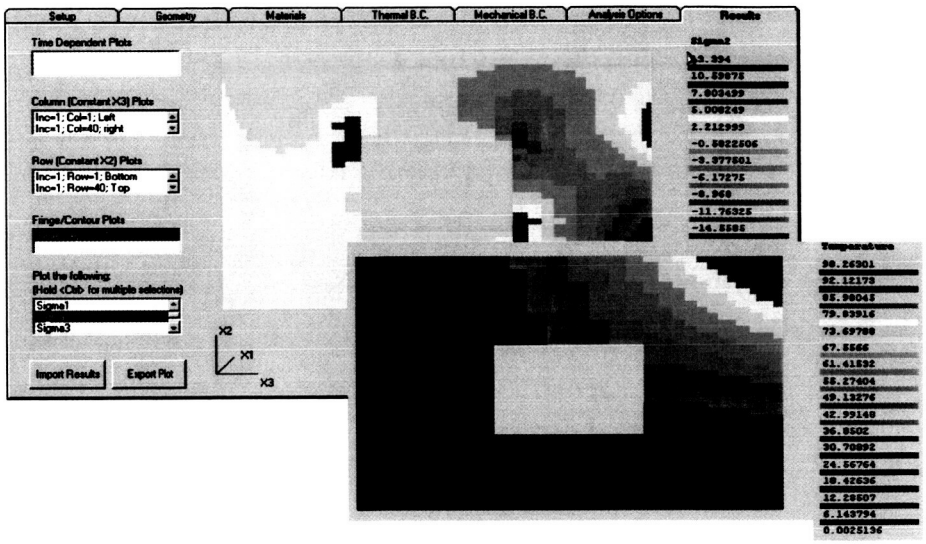

Fig. 49. The HyperSizer NCell results tab.

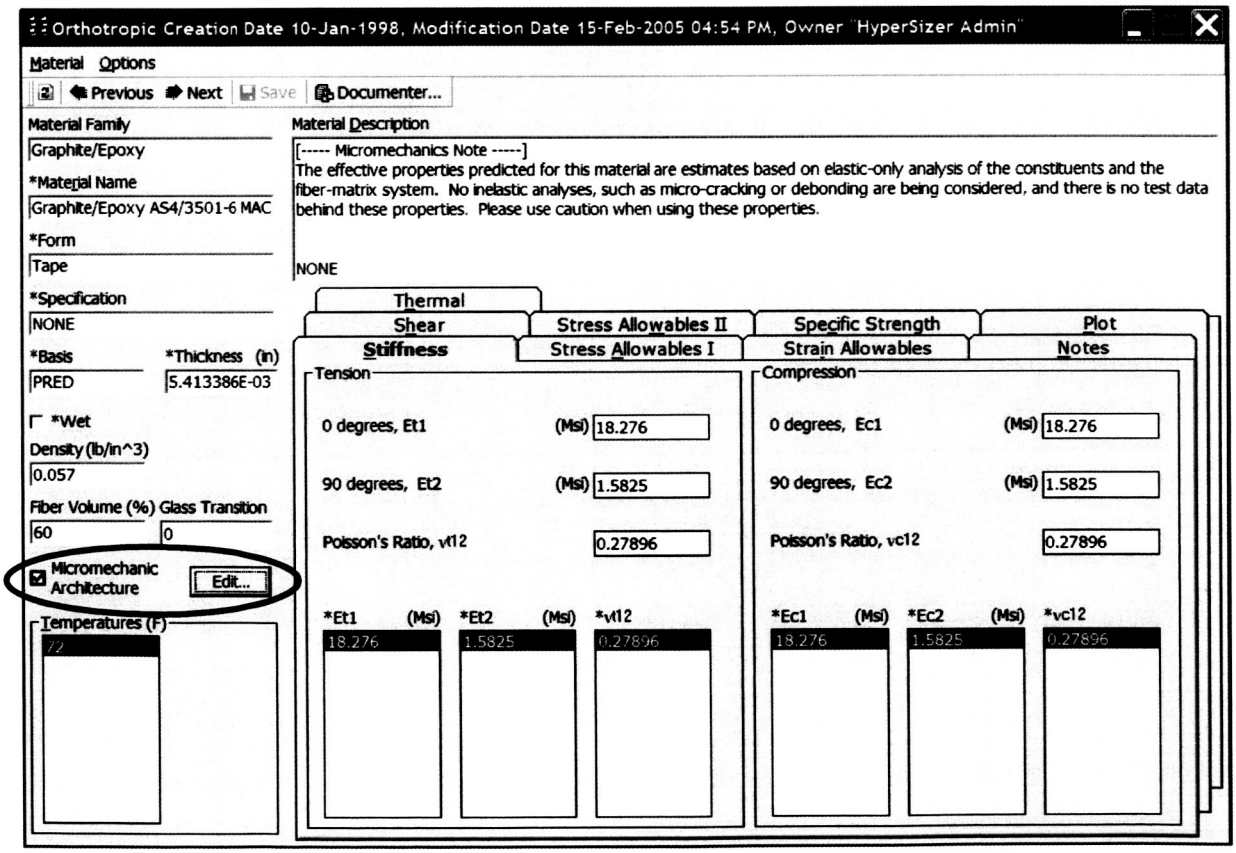

Fig. 50. HyperSizer Orthotropic Material form with Micromechanics Architecture checkbox highlighted.

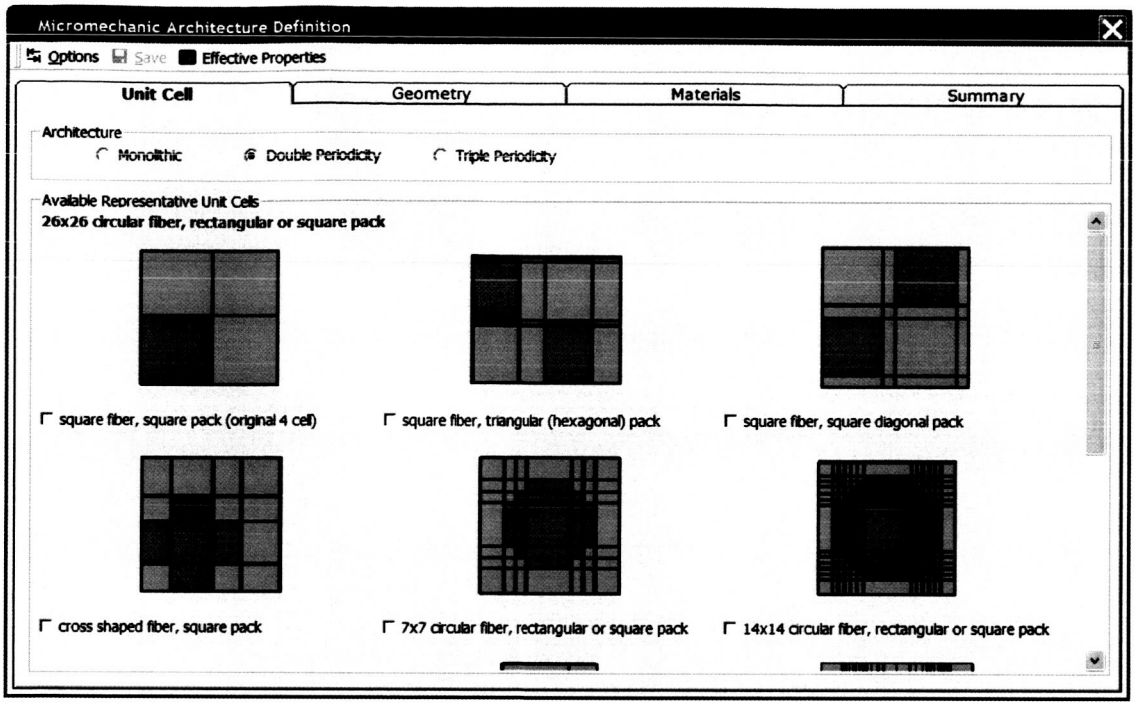

Fig. 51. New HyperSizer Micromechanics Architecture Definition interface – Unit Cell tab.

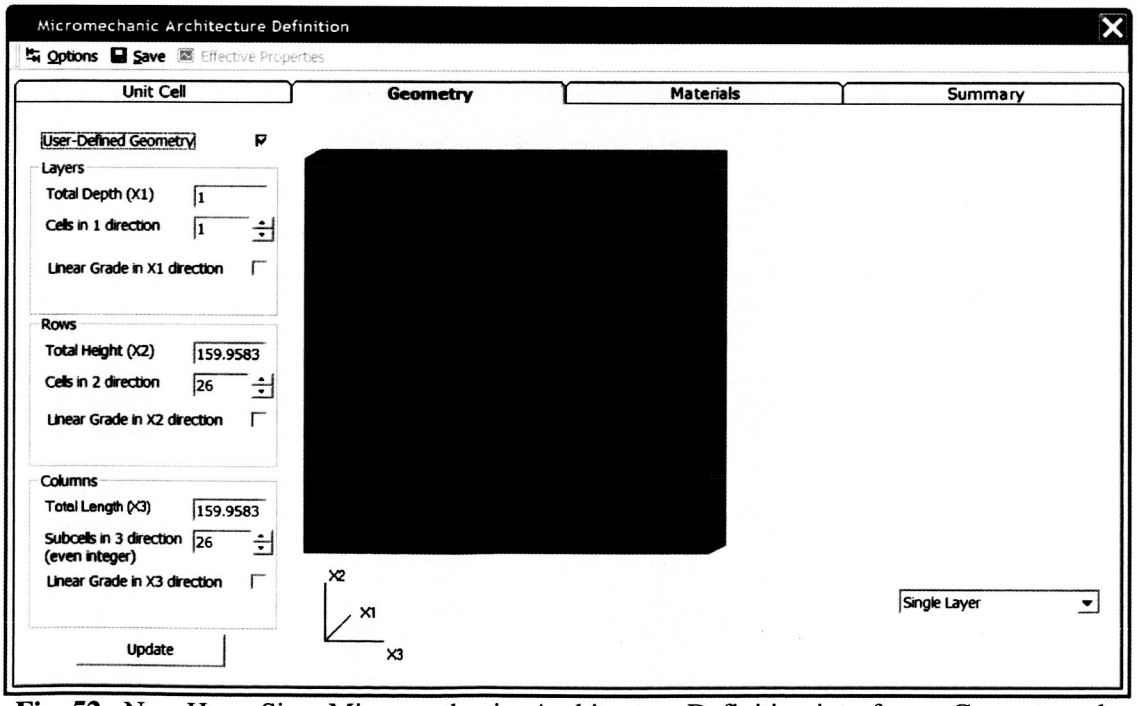

Fig. 52. New HyperSizer Micromechanics Architecture Definition interface – Geometry tab.

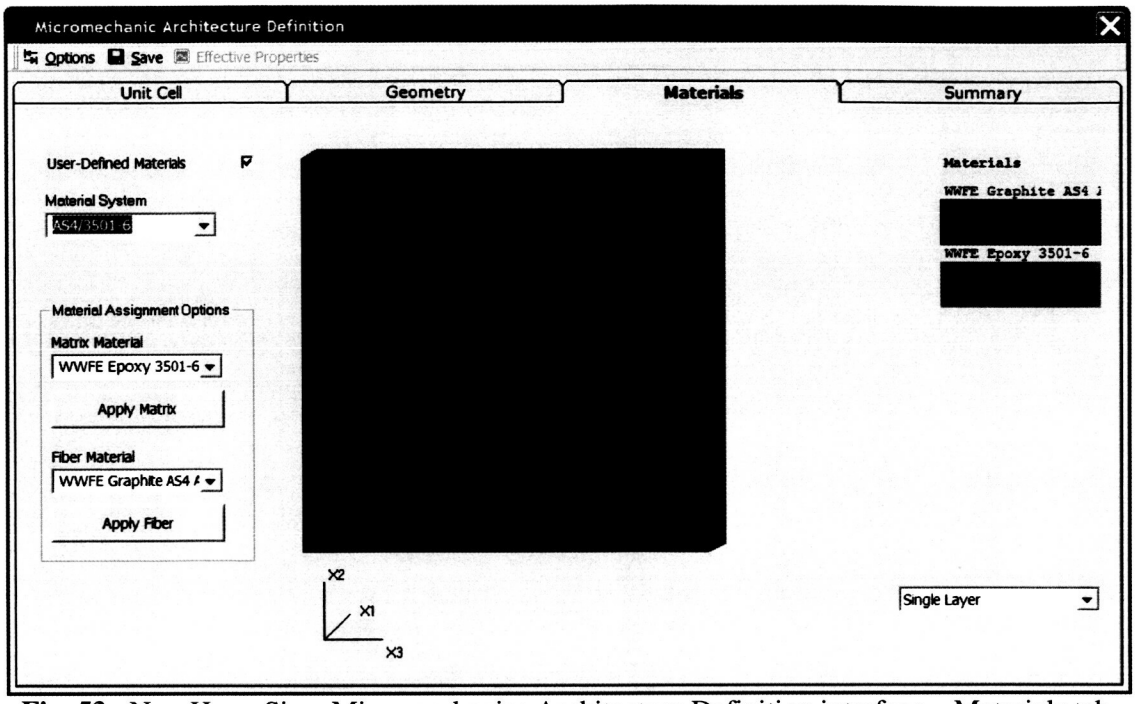

Fig. 53. New HyperSizer Micromechanics Architecture Definition interface – Materials tab.

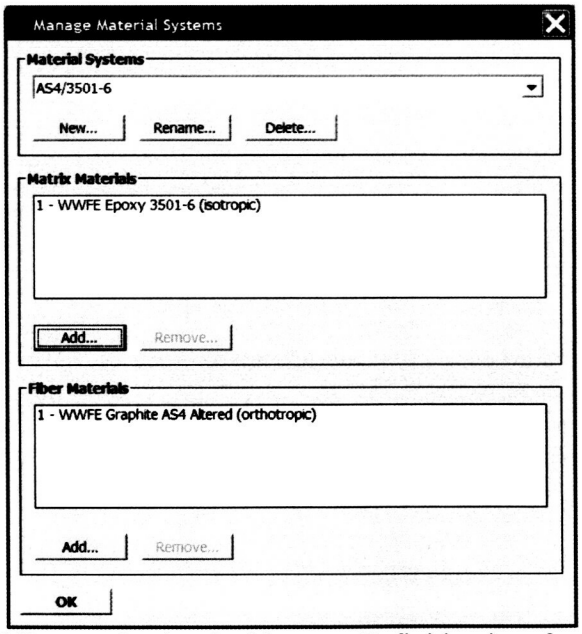

Fig. 54. New HyperSizer Micromechanics Architecture Definition interface –Material Systems Form.

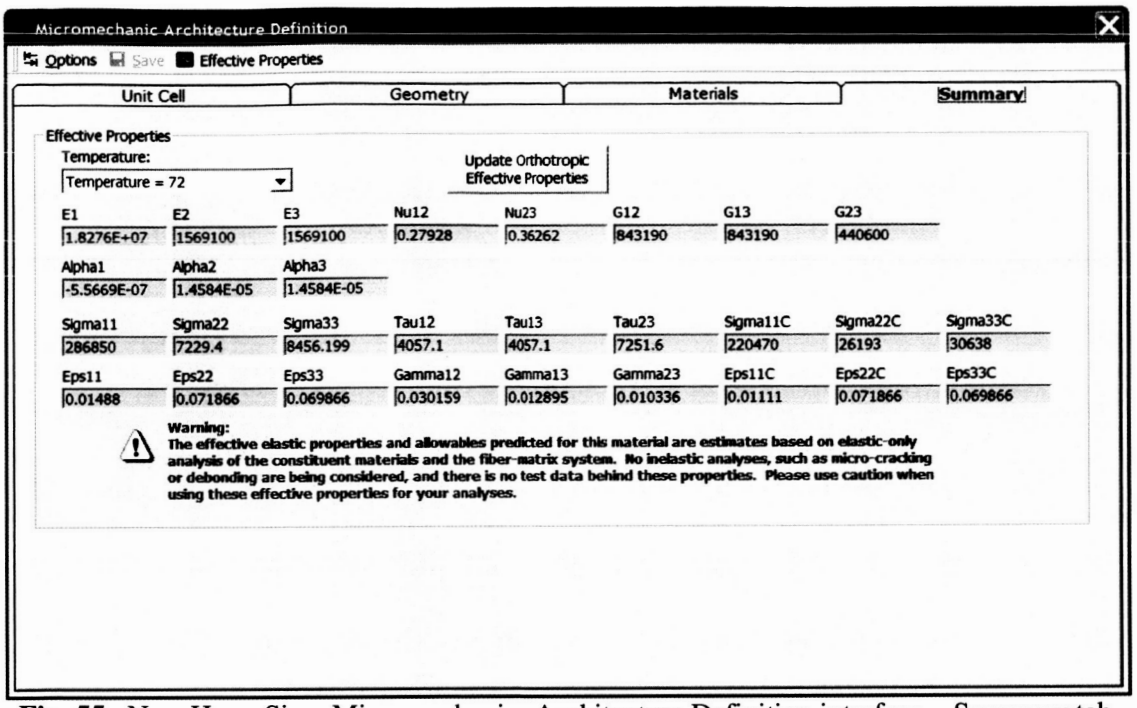

Fig. 55. New HyperSizer Micromechanics Architecture Definition interface – Summary tab.

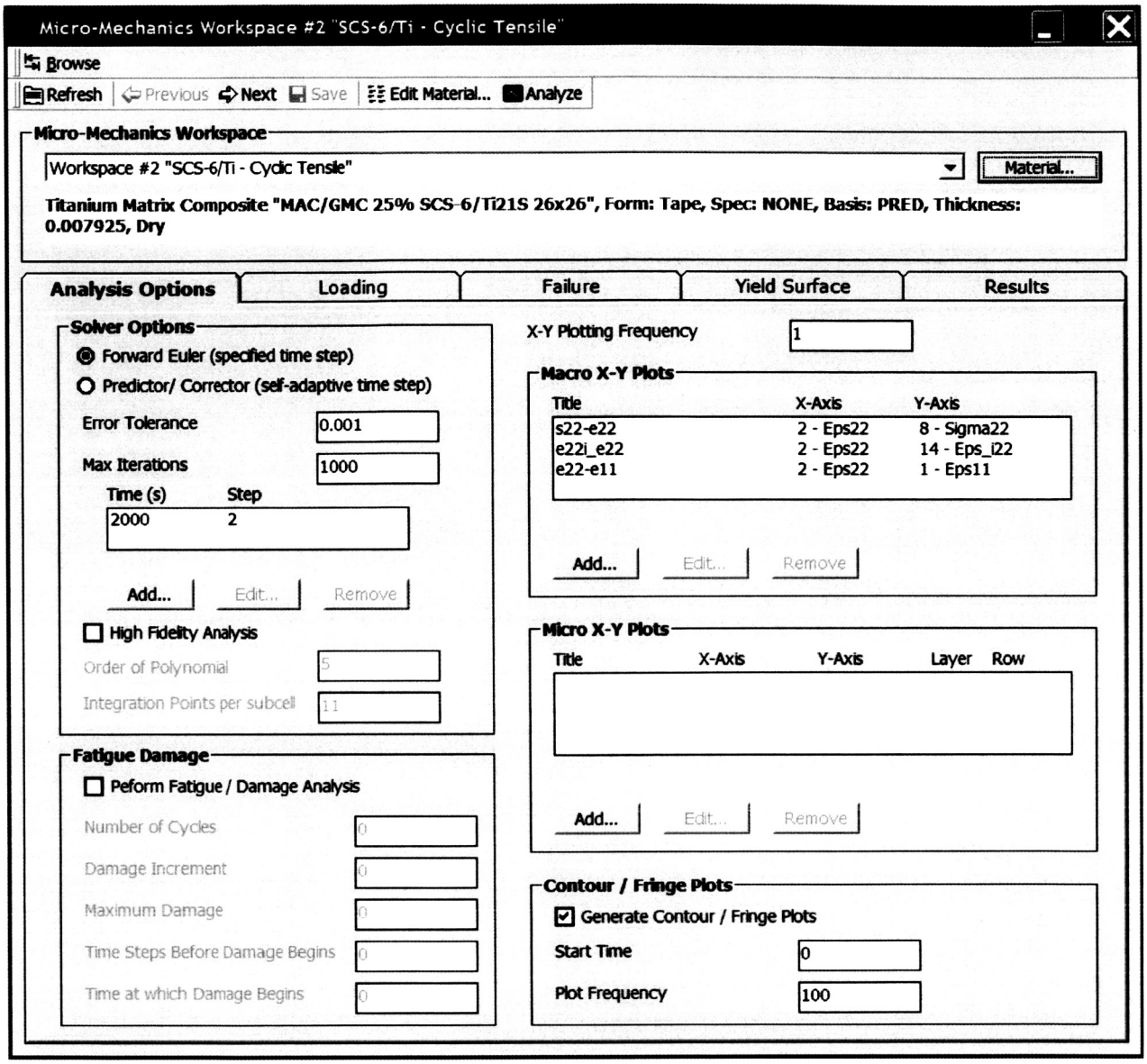

Fig. 56. The HyperSizer "Micromechanics Workspace" form, which allows users to model the response of composite materials to applied thermo-mechanical loading and display the results.

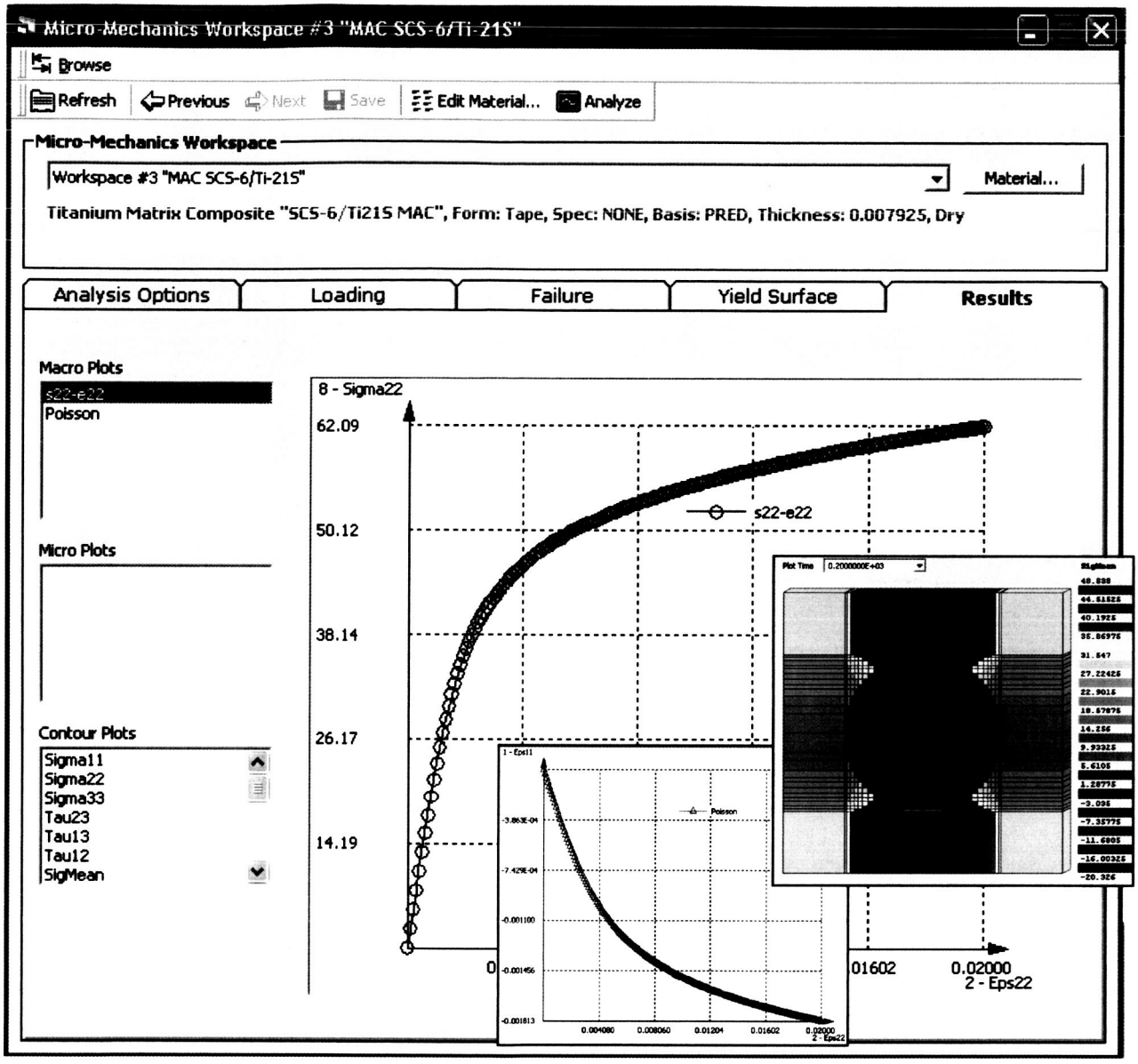

Fig. 57. The HyperSizer "Micromechanics Workspace" form results tab.

4.4 Develop HyperSizer Linkage Code

As discussed in Tasks 2 and 4.2, the tight linkage with HyperSizer was not pursued with respect to HOTFGM. The linkage code developed with respect to MAC/GMC has enabled full access to the HyperSizer iterative optimization capabilities. This linkage is thus discussed in Task 5.1.

Task 5. Full Synthesis of Models

The full integration of HyperSizer and MAC/GMC, depicted in Fig. 1, has been accomplished. As discussed in Tasks 2 and 4.2, standard HOTFGM (i.e., non-homogenized HOTFGM) has only been loosely coupled with HyperSizer through the HyperSizer NCell product. The homogenized version of HOTFGM, now called HFGMC, has been incorporated within MAC/GMC (see Task 1.2), and is thus fully integrated within the multi-scale HyperSizer framework. Now, for the first time, design and analysis can progress from the full vehicle finite element model, to the HyperSizer stiffened panel and laminate analysis, and finally to the fiber and matrix scale with the coupled MAC/GMC capability.

5.1 Coding to Allow Iterative Optimization

The coding that has enabled iterative optimization down to the micro scale had taken advantage of the streamlining of MAC/GMC performed in Task 4.1. MAC/GMC was rewritten in the FORTRAN 90 standard, enabling use of data structures and derived types. This was critical to establishing the tight linkage between HyperSizer and MAC/GMC that is used in multi-scale problems in which HyperSizer calls MAC/GMC thousands of times in a given problem. The core MAC/GMC computational code, outlined in Fig. 2, has been implemented as a dynamic link library (dll) that is callable by HyperSizer to represent a particular composite ply within a stiffened panel. All data needed by MAC/GMC for a particular ply are stored in three large data structures, which are passed to MAC/GMC as arguments. These three data structures are described as follows:

1) Contains the complete definition of the MAC/GMC material as defined in the Micromechanics Architecture Form. That is, the constituent material properties and the repeating unit cell dimensions and material arrangement.

2) Contains information on the maximum dimensions of arrays across all MAC/GMC definitions that will be used in the current coupled HyperSizer – MAC/GMC problem.

3) Contains the ply-level load (stresses and/or strains) for the current call to MAC/GMC along with all current state variable information for each subcell in the MAC/GMC composite repeating unit cell.

The effective property information determined by MAC/GMC is then passed back to HyperSizer as a fourth data structure argument. Thus, all communication between the codes during a coupled HyperSizer – MAC/GMC problem is accomplished via the four data structure arguments along with one integer argument that defines the MAC/GMC state variable partitioning. The only source code shared by HyperSizer and MAC/GMC is a single module defining data types and these four structures. Both codes are thus free to progress independently without the need for the other's source code, resulting in high level of maintainability.

Fig. 42 shows an example of a full multi-scale coupled analysis in which a T-Stiffened panel is modeled to level of the ply by HyperSizer and then to the level of the fiber and matrix constituents by MAC/GMC. The results of such an analysis are presented and discussed in Task 3.3.

Two additional capabilities specifically incorporated within MAC/GMC to support the full integration with HyperSizer should be mentioned. These enable quick estimation of composite failure based on linear elastic calculations, as opposed to a full time-dependent simulation. MAC/GMC's new elastic allowables calculation enables determination of a composite-level load at which local subcell failure will occur based on the allowables of the constituent materials. This is a simple elastic concentration calculation within MAC/GMC that can be performed extremely efficiently. MAC/GMC provides these allowables based on first subcell failure, average fiber and matrix material failure, or failure of all subcells, as shown in Fig. 58. In addition, a new load margin capability enables users to input a composite level load and determine the composite level margin of safety based on the same type

of elastic concentration calculation in conjunction with local failure theories (currently the maximum stress and strain theories, the Tsai-Hill theory, and the strain invariant failure theory (SIFT)). Sample MAC/GMC load margin results are shown in Fig. 59.

The new elastic allowables and load margin capabilities are important because they enable HyperSizer to utilize MAC/GMC, and thus perform a full coupled multi-scale analysis, even in the linear elastic case. Even when the new HyperSizer time-dependence is not operative, new micromechanics-based allowables can be generated with no additional input or knowledge required by the user.

```
     ************************************************************
     ** CAUTION - These allowables have not been validated and  **
     **           are based only on linear elastic calculations **
     ************************************************************

          --- 1st Subcell ---        --- Avg Material ---     - All Subcells -
          ALLOWABLE    CRITICAL      ALLOWABLE    CRITICAL       ALLOWABLE
COMP       STRESS      SUBCELL        STRESS      MATERIAL        STRESS
----     ----------   --------      ----------   --------       ----------
 1       0.2112E+04     325         0.2112E+04       1          0.5599E+04
 2       0.6808E+02      13         0.8416E+02       1          0.1199E+03
 3       0.6808E+02     339         0.8416E+02       1          0.1199E+03
 4       0.3140E+02      39         0.3140E+02       1          0.4000E+02
 5       0.2489E+02     313         0.5764E+02       2          0.3179E+03
 6       0.2489E+02      13         0.5764E+02       2          0.3179E+03
----     ----------   ---------     ----------   --------       ----------
 1      -0.2112E+04     325        -0.2112E+04       1         -0.5599E+04
 2      -0.6808E+02      13        -0.8416E+02       1         -0.1199E+03
 3      -0.6808E+02     339        -0.8416E+02       1         -0.1199E+03

                * ESTIMATED ELASTIC STRAIN ALLOWABLES *

     ************************************************************
     ** CAUTION - These allowables have not been validated and  **
     **           are based only on linear elastic calculations **
     ************************************************************

          --- 1st Subcell ---        --- Avg Material ---     - All Subcells -
          ALLOWABLE    CRITICAL      ALLOWABLE    CRITICAL       ALLOWABLE
COMP       STRAIN      SUBCELL        STRAIN      MATERIAL        STRAIN
----     ----------   --------      ----------   --------       ----------
 1       0.9000E-02      39         0.9000E-02       1          0.2300E-01
 2       0.1283E-01     325         0.1417E-01       1          0.2770E-01
 3       0.1283E-01     351         0.1417E-01       1          0.2770E-01
 4       0.1704E-01      39         0.1704E-01       1          0.2147E-01
 5       0.6549E-02     313         0.1517E-01       2          0.8454E-01
 6       0.6549E-02      13         0.1517E-01       2          0.8454E-01
----     ----------   ---------     ----------   --------       ----------
 1      -0.9000E-02      39        -0.9000E-02       1         -0.2300E-01
 2      -0.1283E-01     325        -0.1417E-01       1         -0.2770E-01
 3      -0.1283E-01     351        -0.1417E-01       1         -0.2770E-01

NOTE: 1st subcell  --> based on 1st subcell reaching specified constituent allowable
      Avg material --> based on 1st material whose avg stress/strain reaches allowable
      All subcells --> based on all subcells reaching specified constituent allowable
```

Fig. 58. MAC/GMC elastic allowables calculation ASCII output. The elastic allowables calculation enables HyperSizer to utilize MAC/GMC results even in the linear elastic case, without resorting to time-dependent progressive failure simulations.

```
* ELASTIC LOAD-BASED MULTI-AXIAL MARGIN OF SAFETY ESTIMATES *
      ************************************************************
```

```
** CAUTION - These margins have not been validated and are **
**           based only on linear elastic calculations     **
*************************************************************

User-Specified Load Level            Calculated components
-------------------------            ---------------------
  S11 =  0.6500E+02                    E11 =  0.2279E-03
  S22 =  0.3000E+02                    E22 =  0.5064E-02
  S33 =  0.0000E+00                    E33 = -0.2570E-02
  S23 =  0.0000E+00                    E23 =  0.0000E+00
  S13 =  0.0000E+00                    E13 =  0.0000E+00
  S12 =  0.2000E+02                    E12 =  0.5314E-02

Max. Stress-Based Margins of Safety:
-----------------------------------
  1st Subcell Failure-Based Margin of Safety:      0.2444
  Avg. Material Failure-Based Margin of Safety:    1.8044
  All Subcells Failure-Based Margin of Safety:     3.0020

Max. Strain-Based Margins of Safety
-----------------------------------
  1st Subcell Failure-Based Margin of Safety:      0.2325
  Avg. Material Failure-Based Margin of Safety:   -8.5179
  All Subcells Failure-Based Margin of Safety:     4.4859

Tsai-Hill Based Margins of Safety:
----------------------------------
  1st Subcell Failure-Based Margin of Safety:      0.1559
  Avg. Material Failure-Based Margin of Safety:    1.3014
  All Subcells Failure-Based Margin of Safety:     3.3462

SIFT Based Margins of Safety:
-----------------------------
  1st Subcell Failure-Based Margin of Safety:     -0.2049
  Avg. Material Failure-Based Margin of Safety:   -0.0941
  All Subcells Failure-Based Margin of Safety:     2.3389
```

Fig. 59. MAC/GMC elastic load margin calculation ASCII output. The load margin calculation enables HyperSizer to utilize MAC/GMC results even in the linear elastic case, without resorting to time-dependent progressive failure simulations.

5.2 Verification, Development of Test Suite

Significant verification has been performed on all scales for the new stand alone capabilities of HyperSizer, MAC/GMC, and HOTFGM developed in the course of the project. This was typically accomplished by considering a simplified case with known results that still exercised the new capabilities. In particular, the new smart capabilities incorporated within MAC/GMC were verified with ABAQUS and, using the so-called "thermal analogy" discussed in Task 3.2, with MSC/NASTRAN. The latter enabled the new piezo-electro-magnetic capabilities to be verified using existing thermal capabilities that were known to be correct. Further, significant verification was performed on the coupled HyperSizer – MAC/GMC product. Again, via simplification to a problem that could be handled using existing capabilities, the new features were exercised and shown to be functioning correctly. Examples of this verification are given in Figs. 37 and 38, in which progressive failure analysis of a laminate (as opposed to a stiffened panel) was performed using stand alone MAC/GMC and the coupled HyperSizer – MAC/GMC product.

Test suites have been developed for the stand alone codes, as well as the integrated HyperSizer – MAC/GMC product. The MAC/GMC test suite consists of 43 new example problems developed and documented in the course of releasing MAC/GMC 4.0, as discussed in Task 4.1. The test suite for the coupled HyperSizer – MAC/GMC product is more easily maintained because all data are stored in a single HyperSizer database. In the case of stand alone MAC/GMC and HOTFGM, the test cases are each stored as an individual file.

Education/Public Outreach

The Education/Public Outreach portion of the project was conducted by Melissa J.B. Rogers, an Educational Specialist at OAI. The original Education/Public Outreach elements proposed for this project were rather broad and designed for multiple winning NRA proposals from OAI. Following discussions with the NASA Glenn Research Center Office of Educational Programs personnel and with the project PI, investigations into center of mass was selected as the target subject for an elementary classroom module on Forces and Motion. Although this topic is not explicitly identified as a stand-alone piece of national science content standards, its intrinsic importance in aircraft and spacecraft design tied in nicely with the technical part of this project.

The classroom activities were designed to introduce the concept of center of mass to students and have them investigate ways to find the center of mass of simple and complex two-dimensional shapes. Students construct a model vehicle and see how the center of mass of the whole changes as additional components are added. Students also investigate ways to find the center of mass of simple three-dimensional objects. The connection to NASA's vehicle design efforts adds a strong component of "Science and Technology" and "Nature of Science" standards to the project.

A proposal reflecting the activity package was accepted by the National Science Teachers Association and a workshop introducing the guide to teachers was presented as a session during their Spring 2003 Convention in Philadelphia, PA. This workshop was preceded by a similar (but more in-depth) workshop sponsored by the NASA Glenn Office of Educational Programs in November 2002. From these two workshops, four teachers were selected to serve as pilot testers of the guide. They used the product in their classrooms and submitted their comments for inclusion in the final guide. The completed guide was submitted to NASA's Education Office in 2004 and is included in Appendix B.

Commercialization

The goal of this project was to develop new, state of the art, multi-scale, multifunctional structural design and analysis tools for release in a commercial product. That commercial product is the HyperSizer software package sold by Collier Research Corporation. The Ohio Aerospace Institute has informed NASA of its intent to copyright and the software developed in this project and commercialize the software through an agreement with Collier Research Corporation. This has been approved by NASA, and the licensing agreement between the Ohio Aerospace Institute and Collier Research Corporation is being finalized. Collier Research Corporation is being granted a nonexclusive license to sell the software, while NASA retains government use rights and several free licenses of the final commercial product.

References

Aboudi, J., Pindera, M.J. and Arnold, S.M. (2001) "Linear Thermoelastic Higher-Order Theory for Periodic Multiphase Materials" *Journal of Applied Mechanics* 68, 697-707, 2001.

Aboudi, J., Pindera, M.-J., and Arnold, S.M. (2002) "High-Fidelity Generalized Method of Cells for Inelastic Periodic Multiphase Materials" NASA/TM-2002-211469.

Aboudi, J., Pindera, M.-J., and Arnold, S.M. (2003) "Higher-Order Theory for Periodic Multiphase Materials with Inelastic Phases" *International Journal Plasticity* 19, 805-847.

Arnold, S.M., Bednarcyk, B.A., and Aboudi, J. (2004) "Comparison of the Computational Efficiency of the Original versus Reformulated High-Fidelity Generalized Method of Cells" NASA/TM-2004-213438.

Bansal, A. and Ramaswamy, A. (2002) "FE Analysis of Piezo-laminate Composites Under Thermal Loads" *Journal of Intelligent Material Systems and Structures* 13, 291-301.

Bansal, Y. and Pindera, M.-J. (2002) "Efficient Reformulation of the Thermoelastic Higher Order Theory for FGMs" NASA/CR –2002-211909.

Bednarcyk, B.A. (2003) "An Inelastic Micro/Macro Theory for Hybrid Smart/Metal Composites" *Composites: Part B*, 34, 175-197.

Bednarcyk, B.A. and Arnold, S.M. (2000) "A New Local Debonding Model with Application to the Transverse Tensile and Creep Behavior of Continuously Reinforced Titanium Composites" NASA/TM-2000-210029.

Bednarcyk, B.A. and Arnold, S.M. (2002a) "MAC/GMC 4.0 User's Manual Volume 2: Keywords Manual" NASA-TM-212077/Vol 2.

Bednarcyk, B.A. and Arnold, S.M. (2002b) "MAC/GMC 4.0 User's Manual Volume 3: Example Manual" NASA-TM-212077/Vol 3.

Bednarcyk, B.A. and Arnold, S.M. (2002c) "Transverse Tensile and Creep Modeling of Continuously Reinforced Titanium Composites with Local Debonding" *International Journal of Solids and Structures* 39, 1987-2017.

Carrera, E. (1997) "An Improved Reissner-Mindlin-type Model for the Electromechanical Analysis of Multilayered Plates Including Piezo-layers" *Journal of Intelligent Material Systems and Structures*, 8, 232-248.

Collier, C.S. (1993) "Stiffness, Thermal Expansion, and Thermal Bending Formulation of Stiffened, Fiber- Reinforced Composite Panels" AIAA Paper No. 1993-1569.

Collier Research Corp. (1998) *HyperSizer Structural Sizing Software*. Hampton, VA.

Côté, F., Masson, P., Mrad, N., and Cotoni, V. (2004) "Dynamic and Static Modeling of Piezoelectric Composite Structures Using a Thermal Analogy with NSC/NASTRAN" *Composite Structures* 65, 2004.

Crawley, E.F. and Lazarus, K.B. (1991) "Induced Strain Actuation of Isotropic and Anisotropic Plates" *AIAA Journal* 29, 944-951.

Fernandes, A. and Pouget, J. (2004) "Analytical and Numerical Modelling of Laminated Composites with Piezoelectric Elements" *Journal of Intelligent Material Systems and Structures* 15, 753-761.

Gandhi, M.V. and Thompson, B.S. (1992) *Smart Materials and Structures*. Chapman & Hall, New York.

Gopinathan, S.V., Varadan, V.V., and Varadan, V.K. (2000) "A Review and Critique of Theories for Piezoelectric Laminates" *Smart Materials and Structures* 9, 24-48.

Herakovich, C.T. (1998) *Mechanics of Fibrous Composites*. John Wiley & Sons, New York.

Heyliger, P.R., Ramirez, F., and Pan, E. (2004) "Two-dimensional Static Fields in Magnetoelectroelastic Laminates" *Journal of Intelligent Material Systems and Structures* 15, 689-709.

Jones, R.M. (1975) *Mechanics of Composite Materials*. Hemisphere, New York.

Jonnalagadda, K.D., Blanford, G.E., and Tauchert, T.R. (1994) "Piezothermoelastic Composite Plate Analysis Using a First-Order Shear Deformation Theory" *Computers and Structures* 51, 79-89.

Krudryavtsev, B.A., Parton, V.Z., and Senik, N.A. (1990) "Magnetothermoelasticity" in *Applied Mechanics: Soviet Reviews Volume 2: Electromagnetoelasticity*. G.K. Mikhailov and V.Z. Parton (Eds.), Hemisphere Publishing Corp., New York.

Lee, C.K. (1990) "Theory of Laminated Piezoelectric Plates for the Design of Distributed Sensors/Actuators. Part I: Governing Equations and Reciprocal Relationships" *Journal of the Acoustical Society of America* 87, 1145-1158.

Lee, H.J. and Saravanos, D.A. (1997) "Generalized Finite Element Formulation for Smart Multi-Layered Thermal Piezoelectric Composite Plates" *International Journal of Solids and Structures* 34, 3355-3371.

Lee, H.J. and Saravanos, D.A. (2000) "A Mixed Multi-Field Finite Element Formulation for Thermopiezoelectric Composite Shells" *International Journal of Solids and Structures* 37, 4949-4967.

Paley, M. and Aboudi, J. (1992), "Micromechanical Analysis of Composites by the Generalized Cells Model" *Mechanics of Materials* 14, 127-139.

Pan, E. (2001) "Exact Solution for Simply-Supported and Multilayered Magneto-Electro-Elastic Plates" *Journal of Applied Mechanics* 68, 608-618.

Pan, E. and Heyliger, P.R. (2003) "Exact Solutions for Magnetoelectroelastic Laminates in Cylindrical Bending" *International Journal of Solids and Structures* 40, 6859-6876.

Parton, V.Z. and Krudryavtsev, B.A. (1988) *Electromagnetoelasticity Piezoelectrics and Electrically Conductive Solids*. Taylor & Francis, New York.

Pindera, M.-J., and Bednarcyk, B.A. (1999) "An Efficient Implementation of the Generalized Method of Cells for Unidirectional, Multi-Phased Composites with Complex Microstructures" *Composites: Part B* 30, 87-105.

Robbins, D.H. and Reddy, J.N. (1993) "Modelling of Thick Composites Using a Layerwise Laminate Theory" *International Journal for Numerical Methods in Engineering* 36, 655-677.

Saravanos, D.A., Heyliger, P.R., and Hopkins, D.A. (1997) "Layerwise Mechanics and Finite Element for the Dynamic Analysis of Piezoelectric Composite Plates" *International Journal of Solids and Structures* 34, 359-378.

Saravanos, D.A. and Heyliger, P.R. (1999) "Mechanics and Computational Models for Laminated Piezoelectric Beams, Plates, and Shells" *Applied Mechanics Reviews* 52, 305-320.

Schultz, M.R. and Hyer, M.W. (2003) "Snap-through of Unsymmetric Cross-ply Laminates using Piezoceramic Actuators" *Journal of Intelligent Material Systems and Structures* 14, 795-814.

Soden, P.D., Hinton, M.J., and Kaddour, A.S. (1998) "Lamina Properties, Lay-Up Configurations and Loading Conditions for a Range of Fibre-Reinforced Composite Laminates" *Composites Science and Technology* 58, 1011-1022.

Soden, P.D., Hinton, M.J., and Kaddour, A.S. (2002) "Biaxial Test Results for Strength and Deformation of a Range of E-Glass and Carbon Fibre Reinforced Composite Laminates: Failure Exercise Benchmark Data" *Composites Science and Technology* 62, 1489-1514.

Tauchert, T.R. (1992) "Piezothermoelastic Behavior of a Laminated Plate" *Journal of Thermal Stresses* 15, 25-37.

Tzou, H.S. (1993) *Piezoelectric Shells: Distributed Sensing and Control of Continua*, Kluwer Academic, Norwell, MA.

Uchino, K. (1997) *Piezoelectric Actuators and Ultrasonic Motors*. Kluwer Academic Publishers, Hingham, MA.

Yarrington, P. (2001) "User's Manual and Final Report for HOT-SMAC GUI Development" NASA/CR-2001-211294.

Appendix A: Complete list of publications resulting all or in part from the project

Journal Publications

1 Aboudi, J., Pindera, M-J., and Arnold, S.M. (2001) "Linear Thermoelastic Higher-Order Theory for Periodic Multiphase Materials" *Journal of Applied Mechanics* 68, 697-707.

2 Aboudi, J., Pindera, M-J., and Arnold, S.M. (2002) "Higher-Order Theory for Periodic Multiphase Materials with Inelastic Phases" *International Journal of Plasticity* 19, 805-847.

3 Arnold, S.M., Bednarcyk, B.A., and Aboudi, J. (2004) "Analysis of Internally Cooled Structures Using a Higher Order Theory" *Computers and Structures* 82, 659-688.

4 Bednarcyk, B.A., Zhang, J., Collier, C.S., Bansal, Y., and Pindera, M.-J. (2005) "Analysis Tools for Adhesively Bonded Composite Joints, Part I: Higher-Order Theory" *AIAA Journal*, In Press.

5 Bednarcyk, B.A. (2003) "An Inelastic Micro/Macro Theory for Hybrid Smart/Metal Composites" *Composites: Part B* 34, 175-197.

6 Bednarcyk, B.A., Arnold, S.M., Aboudi, J., and Pindera, M.-J. (2004) "Local Field Effects in Titanium Matrix Composites Subject to Fiber-Matrix Debonding" *International Journal of Plasticity* 20, 1707-1737.

7 Pindera, M-J., Aboudi, J., and Arnold, S. M. (2002) "Analysis of Spallation Mechanism in Thermal Barrier Coatings with Graded Bond Coats Using the Higher-Order Theory for FGMs" *International Journal of Engineering Fracture Mechanics* 69, 1587-1606.

NASA Publications

1 Aboudi, J., Pindera, M-J., and Arnold, S.M. (2002) "High-Fidelity Generalized Method of Cells for Inelastic Periodic Multiphase Materials" NASA/TM-2002-211469.

2 Bednarcyk, B.A. (2002) "A Fully Coupled Micro/Macro Theory for Thermo-Electro-Magneto-Elasto-Plastic Composite Laminates" NASA/CR-2002-211468.

3 Bednarcyk, B.A. and Arnold, S.M. (2002) "MAC/GMC 4.0 User's Manual Volume 2: Keywords Manual" NASA/TM-2002-212077/Vol 2.

4 Bednarcyk, B.A. and Arnold, S.M. (2002) "MAC/GMC 4.0 User's Manual Volume 3: Example Manual" NASA/TM-2002-212077/Vol 3.

5 Bednarcyk, B.A. and Yarrington, P.W. (2005) "Coupled Thermo-Electro-Magneto-Elastic Response of Smart Stiffened Panels" NASA/CR In Preparation.

6 Bednarcyk, B.A. and Yarrington, P.W. (2005) "Multi-Scale Progressive Failure of Polymer Matrix Composite Stiffened Panels" NASA/CR In Preparation.

7 Bednarcyk, B.A. and Yarrington, P.W. (2004) "Elasto-Plastic Analysis of Tee Joints Using HOT-SMAC" NASA/CR-2004-213067.

8 Pindera, M-J., Aboudi, J., and Arnold, S. M. (2002) "Analysis of Plasma-Sprayed TBCs with Homogeneous and Heterogeneous Bond Coats Under Spatially Uniform Cyclic Thermal Loading" NASA/TM-2001-210803.

9 Yarrington, P. (2001) "User's Manual and Final Report for HOT-SMAC GUI Development" NASA/CR-2001-211294.

Conference Papers/Presentations and Invited Lectures

1 Arnold, S.M. (2003) "The Impact of Smart Materials and Structures on Revolutionary Aeropropulsion Concepts" invited seminar, April 21, 2003, University of Virginia, Dept. Materials Science and Engineering.

2 Bednarcyk, B.A. (2002) "Micromechanics of Fiber-Matrix Debonding in Titanium Matrix Composites" invited seminar, Feb. 21, 2002, University of Virginia, Dept. Civil Engineering.

3 Bednarcyk, B.A. (2003) "An Inelastic Micro/Macro Theory for Hybrid Smart/Metal Composites" in Proc. Tenth International Symposium on Plasticity, July, Quebec City, Canada.

4 Bednarcyk, B.A., (2005) "Multi-Scale Design and Analysis of Advanced Materials and Structures" invited seminar, March 28, 2003, United States Naval Academy, Dept. Mechanical Engineering.

5 Bednarcyk, B.A., Arnold, S.M., Aboudi, J., and Pindera, M-J. (2002) "Accurate Micro/Macro Field Simulation for Composites Subject to Fiber-Matrix Debonding Using HFGMC" in Proc. 15th ASCE Engineering Mechanics Conference, June 2-5, New York.

6 Bednarcyk, B.A., Arnold S.M., and Powers, L.M. (2005) "Micromechanics-Based FEA of Composite Structures" in Proc. The Eleventh International Symposium on Plasticity, January, Kauai, Hawaii.

7 Collier, C.S., Yarrington, P.W., Aboudi, J., Pindera, M.-J., Arnold, S.M., and Bednarcyk, B.A. (2002) "Higher Order Theory – Structural/Micro Analysis Code (HOT-SMAC) for Thermo-Mechanical Analysis of FGMs" in Proc. MPIF 2002 International Conference on Functionally Graded Materials, May 6-7, Denver, Colorado.

8 Rogers, M.J.B. and Bednarcyk, B.A. (2003) "What's the Point?" presented at the National Science Teachers Association National Convention, March, Philadelphia, Pennsylvania.

9 Shen, L., Lissenden, C.J., Bednarcyk, B.A., and Arnold, S.M. (2002) "Flow Surfaces for Fibrous Metal Matrix Composites Predicted by the Method of Cells" presented at the 39th Society of Engineering Science Technical Meeting, Oct. 13-16, 2002.

10 Yarrington, P.W., Collier, C.S., Bednarcyk, B.A., Arnold, S.M., Pindera, M.-J., and Aboudi, J. (2003) "Higher Order Theory –Structural/Micro Analysis Code (HOT-SMAC) Software for Thermo-Mechanical Analysis of FGMs" in Proc. Fifth International Congress on Thermal Stresses and Related Topics, June, Blacksburg, Virginia.

11 Zhang, J., Bansal, Y., Bednarcyk, B.A., Collier, C.S., and Pindera, M.-J. (2004) "Analysis of Adhesively Bonded Composite Joints Using a Higher-Order Theory" in Proc. 45nd AIAA/ASME/ASCE/AHS/ASC Structures, Structural Dynamics, and Materials Conference, Palm Springs, California.

Appendix B: E/PO Classroom Module on Center of Mass

Everyday your students push chairs around the room, slide books across their desks, and play balancing games with random items. Meanwhile, you are challenged to teach them the basics of forces and motion. What's the Point? directs your students' observations of how things move to a focus on what makes them move. In particular, investigations lead your students to identify the concept of an object's center of mass. The activities are built around a practical theme of moving furniture. The lessons learned will help them to plan a real or virtual re-arrangement of your classroom.

Each activity involves hands-on work to prompt student discussions of basic properties of matter and how matter moves because of a force. This set of activities can be used as a first introduction of these concepts and may also be useful as a review in support of special projects such as model/bottle rockets. Each activity is designed for use in 45-60 minute classroom periods and can be adapted as needed to work with your schedule.

Through Whatcha Made Of? your class will measure the mass of a variety of objects and think about how mass, density, and volume are interrelated.

In I've Fallen and I Can't Get Up! students think about forces and non-motion. What exactly is going on when a book rests on a desktop? Are there forces acting on the book or not? Discussion and some definitions guide them towards the topic of equilibrium. If your students are prepared, you may also want to tie in previous lessons about potential energy.

And then, students get to Make That Thing Move! Through tests on simple objects, your students will realize that they can change how something moves by applying different forces at different locations. Questions and discussions will help your students understand what an object's center of mass is and they will work to develop a method for finding this location for two-dimensional objects.

This will place them at the Center of Attention—designing objects, predicting the locations of the objects' centers of mass, and using their own methods to test their predictions. An assessment piece called Tie To Move! has students applying what they have learned to the furniture move scheme.

Through individual or group research, students will discover Who Cares? about center of mass. They may be surprised how important this concept is for things they are involved with every day—sport utility vehicles, book cases, stair railings—and maybe not quite every day—satellite launches, ski jumping, parachuting.

We hope your students Get The Point!

Introduction to What's The Point?

By the time students reach middle school, they have typically been taught some basics of physical science

- everything is made from stuff, and we can measure how much stuff and call it mass
- stuff takes up space, and we call that amount of space volume
- stuff can be packed together tightly or loosely, varying the density of the stuff
- and if you push or pull on the stuff it moves, the study of forces and motion.

If your students have mastered this information, put this book away. But if you need to spend some time on any or all of these important basics, work with your students on the following activities to help them answer What's The Point?

This guide is designed as a supplement or replacement of your existing lesson plans for forces and motion. The activities are designed to lead your students through the basics of mass, density, forces, and equilibrium to the center of mass. While center of mass is not explicitly identified in national science benchmarks and standards, it is a vital element in predicting the motion resulting from the application of a force. It is a key factor in understanding how airplanes fly, in designing safety railings of an appropriate height, in perfecting your ski-jumping technique, and in most easily rearranging the furniture in your classroom. We think your students will be interested in learning about the Point.

Timing

If you include a classroom discussion of What Do They Know? with the introduction of this unit, you will probably need a full classroom period. Otherwise, Setting the Scene may only take a small amount of time. We suggest that as part of the unit introduction you ask students to bring in the items they will study in Whatcha Made Of?

What Do They Know?

Whether you are using these activities as a complete instructional unit or as a review in preparation for a related unit such as bottle rockets, you may want to assess your students' current understanding of some key topics. As an individual journaling exercise or as a class discussion, have your students address the following questions.

- How do you define the mass of an object?
- How would you determine the mass of a banana?
- What would you do to make a book move across a desk?
- Would you do anything differently if you needed to move a desk across the floor?

Setting the Scene

Tell your students that you are thinking about rearranging the furniture in your classroom. (If you don't have any free-standing tall bookcases or filing cabinets in your room, you will need to refer to some other room, maybe the main office.) You would like them to develop a scheme for

the actual movement of the furniture. The activities they do over the next several classes will give them some background for this task.

Note: If you have the time or can work with your mathematics and computer teachers, you may want to take the classroom move idea further. Students can create a scale model of the room and furniture on paper, in three-dimensions, or using computer drafting software.

As you facilitate the class discussions related to each activity, you may want to capture key ideas for reference throughout the unit.

Activity One: Whatcha Made Of?

In this activity, your students will investigate the physical properties of objects. They will become more comfortable with the "feel" of different masses and will explore ways in which mass can be distributed, that is, variations in volume and density.

Timing

The Students Introduction and Exploring Mass should take one class period. Activity Summary discussions will probably take part of another period and you may want to combine it with the Students Introduction to Activity Two.

Materials and Supplies

- ask students to bring in items to study (you may want to set some restrictions) or provide a variety of objects for which students can measure dimensions (length, width, height, diameter, etc. and mass) such as
    - pencils
    - tennis balls
    - marbles
    - coins
    - calculators
- metric rulers
- metric scales/balances
- at least one 1 g mass
- at least one 1 kg mass
- household items with mass labeled such as
    - package of butter
    - package of flour
    - bag of pet food
- Whatcha Made Of? Team Report (one copy for each team/student)
- Whatcha Made Of? Journal Questions (one copy for each student)

Preparation

→ Decide how you will group students.
→ Make copies of the Whatcha Made Of? Team Report and Journal Questions.
→ If students will not be supplying their own objects to study, gather a variety of items for the students to use. Try to have at least two items per team. See Materials and Supplies list above for ideas.
→ Collect several items of known mass. These should include standard measuring masses (1 g and 1 kg) and everyday items for comparison, see Materials and Supplies list for ideas.
→ Familiarize yourself with the scales your students will use. Review mass measurement with your students, if needed.
→ If possible, determine the mass of the different pieces of furniture in your room.

Student Introduction

→ Remind your students that you are planning to rearrange the classroom and need their help.
→ Tell your students that as a first step in their planning they will measure the mass of a variety of objects.
→ Review the Whatcha Made Of? Team Report with your class. Discuss ways to describe and measure the size of sample objects. Have students suggest Physical Characteristics that could be listed—for example, color, apparent material, surface texture, how firm the object is.
→ If you have fewer scales than teams, instruct students that some teams will need to complete the Size and Physical Characteristics parts of the Team Report while other teams are measuring mass.
→ Have your students form their teams and select two items per team to study. Distribute Team Reports to the students and have them start on the activity. Depending on time constraints and number of teams, you may want to limit the teams to one item each.

Exploring Mass

→ After the teams have completed their Team Reports, have them arrange their objects in a line on the floor in order of increasing mass.
→ Distribute Whatcha Made Of? Journal Questions. Lead a class discussion centered on question 2. Have the students complete the Journal Questions in the remaining classroom time or as an at-home assignment.

Activity Summary

→ After your students complete the Journal Questions, lead them in a group discussion of their responses.
→ Have students pass around the 1 g and 1 kg masses and share the items of similar mass they found at home.
→ Questions 5 and 6 are designed to get students thinking about the relationship among density, mass, and volume: $\rho=m/V$. Our perception of mass is often affected by the size and shape of an object, as well as other physical characteristics such as the material. Hence the age old question—what weighs more, a pound of iron or a pound of feathers?
→ To bring the students back to the furniture-moving theme, have the students estimate the mass of pieces of furniture in the classroom. Ask them what makes up the mass of a bookcase, a filing cabinet, a chair. How is the mass arranged?
→ As an additional challenge, have your students brainstorm some ways to measure the mass of your classroom furniture.

Activity Two: I've Fallen and I Can't Get Up!

Your students may have already learned that a force is a push or pull, but how deeply do they understand this? This activity will get your students thinking about why and how things move and what's going on when something isn't moving. They will consider balanced forces and stable and unstable equilibrium.

Timing

Students should be able to complete their Team Reports and start on the Journal Questions in one class period. Summary discussions may be combined with your introduction to Activity Three.

Materials and Supplies

- a variety of objects for your students to investigate such as
  - unsharpened and sharpened wood pencils
  - empty and full toilet paper and/or paper towel tubes
  - marbles of various sizes (these may be paired with a container of some sort)
  - video cassette cases
  - tissue boxes
  - toy cars (these may be paired with simple ramps)
  - shoe boxes
- materials to construct "top-heavy" objects
  - masses such as those used on your scales/balances or rolls of pennies
  - tape
- I've Fallen and I Can't Get Up! Team Report (one copy for each team/student)
- I've Fallen and I Can't Get Up! Journal Questions (one copy for each student)

Preparation

→ Review/research for yourself the concepts of force, balanced forces and equilibrium, and potential energy. Decide what, if any, background information you would like your students to have before doing this activity.
→ Decide how you will group students.
→ Make copies of the I've Fallen and I Can't Get Up! Team Report and Journal Questions.
→ Collect a variety of objects for the activity. Each team should have at least one item to study. See the Materials and Supplies list above for some ides. You may want to construct some "top-heavy" items to use. Secure a mass such as a roll of pennies at one end of a tissue box and replace the tissues or add mass to the inside of an empty shoe box and seal the box.
→ Experiment with several of the items to see what problems the students may encounter.

Student Introduction

→ Tell your students that it is time to think some more about rearranging the classroom. Ask them for ideas on HOW to move the furniture. Students will suggest ideas such as pushing,

pulling, pushing and pulling together, lifting, using a dolly, or maybe having certain persons do the work. Have them explain their ideas.

→ After several suggestions have been discussed, ask them to use scientific vocabulary to describe their ideas, if they are not doing so.

→ Tell your students that before they move anything, you want them to think some more about what is going on with the furniture RIGHT NOW. Discuss with your students the I've Fallen and I Can't Get Up! Team Report and show them the various objects you have available for study.

→ Have your students form their teams. Distribute the Team Reports and study objects, and have them start their investigations.

Exploring Equilibrium

→ Circulate among the teams as they complete their Team Reports.

→ Some students may need help realizing that Earth's gravity is a force acting on all the items. But if that is true, why aren't the items moving?

→ Some students may know that gravitational forces exist between their item and everything else in the room. Suggest that these forces are so small compared to Earth's gravity that they need not include them in a sketch.

→ Some students may want to discuss the meaning of stable. If enough students are concerned about this, you may want to initiate a full-class discussion.

→ When all the teams have completed the Team Report, have each group share their data. As they compare their results, ask them to think about similarities and differences among items and what might be responsible.

→ Distribute the I've Fallen and I Can't Get Up! Journal Questions. Review the definitions and have students work on Question 1, drawing out any additional questions about forces and how to represent forces on their sketches. Have your students complete the questions in the remaining classroom time or as an at-home assignment.

Activity Summary

→ After your students complete the Journal Questions, lead them in a class discussion of their responses.

→ Questions 2 and 4 may get the students thinking about the shape of an object and the distribution of mass within an object.

→ Question 3 may have some more advanced students thinking about reference frames—we are rotating with Earth as we all revolve around the Sun.

→ As you discuss question 4, ask your students if their results for this activity have given them any more insight into HOW they should move the furniture. Are some pieces of furniture inherently stable or unstable? How can you keep an unstable piece of furniture from toppling over during a move? These questions lead into the next activity.

→ As an additional challenge, have your students think about/research what is done to "stabilize" furniture in moving trucks or in earthquake-prone regions.

Activity Three: Make That Thing Move!

Your students should be just about ready to move some furniture. Hope you know where you want it!! In this activity, your students will see that WHERE you apply a force has an impact on how an object moves. They're probably already thinking about this. Do they want to push that top-heavy bookcase near the top or near the bottom? This activity does not explicitly address the direction in which a force is applied, but you could certainly add this concept to your directions for the Team Report.

Timing

The hands-on student work in this activity should go relatively quickly, so you should be able to include a fair amount of discussion time in a classroom period.

Materials and Supplies

- a variety of simple, rectangular prism-like items such as
  - tissue boxes
  - videocassette cases
  - books
  - toothpaste boxes
  - cereal boxes
- materials to construct objects with "off-center" centers of mass
  - masses such as those used on your scales/balances or rolls of pennies
  - tape
- Make That Thing Move! Team Report (one copy for each team/student)
- Make That Thing Move! Journal Questions (one copy for each student)
- a copy of Figure 1 for display purposes

Preparation

→ Review/research for yourself the concept of center of mass. Review this guide's directions for finding the center of mass of two-dimensional objects and try the method so you understand how/why it works. Search for alternative methods. Discuss with your team teachers methods that involve mathematics.

→ Decide how you will group your students.

→ Make copies of the Make That Thing Move! Team Reports and Journal Questions.

→ Collect a variety of simple rectangular prisms such as those in the Materials and Supplies list above. Each team needs one object to study. You may want to construct some objects with "off-center" centers of mass. See the Preparation section of Activity Two for some ideas.

→ Test the activity with the different items on various surfaces (desks, work tables, floor) in your classroom. The smoothness of the surfaces and items may have an impact on student results.

→ If you have constructed items with "off-center" centers of mass, make sure you test these items ahead of time so that you know how they will react to the applied forces.

→ Prepare a version of Figure 1 you can show to your class.

Student Introduction

→ Remind your students of the discussion about I've Fallen Journal Question 4. Tell them that they will do a simple investigation related to their discussion. They may be expressing an understanding of center of mass, with or without using those words. If so, you may want to introduce the term and concept prior to the activity rather than afterwards.
→ Show the students a sample object and Figure 1. Make sure they understand where they will apply forces to their items.
→ Stress that they are to apply a constant (steady) force in a single direction (perpendicular to the wall). Discuss ways they can attempt this (fingertip, eraser end of pencil).
→ Have your students form their teams. Distribute the Team Reports and study objects and have them begin their investigation.

Exploring Center of Mass

→ Circulate among the teams as they complete their Team Report. Watch for students who are not applying forces at the appropriate locations or in the appropriate directions. Note any discussion topics you may want students to bring up later.
→ When all the teams have completed the Team Report, have them share their data. If, as you observe your students, you find that they had consistent results, you may want to have them move onto the Journal Questions without discussing their results.
→ If all your teams have simple objects with fairly evenly-distributed mass (videotape, paperback book) their results should be consistent. The center of mass for such objects should be close to the physical center. Forces applied at points A and C should cause the object to translate in the direction of the force. Forces applied at points B and D should cause the object to rotate around the center of mass.
→ If you have constructed items with "off-center" centers of mass, your student results will be different. Make sure you test these items ahead of time so that you know how they will react to the applied forces.
→ Distribute the Make That Thing Move! Journal Questions. Have students complete the Journal Questions in the remaining classroom time or as an at-home assignment.

Activity Summary

→ Lead your students in a class discussion of their Journal Question responses. Focus on questions 3b, 4, and 5, especially if you have already discussed your students' observations.
→ Tests of center of mass location (question 4) will probably involve balancing the items on a fingertip or pencil eraser.
→ Student discussions should include conversations about the role of gravity in testing and locating an object's center of mass. In fact, center of mass is often called center of gravity.
→ Have your students compare their plans for finding an object's center of mass. As a class, develop a single method to use for Activity 4.
→ Refer back to your previous class discussions about moving furniture. Have your students revisit their plans, keeping the concept of center of mass in mind. How can they determine

or estimate the location of the centers of mass of the furniture? Some thoughts—Are books evenly distributed on all shelves of bookcases? Are file cabinets fully loaded?

→ As an additional challenge, have your students think about/research how to find the location of the center of mass of three-dimensional objects.

NOTE: This is a good time to introduce/assign the research project Who Cares? to your students. If you are using this unit as an introduction or supplement to a model rocket or some other unit, this is a good time to start focusing on aspects of the other unit.

Activity Four: The Center of Attention

For small, regularly-shaped objects made out of the same material, like a book, the center of mass is very close to the center of the object. But many things are made of more than one material. If you think about it, even books aren't made of just one thing. Besides the paper of the pages, you have the cover, which may be made of one or more materials, and there is glue or thread of some sort in the binding. Some of these materials you can't easily see.

Larger, more complex objects like airplanes, satellites, and buildings are also made from a mix of materials. Sometimes these large, complicated items are designed and built a piece at a time. It is important to understand the properties of the individual pieces, called components.

In this final hands-on activity, your students will design a two-dimensional "spacecraft" using at least three different components. They will use the method the class developed to locate the center of mass of each component prior to construction. After they have constructed the spacecraft, they will predict where the overall center of mass is located and then test their prediction.

Timing

With discussion, planning, construction, and testing, this activity might take two classroom periods to complete.

Materials and Supplies

- directions for finding the center of mass
- two-dimensional construction materials such as
    - paper
    - card stock
    - fabric (not stretchy)
    - aluminum foil
    - cellophane/transparencies
- tape
- glue
- stapler/staples
- scissors
- materials required for finding the center of mass, may include
    - string/thread/dental floss
    - paper clips or other fasteners
    - weights

Preparation

→ Create a clean set of step-by-step directions for finding the center of mass that can either be posted or distributed. Make enough copies, if it is to be passed out.

→ Decide whether students will work individually or as teams.
→ Gather a variety of supplies for your students to use. Consider setting up several similarly-stocked stations around the room to ease traffic flow.
→ Decide how much time you will devote to this activity. Will you have students plan their design in advance (overnight?) or do the design, test, and construct phases all in class? Do you have time for a class discussion in the middle of the activity?
→ Prepare a rubric for the unit assessment piece, Time To Move. Make enough copies of the Time To Move! assignment and rubric for each student.

Student Introduction

→ Remind students of your summary discussions in Activities 2 and 3. When talking about the furniture center of mass, it matters where mass is located. Most classroom furniture is a good example of something made out of different components. The screws or bolts that hold a bookcase together are probably made from a different material than the bulk of the bookcase. Add books, containers of calculators, and a box of spare pencils and you have all kinds of components to consider. While they may not normally care about the center of mass of a book when they return it to the bookcase, they should now realize that they alter the bookcase's center of mass each time they borrow and return a book.
→ Tell your students that they will design a two-dimensional "spacecraft" from at least three different components (you may want to limit them to only three components). Show them the different materials they have available.
→ Tell the students they will first design their spacecraft on paper, indicating the approximate dimensions and specific materials to be used. Following the design phase, they will cut out their components and find and mark the center of mass of each component using the specified method.
→ Let your students know that after they have found the center of mass of their components they should
    - o construct their spacecraft,
    - o predict the center of mass of the spacecraft and mark the predicted location with a P; have them show their work to you before proceeding,
    - o find the center of mass of the spacecraft and mark the location with an X.
→ Tell them what breaking points you plan to have during the activity so that some students do not get ahead of your planned timetable.

NOTE: Through the design phase, students may not think about how they will connect their components and what impact this may have on the final spacecraft's center of mass. You may want to introduce this thought before they start working or you may want to have a discussion when students have found the center of mass of their components and are ready to predict the overall center of mass location.

Exploring Components

→ Circulate among the students as they are designing their spacecraft (if not an at-home assignment) and finding the components' centers of mass. Help troubleshoot any difficulties they may have finding the centers of mass and address/announce any common pitfalls you find.

→ Make sure students mark their predicted spacecraft center of mass position before testing it.
→ As they are finishing, ask students to think about how the components (shape and material) and connections impacted with centers of mass of the spacecraft.

Activity Summary

→ Lead a class discussion of the component nature of most things we deal with. See if they can think of anything that is NOT made up of several components. Pure metal is one example, although we often see alloys used in jewelry and sculpture.
→ If your students are working on the Who Cares? Research Activity, ask them to think about the role of components in the situation they are researching.
→ Assign the Time To Move! assessment activity and distribute copies of it and your grading rubric.

Time To Move! Assignment

You have been planning to rearrange your classroom for a while, and it is almost time to move. Before the move can take place, you need to create a detailed move plan for one piece of furniture. Your plan must include the following.

- A scaled sketch of the piece of furniture with the following labeled
  - location and materials of the major components,
  - dimensions,
  - approximate overall center of mass location,
  - an estimate of the mass.
- A second scaled sketch (same size and scale) showing the following
  - approximate overall center of mass location,
  - all forces acting on the piece of furniture when stationary,
  - the force(s) planned to move it one meter across the floor (indicate the point of application and direction of application for all forces).
- A written description using scientific vocabulary of where the force(s) will be applied and why you developed the plan you did.

Research Activity: Who Cares?

Although your students have been looking at the authentic application of forces and motion and the role of center of mass in moving furniture, you may want them to research the many other situations where centers of mass are important. You may want to assign the suggested situations provided here, or use situations you or your students think of.

Timing

How much classroom time you devote to this activity is up to you. You may want students to do book/computer research during class time. Oral presentation will take additional classroom time.

Materials and Supplies

- library/classroom textbooks and reference material
- the internet
- some general URLs that may be helpful
    - www.discoverengineering.org
    - www.av8n.com/how/
    - www.crestedbutteacademy.com/athletics/skiprogcurriculum.html
    - www.thetech.org/exhibits/online/satellite/home.html
    - pumas.jpl.nasa.gov/
    - www.howstuffworks.com/index.htm
    - whyfiles.org/
    - www.youngastronauts.org/yac/
    - www.challenger.org
    - education.nasa.gov

Preparation

→ Decide whether your students will work individually or in teams. Decide how you will form teams.
→ Decide whether reporting will be written or oral.
→ Create a rubric for the research report and make enough copies.
→ Decide how you will assign topics to students.

Student Introduction

→ Tell students that they will work on a research project to find out Who Cares? about centers of mass.
→ Introduce the rubric to explain what you expect them to learn and how you want them to present their research.
→ Discuss possible reference sources, asking your students for suggestions.
→ Assign the project, giving the due date or schedule for oral presentations.

Suggested Situations for Study

- a rocket on the launch pad
- a commercial airplane loaded with passengers and cargo
- a telecommunications satellite orbiting Earth
- a motorcycle going around a curve
- a backpack being filled for a long hiking trip
- a pair of high-heel shoes
- a railing on a ship deck
- a bicycle with training wheels
- a snowman, under construction
- a ski jumper leaving the jump
- a ski jumper landing
- the International Space Station, under construction
- the Space Shuttle, seconds after leaving the launch pad
- a jet, refueling in flight

What's The Point? Summary

After you have reviewed your students' Time To Move! and Who Cares? assignments, lead a closing discussion about this unit. Refer back to your early What Do They Know? questions and ask students to think about why you talked about mass, density, and volume and force, equilibrium, and potential energy. Do they have a better appreciation for how the force you apply makes an object move and why the objects move the way they do? Do they Get The Point?